The Role of the RNA Exosome Component, EXOSC3, in the Pathogenesis of Atypical Haemolytic Uraemic Syndrome

Patrick R. Walsh

Submitted for the degree of Doctor of Philosophy

Newcastle University, Faculty of Medical Sciences

November 2023

Acknowledgements

This project would not have been possible without the support of my supervisors Professor David Kavanagh and Professor Kevin Marchbank, they have been a continued support throughout this project and have allowed me to flourish and grow as a scientist. I would also like to acknowledge the support of all of the team in the complement therapeutic group and the national renal complement therapeutic centre, who have guided me in new techniques and maintaining the mouse colony, finally I would like to acknowledge the patients and families who have helped to identify these causes of aHUS.

Dedication

This thesis is dedicated to my wonderful wife Nicole and my little girl Olive, with whose love and support this would not have been possible.

Abstract

Haemolytic uraemic syndrome (HUS) is a rare kidney disease characterised by microangiopathic haemolytic anaemia, thrombocytopenia, and acute kidney injury, histologically this is as a result of thrombotic microangiopathy (TMA). Work over the last 25 years has identified inherited and acquired dysregulation of the complement system as the underlying cause in complement associated HUS (C-aHUS); leading to the introduction of the complement inhibitor, eculizumab. It is now clear that there is a subgroup of patients who do not respond to eculizumab. The National Renal Complement Therapeutic Centre (NRCTC) maintains one of the world's largest repositories of HUS cases, with approximately 2000 individuals. This project aimed to review eculizumab non-responsive patients for an alternative genetic diagnosis.

Using a combination of Whole Exome and Sanger sequencing eleven patients with variants in five RNA surveillance genes (*EXOSC3, POLR3B, POLR3H, RNU4ATAC* and *TSEN2*) were identified. These patients uncover a previously undescribed pathway for TMA pathogenesis.

To further understand the effects of RNA surveillance in a conditional knockout mouse of one of these genes ($Exosc3^{fl/fl}$) was utilised. A whole-body knockout model ($Exosc3^{gfp/gfp}.Rosa26Cre^{ERT2/ERT2}$) did not develop HUS but did show evidence of ribosomal dysfunction in the form of bone marrow and intestinal failure secondary to cell cycle arrest and apoptosis. P53 inhibition resulted in significant improved survival.

To determine whether TMA would develop in an endothelial specific knockout model, *Exosc3*$^{fl/fl}$ were crossed with an endothelial specific cre model (*Exosc3*$^{gfp/gfp}$*.Tie2Cre*$^{ERT2/ERT2}$), unfortunately these mice did not show evidence of recombination.

Overall, this project has identified five genes in the RNA surveillance pathway that result in TMA via complement non-responsive pathways. Whilst the mouse models did not develop TMA, the mice demonstrated evidence of ribosomal dysfunction that was partially rescued with a p53 antagonist; suggesting ribsomopathy is central to the pathogenesis of EXOSC3-mediated TMA and offering new insights in to other forms of TMA.

Contents

3′SSPI	-	3′ splice site
4-OHT	-	4-Hydroxytamoxifen
7-AAD	-	7-aminoactinomycin D
A/E	-	Attaching and effacing
AdoCbl	-	Adenosylcobalamin
aHUS	-	Atypical Haemolytic uraemic syndrome
AKI	-	Acute kidney injury
Anti-RNAPIII	-	Anti-RNA polymerase III
ARE	-	AU-Rich elements
ARE-BP	-	ARE-binding proteins
ARS	-	Acute radiation syndrome
BAC	-	Bacterial artificial chromosome
BFU	-	Burst forming unit
BrdU	-	Bromodeoxyuridine
BSA	-	Bovine Serum albumin
C3	-	Complement component 3
C5aR1	-	C5a Receptor 1
C-aHUS	-	Complement associated Haemolytic uraemic syndrome
CblC	-	Cobalamin C
CCP	-	Complement control proteins
cDNA	-	Complementary DNA
CFB	-	Complement factor B
CFH	-	Complement factor H
CFHR	-	Complement factor H related
CFI	-	Complement factor I
CMT	-	Charcot-Marie Tooth
COIN	-	Conditional by Inversion
DGKε	-	Diacylglycerol kinase epsilon
DNA	-	Deoxyribonucleic acid
dPBS	-	Dulbecco Phosphate buffered saline
DSB	-	Double strand break
EDTA	-	Ethylenediaminetetraacetic acid
EF1	-	Elongation factor 1
EF2	-	Elongation factor 2
ELISA	-	Enzyme linked immunosorbent assay
ER	-	Endoplasmic reticulum
eRNA	-	Enhancer RNA
FACS	-	Fluorescence-activated cell sorting
FHAA	-	Factor H autoantibodies
FSC	-	Forward Scatter
FSGS	-	Focal segmental glomerulosclerosis
GAG	-	Glycosaminoglycan
Gb_3	-	Globotriaosylceramide 3
gDNA	-	Genomic DNA
GFP	-	Green fluorescence protein
GI-ARS	-	Gastrointestinal acute radiation syndrome

H&E	-	Haematoxylin and Eosin
H-ARS	-	Haemopoetic acute radiation syndrome
HIV	-	Human immunodeficiency virus
HMEC-1	-	Human microvascular endothelial cells
HRP	-	Horseradish Peroxidase
HSC	-	Haemopoetic stem cells
HUS	-	Haemolytic Uraemic Syndrome
I.P.	-	Intraperitoneal
Ifnar	-	Interferon receptor
INF2	-	Inverted formin-2
IPA	-	Ingenuity Pathway Analysis
ISG	-	Interferon stimulated genes
IV	-	Intravenous
LDH	-	Lactate dehydrogenase
LEE	-	Locus of enterocyte effacement
LSK	-	$Lin^{-}Sca1^{+}c\text{-}Kit^{+}$
MAC	-	Membrane attack complex
MAHA	-	Microangiopathic haemolytic anaemia
MCP	-	Membrane cofactor protein
MeCbl	-	Methylcobalamin
MLPA	-	Multi-ligation probe amplification
MMA	-	Methylmalonic acid
MMACHC	-	Methylmalonic aciduria and homocystinuria type C
mRNA	-	Messenger RNA
MSB	-	Martius Scarlet Blue
NADPH	-	Nicotinamide adenine dinucleotide phosphate
NAHR	-	Non-allelic homologous recombination
N-ARS	-	Neurological acute radiation syndrome
ncRNA	-	Non-coding RNA
NHEJ	-	Non-homologous end joining
NRCTC	-	National Renal Complement Therapeutic Centre
pA	-	Polyadenylation
PAS	-	Periodic Acid-Schiff
PCH	-	Pontocerebellar hypoplasia
PCR	-	Polymerase chain reaction
PFT-α	-	Pifithrin-α
PGE_2	-	Prostaglandin E2
p-HUS	-	Streptococcal Pneumoniae Haemolytic uraemic syndrome
PI	-	Propidium Iodide
POLR3-HLD	-	POLR3 related Hypomyelinating Leukodystrophy
PROMPTs	-	Promoter upstream transcripts
PRR	-	Pattern recognition receptors
qPCR	-	Quantitative polymerase chain reaction
RCA	-	Regulator of complement activation
RIP	-	Ribosome Inactivating Proteins

RIPA	-	Radioimmunoprecipitation assay
RLR	-	RIG-I Like Regulators
RNA	-	Ribonucleic acid
RNAP	-	RNA polymerase
RP	-	Ribosomal protein
rRNA	-	Ribosomal RNA
RSV	-	Respiratory syncytial virus
RT-qPCR	-	Reverse transcriptase quantitative PCR
SLE	-	Systemic Lupus Erythematous
snoRNA	-	Short nucleolar RNA
snRNA	-	Short nuclear RNA
SRC	-	Scleroderma renal crisis
SSc	-	Systemic Sclerosis
SSC	-	Side Scatter
ssRNA	-	Single stranded RNA
STEC	-	Shiga toxin producing *E.coli*
STEC-HUS	-	Shiga toxin associated Haemolytic uraemic syndrome
Stx.	-	Shiga toxin
TAE	-	Tris-acetate-EDTA
TBST	-	Tris-buffered saline with 0.05% Tween® 20 detergent
TMA	-	Thrombotic microangiopathy
TMB	-	3,3',5,5'-Tetramethylbenzidine
TNF-α	-	Tumour necrosis factor α
tRNA	-	Transfer RNA
TTP	-	Thrombotic thrombocytopenic purpura
VEGF2	-	Vascular endothelial growth factor 2
vWf	-	von Willebrand factor

Figure List

1. Introduction

1.1. Haemolytic Uraemic Syndrome

Haemolytic Uraemic Syndrome (HUS) is the clinical triad of microangiopathic haemolytic anaemia (MAHA), thrombocytopenia, and acute kidney injury (AKI) (Moake, 2002; Walsh and Johnson, 2018; Brocklebank *et al.*, 2020).

1.1.1. Pathology

Pathologically, HUS is characterised by thrombotic microangiopathy (TMA) in affected organs, most commonly the kidney (Figure 1-1). TMA can be recognised in the acute phase with the appearance of intraluminal thrombi within glomeruli, subendothelial space, and mesangium. Endothelial activation results in mesangiolysis, endothelial swelling within the glomeruli that can be seen on both light and electron microscopy. Chronic changes of TMA include duplication of glomerular basement membrane, intimal proliferation and fibrosis with narrowed arterioles lumen resulting in “onionskin” lesions. Immunofluorescence in TMA confirms fibrin rich thrombi as well as non-specific Immunoglobulin staining (Lusco *et al.*; Goodship *et al.*, 2017; Brocklebank;Wood and Kavanagh, 2018).

1.1.2. Classification of TMAs

TMA classification has evolved through its history with the identification of new causative genes, understanding of pathogenic mechanisms and the introduction of therapies. Broadly speaking, TMAs can be categorised in to primary, due to genetic variants or acquired autoantibodies, infection associated, and secondary TMAs, occurring in the setting of other disease processes (Brocklebank;Wood and Kavanagh, 2018).

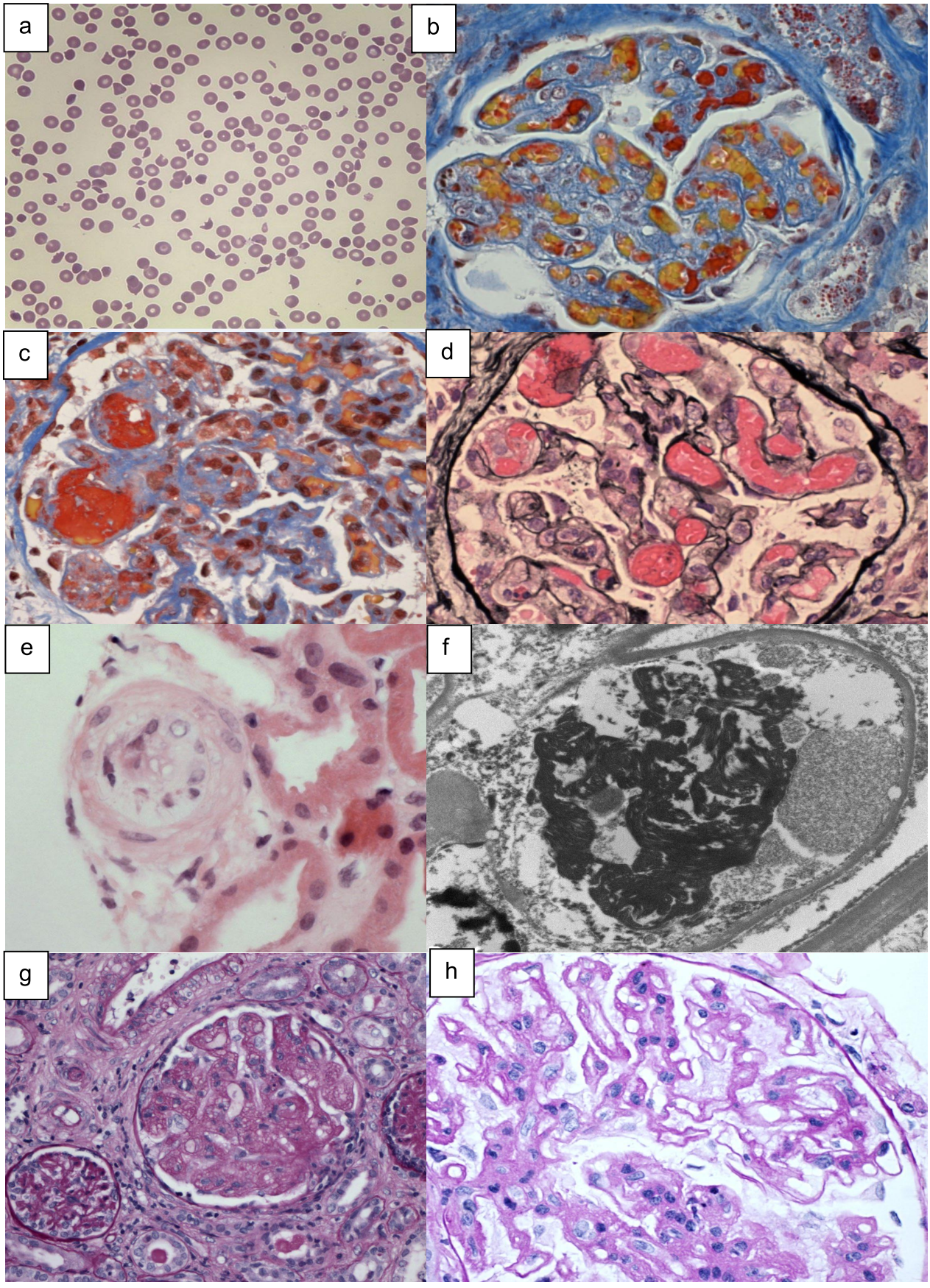
a
b
c
d
e
f
g
h

Figure 1-1 Pathological features of thrombotic microangiopathies.

a. Blood film showing MAHA and thrombocytopenia schistocytes evident. b. & c. Glomerular capillary lumina containing fibrin thrombi (red) and erythrocytes (yellow) (Martius Scarlet Blue, ×400) d. Glomerular paralysis with capillary loops containing abundant erythrocytes (silver, ×400) e. Mucoid thickening and obliteration of the lumen of a small artery, typical onion-skin lesion (haematoxylin and eosin, ×400) f. Electron micrograph demonstrating fibrin tactoids (black) in glomerular capillary (×10,000) g. Reduplication of glomerular basement membrane (arrow) and fibrillary mesangium (periodic acid–Schiff, ×400) h. Reduplication of the glomerular basement membrane (Periodic acid-Schiff x400)

1.2. Shiga Toxin HUS (STEC-HUS)

Shiga toxin HUS (STEC-HUS) is the most common form of TMA, responsible for approximately 90% of cases. STEC-HUS occurs as a result of infection with Shiga toxin producing *E.coli* (STEC) infection, most commonly serotype O157:H7 (Lynn *et al.*, 2005; Dallman *et al.*, 2022). Additional shiga toxin producing organisms can result in HUS, including Non-O157 *E.coli* (including O26, O145, O111, O13-O135, O146, O45, O80 and O85), *Shigella dysentriae*, *Shigella flexneri, Shigella sonnei and Citrobacter* (Walsh and Johnson, 2018; Michael *et al.*, 2022; UKHSA, 2022).

1.2.1. Epidemiology

STEC has an annual incidence of 0.91 per 100,000 in the UK. Children under five years of age are at highest risk of both STEC infection, with an incidence of 3.28 per 100,000 population, and progression to STEC-HUS (Lynn *et al.*, 2005; Adams *et al.*, 2019b; UKHSA, 2022). Following infection with STEC, haemorrhagic colitis occurs in the majority of infected people. In over 80-90% of cases this resolves within a week with no further sequalae. In the remaining 10-20% STEC-HUS develops 7-10 days after symptom onset (Tarr *et al.*, 2005). The most commonly affected organ is the kidney with 50-75% of patients needing dialysis (Walsh and Johnson, 2018). Extra-renal manifestations occur in approximately 20% of cases.

This can involve the gastrointestinal tract in the form of bowel ischaemia, perforation, and bowel necrosis. Pancreatic involvement can include pancreatitis and insulin dependent diabetes mellitus, cardiovascular involvement commonly results in hypertension and myocarditis (Khalid and Andreoli, 2019). Of all the extra-renal manifestations neurological involvement is the most serious and results in seizures, encephalopathy, hemiplegia, cortical blindness, dysphasia diplopia, facial nerve palsy and coma, which represents the major cause of mortality in HUS (Swick and Haworth, 1986; Oakes *et al.*, 2006). Acutely, mortality remains between 3-5%, with long-term sequelae (hypertension, chronic kidney disease) affecting approximately 30% (Lynn *et al.*, 2005).

1.2.2. Source of disease

Cattle are the major reservoir for STEC globally, with other ruminants, including deer, sheep and goats carrying STEC (Callaway *et al.*, 2007; Fernández *et al.*, 2009; Ferens and Hovde, 2011; Ferreira *et al.*, 2014; Mellor *et al.*, 2016; Venegas-Vargas *et al.*, 2016; Ross *et al.*, 2019; Dallman *et al.*, 2022; Jenkins *et al.*, 2022). Human infection usually occurs as a result of consumption of poorly cooked contaminated beef (Kassenborg *et al.*, 2004; Rangel *et al.*, 2005; Vogt and Dippold, 2005). Other sources include consumption of unpasteurised contaminated milk (Adams *et al.*, 2019a; Dallman *et al.*, 2022; Jenkins *et al.*, 2022), and contaminated vegetables (Franz and van Bruggen, 2008). Beansprouts were responsible for one of the largest outbreaks in 2011 (Buchholz *et al.*, 2011; Kintz *et al.*, 2019). STEC infection commonly occurs as part of an outbreak, partially due to the remarkably low number of bacteria required for disease to develop. STEC infection has been described in individuals exposed to ten bacteria (Schmid-Hempel and Frank, 2007), this compares to $>10^5$ organisms required for infection with other *E.coli* species

(Kothary and Babu, 2001). STEC-HUS displays a seasonal variation, with the peak incidence in summer months (UKHSA, 2022). Whilst the exact reason for this is unclear, one explanation is that contaminated beef consumption increases with poorly prepared barbeques in the summer months and an increase in visits to petting zoos. One potential public health intervention that has been suggested to prevent the transmission of *E.coli* from cattle is vaccination, this has been predicted to reduce the human infection rate by up to 85% (Matthews *et al.*, 2013).

1.2.3. Pathogenesis of disease

Following ingestion, STEC traverses the acid stomach environment and enters the intestine, the site of infection. One of the hallmarks of STEC, that is shared with enteropathogenic *E.coli*, is the ability to bind to the intestinal epithelium through the production of “attaching and effacing” (A/E) lesions (Lai *et al.*, 2013). This is due to the presence of the locus of enterocyte effacement (LEE) (McDaniel and Kaper, 1997; Elliott *et al.*, 1998). This region codes for numerous proteins that aid the attachment of STEC to the plasma membrane including adhesin intimin, chaperones, a filamentous type III secretion system composed of the translocators proteins (EspA, EspB and EspD), and six effectors (Tir, EspF, Map, EspG, EspH, and EspZ) (Gaytán *et al.*, 2016). A/E lesions are characterised by effacement of the intestinal brush border, bacterial attachment to the enterocyte cell membrane, and accumulation of actin which appears as electron dense material (Lai *et al.*, 2013). These A/E facilitate the strong binding of STEC to the intestinal tract. STEC infection does not result in bacteraemia, instead luminal bound STEC produces shiga toxin (Stx.), the pathogenic toxin in HUS (Chan and Ng, 2016). The exact mechanisms of toxin translocation is currently unknown. Once in the blood stream Stx. binds to

circulating polymorphonuclear neutrophils and is transferred onwards (te Loo *et al.*, 2000).

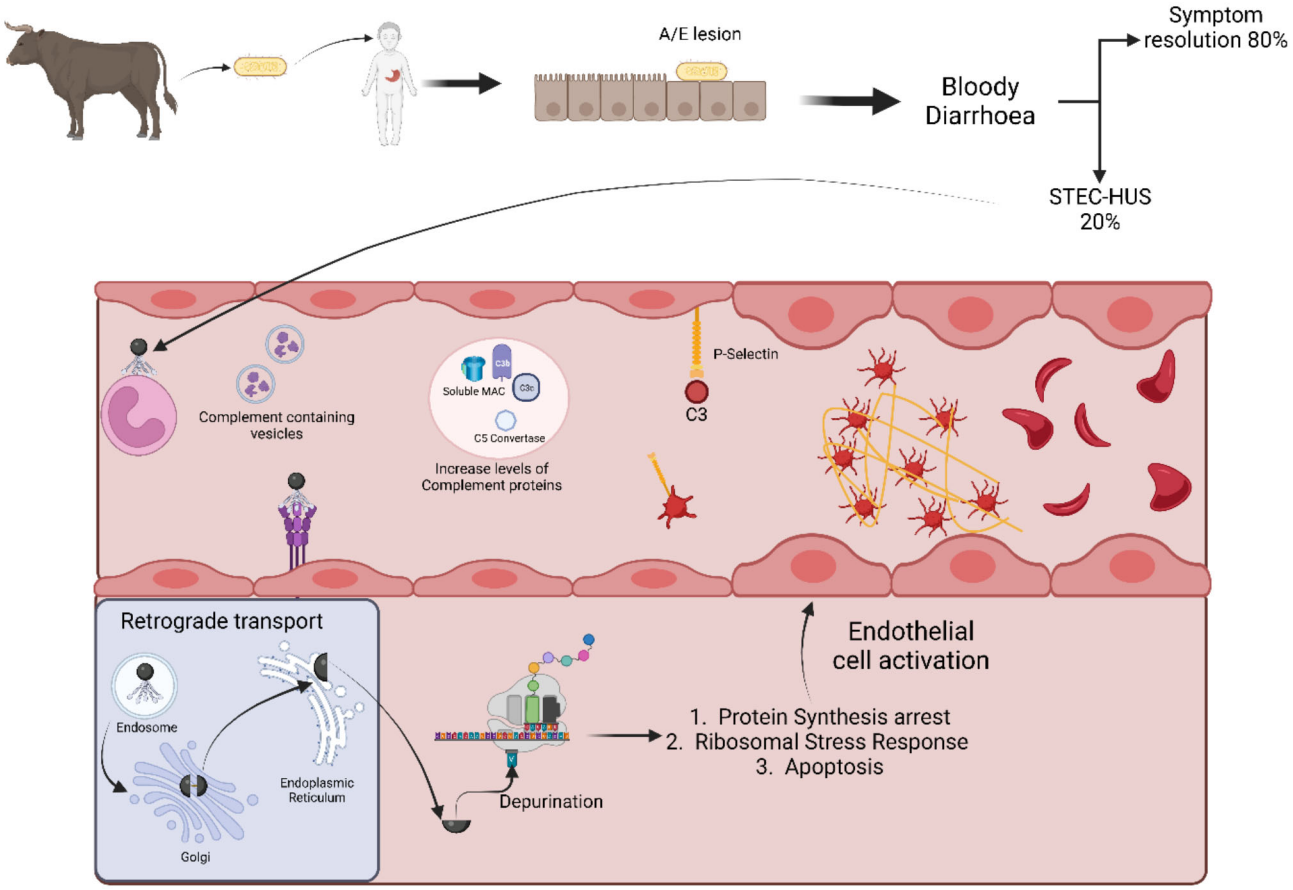

Figure 1-2: Pathogenesis of STEC-HUS. *Following ingestion of STEC, most commonly from consumption of contaminated dairy or beef, STEC binds to the intestinal lumen via Attaching and Effacing lesion. This results in bloody diarrhoea lasting 7 -10 days. In 80% of people this resolves without further sequalae. In the remaining 20% STEC-HUS occurs. Stx. released from STEC translocates from the intestinal lumen to the bloodstream, through mechanisms that are so far unknown. Once in the bloodstream Stx. binds to circulating neutrophils and is transported systemically. Stx. binds to the Gb3 receptor that is found on endothelial surfaces, in particular on the glomerular surface. This is then internalised and enters the endosome where it is then transported to the Golgi and subsequently the ER before release into the cytoplasm (a process known as retrograde transport). Once the A1 subunit is released into the cytoplasm it hydrolyses the depurination of the alpha-sarcin loop ultimately leading to ribosomal dysfunction, protein synthesis arrest, ribosomal stress response and apoptosis. This activates the endothelium and causes the formation of platelet rich thrombi which occlude the lumen, these result in haemolysis as red cells are forced through this network. Ultimately this leads to downstream organ dysfunction. There is evidence of complement activation in STEC-HUS, complement containing microvesicles have been identified in patients with STEC-HUS, complement components have been shown to be raised in*

patients with STEC-HUS and there is evidence that Stx. activates and upregulates P-Selectin on both the endothelium and platelets, which can subsequently activate C3. (Images created in BioRender)

1.2.4. Shiga toxin structure and function

Stx. produced by *S. dysentriae* was first described 120 years ago (Shiga, 1898). Stx. was later discovered to be produced by *E.coli* species (Konowalchuk *et al.*, 1977). Two subtypes of shiga toxin have been identified, Stx. 1 and 2 (Melton-Celsa, 2014). Stx2 accounting for a greater likelihood of developing STEC-HUS, following infection (Taylor *et al.*, 1999; Adams *et al.*, 2019b). Stx. 1 and 2 are both examples of AB_5 toxins composed of two subunits A and B. The B subunit is a pentamer that enables binding to the target receptor, the Globotriaosylceramide 3 (Gb3) receptor; the A subunit is comprised of an A_1 and A_2 chain that are responsible for effects on the ribosome. Following binding to the Gb3 receptor the toxin is internalised and utilises retrograde pathways to enter the endosome, into the Golgi, where the A subunit is proteolytically cleaved in to A_1 and A_2 (but continues to be held together by disulphide bonds) (Garred *et al.*, 1995), then subsequently the Endoplasmic Reticulum (ER) (Bonifacino and Rojas, 2006; Falguières *et al.*, 2006). Once within the ER the disulphide bonds holding the A_1 and A_2 chains together are reduced and only the A_1 chain is released into the cytoplasm (Figure 1-2). A_1 is a Ribonucleic Acid (RNA) N-glycosidase that hydrolyses the N-glycosidic bond between a specific adenine (differing between species) and its associated sugar, releasing this adenine from the alpha-sarcin loop in the 28S ribosomal subunit, thus preventing its normal function (Furutani *et al.*, 1992). The ribosome is responsible for translating messenger RNA (mRNA) into polypeptides. The ribosome is formed of two subunits, each comprised of combination of non-coding ribosomal RNA (rRNA) and ribosomal proteins (RP), together forming ribonucleoprotein particles (RNPs).

Together these subunits perform the intricate task of decoding mRNA, matching to the corresponding transfer RNA (tRNA) and finally catalysing the formation of peptide bonds. The alpha-sarcin loop is essential for binding of Elongation factors 1 and 2 (EF1 and EF2) to the ribosome (Voorhees *et al.*, 2010). EF1 mediates the entry of aminoacyl tRNA (tRNA with amino acid attached) to the ribosome, EF2 mediates the elongation of the polypeptide change. The removal of this adenine by the A_1 chain prevents binding of EF1 and EF2 (Sperti *et al.*, 1975), resulting in ribosomal translation and protein synthesis arrest. In addition to the specific depurination in the alpha-sarcin loop of rRNA resulting from A_1 chain, there is evidence that purified Ribosome Inactivating Proteins (RIPs) (of which Stx1 and Stx2 are forms) cause depurination of Deoxyribonucleic Acid (DNA), tRNA and viral nucleic acids (Peumans *et al.*, 2001). It is now clear that Stx. has a direct effect on rRNA and tRNAs, resulting in abnormal modifications that target these for degradation by the RNA exosome (4.5) (Jobst *et al.*, 2016).

1.2.5. Downstream effects of Stx. on ribosome function

Stx. results in up regulation of pro-apoptotic and inflammatory pathways through three interdependent mechanisms (Jobst *et al.*, 2016), translation arrest, ribotoxic stress response and unfolded protein response. Translation arrest has been found to up-regulate apoptosis, as a response to cell stress (Holcik and Sonenberg, 2005). Ribotoxic stress response was initially described in response to anisomycin, a 28S inhibitor (Iordanov *et al.*, 1997); upon depurination of 28S rRNA there is activation of a number of pro-apoptotic and pro-inflammatory pathways that ultimately result in apoptosis. Induction of the ribotoxic stress response using Deoxynivalenol has been shown to result in upregulation of a wide number of proteins responsible for cell cycle regulation, RNA processing (through the RNA exosome) and ribosomal

biogenesis (Pan *et al.*, 2013). Finally, the unfolded protein response is thought to be initiated by the unfolding of Stx. within the ER, (Tesh, 2012) resulting in up-regulation of pro-apoptotic pathways. Ultimately the cellular result of Stx. is upregulation of pro-apoptotic pathways and cell death.

1.2.6. Management of STEC-HUS

The mainstay of treatment for STEC-HUS is supportive management, with approximately half of children requiring dialysis and up to 80% needing red cell transfusion (Walsh and Johnson, 2018). Multiple interventions have been trialled, with limited evidence of success. One potential reason for this is due to trail design. As previously noted 85-90% of people infected with STEC have complete resolution of symptoms, without progression to HUS. The majority of trails have used a definition of HUS (MAHA, thrombocytopenia and AKI) as entry criteria. It is possible and in some cases likely that this is too late for effective intervention.

1.2.6.1. Intravenous fluids

On acute presentation with STEC-HUS it is common for patients to have evidence of hypovolaemia. One management strategy that has been employed is the administration of Intravenous (IV) fluids, on presentation with STEC associated diarrhoea, prior to established STEC-HUS to maintain intrarenal blood flow and prevent thrombus formation, this has demonstrated some promise in preventing the need for intensive care and dialysis (Ardissino *et al.*, 2015).

1.2.6.2. Antibiotics

Antibiotic use is generally avoided, as there is *in vitro* evidence of upregulation of Stx. production and release following exposure to antibiotics (in particular ciprofloxacin) (Bielaszewska *et al.*, 2012). Retrospective data has demonstrated an

increased likelihood of developing HUS following treatment with antibiotics in the diarrhoeal stage of disease (Wong *et al.*, 2000; Adams *et al.*, 2019b). There is some promising data that Azithromycin may be of benefit in STEC-HUS, due to its ability to block protein synthesis within *E.coli* (Ohara *et al.*, 2002; Bielaszewska *et al.*, 2012; Seifert and Tarr, 2012), however this is in the early stages of investigation. As previously noted, bacteraemia is rare in STEC infection, however intra-abdominal sepsis is a recognised complication, due to breakdown in the intestinal integrity.

1.2.6.3. Gb3 binding agents

SYNSORB Pk (SYNSORB Biotech Inc., Canada) was once a promising treatment for STEC-HUS. This agent consists of silicon dioxide particles linked to the trisaccharide moiety of the Globotriaosylceramide molecule. This agent competes for Gb3 binding thus preventing Stx. binding and internalisation. Unfortunately despite promising results in preclinical models, there were no benefits seen in the randomised clinical trial (Trachtman, 2003), potentially as patients were treated only after the onset of HUS, at a time point where Stx. has already internalised.

1.2.6.4. Shiga toxin neutralising antibodies

Several agents that bind to Stx. and prevent binding to cells have been investigated including STARFISH (Kitov *et al.*, 2000), NEAST (Hiriart *et al.*, 2019), and Urtoxazumab (Moxley *et al.*, 2017), whilst these have all shown promise in preclinical models, all have failed to translate to clinical effectiveness in patients with STEC-HUS.

1.2.6.5. Plasma Exchange

Once the mainstay treatment for salvage treatment in cases of neurological involvement, plasma exchange has failed to demonstrate clinical improvement outside small anecdotal studies (Colic *et al.*, 2011; Kielstein *et al.*, 2012)

1.2.6.6. Anti-complement therapy

The role of anti-complement therapy is examined below (1.3.5).

1.3. Atypical HUS (aHUS)

The term aHUS has traditionally been used for HUS not due to STEC. However, with an increase in understanding of the underlying pathogenesis of disease the term is now generally used to describe complement mediated disease, alternatively the term Complement-associated haemolytic uraemic syndrome (C-aHUS) has been used.

1.3.1. Epidemiology

C-aHUS is a rare disease with an annual incidence of 0.41/million/year in England (Brocklebank *et al.*, 2023). Whilst aHUS has been reported at any age there are two recognised peaks, in early childhood and subsequently in early adulthood in women of child bearing age (Noris *et al.*, 2010; Brocklebank *et al.*, 2023) likely due to complement activation during and immediately after pregnancy (Smith-Jackson and Harrison, 2023). Triggering events, most commonly viral infection and pregnancy, are identified in between 30-70% of patients (Noris *et al.*, 2010; Brocklebank *et al.*, 2023) .

Since the first identification of pathogenic variants in complement factor H (*CFH*) 25 years ago (Warwicker *et al.*, 1998) the number of complement genes that have been documented in aHUS has grown to include: Complement Factor I (*CFI*), Membrane

Cofactor Protein (*MCP* or *CD46*), Complement Factor B (*CFB*), Complement component 3 (*C3*), Complement Factor H Related genes (*CFHR*) and autoantibodies to CFH (Caprioli *et al.*, 2006; Noris *et al.*, 2010; Brocklebank *et al.*, 2017). Approximately 50% of patients with C-aHUS have a pathogenic variant in a complement gene identified and/or factor H autoantibody identified (Brocklebank *et al.*, 2023)

1.3.2. Complement system

The complement system is an arm of the innate immune system comprising of over 30 serum and membrane bound proteins (Walport, 2001). The complement system is comprised of three separate activation pathways that converge on a common final pathway. Namely the classical, alternative and mannose binding lectin pathway. The complement system acts in three main ways firstly, as part of the host innate response to infection, resulting in opsonisation, chemotaxis, and direct cell lysis. Secondly, it acts at the interface between the innate and adaptive immune system, by augmenting antibody responses, and enhancing immune memory. Finally, it is involved in cellular waste disposal, by clearing immune complexes and apoptotic cells.

1.3.2.1. The Alternative complement pathway

C-aHUS is a disease of alternative complement (AP) dysregulation (Kavanagh *et al.*, 2013). Under normal physiology the alternative complement pathway is constitutively active, due to the spontaneous hydrolysis of C3 (the first protein in the alternative complement pathway) to C3(H_2O) (Pangburn *et al.*, 1981). This process exposes the binding site for a CFB, resulting in the formation of C3(H_2O)-Bound FB. This is cleaved by circulating Factor D to form the C3 convertase (C3(H_2O)Bb), which can convert circulating C3 to C3a and C3b. This C3b binds to available cell

surfaces where it is able to generate additional C3 Convertase (C3bBb) with Factor D and CFB acting as described. This generates an amplification loop whereby there is rapid conversion of circulating C3 to C3a and C3b by the C3 convertase. The generated C3a and C3b have a role in chemotaxis and opsonisation, respectively (Walport, 2001). The membrane bound C3 convertase continues to amplify this C3 conversion and ultimately binds a further molecule of C3b to become C3bBbC3b, the C5 convertase. The C5 convertase is responsible for the conversion of circulating C5 to C5a (a chemotactic molecule) and C5b, which complexes with C6-C9 to become the Membrane attack complex (MAC), which binds to the cell surface to create a pore in the cell membrane that results in cell lysis through osmosis (Merle *et al.*, 2015).

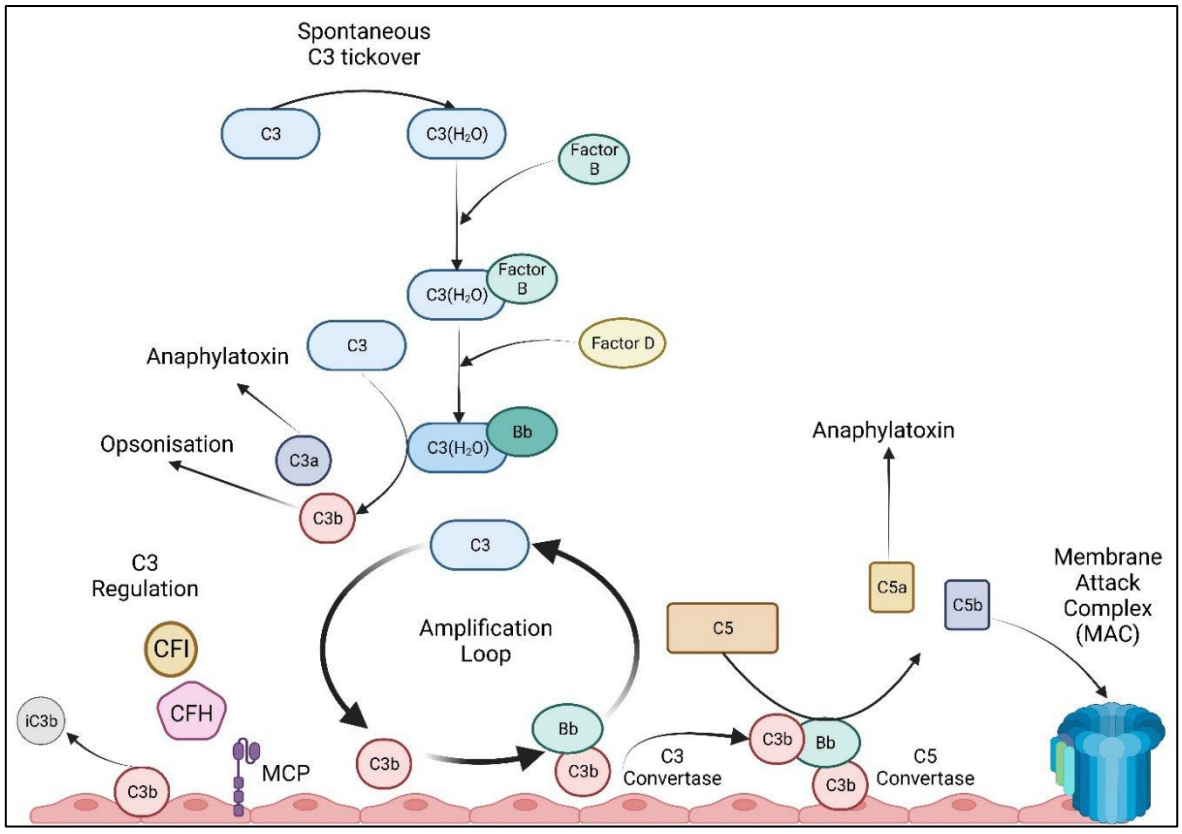

Figure 1-3: The alternative pathway of complement activation.

C3 spontaneously hydrolyses to C3(H_2O), a process known as C3 tick-over. This exposes the factor B binding site; following Factor B binding this is further cleaved by factor D, resulting in the C3 convertase C3(H_2O)Bb. The C3 convertase is then able to convert circulating C3 to C3a

(anaphylatoxin) and C3b (opsonisation). C3b binds to the cell surface and finds circulating Factor B to become the C3 convertase (C3bBb). This generates a positive feedback amplification loop where circulating C3 is converted to C3a and C3b. Ultimately the C3 convertase binds a further molecule of C3b to become the C5 convertase (C3bBbC3b). The C5 convertase catalyses the conversion of C5 to C5a (Anaphylatoxin) and C5b, which complexes with C6-C9 to generate the membrane attack complex that creates an osmotically active pore on the cell surface, resulting in cell lysis. To prevent inappropriate activation on host cells there are a number of regulators that prevent unchecked complement activity. C3 and the amplification loop are regulated by CFI, CFH and MCP. These regulators degrade surface bound C3b to iC3b, which can no longer bind factor B, preventing it from amplifying the complement cascade.

1.3.2.2. Complement regulation

To prevent indiscriminate complement activation that would result in host cell damage, a number of complement regulators exist, CFH, CFI, MCP (CD46), CR1 and C4BP (Merle *et al.*, 2015). Of these pathogenic variants in CFI, CFH and MCP have been described in C-aHUS (Caprioli *et al.*, 2006; Noris *et al.*, 2010; Goodship *et al.*, 2017).

CFI is a serine protease that cleaves C3b in the presence of co-factors, including CFH and MCP. CFI activity on C3b results in the degradation to iC3b, which is unable to bind CFB, preventing downstream processes. MCP is a membrane bound CFI cofactor that is present on all nucleated cells (M K Liszewski *et al.*, 1991), composed of four complement control proteins (CCPs) MCP is required for CFI mediated C3b inactivation on the cell surface.

CFH is described as the master regulator of the alternative pathway. CFH is composed of 20 CCPs oriented in a “Bead on string” configuration. There are two domains that are of particular interest in complement regulation, the N-terminal CCPs (1-4) are responsible for the cofactor activity with CFI, compete with circulating CFB for C3b binding, therefore preventing the conversion to the C3 convertase and accelerate the degradation of formed C3 convertase (Kavanagh *et*

al., 2013). The final two CCPs at the C-terminus enable CFH to bind to the cell surface through binding to glycosaminoglycans (GAGs) in the kidney (Ferreira *et al.*, 2010). CFH therefore has complement regulatory properties in both the fluid phase and as a surface bound protein.

1.3.3. Historical outcomes of pathogenic variants in C-aHUS

Pathogenic variants in *CFH* were the first identified in aHUS 25 years ago (Warwicker *et al.*, 1998). *CFH* are the most commonly identified variants in C-aHUS, detected in 47% of the historical NRCTC cohort. These were historically associated with a poor prognosis, with a five-year end stage kidney disease (ESKD) free survival of 16% (Brocklebank *et al.*, 2023). Pathogenic variant in *CFH* cluster at the C-terminus in CCP19-20 affecting the cell surface binding (Kavanagh;Goodship and Richards, 2013; Brocklebank *et al.*, 2023). In addition to point mutations in *CFH*, the region of the genome in which *CFH* resides is particularly susceptible to genomic rearrangement events (4.2). These genomic rearrangement events result in disruption of the C terminus and therefore have similarly outcomes to the *CFH* variants (15% five-year ESRD free survival).

CFI and *C3* variants have had historically poor outcomes similar to *CFH* variants (5 year ESKD free survival of 17 and 21%, respectively). Whilst *CD46* variants were associated with the lowest chance of disease progression (84.75% five-year ESKD free survival) (Brocklebank *et al.*, 2023). In addition to pathogenic genetic variants, there are patients with autoantibodies directed against CFH (FHAA), these are associated with a five-year ESKD risk of 75% (Brocklebank *et al.*, 2017; Brocklebank *et al.*, 2023)

1.3.4. Anti-complement therapy in aHUS

Eculizumab (Alexion, USA) is a recombinant humanised monoclonal $IgG_{2/4k}$ antibody that binds to C5 and inhibits the activation of terminal complement pathway, preventing the formation of MAC. Eculizumab has transformed the outlook for patients with C-aHUS, consistently demonstrating life-changing benefit for patients with C-aHUS (Legendre *et al.*, 2013; Licht *et al.*, 2015; Greenbaum *et al.*, 2016; Menne *et al.*, 2019). Eculizumab effectively blocks the conversion of C5 to C5a and C5b, with the effect of preventing the formation of MAC, which appears to be the pathogenic process in C-aHUS (Figure 1-4). Patients treated with eculizumab are at 1000-2000 times increased risk of *Neisseria meningitidis,* underpinning the important role of complement in preventing infection (Struijk *et al.*, 2013; McNamara *et al.*, 2017). Current practice in England is to ensure patients treated with eculizumab are vaccinated with both the meningitis ACWY and B vaccines, additionally patients are treated with prophylactic penicillin to reduce the risk. Recently a modified version of eculizumab, Ravulizumab (Alexion, USA), has been developed that allows for extended dosage interval, this is has been shown to be efficacious for patients with C-aHUS (Rondeau *et al.*, 2020; Tanaka *et al.*, 2021).

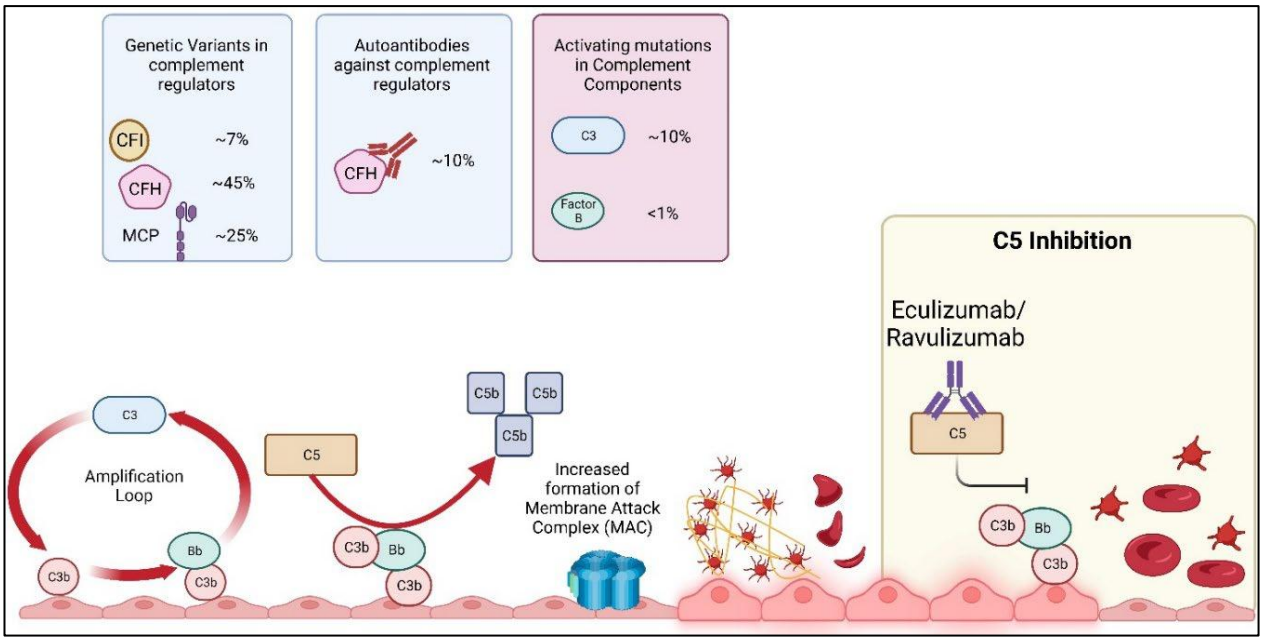

Figure 1-4: Complement dysregulation in C-aHUS and the role of anti-C5 antibodies.

Genetic variants in complement regulators, autoantibodies against CFH or activating variants in complement components (Approximate percentages of variants identified in C-aHUS given), result in unchecked complement activation on the cell surface. This ultimately leads to an increase in conversion of C5 toC5a and C5b, which leads to increased deposition of the MAC on the cell surface and endothelial cell activation and thrombus formation. Treatment with C5 inhibition blocks the conversion of C5 to C5a and C5b, preventing endothelial activation and restoring the endothelium to its normal state.

1.3.5. The role of complement in STEC-HUS

The similarity between C-aHUS and STEC-HUS pathology raises the question of whether complement activation participates in STEC-HUS. There is evidence to suggest that patients with STEC-HUS have complement activation (Figure 1-2) as measured by higher plasma levels of the alternative complement activation products, C3b, C3c, C3d, CFB, C5 convertase and soluble C5b-9 (Thurman *et al.*, 2009; Morigi *et al.*, 2011; Ferraris *et al.*, 2015; Westra *et al.*, 2017). Additionally there is evidence of complement containing microvesicles in affected patients (Stahl;Sartz and Karpman, 2011; Arvidsson *et al.*, 2015). This data suggests that complement is activated in patients with STEC-HUS; however, complement activation is frequently seen in patients presenting with infections, most notably in

recent history with COVID-19 (Holter *et al.*, 2020; Java *et al.*, 2020; Noris;Benigni and Remuzzi, 2020). A direct implication for the role of complement in the pathogenesis of STEC-HUS comes from the finding that incubation of Stx. (at levels higher than found in patients) with normal human serum results in increased levels of soluble C5b-C9, via activation of the AP (Orth *et al.*, 2009). In the same study Stx2 was demonstrated to bind to CFH, CCPs 6–8 and 18–20, the regions responsible for binding GAGs in the eye and kidney respectively (Kavanagh *et al.*, 2013). This results in decreased cell surface binding, with preserved fluid phase regulation. P-Selectin (CD62P) is a cell adhesion molecule that is found on the surface of endothelial and activated platelets, it is responsible for recruitment of platelets to the site of vascular injury and induction of thrombus formation (André, 2004). P-Selectin levels have been found to be increased in patients with STEC-HUS (Kamitsuji *et al.*, 1999) and Stx2 has been shown to significantly upregulate P-selectin in human microvascular endothelial cells (HMEC-1) (Ferraris *et al.*, 2015). This increased P-selectin has been shown to bind and activate circulating C3 resulting in greater thrombus burden, the use of a P-selectin antibody reduced both the C3 deposition and thrombus burden in this HMEC-1 model, suggesting a role for P-selectin in activating complement in response to Stx.

1.3.6. Eculizumab in STEC-HUS

Until very recently the only available data on eculizumab efficacy came from small cases series and uncontrolled observational data. For example, the first reported use of eculizumab in STEC-HUS was published (Lapeyraque *et al.*, 2011) in which three young children with STEC-HUS, complicated by dialysis-dependent AKI and severe neurological involvement, were treated with eculizumab. All three patients showed dramatic improvement in their neurological symptoms within 24 hours of

the first dose and normalisation of their haematological parameters within 5 days. On the basis of this report eculizumab was used in the large outbreak of STEC O104 in 2011 (Buchholz *et al.*, 2011). Eculizumab was used in a non-blinded open-label fashion in patients with the most severe disease, AKI stage 3, neurological involvement, or thromboembolic events. No benefit of eculizumab over best supportive care or plasma exchange was found even after adjustment for potential confounding factors (Menne *et al.*, 2012). Recently the first randomised controlled trial of eculizumab in STEC-HUS was published (Garnier *et al.*, 2023), in which 100 children were randomised to either eculizumab or placebo (50 to each group). This study failed to achieve the primary endpoint of dialysis discontinuation at 48 hours, however there was a significant difference in the percentage of patients with renal sequelae at 1 year (20/50 in the eculizumab group vs. 29/50 in the placebo group). As with the other studies described above (1.2.6) one of the essential inclusion criteria was eGFR<75ml/min/1.73m^2 i.e. patients were required to have established AKI, prior to enrolment. This resulted in a median eGFR at enrolment of 15.2 ml/min/1.73m^2 and 29 patients were receiving renal replacement therapy. Additionally, only 54.3% and 42.1% of children had therapeutic complement blockade (as measured by CH50) at day 7 and 21 respectively. Whilst this study is one of the first studies to show any positive intervention in STEC-HUS, it appears that treatment may have been commenced too late in the disease timeline, at a time when renal injury is established meaning that is difficult to conclude definitively the effects of C5 inhibition in STEC-HUS. Ultimately to answer this question pre-clinical models of disease will be required.

1.4. Animal models of HUS

1.4.1. STEC-HUS

1.4.1.1. Rodent models

Rodent models of STEC-HUS have so far failed to recapitulate the HUS phenotype (Richards and Kavanagh, 2009). Mouse models have be based on administering either *E.coli* O157:H7 orally (Eaton *et al.*, 2017) or purified Stx. parenterally (Tesh *et al.*, 1993). Whilst these mice develop evidence of renal dysfunction, this is in the form of tubular necrosis. The failure to recapitulate TMA in these mice is felt to be due to the distribution of the Gb_3 receptor in mice, which is predominantly tubular and absent within the glomerulus (Tesh *et al.*, 1993; Morace *et al.*, 2019).

1.4.1.2. Non-rodent models

“Alabama Rot” or Cutaneous and Renal Glomerular Vasculopathy is a naturally occurring model of HUS that was first recognised at a greyhound race track in Alabama. Racing greyhounds were fed raw meat from rendering plants which commonly contains pathogenic *E.coli*. Whilst reported in the UK, the cause of this is currently unknown (Stevens *et al.*, 2018). TMA has been seen in Baboons given IV Stx. (Taylor *et al.*, 1999), however, given the expense and complexity of maintaining non-human primate colonies this is not a practical model for widespread research in HUS. Currently there are no animal models that have widespread utility for examining STEC-HUS.

1.4.2. Complement mediated HUS

1.4.2.1. $Cfh^{\Delta 16\text{-}20}$

There have been several mouse models of C-aHUS, the first model was described in 2007 (Pickering *et al.*, 2007). In this model a stop codon was introduced at the

beginning of CCP16, resulting in mice that expressed this truncated $Cfh^{\Delta 16\text{-}20}$. As previously highlight (1.3.2.2) the N-terminus CCPs are responsible for cell surface binding, and are enriched in aHUS (Kavanagh *et al.*, 2013). These mice developed red cell fragmentation, thrombocytopenia, and renal failure i.e., TMA, spontaneously. Unfortunately, this model is no longer available.

1.4.2.2. Cfh^{W1206R}

A mouse model containing a point mutation identified in patients with aHUS, *Cfh* W1206R (W1183R in humans) has been developed (Ueda *et al.*, 2017). The W1206R variant resides in the C-terminus of CFH, therefore preventing cell surface binding, but as predicted this mouse has normal plasma complement regulation. This mouse has been shown to develop features of TMA in the kidney with systemic thrombophilia, in the liver, lung, spleen, kidney, and brain (in the form of thrombotic strokes), features that are not seen in C-aHUS. Further work on these mice has demonstrated that these macrovascular changes can be ablated by a C5a Receptor deficiency (C5aR1), without effect on the renal TMA. Conversely, C6 or C9 deficiency results in improvement in renal TMA, without an effect on the macrovascular phenotype (Ueda *et al.*, 2019). Suggesting that TMA, in this model at least, is mediated through MAC formation, rather than C5a signalling.

1.4.2.3. $C3^{D1115N}$

The $C3^{D1115N}$ model, originally developed in Newcastle and used as the mouse model of aHUS in this study, contains a point mutation in C3 that has been identified in patients with C-aHUS (Smith-Jackson *et al.*, 2019). This model represents the most accurate model of non-human C-aHUS developed. The C3 point mutation introduced into the mouse results in a “Gain of Function” variant, this variant binds CFH with lower affinity than wild type CFH, resulting in a reduced ability to regulate

complement. C3b^{D1115N} deposited on the cell surface results in resistance to CFH mediated inactivation, therefore resulting in complement dysregulation. This model has been shown to result in TMA through terminal complement activation, the TMA in this model was prevented by therapeutic and genetic C5 blockade, using BB5.1 (C5 specific monoclonal antibody, an orthologue of eculizumab) and C5 knockout, respectively.

Interestingly, the *Cfh*^{W1206R},*Cfh*$^{\Delta 16\text{-}20}$ and *C3*^{D1115N} models all require the transgene in homozygosity, despite the human variants being found in heterozygosity. The reason for this is not entirely clear, however is likely due to differences in complement regulators in mice compared to humans, such as the presence of Crry in mice.

1.5. Eculizumab non-responsive TMA

Whilst the outlook for C-aHUS has been transformed by the introduction of anti-C5 therapy. There are a group of patients that demonstrate variable respond to eculizumab or show no response at all (Palma *et al.*, 2021). This group includes patients with C-aHUS, who present at a late stage of disease (Brocklebank *et al.*, 2023), and patients with eculizumab resistance due to a C5 polymorphism that alters the eculizumab binding site (Nishimura *et al.*, 2014). In addition, this group includes patients with genetic variants in non-complement genes.

1.5.1. DGKE

Diacylglycerol kinase epsilon (DGKε) is a ubiquitously expressed lipid kinase that converts diacylglycerol to phosphatidic acid as part of the phosphatidylinositol cycle (Lemaire *et al.*, 2013). This increase in intracellular diacylglycerol results in downstream effects through activation of protein kinase C that ultimately results in

changes in vascular tone (Khalil, 2013), release of prothrombotic factors and platelet activation (Lemaire *et al.*, 2013). Autosomal recessive variants in *DGKε* in patients who develop TMA were first reported in 2013 (Lemaire *et al.*, 2013). A long-term outcome study performed in the NRCTC of patients with *DGKε* mediated TMA revealed an estimated incidence of 0.009/million/year. Unlike C-aHUS, patients do not respond to eculizumab (Brocklebank *et al.*, 2020). *DGKε* mediated TMA is also associated with childhood presentation and significant persistent proteinuria. The prognosis of DGKε mediated TMA is favourable compared to C-aHUS, in the long-term outcomes study from the NRCTC 2/14 patients developed ESKD and one of these was successfully transplanted without relapse.

A mouse model of *DGKε* mediated TMA recapitulated the TMA phenotype by using a *Dgkε*$^{fl/fl}$ mouse crossed with an endothelial specific cre promoter, Tie2^{Cre} (Liu *et al.*, 2021). This mouse developed TMA due to defective vascular endothelial growth factor 2 (VEGF2) production that led to reduced induction of cyclooxygenase 2 and production of prostaglandin E2 (PGE_2). Interestingly this mouse phenotype was rescued with a PGE_2 analogue.

1.5.2. MMACHC

Autosomal recessive variants in Methylmalonic aciduria and homocystinuria type C (*MMACHC*) are the most common inherited disorder in vitamin B_{12} metabolism with an incidence of approximately 1/100,000 live births (Weisfeld-Adams *et al.*, 2010). Variants in *MMACHC* result in defective cobalamin C (CblC) protein. CblC is a member of the intracellular vitamin B_{12} complementation group, which is responsible for the intracellular metabolism of vitamin B_{12}. Specifically, CblC is essential for the production of 2 coenzymes adenosylcobalamin (AdoCbl) and methylcobalamin (MeCbl) (Gravel *et al.*, 1975). MeCbl converts homocysteine to methionine. Whilst

AdoCbl converts L-methylmalonyl-CoA to succinyl-CoA. In CblC deficiency failure to produce AboCbl and MeCbl results in increased methylmalonic acid (MMA), homocysteine, and decreased methionine.

CblC deficiency results in a multi-system disorder that compromises, hematologic involvement megaloblastic anaemia, MAHA and thrombocytopenia, neurological involvement including developmental delay, microcephaly, hypotonia, seizures, macrocephaly, and dementia; myelopathy, metabolic acidosis, and ophthalmological involvement with pigmentary retinopathy, decreased visual acuity, and nystagmus (Lerner-Ellis *et al.*, 2009).

HUS in CblC deficiency presents in infancy (Beck *et al.*, 2017), with few cases reported in older children and young adults (Cornec-Le Gall *et al.*, 2014). Without treatment, the prognosis is poor, however treatment with hydroxycobalamin and betaine results in stabilisation of the kidney function (Beck *et al.*, 2017). Currently the exact mechanism is unclear; however, there is some evidence that increased homocysteine results in endothelial dysfunction that may explain the phenotype (Carrillo-Carrasco and Venditti, 2012).

1.5.3. INF2

Pathogenic variants in Inverted formin-2 (INF2) are the most common inherited form autosomal dominant form of focal segmental glomerulosclerosis (FSGS) (Brown *et al.*, 2010; Boyer *et al.*, 2011a; Gbadegesin *et al.*, 2012), additionally *INF2* is associated with the neurological condition Charcot-Marie Tooth (CMT) (Boyer *et al.*, 2011b). Two families have been identified in the NRCTC cohort that develop TMA with pathogenic variants in *INF2* (Challis *et al.*, 2017). INF2 is a ubiquitously expressed formin protein that is responsible for actin polymerisation

/depolymerisation. Functional analysis of pathogenic variants in INF2 are linked to disordered cytoskeletal organisation (Brown *et al.*, 2010; Boyer *et al.*, 2011a), which may explain the FSGS in these patients. It is currently unclear whether the TMA phenotype is a direct effect of INF2, or secondary to FSGS as TMA has been associated with other causes of FSGS (Siegler *et al.*, 1989).

1.5.4. G6PD

Glucose-6-phosphate dehydrogenase (G6PD) deficiency has been identified as a mimic of HUS in a small number of patients presenting clinically with HUS (Walsh *et al.*, 2018) within the NRCTC cohort. This presents following oxidative stress (secondary to infection, and/or medications) with profound non-immune haemolysis, moderate thrombocytopenia, and acute kidney injury. G6PD deficiency is an X-linked recessive disorder that results in reduced nicotinamide adenine dinucleotide phosphate (NADPH) in cells, In anucleated cells (platelets and erythrocytes) there is no alternative pathway for NADPH production, therefore resulting there is increased production of free radical damage and reactive Oxygen species formation, this ultimately results in destruction of these cells. In mild variants, this results in shortened erythrocyte lifespan and increased haemolysis following oxidative stress, for example secondary to medications, infection and consumption of Fava beans. In patients with variants that result in severely suppressed G6PD levels there is chronic non-spherocytic haemolytic anaemia, which leads to platelet destruction, and thrombocytopenia as the residual G6PD activity is too low to maintain the redox state, even in younger cells. Following exposure to oxidative stress these patients experience profound haemolytic anaemia and thrombocytopenia, they may also develop AKI secondary to haem-mediated damage within the glomeruli.

1.6. Secondary TMAs

1.6.1. Thrombotic Thrombocytopenic Purpura

Thrombotic thrombocytopenic purpura (TTP) is the name given to TMA occurring secondary to ADAMTS13 deficiency (<10% of normal) (Page *et al.*, 2017; Chiasakul and Cuker, 2018). TTP is a rare form of TMA (2/1,000,000 people/year) (Page *et al.*, 2017) and is characterised by MAHA and thrombocytopenia, in contrast to C-aHUS renal failure is not universal, and neurological involvement, and fevers are common. Historically, TTP was defined as a classic pentad of MAHA, thrombocytopenia, renal involvement, fevers and neurological involvement, however this is found in fewer than 10% of patients at presentation (Page *et al.*, 2017). Since the introduction of plasmapheresis in the management of TTP the mortality rate has improved substantially, from approximately 90% (Phillips *et al.*, 2016) to 10% acutely in the UK (Scully *et al.*, 2008). ADAMTS13 is a metalloprotease enzyme that cleaves von Willebrand factor (vWf) (Sonneveld;de Maat and Leebeek, 2014). The pathogenesis of TTP occurs due to the formation of ultra large VWF multimers in the absence of ADAMTS13. This ultimately results in platelet aggregation and thrombus formation. TTP may be either acquired, due to autoantibodies against ADAMTS13, or congenital due to pathogenic variants in *ADAMTS13.* Recently, Caplacizumab has been introduced in the treatment of acute acquired TTP in combination with plasma exchange and immunosuppression (Hughes *et al.*, 2021).

1.6.2. Streptococcal Pneumoniae HUS

Streptococcal Pneumoniae HUS (p-HUS) is a rare complication of invasive *S.pneumoniae.* Acute mortality from p-HUS ~10%, however the majority of deaths occur in patients with *S.pneumoniae* meningitis (Copelovitch and Kaplan, 2008).

S.pneumoniae secretes neuraminidase, which is results in desialylation of glycoproteins on the surface of red blood cells, platelets, and endothelial cells, this is hypothesised to prevent CFH binding to the cell surface (Blaum *et al.*, 2015). This reveals a cryptic antigen, the Thomsen-Friedenreich antigen, this antigen reacts with circulating IgM resulting in HUS.

1.6.3. Pregnancy associated TMA

There is a peak in presentation with C-aHUS in women of child-bearing age. During pregnancy there are significant changes to the physiological complement profile, which may explain this peak in presentation (Smith-Jackson and Harrison, 2023). The frequency of complement variants, severity outcomes and response to treatment of pregnancy associated TMA are similar to that of C-aHUS (Bruel *et al.*, 2017)

1.6.4. Transplant associated TMA

TMA can occur in the setting of solid organ transplantation (Ponticelli and Banfi, 2006; Verbiest *et al.*, 2014). The underlying mechanism for this is not clear, with a multifactorial nature with ischaemia/reperfusion injury, immunosuppressive drugs, antibody mediated rejection and viral infection all causing endothelial stress that can result in TMA. Patients with C-aHUS who undergo transplantation were traditionally at high risk of relapse, with the exception of patients with *MCP* variants, due to the local production of *MCP* on the endothelial surface. The introduction of prophylactic eculizumab has enabled patients with C-aHUS, in whom recurrence of aHUS occurred in one third of patients, to undergo successful transplantation, with one year graft survival of 94%(Glover *et al.*, 2022).

1.6.5. Bone marrow transplant associated TMA

Multi-system TMA has been reported after bone marrow transplantation, this is associated with a poor prognosis. Unlike C-aHUS there is a high proportion of patients that present with serositis, particularly with pericarditis. There are reports of improved outcomes with anti-complement therapy (Jodele *et al.*, 2013; Jodele *et al.*, 2014a; Jodele *et al.*, 2014b; Elfeky *et al.*, 2020), but as yet there are no randomised control trials available. Similarly, to solid organ transplantation this is likely to be multifactorial in nature. Genetic screening of patients with Post bone marrow TMA has revealed only a small number of patients with variants in complement regulatory proteins (2/25) (Elfeky *et al.*, 2020).

1.6.6. TMA associated with autoimmune disease

TMA can occur in association with Systemic Lupus Erythematous (SLE), catastrophic antiphospholipid syndrome and Scleroderma renal crisis (SRC). The mechanisms behind the development of TMA in these conditions is unclear.

SRC occurs in up to 15% of patients with Systemic Sclerosis (SSc) (Woodworth et al., 2016), despite dramatic improvements in outcomes with the introduction of Angiotensin converting enzyme inhibition; the prognosis remains poor with an estimated mortality of 31 - 50%; whilst dialysis is required in 25-40% of survivors (Penn et al., 2007; Bussone et al., 2011; Hudson et al., 2014). Autoantibody production is a cardinal feature of SSc (van den Hoogen et al., 2013), with specific antibodies predictive of disease phenotype, for example anti-topoisomerase I are associated with diffuse SSc and anti-centromere with limited cutaneous sclerosis. Anti-RNA Polymerase III (Anti-RNAPIII) antibodies are found in up to 60% of patients with SRC (Penn et al., 2007; MEYER et al., 2010; Hudson et al., 2014), however whether these antibodies are pathogenic or an epiphenomenon is unclear

(Fritzler and Choi, 2016). Purified IgG from patients with anti-RNAPIII antibodies inhibit the RNA polymerase III ability to transcribe DNA in vitro (Kuwana et al., 1993). Anti-RNAPIII have been found to be detectable years before the clinical manifestations of SSc, with a rapid rise short before patients develop SRC (Burbelo et al., 2019), indicating that the rapid rise in antibody may result in direct damage to the kidney resulting in TMA. A potential link between RNA Polymerase III and TMA is explored later (4.5.3).

1.6.7. Drug induced TMA

TMA has been associated with a more than 75 drugs reviewed in (Al-Nouri *et al.*, 2015), with very few mechanistic studies ascribing a cause in this group. For the majority of cases withdrawal of the offending drug results in resolution of the TMA.

1.6.8. Interferon-mediated TMA

TMA has been described as a rare complication of treatment with interferon-β for multiple sclerosis (Hunt *et al.*, 2014). Patients with interferon induced TMA present following years of uneventful management, at presentation patients show evidence of severe hypertension in addition to TMA, management of interferon induced TMA is principally withdrawal of interferon-β. A mouse model that overexpresses interferon, restricted to the brain, has been developed (Kavanagh *et al.*, 2016), which demonstrates TMA-like lesions in the brain vasculature at 2-3 months of age. Together these data suggest that chronic interferon exposure to the endothelium results in TMA. The mechanism underlying this is currently unclear.

1.7. Summary

HUS describes a heterogeneous group of disorders that share a histological legion i.e. TMA, the introduction of anti-complement therapy has revolutionised the

management of C-aHUS. There are still questions about how eculizumab will affect the disease course of other forms of HUS (e.g. STEC-HUS). However, it is evident that some forms of inherited and acquired forms of TMA that are eculizumab non-responsive e.g. TTP, SRC, as well as *DGKε, MMACHC and INF2* have alternative pathological processes.

2. Aims of this Project

1. The first aim of this project was to review the NRCTC cohort of aHUS patients to describe the current cohort of complement genetics in this cohort.
2. The second aim was to identify novel eculizumab non-responsive genetic causes of TMA.

3. Methods

3.1. Diagnostic testing

Genetic analysis of the NRCTC cohort was performed in collaboration with the NHS clinical genetics service based at the Centre for Life (Newcastle, UK), this included Sanger sequencing, Multiplex ligation-dependent probe amplification (MLPA) and Factor H autoantibody screening.

3.1.1. Sanger sequencing of HUS associated gene

Sanger sequencing of coding exons of C-aHUS associated genes *CFH, CFI, CD46, C3, CFB* and the *C5* polymorphisms that result in Eculizumab non-responds was performed. Non-complement responsive genes *DGKE* and *MMACHC* were also tested.

3.1.2. MLPA of HUS-associated genes

MLPA was utilised to determine copy number variant (CNV) of CFH and CFHRs. MLPA was performed by the clinical laboratory, following manufacturer's instruction at the Centre for Life (Newcastle, UK) utilising the MLPA probe mix P236-B1 and P296 (MRC Holland). MLPA allows the copy number of multiple genomic regions to be determine in a single reaction (Figure). Briefly, sample DNA was denatured at 95°C and probes hybridised to the DNA at 60°C overnight. For each target site a right and left probe anneal, both probes are required to allow ligation to proceed. The right and left probes contain the complementary sequence to allow hybridisation, a common PCR primer sequence that is shared with all probes (to allow a single primer to be used to amplify all probes) and a stuffer sequence of varied lengths (this generates amplicons of unique sizes that are separated by capillary electrophoresis). Following hybridisation, a ligation step is performed, DNA

ligase is added to the reaction and incubated at 54°C for 15 minutes to generate a single probe from the left and right probes, the DNA ligase is inactivated by heating to 98°C for 5 minutes. This stage of the reaction generates ligated probes of varied lengths from multiple targets within the genome. PCR amplification is performed with a common fluorescently tagged PCR primer (35 cycles [95°C 30 seconds, 60°C 30 seconds, 72°C 60 seconds], 72°C 20 minutes). Following amplification the amplicons are separated by capillary electrophoresis to determine relative abundance of each probe. The results of this were subsequently analysed using Coffalyser.Net. Ultimately this generated a relative abundance of each probe compared to known reference probes within the mix. This data can be used to calculate CNV of each probe.

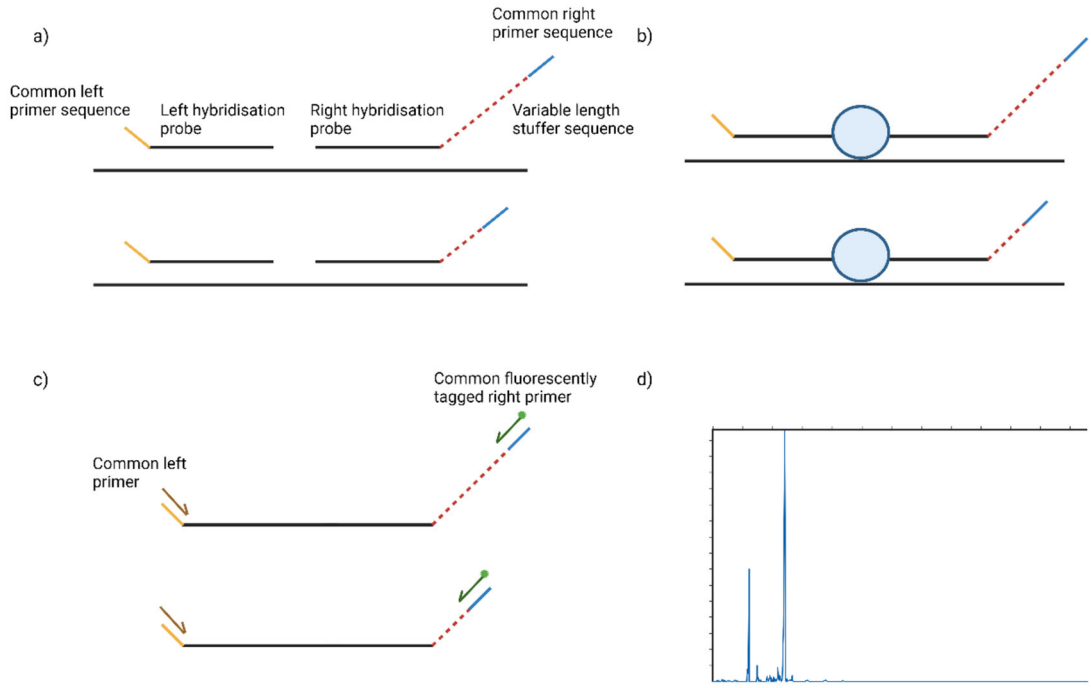

Figure 3-1: MLPA Workflow

a) Probe mix containing sequence specific probes, each probe pair contains a sequence specific hybridisation region, a variable length stuffer sequence and common primer sequences. This design

later generates probes of various sizes containing common primer sequences, which allows amplification of all amplicons using a single sequencing primer, during the hybridisation stage the sequence specific probes bind to the complementary region in the genomic DNA. b) The addition of DNA ligase generates single probes from the probe pair. c) PCR amplification using the common primers generates amplicons of unique sizes, the addition of a fluorescently labelled primer enables separation by capillary electrophoresis d) capillary electrophoresis is used to separate the amplicons, which can be subsequently analysed to determine CNV

3.1.3. Factor H antibody screening

Factor H (FH) antibody screening was performed by Enzyme linked immunosorbent assay (ELISA) as previously described (Watson *et al.*, 2014). Briefly, Maxisorb ELISA plate (Thermofisher) were coated with 50µl of 5µg/ml FH (Comptech, USA) in dPBS per well, control wells without FH were prepared in tandem. These plates were incubated overnight at 4°C. Following incubation, the wells were aspirated and washed with 200µl PBS/Tween 0.1% (PBS-T) three times. 200µl PBS-T was added to each well on plate and incubated at room temperature for one hour. Test sera and negative control (pooled sera) was prepared in triplicated at 1/50 concentration in PBS-T. The positive control was prepared at 1/25. PBS-T was then aspirated from plates and washed with 200 µl PBS-T. 50µl of serum was added per well on both FH coated and control plate and incubated at room temperature for one hour. The plates were then washed three times with PBS-T; followed by 50µl of Goat anti-human IgG Fcγ specific-horseradish peroxidase (HRP) at 1/20,000 in PBS-T (Stratech Scientific) for one hour at room temperature. A final wash step with PBS-T was performed three times. 50µl of 3,3',5,5' tetramethylbenzidine (TMB) (Universal Biologics, UK) was added for 5 min at room temperature. To stop the reaction 50µl of 10% Sulphuric acid was added to each well. Absorbance was read at 450nm using EL-800 plate reader (Biotek, UK). Triplicate samples were averaged

and background subtracted using the corresponding control plate sample. Samples were standardised to an Optical density was 1.6 at 450nm for the positive sample. To generate the Relative Units (RU) a standard curve was generated using the positive value of 1.6 (GraphPad prism). A value of >100RU/ml was considered positive (Brocklebank *et al*., 2017).

3.2. Whole exome sequencing

Whole exome sequencing had previously been performed in selected patients and families with a diagnosis of aHUS. Briefly, DNA was sent to AROS AB and GATC Biotech. Three exome enrichment kits were used, TruSeq exome enrichment kit (Illumina), Nextera Rapid Capture Exome kit 37Mb (Illumina) and SureSelect^{XT} Human all exon V5 (Agilent). The resultant data was subsequently analysed using our bioinformatics pipeline

3.2.1. Bioinformatics pipeline and analysis

The sequencing reads were analysed using the following workflow to generate a list of variants per family or case. I then performed analysis of the candidate genes for evidence of pathogenicity utilising *in silico* analysis programs, including Polyphen-2, Mutation Taster, Functional Analysis through Hidden Markov Models (FATHMM), and Mutation Assessor. This process identified genetic variants in novel genes.

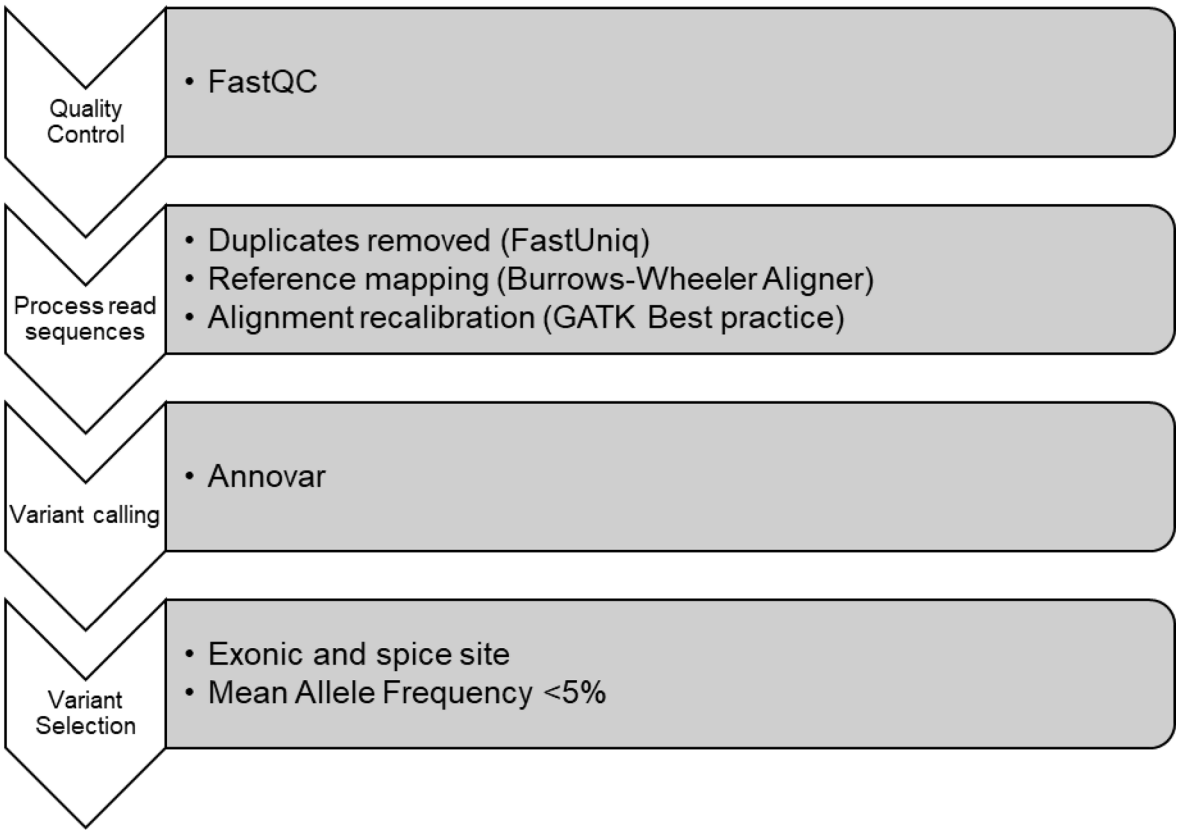

Figure 3-2: Bioinformatics pipeline workflow used to generate the list of candidate genes

3.3. Mouse methods

3.3.1. Mouse housing

Mice were housed within the Comparative Biology Centre (Newcastle University, UK). Mice were caged in individually ventilated cages; and were provided standard chow food and water ad libitum. Additionally, experimental mice, following treatment with tamoxifen, were given a soaked diet, to increase fluid intake and reduce the risk of AKI secondary to dehydration. A standard 12-hour light/dark reverse cycle and an ambient temperature of 21 ± 1ºC was maintained. The wellbeing of mice was monitored daily, and clinical scoring of mice were performed, as previously developed within the complement therapeutics group (daily following treatment with tamoxifen; this scoring system assigns value between 0 (least severe) and 3 (most severe) on a number of observable parameters indicative of ill health; weight loss, piloerection, decreased activity, movement impairment, and respiratory rate. The score for all of these parameters were summated and any mouse with a clinical score greater than 15 was promptly euthanised to avoid any unnecessary suffering. All mice were euthanized either by cervical dislocation, exposure to increasing levels of Carbon Dioxide or terminal exsanguination via cardiac puncture, performed under deep anaesthetic with Isoflurane, with a secondary method to confirm cessation of life.

3.3.2. Mouse strains

3.3.2.1. *Exosc3 inducible conditional mouse*

The Exosc3 conditional mouse model, Exosc3$^{tm1.1Uba}$, was a kind gift from Professor Basu (Columbia University, New York) (Pefanis *et al.*, 2015b). Mice were originally derived on a C57BL/6/Tec background. This model contains a Conditional by Inversion (COIN) module. This module contains an inverted sequence of enhanced

Green fluorescence protein (GFP), preceded by a 3′ splice site (3′SSPI) and followed by a polyadenylation region (pA). To enable inversion by Cre recombinase, the COIN module is flanked by LoxP and Lox2372 sites in a head-to-head orientation. To achieve temporospatial control of Exosc3 knock-out these mice have been crossed with Cre-expressing lines, this allows inversion of the floxed allele.

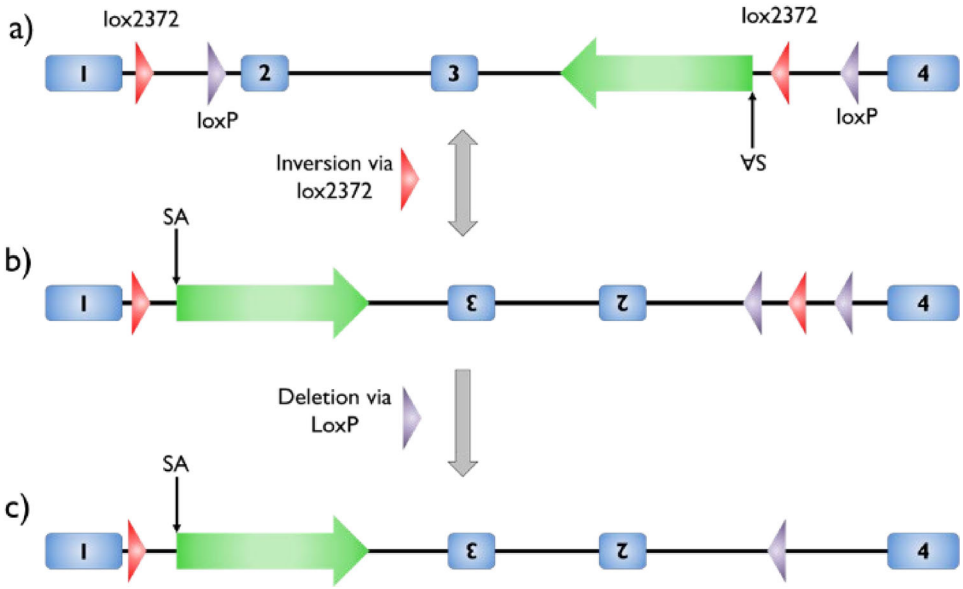

Figure 3-3: Schematic view of Exosc3 COIN allele (Exosc3^{fl})

Exon 2 and 3 and inverted eGFP cassette floxed with Lox2372 and LoxP sites. a. Prior to cre-recombination, resulting in normal expression of Exosc3 with no GFP expression, Lox sites in head-to-head orientation. b) Following cre mediated inversion of floxed region between Lox2372 sites resulting in inversion of exon 2-3 with GFP cassette in normal orientation and therefore GFP expression, Lox2372 sites remain in head-to-head orientation, with LoxP sites in head-to-tail orientation. c) Final orientation following recombination event resulting in deletion of Floxed region between LoxP sites leading to abrogation of lox2372 site and therefore irreversibility of recombination. Adapted from (Economides et al., 2013b)

3.3.2.2. ROSA26Cre^{ERT2} mouse

To allow temporospatial control of Exosc3 knock-out mice were bred with mice containing Tamoxifen sensitive Cre recombinase. To allow whole body cre-

expression the B6.129-Gt(ROSA)26Sortm1(cre/ERT2)Tyj/J (Rosa26Cre^{ERT2}) was purchased from Jackson Laboratory (Maine, USA).

3.3.2.3. Tie2Cre^{ERT2} mouse

To restrict Cre expression to the endothelium The B6.Cg-Tg(Tek-cre/ERT2)1Arnd/ArndCnrm (Tie2Cre^{ERT2}) mice were used; these mice have previously been shown to have cre-expression restricted to the endothelium in adult mice (Forde *et al.*, 2002). B6.Cg-Tg(Tek-cre/ERT2)1Arnd/ArndCnrm were purchased from The European Mouse Mutant Archive (München, Germany).

3.3.2.4. Ifnar mouse

To investigate the effects of interferon on this phenotype a type 1 interferon receptor (Ifnar) knock out model was used, B6(Cg)-Ifnar1tm1.1Ees/J (Ifnar$^{-/-}$), these were previously held in the facility and a gift from Dr. Chris Duncan (Newcastle University)

3.3.3. Mouse monitoring

Mouse monitoring was performed using a purpose designed clinical monitoring tool (Smith-Jackson *et al.*, 2019). Mice were weighted daily initially and monitoring adjusted according to severity (e.g. relaxed to every other day after completing treatment and then no observable phenotype developing.) Urinalysis was performed using Multistix 10SG Urinalysis Strips (Siemens).

3.3.4. Mouse nomenclature

Mouse Line	Function	Synonym given
Exosc3tm1.1Uba	Floxed Exosc3 exon 2&3 with antisense GFP	*Exosc3^{fl}* Heterozygous *Exosc3$^{fl/fl}$* Homozygous
B6.129-Gt(ROSA)26Sortm1(cre/ERT2)Tyj/J	Ubiquitous cre expresser (tamoxifen sensitive)	*Rosa26Cre^{ERT2}* Heterozygous Rosa26Cre$^{ERT2/ERT2}$ Homozygous
B6.Cg-Tg(Tek-cre/ERT2)1Arnd/ArndCnrm	Endothelial specific cre expresser (tamoxifen sensitive)	*Tie2Cre^{ERT2}* Heterozygous Tie2Cre$^{ERT2/ERT2}$ Homozygous
B6(Cg)-Ifnar1tm1.1Ees/J	Constitutive type 1 interferon receptor knock-out	*Ifnar^{-}* Heterozygous *Ifnar$^{-/-}$* Homozygous
Exosc3$^{fl/fl}$ x Rosa26Cre^{ERT2}	Exosc3 floxed allele (always maintained in homozygosity) crossed with ubiquitous cre expresser (tamoxifen sensitive), prior to Tamoxifen treatment expresses normal levels of Exosc3	*Exosc3$^{fl/fl}$.Rosa26Cre^{ERT2}* Heterozygous Exosc3$^{fl/fl}$.Rosa26Cre$^{ERT2/ERT2}$ Homozygous
Tamoxifen Treated Exosc3$^{fl/fl}$ x Rosa26Cre^{ERT2}	Following tamoxifen treatment, floxed allele is inverted resulting in inversion of exon 2&3 and sense expression of GFP	Exosc3$^{gfp/gfp}$.Rosa26Cre^{ERT2} Heterozygous (Rosa26CreERT2 allele) Exosc3$^{gfp/gfp}$.Rosa26Cre$^{ERT2/ERT2}$ Homozygous
Exosc3$^{fl/fl}$ x Rosa26Cre$^{ERT2/ERT2}$ x Ifnar$^{-/-}$	Exosc3 floxed allele, crossed with ubiquitous cre expresser (tamoxifen sensitive) crossed with constitutive interferon receptor knock-out	Exosc3$^{fl/fl}$.Rosa26Cre$^{ERT2/ERT2}$ .Ifnar$^{-/-}$
Exosc3$^{fl/fl}$ x Tie2Cre$^{ERT2/ERT2}$	Exosc3 floxed allele crossed with endothelial specific cre expresser (tamoxifen sensitive), prior to Tamoxifen treatment expresses normal levels of Exosc3	Exosc3$^{fl/fl}$.Tie2Cre$^{ERT2/ERT2}$
Tamoxifen Treated Exosc3$^{fl/fl}$ x Tie2Cre$^{ERT2/ERT2}$	Following tamoxifen treatment, floxed allele is inverted resulting in inversion of exon 2&3 and sense expression of GFP in the endothelium	Exosc3$^{gfp/gfp}$.Tie2Cre$^{ERT2/ERT2}$

3.3.5. Clinical monitoring sheet

Mouse health was tracked using the scoring system below

Characteristic	Grading guidance – for use in moderate and severe protocols			
Score	0	1	2	3
Activity	Normal, stands upright, explores, climbs	Active but avoids being upright on hind legs	Inactive, moves around bottom of cage only ([2b])	No activity, only moves when provoked ([3b])
Appearance	Normal, well groomed	Patches of piloerection covering >25 but <50% of body	>50 but less than 75% of back showing piloerection	Mouse appears puffy, >75% piloerection ([3b])
Body condition score (BCS)	3 or 4	Change in BCS ([1a])	2 or 5 ([2b])	1 ([3b])
Body weight change	< 5%	5-12% ([1a])	13-19% ([2b])	>20 < 30% ([3a])
Hydration	Normal skin turgor	Skin folds on back but returns to normal within 2 seconds ([1a])	Skin fold remains > 2 seconds but returns to normal after 5 seconds ([2a])	Skin fold on back remains > 5 seconds or does not resolve ([3b])
Faeces	Normal	Soft, but formed	Soft, wet in appearance ([2c])	Watery, v. loose (diarrhoea) ([3a])
Respiration	Normal rapid mouse breathing	Periods of laboured breathing for 5-10 secs,	Laboured breathing for >10 secs and/or abdominal breathing, no gasping ([2c])	Laboured and/or abdominal breathing with gasps >1s between breaths ([3b])
Proteinuria (mg/dl)	Normal (0-30)	>31	>100 (2c)	>800 ([3b])

Haematuria (Ery/µl)	Normal (0)	>10	>50 (2c)	>100 (3[b])
TOTAL SCORE				

Notes: 1[a] – add soaked diet to cage.

1[b]- treat affected area with green clay or Vetericyn spray twice daily for 3 days and trim nails

2[a]- give subcutaneous fluids, reassess in 1 hour, can be given up to 3 times then consult vet for further advice

2[b] - consult vet – interventions maybe available;

2[c] –increase monitoring or for **moderate protocols refer to 3[b]**

3[a]- if associated with BCS of 2 this finding may require humane killing, consult NAWCO/NVS, and ensure you have checked correct protocol;

3[b]- arrange to humanely kill a.s.a.p.; preferably - Terminal exsanguination via Cardiac Puncture followed by schedule 1 technique.

Guide to cumulative score and suggested outcome – severe protocols
0-6 Continue normal monitoring. 7-11 Examine and rescore daily; treat animals; use soaked diet if not already used. Consult with NACWO/NVS as needed, **particularly if moderate severity study**. ‡12-15 Treat animals ASAP or Consult NACWO/NVS (with view to humane killing). >15 Humanely Kill. **N.B. * compared to baseline evaluation** and please see below for Body conditioning score diagrams

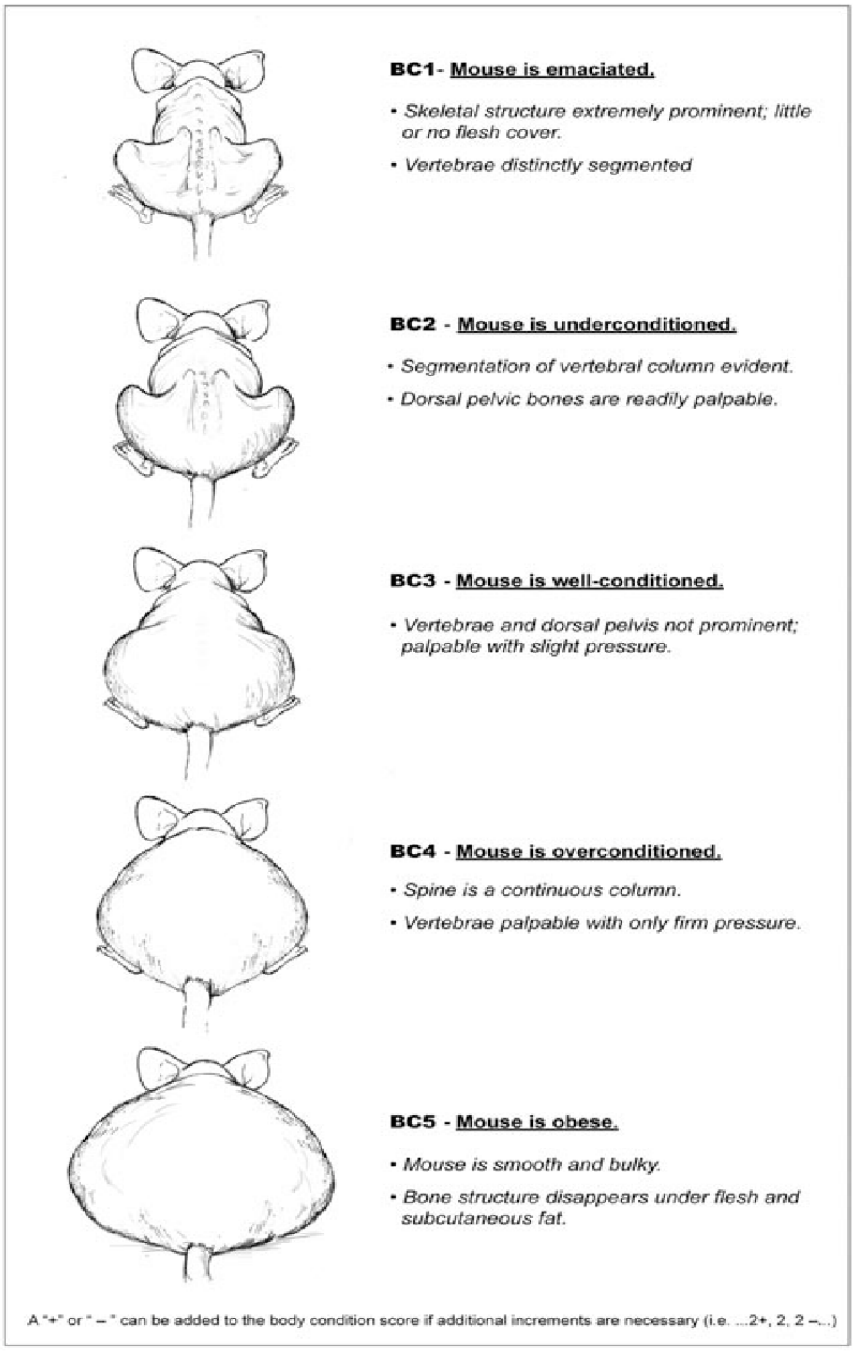

Figure 3-4: Body condition score.

Condition scoring used as part of the clinical scoring system, used to determine overall mouse health. Adapted from (Ullman-Culleré and Foltz, 1999)

3.4. Tamoxifen induction

3.4.1. Intraperitoneal injection

Tamoxifen was administered via intraperitoneal (I.P.) injection to induce recombination in mice containing the Tamoxifen sensitive Cre cassette. Tamoxifen base (Sigma-Aldrich, UK) was dissolved in filter sterilised corn oil (Sigma-Aldrich, UK) at a concentration of 20mg/ml, and incubated in a 55°C water bath for 1-2 hours, with regular agitation, until fully dissolved. This was stored at 4ºC for up to two weeks in the dark. To induce recombination mice were treated with 75mg/Kg dose every 24 hours for four days as standard, some mice received different dosage strategy as described (6.2.3).

3.4.2. Oral route

To enable long-term tamoxifen dosing studies, mice received tamoxifen orally. This was achieved via chow (Envigo, UK) or via oral gavage, to perform this Tamoxifen was dissolved in either corn oil or Kolliphor HS (Sigma, UK) at 10mg/ml. Oral gavage was performed every 24 hours at a dosage of 2mg a day for up to eight weeks.

3.5. Mouse dissection and tissue preservation

3.5.1. Terminal exsanguination

Terminal exsanguination was performed to collect blood at the end of the study. Mice were first anesthetised using isoflurane inhalation. Once mice where under deep anaesthesia, blood was collected via cardiac puncture into heparinised tubes (SARSTEDT, Germany) and placed on ice for downstream processing.

3.5.2. Storage for RNA analysis

Following dissection of organs these were snap frozen in liquid Nitrogen for RNA analysis. Samples were stored at -80°C for downward processing.

3.5.3. Storage for formalin fixation

Samples for histology were fixed in 10% neutral buffered formalin (CellStor, UK)

3.5.4. Storage for electron microscopy

Kidneys were cut in to 2mm cubes and fixed in 2% glutaraldehyde.

3.5.5. Plasma collection

Plasma was isolated from heparinised blood; blood was centrifuged at 1000 x g for 10 minutes at 4°C to separate plasma and cells. Plasma was removed, separated into 50µl aliquots and stored at -80°C.

3.5.6. Histology

Histology was performed on formalin fixed tissue. Haematoxylin and Eosin (H&E) staining was performed by Charles River Labs. Periodic Acid-Schiff (PAS) and Martius Scarlet Blue (MSB) were performed by Newcastle-Upon-Tyne Pathology labs.

3.6. Treatments

3.6.1. Bromodeoxyuridine

To investigate cell cycle dynamics mice were treated with 100mg I.P. bromodeoxyuridine (BrdU, Biolegend). BrdU is a synthetic nucleoside analogue that is incorporated in to dividing cells in place of thymidine, utilising an anti-BrdU antibody this can be used to determine which cells are actively dividing.

3.6.2. Pifithrin-α

Pifithrin-α (PFT-α, Selleckchem) is a p53 antagonist that has been shown to protect mice from irradiation damage (Komarov *et al.*, 1999). PFT-α was made up in sterile conditions (Table 3-1). PFT-α (2.2mg/Kg, I.P.) was administered to mice 24 hours before commencing tamoxifen treatment and then every 48 hours for a maximum of 5 doses (Kuang *et al.*, 2016).

Component	Volume (%)
Dimethyl sulfoxide (DMSO) (Sigma)	5
PEG300 (Sigma)	40
Tween80	5
Double distilled water	50

Table 3-1: PFT-α recipe

3.7. Genotyping

3.7.1. DNA extraction from mouse

3.7.1.1. Sodium Hydroxide boiling for standard PCR

Exosc3COIN, Ifnar and Rosa26Cre^{ERT2} genotyping was performed via conventional Polymerase chain reaction (PCR) using ear punch biopsy following weaning (three weeks onwards). Ear punch biopsies were added to 100µl of lysis buffer (0.1µM Ethylenediaminetetraacetic acid (EDTA), 10mM sodium hydroxide). This was incubated at 95˚C for 30 minutes and stored at -20°C prior to use.

3.7.1.2. DNA Extract All Reagent

To perform Tie2Cre^{ERT2} genotyping, quantitative PCR (qPCR) was used to determine copy number of Cre allele. This was performed using the TaqMan® Sample-to-SNP™ Kit (Thermofisher, UK) following the manufacture's instruction. Ear punch biopsies were added to 50µl of DNA Extract All Lysis reagent and incubated at 95°C for 5 minutes, 50µl of DNA Extract All Stabilisation reagent was then added to halt lysis, and samples were stored at -20 ºC.

3.7.2. Standard PCR

Standard genotyping PCR was performed for Exosc3^{fl}, Ifnar, and Rosa26CreERT2 and Exosc3 genomic recombination alleles. This was performed using Immomix™ (Meridian, UK), amplification was performed on the Bio-Rad thermocycler using conditions in (Table 3-2 &Table 3-3).

PCR Stage	Temperature (ºC)	Time (Seconds)	Cycle number performed
Initialization	95	600	1
Denaturation	95	30	10
Annealing	65 (-0.5 per cycle)	30	
Elongation	72	30	
Denaturation	95	30	28
Annealing	60	30	
Elongation	72	30	
Final Elongation	72	600	1
Storage	12	∞	1

Table 3-2: PCR conditions used for both Exosc3 and Rosa26Cre^{ERT2} alleles.

PCR Stage	Temperature (ºC)	Time (Seconds)	Cycle number performed
Initialization	95	600	1
Denaturation	95	15	37
Annealing	57	15	
Elongation	72	90	
Final Elongation	72	600	1
Storage	12	∞	1

Table 3-3: PCR conditions used for Ifnar allele

Primer Name	Sequence (5'→ 3')
Rosa26Cre Forward	AAGGGAGCTGCAGTGGAGTA
Rosa26Cre Reverse	TCTTGCGAACCTCATCACTC
Rosa26 Cre alternative	CCGAAAATCTGTGGGAAGTC
Exosc3 Forward	GTCCCAGTTGCAATGAGTCC
Exosc3 Reverse	TGGTCCCCTTTCACAGGTAC
Ifnar Forward	GACAATTCAAGTAGCCCTCTGG
Ifnar Reverse	CGTCTGCTGAATGGTCTTAGC
Exosc3 Post-recombination Forward	GACAATTCAAGTAGCCCTCTGG
Exosc3 Post-recombination Reverse	CGTCTGCTGAATGGTCTTAGC

Table 3-4: PCR primers used for conventional PCR (all primers ordered from Integrated DNA technologies (USA))

3.7.3. Visualisation of PCR products on agarose gel

Following PCR reactions amplicons were separated using gel electrophoresis. Agarose gel (0.5 -2%) was made up with Tris-acetate-EDTA (TAE) (stock at 50x, diluted to 1x with water prior to use) and stained with SYBR™ Safe DNA Gel Stain (1:10000) (Thermofisher).

Gels were submerged in TAE in gel running tank, 10µl of PCR product and 5µl of DNA ladder (Generuler 1Kb plus, Thermofisher) was loaded on to gel and electrophoresis was performed for two hours at 100V. Images were captured on the Li-cor Odyssey® FC using the 600nm acquisition channel and analysed using ImageStudio.

Component	Concentration (M)
Tris Base (Sigma)	2
Acetic acid	1
EDTA disodium salt dihydrate	0.05

Table 3-5: 50x TAE recipe

3.8. qPCR

3.8.1. Genotyping for Cre allele

qPCR was used to determine Cre recombinase copy number (i.e., Wild-type, heterozygous and homozygous) in the Tie2Cre^{ERT2} mouse line, using the TaqMan® Sample-to-SNP™ (Thermofisher, UK) Cre genotyping probes had previously been designed by Jackson Laboratory (Protocol 20627) (Table 3-6).

TaqMan® Probe Cre FAM	0.15µM
TaqMan® Probe ApoE SUN™	0.15µM
Primer (Cre F&R, ApoE F&R)	0.4µM
GTXpress™	5µl
Genomic DNA (gDNA)	2µl
RNase/DNase free water	Up to 10µl

Table 3-6 Cre qPCR recipe

All samples were run in duplicate on Quantstudio3 (Applied biosciences) (Table 3-7).

PCR Stage	Temperature (ºC)	Time (Seconds)	Cycle number performed
Initialisation	95	20	1
Denaturation	95	3	40
Anneal/extend & fluorescence measurement	60	20	

Table 3-7: PCR conditions used for Cre allele genotyping PCR

Copy number was determined using CopyCaller® v2.1 (Applied Biosciences) using a known Cre homozygous sample as the reference, ApoE was used as an internal control to allow for quantification.

3.8.2. RNA preparation for RNA-Seq.

Kidneys were isolated from mice and snap frozen in liquid nitrogen, these were then thawed in RNA*later*™-ICE (Ambion) before being sent to QIAGEN for mRNA

sequencing, utilising polyA enrichment using CLC Genomics Workbench (version 12.0.2) and CLC Genomics Server (version 11.0.2). RNA was analysed using QIAGEN Ingenuity Pathway Analysis (IPA).

3.8.3. RT-qPCR

Reverse transcriptase quantitative PCR (RT-qPCR) was performed on samples to investigate changes in expression levels following recombination.

3.8.4. RNA extraction using Trizol

RNA was extracted from tissue snap-frozen in liquid Nitrogen using Trizol (Sigma, UK) as per manufacturer's instructions. 50mg of tissue was added to 500µl of Trizol (Sigma, UK) and homogenised using a handheld tissue homogeniser. This was incubated for 5 minutes at room temperature, 100µl of chloroform (Sigma, UK) was added and then shaken to ensure proper mixing of Trizol and chloroform. Following incubation for 2 minutes the mixture was centrifuged for 15 minutes at 12,000 × g at 4°C. To isolate RNA the aqueous phase was removed and transferred to a fresh microcentrifuge tube. 250µl of isopropanol was added and incubated for 10 minutes at 4°C, followed by centrifuge for 10 minutes at 12,000 × g at 4°C. RNA precipitate formed a white gel-like pellet. The RNA pellet was washed with 500µl of 75% ethanol and centrifuged for 5 minutes at 7500 × g at 4°C. Supernatant was discarded and the RNA pellet was air dried for 10 minutes. Finally, the RNA pellet was re-suspended in RNAse free water (Ambion, UK) and incubated at 55°C for 10 minutes. RNA concentration was determined using Nano-Drop™ spectrometry, using the A260/280 ratio and then stored at -80°C.

3.8.5. DNase treatment

Following isolation of RNA, samples were treated with TURBO DNA-free™ Kit (Thermofisher, UK) to remove residual gDNA.

RNA	10µg diluted in 50µl of RNAse-free water
10X TURBO DNase™ Buffer	5µl
10X TURBO DNase™ Enzyme	1µl

This was incubated at 37°C for 30 minutes. 5µl of DNase Inactivation Reagent was added and incubated for 5 minutes at room temperature. The sample was then centrifuged at 10,000 × g for 1.5 minutes. The supernatant was transferred to a fresh tube and stored at -80ºC.

3.8.6. RT-qPCR

RT-qPCR was used to determine the mRNA levels of specific genes in mice. RNA was generated using Trizol, as described.

RNA was subsequently converted to complementary DNA (cDNA) using SuperScript III First-Strand Synthesis System (Invitrogen, USA) as per manufacturer's instructions.

Total RNA (TurboDNase treated)	1µg
Random Hexamer 50µM (Invitrogen, UK)	1µl
dNTPs (50µM)	1µl
RT-PCR grade PCR water	Up to 13µl

This was heated to 65°C for 5 minutes and then transferred to ice for 1 minute. cDNA was then generated:

5X first-strand buffer	4µl
0.1 M Dithiothreitol (DTT)	1µl
SuperScript™ III Reverse Transcriptase	1µl

This was incubated at 25°C for 5 minutes, followed by incubation at 50°C for 30 minutes, finally the reverse transcriptase was inactivated by heating to 70°C for 15 minutes.

Primers and probe pairs (Universal Probe Library Set; Roche, Switzerland) were designed on the Universal Probe Library Assay Design Centre (Roche, Switzerland). RT-qPCR was performed using TaqMan™ Gene Expression Master Mix (Applied bioscience) (Table 3-8). All samples were run in duplicate on Quantstudio3 (Applied biosciences), using condition in (Table 3-9).

TaqMan™ Gene Expression Master Mix	5µl
cDNA (diluted 1 in 5)	2µl
10µM forward & reverse primers combined.	0.2µl
0.1µL probe (Roche, universal probe library) (FAM)	0.1µl
2.7µL RT-grade water	2.7µl

Table 3-8: RT-qPCR recipe

PCR Stage	Temperature (ºC)	Time (Seconds)	Cycle number performed
Initialisation	95	600	X 1
Denaturation	95	15	X40
Anneal/extend & fluorescence measurement	60	60	

Table 3-9: PCR conditions for RT-qPCR

Ct values were recorded and then analysed using the $2^{-\Delta\Delta}$ CT method described (Livak and Schmittgen, 2001), β-Actin was used as the housekeeper gene to allow normalisation.

3.9. Blood investigations

Mouse biochemistry and haemoglobin from terminal exsanguination was analysed using the iSTAT system (Abbott) using CHEM8+ cartridges. 100µl of blood collected in heparinised blood was analysed using these cartridges.

3.9.1. Blood films

Blood films were performed to investigate for evidence of haemolysis, specifically looking for schistocytes. 2µl of heparinised blood was placed on a slide and a smear generated by using a second slide to push the blood along the slide. This smear was then stained with the Rapi-Diff II Stain (Atom Scientific) according to manufacturer's instruction. Blood films were immersed in Solution A (Thiazine dye in methanol) for five seconds, followed by immersion in Solution B (Eosin Y dye in phosphate buffer) for five seconds, this was rinsed with water and then immersed in Solution C (Polychromed Methylene Blue in phosphate buffer), excessed solution was rinsed with water and blood films imaged.

3.9.2. Reticulocyte counting

Reticulocyte counting was performed using the BD Retic-count (BD Biosciences), which uses Thiazole Orange as an intercalating DNA/RNA dye, therefore binding nucleated reticulocytes, but not mature anucleated erythrocytes. Two samples were required per test, for the background control 5µl of heparinised blood was added to 1ml Dulbecco Phosphate buffered saline (dPBS, Gibco). To calculate the reticulocyte percentage 5µl of heparinised blood was added to 1ml BD Retic-count,

both were incubated at room temperature in the dark for at least 30 minutes and no longer than 3 hours. Data acquisition was subsequently performed using flow cytometry (3.12.2)

3.9.3. Platelet count

Heparinised whole blood was used for platelet analysis. After collection, samples were immediately stored on ice and kept on ice throughout. 10µl of heparinised blood was added to 400µl platelet flow buffer (dPBS containing 5% w/v Bovine Serum Albumin (BSA), 1 mM Ethylenediaminetetraacetic acid (EDTA), 0.1% w/v Sodium azide). 5µl of this was transferred to 200µl staining buffer (platelet flow buffer containing anti-CD41 (1:400). This was incubated in the dark on ice for 30 minutes. Prior to analysis 50µl CountBright™ Plus Absolute Counting Beads were added to allow a platelet count to be performed. Data acquisition was subsequently performed using flow cytometry (3.12.3)

3.9.4. White blood cell count

Heparinised whole blood was used for white cell counting analysis. 50µl of blood was added to a 5mL Round Bottom Polystyrene FACS Tubes (BD Biosciences). 1µl of CD45 (BD Biosciences), CD19 (BD Biosciences), CD3 (Miltenyi Biosciences), and Ly6G (Miltenyi Biosciences) antibodies were added and incubated in the dark for 15 minutes at room temperature. 450µl of red cell lysis fixation buffer (Biolegend) was added and incubated for 20 minutes in the dark at room temperature. Prior to analysis 50µl of CountBright™ Plus Absolute Counting beads were added to allow white cell count to be performed. Data acquisition was subsequently performed using flow cytometry (3.12.4)

3.9.5. Cell counting formula

CountBright™ Plus Absolute Counting beads (Invitrogen, UK) were used to count cells via flow cytometry. 50µl beads were added to the tube prior to data analysis. Beads were identified via flow cytometry and used to count cells using the formula:

$$\left(\frac{\left(\frac{(Cell\ count\ x\ Counting\ bead\ volume)}{(Counting\ bead\ count\ x\ Cell\ volume)}\ x\ Counting\ bead\ concentration\ \left(\frac{Beads}{\mu l}\right)\right)}{Dilution\ factor}\right) x\ 1000$$

Equation 3-1: Equation used to determine cell count using CountBright™ Plus Absolute Counting Beads (cells/ml).

3.10. Immunoblotting

3.10.1. Sample preparation

Western blot was performed on whole kidney lysate to identify Exosc3 expression. Following isolation kidneys were snap frozen in liquid Nitrogen and stored at -80°C. To isolate lysate 5mg of tissue was homogenised in 900µl of ice cold Radioimmunoprecipitation assay (RIPA) buffer (Table 3-10) with added protease inhibitor (1%) using an electric homogeniser. This was then placed at 4°C under constant agitation for 2 hours. To isolate supernatant the protein lysate was centrifuged for 20 minutes at 17,000 g at 4°C. The supernatant was aspirated and stored at -80°C.

10mM Tris-HCl, pH 8.0
1mM EDTA
0.5mM EGTA
1% Triton X-100
0.1% Sodium Deoxycholate
0.1% SDS
40mM Sodium Chloride
ddH_2O

Table 3-10: RIPA Buffer Recipe

3.10.2. SDS PAGE

Reducing Sample Buffer (Thermo Fisher Scientific, 39000) or Non- reducing Sample Buffer (Thermo Fisher Scientific, 39001) was mixed with protein lysate, diluted to appropriate concentration. Samples were heated at 95°C for 5 minutes. Tris-Glycine gels (Novex, Life Sciences. 1.0mm x 10 well) and the XCell SureLock Mini-Cell (Novex, Life Technologies. EI0002) were set up according to manufacturer's instructions (Life-Technologies, 2012) using 1x Running Buffer (25mM Tris base, 192mM Glycine, 0.1% SDS pH 8.3) (Life Technologies, LC2675-5). 30µL of sample was loaded per well and 15µL of molecular weight ladder (BIO-RAD, 1610324). This was connected to a PowerPac (Bio-Rad. 300V, 400mA, 75W) and run for 90 minutes at 125 volts.

3.10.3. Western Blot

XCell SureLock Mini-Cell was set up for gel transfer, following manufacturer's instructions (Life-Technologies, 2009) for transfer of Novex Tris Glycine Gels onto a nitrocellulose membrane (Invitrogen, Life technologies. LC2001). Gels were transferred for 90 minutes at 25 volts on ice using 1x Tris-Glycine Transfer Buffer (12mM Tris base (Sigma), 96mM Glycine (Sigma), pH 8.3, 20% Methanol (VWR)). After transfer the membrane was then blocked with blocking solution, 5% non-fat milk powder in 1 x TBST (50mM Tris.HCl pH 7.4 (Sigma), 150mM NaCl (Sigma), 0.05% Tween 20 (Sigma)), for 1 hour at 4°C overnight. The blocking solution was removed and the fresh blocking solution with the primary antibody at the appropriate concentration was added (Table 3-11). This was incubated for 1 hour at room temperature. The liquid was discarded and the membrane was washed for 5 minute three times, using fresh TBST. Fresh blocking solution containing

appropriate concentrations of secondary antibody was then added and left for 1 hour at room temperature. A final wash step with TBST was performed.

Antibody used	**Exosc3 (Polyclonal, Proteintech, 15062-1-AP)**	**Exosc3 (Monoclonal, Abcam ab190689)**
Size range	34kDa	30kDa
Gel percentage	4-20%	4-20%
Concentration	1:250	1:1000
Secondary antibody	Goat α-rabbit (Abcam, ab6721)	Goat α-rabbit (Abcam, ab6721)
Concentration	1:20000	1:20000

Table 3-11: Western Blot antibodies

3.10.4. Protein visualisation

SuperSignal West Pico Chemiluminescent Substrate (Thermo Fisher Scientific, 34077) was added to the membrane and left for 1 minute. The membrane was then imaged on the Lic-or Odyssey® at 700nm for 10 minutes. Image Studio Lite Version 5.2 software was used to analyse the image.

3.11. Flow Cytometry

3.11.1. Data collection and analysis

Flow cytometry was performed on the BD Symphony A5 (BD Biosciences) based in the Flow Cytometry Core Facility at Newcastle University. Data was analysed using FCS Express 7 (DeNovo software).

3.11.2. Tissue isolation

3.11.2.1. Spleen

Spleens were isolated in ice cold dPBS. Spleen was then transferred to a petri dish with 5ml of ice-cold dPBS and crushed between the frosted surfaces of two slides to dissociate cells. This was transferred to a fresh 15ml conical centrifuge tube and a further 5ml of dPBS added up to 10ml. This was left to settle for five minutes, the top 9ml of suspension was aspirated, being careful not to disturb the debris, and transferred a 15ml conical centrifuge tube.

This single cell suspension was centrifuged at 400 x g for five minutes to pellet the cells. The supernatant was discarded, and cells were resupended in 1ml of red cell lysis buffer (Gibco, UK) for three minutes on ice, with regular agitation. 9ml of ice-cold dPBS was added and centrifuged at 300 x g for 10 minutes. The supernatant was discarded, and cells were resupended in 10ml of PBS.

3.11.2.2. Kidney

To perform flow cytometry analysis on the kidney, a single kidney was isolated in ice cold RPMI-1640 media (Gibco).To generate a single cell suspension from the kidney enzymatic digestion was performed.

Kidneys were decapsulated and then finely chopped with scissors in 2 ml of pre-warmed dissociation media (2 mg/ml collagenase/dipase (Roche Applied Science, Penzberg, Germany) and 0.2 mg/mL DNase type 1 (Roche Applied Science) in RPMI-1640). Samples were placed in a water bath at 37°C for one hour. Samples were transferred to a 100µm sieve and washed with 10ml of ice-cold dPBS. The resulting flow-through was centrifuged at 400 x g for 5mins and the supernatant discarded. The pellet was resuspended in 1ml of red cell lysis buffer for 3 minutes

on ice. 9ml of ice-cold PBS was added and centrifuged at 300 x g for 10 minutes. The supernatant was discarded, and cells resuspended in 5ml of PBS.

3.11.2.3. Bone marrow

To perform flow cytometry on bone marrow, both femurs and the right tibia were removed, residual muscle was removed by scraping with a scalpel and the bones were placed in ice-cold dPBS. The ends of the bones were removed and discarded with a scalpel, long bones were placed in a 0.6ml microcentrifuge tube that was pierced with an 18G needle at the base to allow bone marrow to exit when centrifuged. The prepared tube was placed inside a 1.5ml microcentrifuge tube and centrifuged at 10,000 x g for 15 seconds, this resulted in complete extraction of the bone marrow. Cells were resuspended in 1ml of red cell lysis buffer for three minutes on ice, with regular agitation. 9ml of ice-cold PBS was added and washed at 300 x g for 10 minutes, cells were resuspended in 10ml of dPBS.

3.11.2.4. Cell count

Cell counting was performed using the Anvajo fluidlab R-300 Cell Counter. Cells were diluted to 1 in 1000 prior to counting in dPBS, 20µl was placed on Anvajo acella 100 sample carrier for counting.

3.11.2.5. Cell surface marker staining

Cells were diluted to $2x10^7$ cells/ml. 50µl ($1x10^6$ cells) was analysed per test. Kidney, spleen and bone marrow cells were incubated with TruStain FcX™ (anti-mouse CD16/32) (Biolegend), in order to prevent non-specific binding of antibodies to Fc receptors, and fixable live/dead stain at appropriate concentrations (Table 11-1) in the dark on ice for 30 minutes.

Antibodies mix was prepared in 50µl of BD brilliant stain buffer (BD biosciences) at the appropriate concentration (Table 11-1). Appropriate antibody mix was added to cells and incubated in the dark on ice for 30 minutes. Following incubation, cells were washed in 200µl of flow buffer (dPBS with 1% w/v BSA and 0.1% sodium azide) three times at 400 x g for 5 minutes. Where biotinylated primary antibody had been used, a second incubation with streptavidin fluorophore was performed for 30 minutes on ice. Cells were washed in 200µl of flow buffer three times at 400 x g for 5 minutes. Cells were resuspended in a final volume of 200µl of flow buffer.

3.11.2.6. Compensation

To allow compensation single stained controls were used, one drop of UltraComp eBeads™ Plus Compensation Beads (Invitrogen) was added to 0.5µl of antibody and incubated in the dark for 15 minutes. This was washed with 3ml of flow buffer and resuspended in a final volume of 200µl of flow buffer. For GFP and viability compensation cells were used instead.

3.11.2.7. Cell cycle analysis

To perform cell cycle analysis bone marrow cells from BrdU treated mice were extracted, treated with red cell lysis buffer, and counted as described. $1x10^7$ cells were centrifuged for 5 minutes at 300 x g. To fix and permeabilise cells, 70% ethanol was used, the cell pellet was dislodged with 5ml of ice-cold (-20ºC) 70% Ethanol added dropwise with constantly vortexing. Cells were then incubated at -20ºC for at least 2 hours and remained suitable for analysis for up to three months.

Anti-BrdU was used to allow actively cycling cells to be identified, fixed cells were washed twice with dPBS and centrifuged for 5 minutes at 300x g. Cells were incubated with 2ml of 2M hydrochloric acid for 20 minutes at room temperature.

Cells were washed twice with dPBS and centrifuged for 5 minutes at 300 x g. Cells were resuspended in 1ml of flow buffer and 100µl was aliquoted to fresh FACS tube. 5µl of anti-BrdU antibody (Biolegend) was added and incubated for 20 minutes at room temperature. Cells were washed in flow buffer and centrifuged for 5 minutes at 300 x g. Cells were treated with 50µl of 100µg/ml Ribonuclease I (Thermofisher), to digest RNA and 10µl of 50µg/ml Propidium iodide (Thermofisher) added to enable DNA content to be calculated prior to data collection.

3.11.2.8. Annexin V staining

Annexin V staining was used to investigate apoptosis. Following isolation of bone marrow cells and treatment with red cell lysis buffer as described $1x10^6$ cells were washed twice in Annexin V buffer (Biolegend) and centrifuged at 300 x g for 5 minutes. Cells were resuspended in 100µl of Annexin V buffer with 5µl of Annexin V antibody (APC, Biolegend) and 5µl of 7-AAD (Biolegend), this was incubated for 15 minutes in the dark at room temperature. 400µl of Annexin V binding buffer was added prior to analysis.

3.11.2.9. Antibody optimisation

Prior to performing multi-antibody flow experiments antibody were optimised. This was performed on single stained samples, $1x10^6$ bone marrow cells were stained with serial dilutions of antibody (Table 3-12).

Well	A	B	C	D	E	F	G	H
Starting Volume (µl)	100	50	50	50	50	50	50	50
Antibody volume (µl)	2	-	-	-	-	-	-	-
Volume after dilution (µl)	50	50	50	50	50	50	50	50
Final Concentration	1:50	1:100	1:200	1:400	1:800	1:1600	1:3200	1:6400

Table 3-12: Serial dilution of antibody to determine optimum staining concentration

3.11.3. Fluorescence minus one controls

For complex staining protocols (e.g. stem cell analysis) a Fluorescence minus one control was used to determine positive staining, $1x10^6$ cells were stained as described with the exception of one. This was used to determine true positive staining versus background.

3.12. Flow cytometry analysis

3.12.1. Solid organs

Data for Forward scatter (FSC), side scatter (SSC) (area, weight, and height) and relevant bandpass filter were recorded on all samples.

3.12.2. Reticulocyte

Forward and side scatter was used to identify red cell population (containing the reticulocytes). Red cells were gated and $1x10^5$ events were recorded for both the control and the test sample. Reticulocyte percentage was determined according to the manufacturer's instructions. The control sample was used to set the background fluorescence (Figure 3-5) and reticulocyte count calculated using Thiazole-orange stained sample.

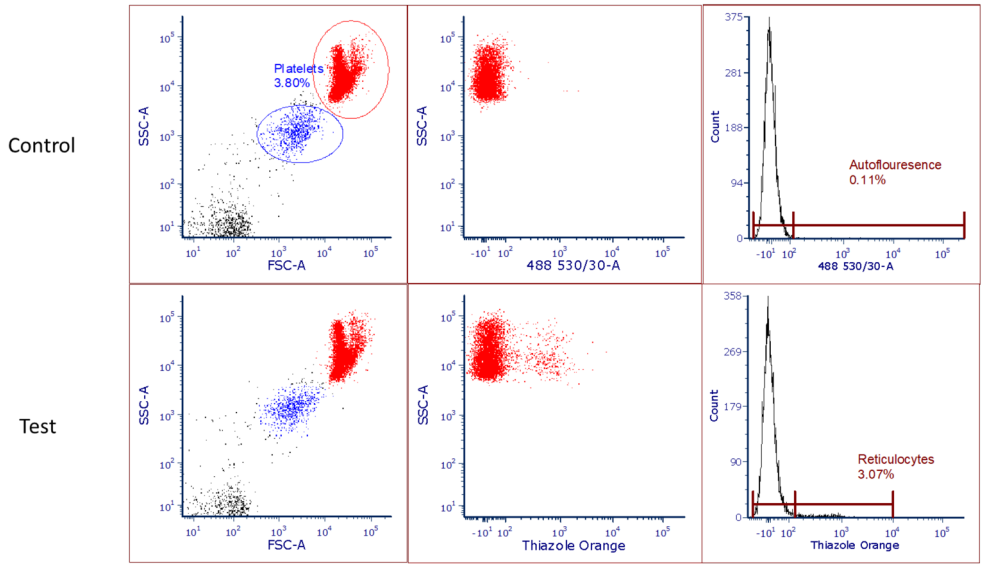

Figure 3-5: Reticulocyte count with BD Retic-Count.

10,000 events were collected for both control and Retic-count samples. FSC and SSC, on a log scale to identify red cells. The red cell gate was then plotted against 488 530/30 channel. A histogram of the results was plotted and the point at which the control sample crossed the X-axis was used to determine background staining level. In the Thiazole-Orange stained sample the percentage of cells beyond this point was determined to be positively stained. Reticulocyte percentage was calculated by Percentage of Thiazole orange gated events - Background percentage.

3.12.3. Platelets

Platelets were identified using FSC and SSC plotted on a log scale, CD41-PE was used to confirm platelets (Figure 3-6), and beads identified to allow platelet count. Platelet count was then determined using the cell counting formula (Equation 1).

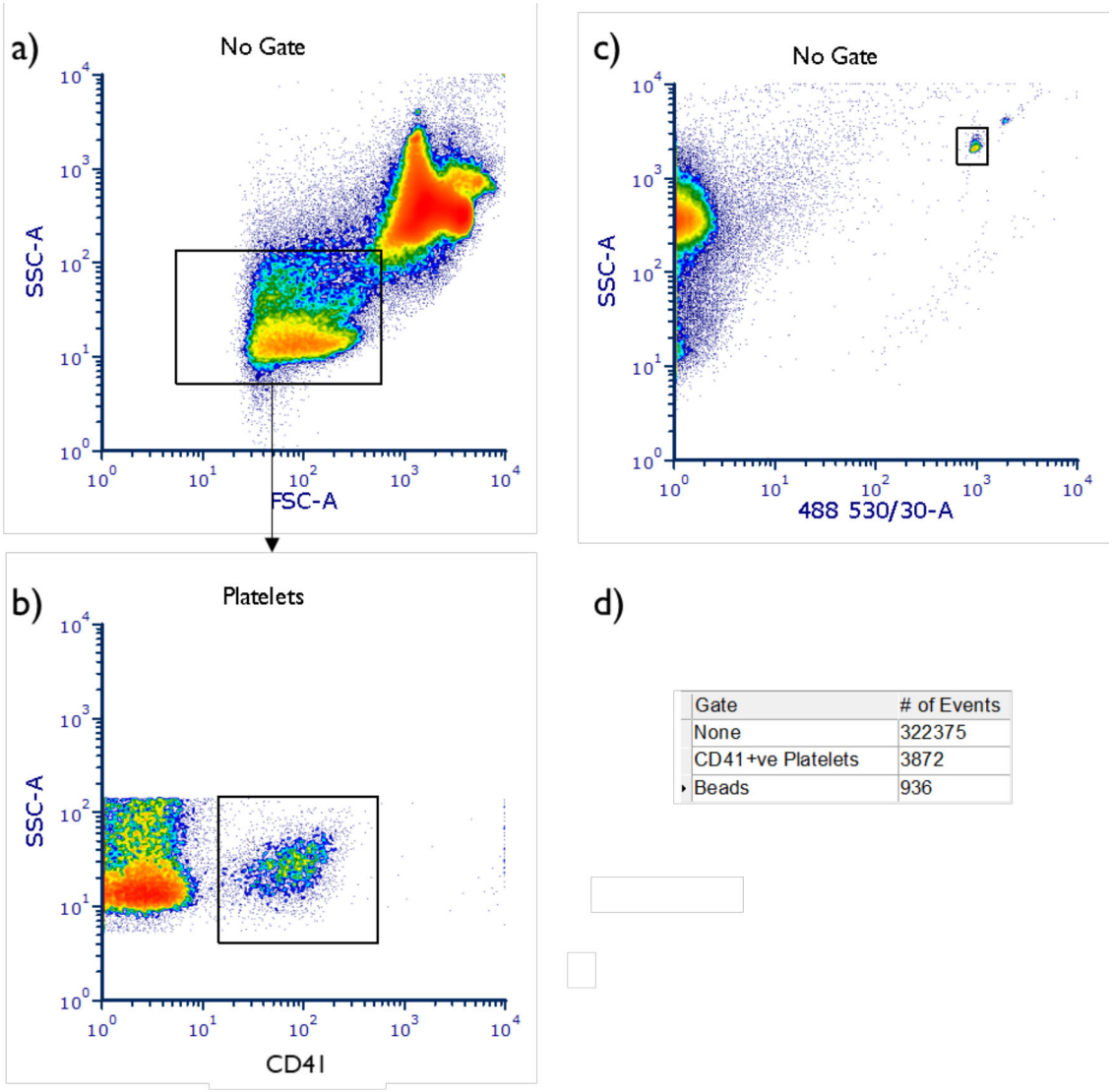

Figure 3-6 Representative flow cytometry of blood sample to determine platelet count.

Heparinised blood was diluted to 1 in 40 in platelet flow buffer. 5µl of diluted blood was added to 200µl of flow buffer containing 1:400 anti-CD41 (PE, BD Biosciences) and incubated on ice for 30 minutes, 50µl of Absolute Counting beads were added to prior to flow cytometry to allow for cell count to be worked out. a) FSC-A vs. SSC-A (log-scale) used to identify platelet containing fraction b) anti-CD41 (PE) used to identify platelets within platelet fraction c) SSC-A vs.488 530/30-A used to identify counting beads d) Gate statistics

3.12.4. White cell count

White blood cells were identified using FSC and SSC, CD3, CD45, CD19 and Ly6G were used to identify cell sub-type, counting beads were used to enable white cell count to be determined (Figure 3-7). White cell count was determined using the cell counting formula (Equation 1).

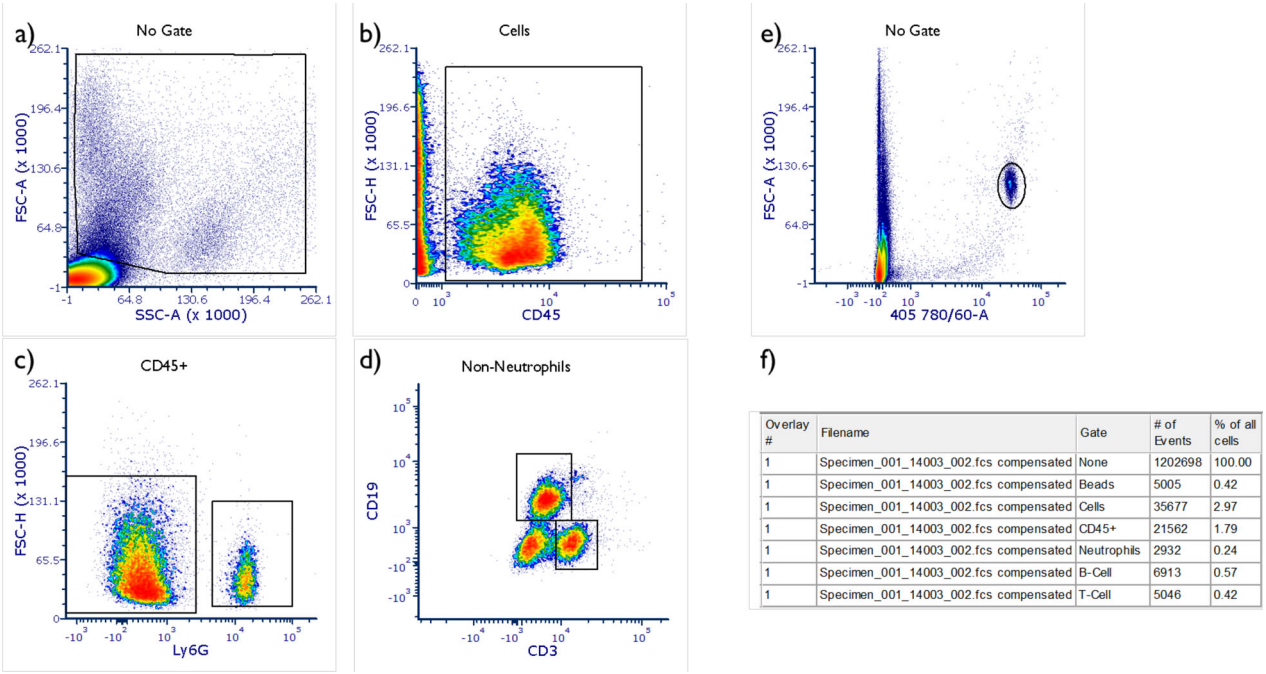

Overlay #	Filename	Gate	# of Events	% of all cells
1	Specimen_001_14003_002.fcs compensated	None	1202698	100.00
1	Specimen_001_14003_002.fcs compensated	Beads	5005	0.42
1	Specimen_001_14003_002.fcs compensated	Cells	35677	2.97
1	Specimen_001_14003_002.fcs compensated	CD45+	21562	1.79
1	Specimen_001_14003_002.fcs compensated	Neutrophils	2932	0.24
1	Specimen_001_14003_002.fcs compensated	B-Cell	6913	0.57
1	Specimen_001_14003_002.fcs compensated	T-Cell	5046	0.42

Figure 3-7: Representative example of white cell counting performed via flow cytometry.

50µl of anti-coagulated blood was stained with 1µl of Anti-CD45, Ly6G, CD19 and CD3 antibodies and incubated on ice for 30 minutes, 450µl of red cell lysis fixation buffer was added and incubated for 20 minutes at room temperature, 50µl of Absolute Counting beads were added to allow cell count to be determined. a) FSC-A vs. SCC-A used to identify differentiate cells from debris. b) FSH-H vs 561 780/60, anti-CD45 (PE-Cy7) used to identify total leucocytes. c) FSH-A vs. 635 670/30, anti-Ly6G (APC) used to identify neutrophils, within the CD45 positive population d) 488 695/40 vs. 561 586/15, anti-CD3 (PerCP-Vio700) and anti-CD19 (PE) used to identify T and B cells respectively. e) Beads identified using 405 780/60 positivity and used to count cells using Equation 1. f) Summary statistics of cell and bead counts.

3.13. TNF-α ELISA

Tumour necrosis factor-α (TNF-α) ELISA was performed on plasma following recombination using Quantikine™ ELISA (R&D Systems) as per manufacturer's instruction. Mouse TNF-α standard was prepared and serially diluted to generate standard curve each sample was performed in duplicate. 50µL of Assay Diluent was added to each well followed by 50µL of standard, control, test sample test samples were performed in triplicate. This was incubated for 2 hours at room temperature. Wells were aspirated and washed four times with 400µL of wash buffer, following

the final wash the plate was blotted on paper towel to completely remove wash buffer. 100µL of Mouse TNF-α Conjugate was added to each well and incubated for 2 hours at room temperature, followed by repeating the wash step. 100µL of Substrate Solution was added to each well and incubated for 30 minutes at room temperature in the dark. 100µL of Stop Solution was added to each well and a plate reader was used to determine optical density at 450nm. Wavelength correction was set to 540nm. Standard curve in GraphPad Prism 9 by plotting the mean absorbance for each standard on the y-axis against the concentration on the x-axis best fit curve through the points on the graph. The data may be linearised by plotting converting the data to log scale, the best fit line was determined by regression analysis.

3.14. Statistical analysis

Statistical analysis was performed using GraphPad Prism 9, to compare two independent samples in normal distribution an unpaired t-test was used. P values of ≤0.05 were considered statistically significant. Mantel-Cox was used to determine survival analysis.

Symbol	p value
n.s.	>0.05
*	≤ 0.05
**	≤ 0.01
***	≤ 0.001

4. Genetic Analysis of the NRCTC aHUS Cohort

4.1. Epidemiology

Approximately 40% of patients presenting with C-aHUS have a pathogenic variant in the complement pathway recognised. Review of the NRCTC data (Brocklebank *et al.*, 2023) identified 1956 patients referred to the NRCTC with a diagnosis of C-aHUS. 243 patients were treated with eculizumab and the control group was composed of patients presenting prior to eculizumab availability through the NRCTC (Figure 4-1). In the eculizumab treated group a complement gene mutation was detected in 90 patients (37%) (Table 4-1). This data confirmed previous studies that have demonstrated *CFH* variants are the most commonly detected (37%), followed by CD46 (26%) (Caprioli *et al.*, 2006). In the total cohort genomic rearrangements resulting in CFH::CFHR1 hybrids were discovered in 12 patients (4.2). The data also revealed that an alternative diagnosis was uncovered in 51/243 who presented with a suspected diagnosis of C-aHUS and were treated with eculizumab. Within this group, a genetic diagnosis was uncovered in 19 patients. In addition to patients treated with eculizumab there were 28 patients identified in the pre-eculizumab with variants in non-complement genes (Figure 4-1).

Characteristic		Eculizumab Treated Cohort (n = 243)	Control Cohort (n = 279)
Age at first presentation, years			
	Median	23	22
	Range	0-80	0-79
Sex			
	Male	98 (41%)	135 (48%)
	Female	145 (59%)	144 (52%)
Plasma exchange			
	Yes	130 (53%)	114 (38%)
	No	94 (39%)	67 (23%)
	Data not available	20 (8%)	116 (39%)
Complement gene mutation		90 (37%)	279 (100%)
	CFH	33 (37%[†])	131 (47%)
	CFHR1:CFH hybrid	1 (1%[†])	11 (4%)
	CFI	6 (7%[†])	19 (7%)
	CD46	23 (26%[†])	61 (22%)
	C3	10 (11%[†])	24 (9%)
	CFB	1 (1%[†])	0
Factor H autoantibody positive		11 (12%[†])	29 (10%)
Combined mutation(s)/autoantibody		5 (6%[†])	4 (1%)
No complement mutation/autoantibody		102 (42%); 24 (10%) with VUS	0
Not CaHUS		51 (21%)	NA

Table 4-1: Summary of complement variants detected in patients referred to the NRCTC with C-aHUS.

Control cohort, patients presenting before the availability of eculizumab through the NRCTC. Data demonstrates that CFH variants are the most commonly detected in C-aHUS. In the eculizumab group only 37% of patients with C-aHUS had pathogenic variants in a complement gene detected.

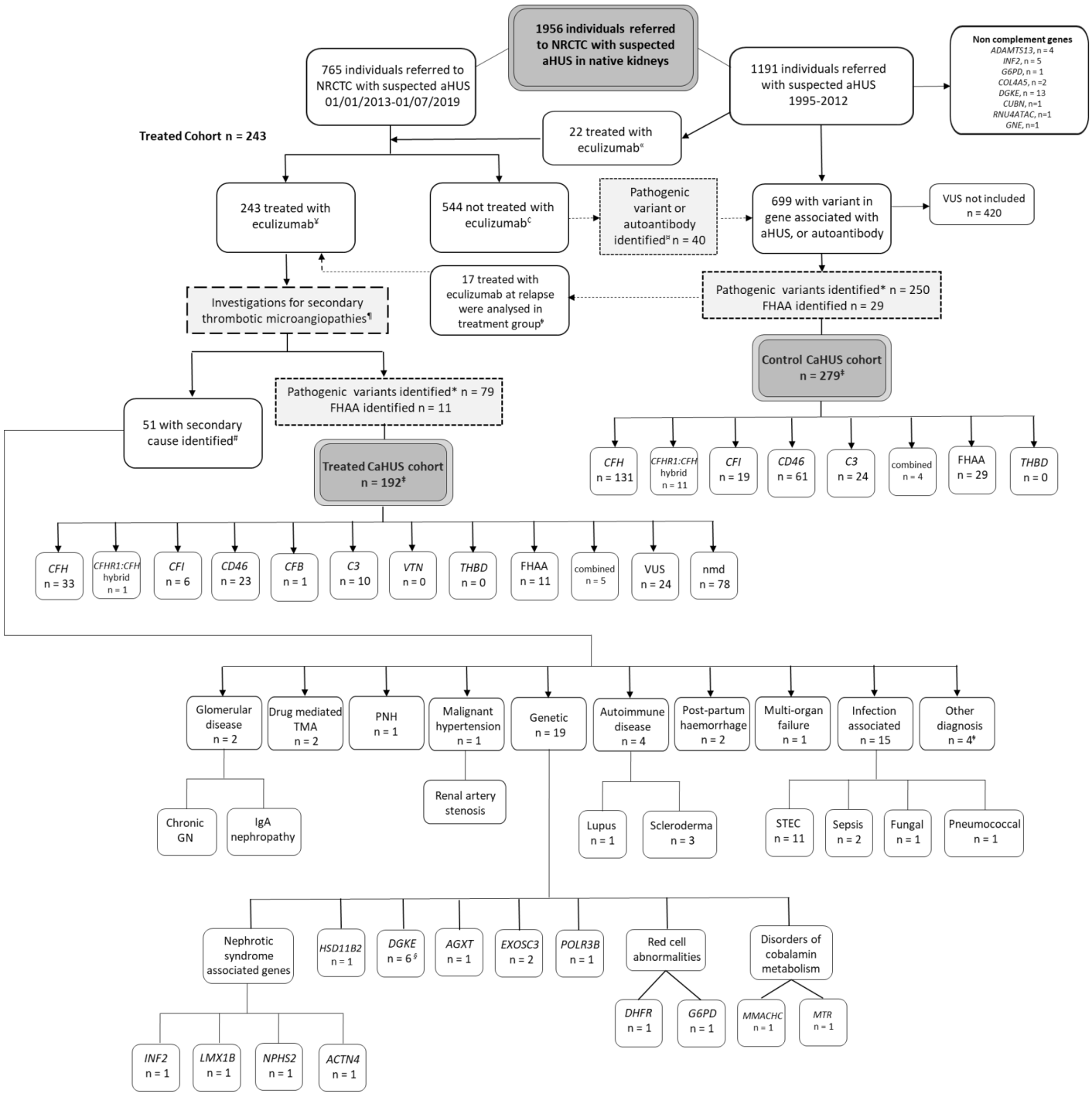

Figure 4-1: Patients referred to the NRCTC with a diagnosis of presumed HUS.

1191 patients presented before the availability of eculizumab (control cohort) within this group 28 patients were identified with variants in genes not thought to be associated with complement mediated HUS. 765 patients presented after the introduction of eculizumab into routine management, within these group 19 patients were identified with variants in genes responsible for non-complement mediated HUS.

4.2. Genomic rearrangements in the RCA cluster

4.2.1. Genomic rearrangements in CFH as a cause of aHUS

The Regulator of complement activation cluster (RCA) is a 360Kb region located on chromosome 1q32; this region contains the complement regulators *MCP* (and the pseudogene MCPL) and *CFH* along with five *CFH* related genes *CFHR* 1-5 (M K Liszewski;T W Post and Atkinson, 1991; Hourcade *et al.*, 1992; Zipfel *et al.*, 1999). This region is thought to have arisen due to multiple duplication events, resulting in an unusually homologous region of the genome (Figure 4-2). This can result in pathology due to errors in double strand break repair.

Double strand breaks (DSB) are common cellular events, occurring 10/day/cell, these DSB have the potential to be devastating to chromosomal integrity and can lead to cell death if not repaired (Lieber, 2010). DSBs occur as a result of exogenous DNA stressors including ionising radiation, and chemical exposure and endogenous protein failures e.g. topoisomerase I failure (Vítor et al., 2020). There are two principal DSB repair pathways. Firstly, Non-homologous end joining (NHEJ), this is a fast but error prone repair mechanisms that joins the two free ends generated by the DSB together to restore chromosomal integrity (Figure 4-3). NHEJ occurs throughout the cell cycle but is vulnerable to insertions and deletions as there is no template and the free ends are simply joined together. The second repair mechanism commonly employed is Homologous Recombination (HR). This is a slow, high fidelity repair pathway that requires a template from the sister chromatid, therefore this is only possible when the DNA is in close proximity, such as cell division. The high degree of homology in the RCA results in an increased risk of errors in double strand break repair, specifically through NHEJ and non-allelic homologous recombination (NAHR) (Figure 4-3). This leads to the generation of

fusion and hybrid genes (Venables et al., 2006; Valoti et al., 2015; Challis et al., 2016; Tschernoster et al., 2022)

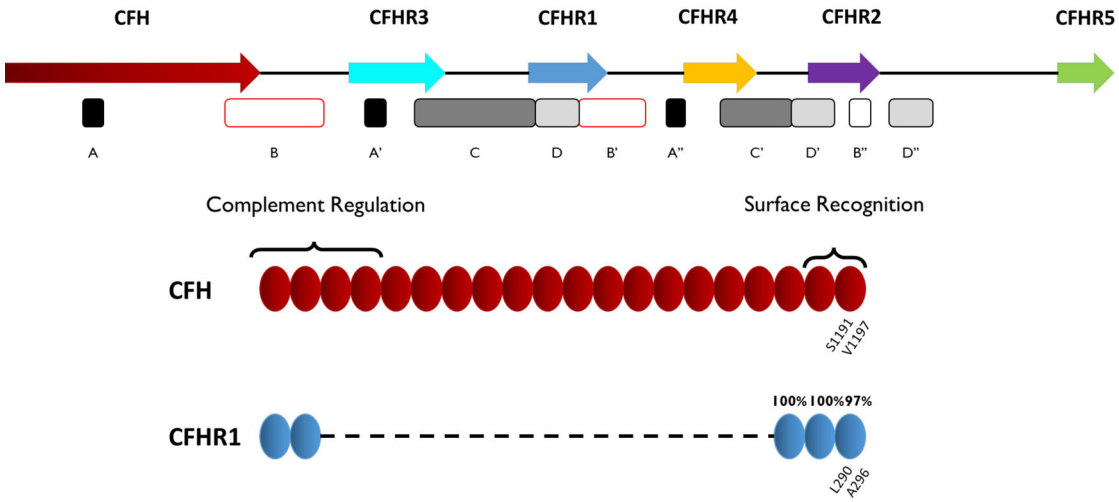

Figure 4-2: Representation of the RCA cluster, with CFH and CFHRs.

The orientation of the genome showing CFH (red) with intergenic sequence followed by CFHR3 (light blue), CFHR1 (blue), CFHR4 (yellow), CFHR2 (purple) and CFHR5 (green). Regions of homology highlighted with letters. Region B and B' highlighted. Region B at the 5' end of CFH, sharing a high degree of homology with B' at the 5' region of CFHR1. Beneath, shows a representation of CFH (Red) aligned with CFHR1 (Blue) at a protein level this high degree of homology between CFH (Red) and CFHR1 (Blue) is reflected by the fact that there is only a two amino acid difference between CFH and CFHR1. These two amino acid changes result in reduced cell surface recognition compared to CFH.

4.2.2. Mechanism of non-allelic homologous recombination in aHUS

Following a double strand break at the 5' end of CFH, the newly generated free ends seek out a template, the high degree of homology can mean that CFHR1 is aligned to this generate the double Holliday junction, leading to NAHR (Figure 4-4). Following strand invasion and DNA synthesis the double Holliday junction must then be resolved, which can occur in one of two ways (Figure 4-4). This can result in either a cross over event or a gene conversion, which can be detected using Multi-ligation probe amplification (MLPA). Both of these processes result in an identical protein, i.e., CFH N-terminus (complement regulatory region) with a CFHR1 C-

terminus (cell surface recognition). CFHR1 is unable to bind to the cell surface with the same affinity as CFH, therefore this protein is unable to regulate complement at the cell surface leading to C-aHUS. It is also possible for the DSB to occur in CFHR1, in which case the resultant CFHR1 molecule contains CFHR1 N-terminus with CFH C-terminus, this protein out competes with wild type CFH for cell surface binding but is unable to regulate complement once bound with the same affinity, resulting in C-aHUS. A review of the MLPA data during this project highlighted a number of patients (Table 4-2) where the MLPA data showed evidence of large genetic recombination events that were not typical of gene conversion events, due to length of DNA affected, nor cross-over events, as the CFHR3 and CFHR1 MLPA indicated there were normal copy numbers of CFHR3, in a cross-over event the entire downstream gene is crossed over and the CFHR3 sequence is therefore lost (Figure 4-4). The proposed mechanism for these recombination events is through two separate cross over events as described in Figure 4-4. This has not been documented in the RCA cluster previously.

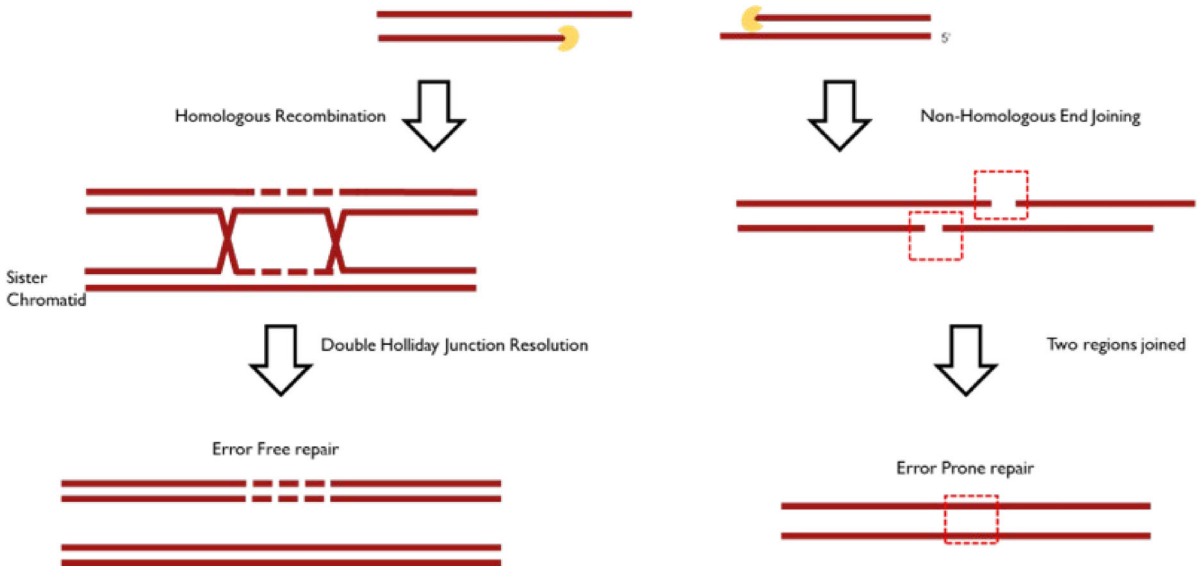

Figure 4-3: Outcome of double strand breaks.

Following a double-strand break the free 5' ends are first digested by exonucleases to generate overhangs. There are two major mechanisms of double strand break repair. Homologous recombination utilises the sister chromatid as the repair template, firstly the sister chromatid invades the double strand break, to form a double Holliday junction, which is subsequently resolved to release the two chromatids (the template chromatid and the newly repaired chromatid) and is therefore occurs mostly during active cell division where sister chromatids are in close proximity with each other. The second repair mechanism is non-homologous end joining in which the free 5' and 3' ends are joined together, this mechanism of repair does not require a template and is therefore utilised throughout the cell cycle, this mechanism of repair is susceptible to insertions and deletions (Indels) and translocations. There is a fine balance between the slow but high-fidelity homologous recombination and the rapid non-homologous end joining mechanism. If these double strand breaks are not repaired the cell activates apoptotic pathways that lead to cell death.

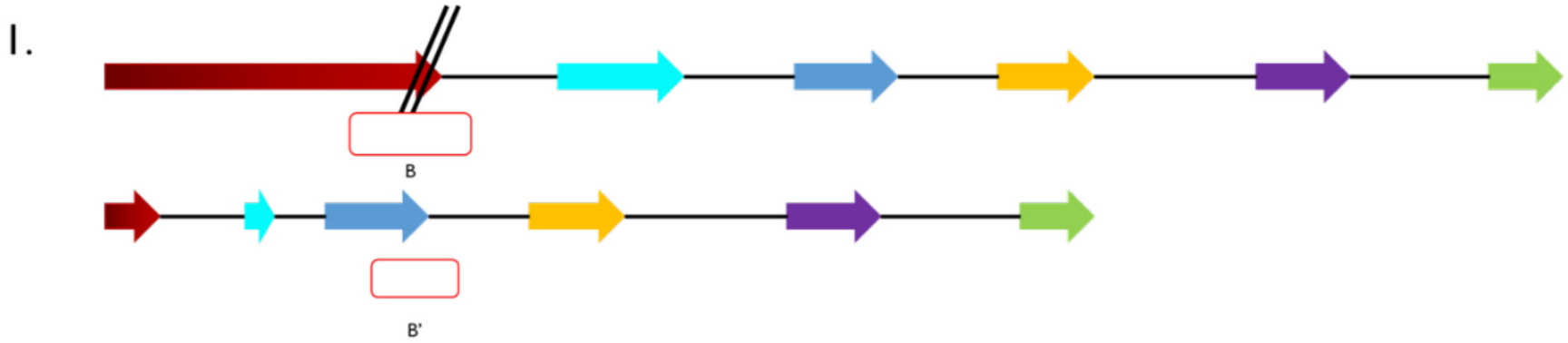
1.
B
B'

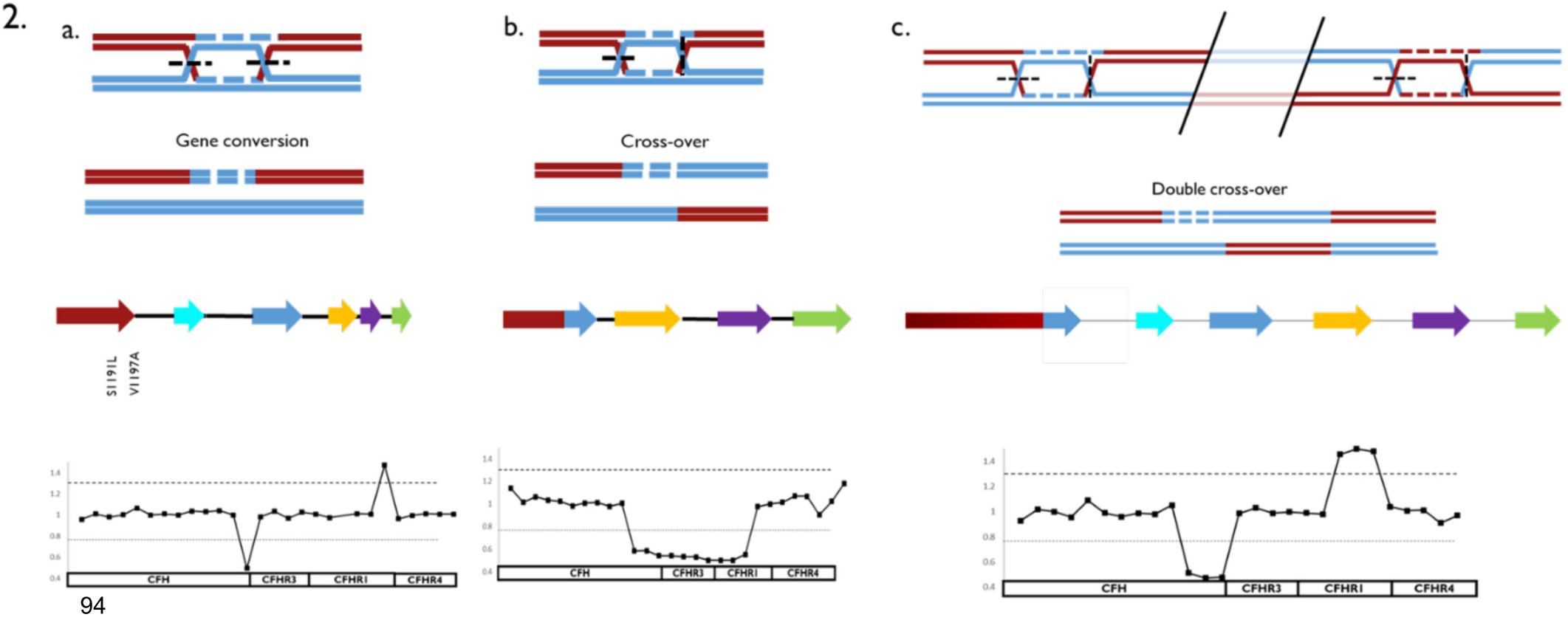
2.
a.
Gene conversion
b.
Cross-over
c.
Double cross-over
S1191L
V1197A
CFH
CFHR3
CFHR1
CFHR4

Figure 4-4: Non-allelic homologous recombination.

1. Following a double strand break at the 5' end of CFH there is misalignment of the sister chromatid, due to the high degree of homology and the CFHR1 sequence is used as the template. The resulting double Holliday junction must then be resolved which can occur in one of two ways. a. Two "horizontal cuts" results in a gene-conversion event, in which there is a small region of the genome is converted. This results in a CFH protein that contains CFH N terminus (complement regulatory region) with two amino acids from CFHR1 (S1191L and V1197A) at the C-terminus (Cell surface recognition), the resultant protein is unable to bind to the cell surface and therefore does not regulate complement. This can be detected using Multi MLPA which shows a drop in the sequence overlying the 5' end of CFH and an increase in the corresponding region of CFHR1 (indicating an extra copy of CFHR1 sequence and loss of the CFH sequence) with normal copy number all other probes, including CFHR3 and CFHR4, therefore only a small genomic region has been exchanged. b. A cross-over event, in which "one horizontal and one vertical cut" are performed by repair complexes. This results in exchange of the sequence following the double Holliday junction. On a protein level this is indistinguishable from the CFH::CFHR1 gene conversion event, however on a gene level this results in loss of the sequence between the 5' end of CFH to the 3' end of CFHR1, this region contains CFHR3 and can therefore be identified using MLPA, which shows loss of the 5' CFH, CFHR3 and 3' CFHR1 (of note CFHR3 and 1 deletion is seen in patients with CFH autoantibodies, this can be differentiate from this due to the retention of two copies of 3' CFHR1, in CFHR3,1 deletion there is only one copy of the whole of CFHR3 and CFHR1, with normal copy number in CFH). c. Proposed mechanism following the discovery of patients with loss of large sequence at the 5' end of CFH and an increase in the corresponding region of CFHR1 resulting in a CFH::CFHR1 hybrid protein that is functionally identical to both the single cross-over and gene conversion (i.e. S1191L, V1197A) on a genetic level there is loss of a large region of 5' CFH normal copy number of CFHR3 and gain of CFHR1 sequence. The proposed mechanism is that there are two cross-over events occurring, the first event results in crossing over of the CFHR1 downstream sequence, as with a cross-over event, the second cross-over results in restoration of the downstream CFH sequence, this results in the MLPA data demonstrating loss of a large sequence at the 5' end of CFH and a gain in the corresponding region of CFHR1. This mechanism has not been proven, and in humans it is not possible to differentiate double cross-over events from large gene conversions. The same processes can result from a DSB in CFHR1, in this scenario the resultant protein contains the N terminus of CFHR1 (complement regulatory region) with the C-terminus of CFH (Surface binding) this results in a CFHR1::CFH hybrid that competes with wild type CFH for cell surface binding To investigate the proposed mechanism long range sequencing could be performed for example using Nano pore technology.

Mechanism		Gene	Number of Cases
Conversion		CFH	18
		CFHR1	2
Crossover	Single	CFH::CFHR1	1
	Double/ Large gene conversion	CFH::CFHR1	14
	Single	CFHR1::CFH	2
	Double/ Large gene conversion	CFHR1::CFH	9
NHEJ		CFH::CFHR3	8

Table 4-2: Genomic rearrangement events detected in patients referred to the NRCTC including unaffected family members, surprisingly single cross-over events are detected at a much lower frequency than large gene conversion/ double cross-over events.

4.3. Genetics of eculizumab non-responsive TMA

Within the NRCTC cohort 47 patients with genetic forms of non-complement mediated TMA were discovered. This included previously described genes associated with aHUS including 19 with *DGKε* (Lemaire *et al.*, 2013; Quaggin, 2013; Brocklebank *et al.*, 2020), two with disorders of cobalamin metabolism, *MTR* (Vaisbich et al., 2017) and *MMACHC* (Sharma *et al.*), and six with *INF2* (Challis *et al.*, 2017). Three children presented with disorders of red cell morphology one with *DHFR* and two with *G6PD*, these have been shown to present in a clinical phenotype indistinguishable from HUS (i.e. haemolytic anaemia, thrombocytopenia and acute renal failure) (Walsh *et al.*, 2018). In addition to variants in these known TMA genes, three individuals were identified with variants in RNA surveillance proteins. These included two patients with *EXOSC3* variants and one patient with *POLR3B.* Review of the NRCTC cohort as part of this project identified five further

patients with variants in RNA processing including one patient with *TSEN2,* two siblings with *RNU4ATAC*, and one patient with *POLR3H*.

4.3.1. Novel genes identified in the RNA processing pathway

4.3.1.1. EXOSC3

Child One

An 8-month-old girl with a background of profound developmental delay, secondary to pontocerebellar hypoplasia (PCH) (Figure 4-5), presented to the paediatric service with a short history of Respiratory syncytial virus (RSV) positive bronchiolitis. She deteriorated rapidly and required ventilation. Blood tests at this time revealed microangiopathic haemolytic anaemia, thrombocytopenia and acute kidney injury. She required renal replacement therapy for 11 days, as well as multiple red cell and platelet transfusions. A diagnosis of presumed C-aHUS was made and she was commenced on eculizumab. After an initial recovery and discontinuation of renal replacement, she represented five months later with a lower respiratory tract infection with relapse of her TMA, despite adequate complement blockade (CH50/AH50 absent) on eculizumab. Due to her underlying neurological disorder, the decision was made to redirect her care, she died shortly after (Figure 4-6). She had extensive work-up as per the NRCTC protocol for patients presenting with TMA, including STEC testing, complement (*C3, CFH,CFI, CD46, CFHR1-5* copy number and *C5* eculizumab non-responsive SNP) and non-complement (*DGKε, INF2, MMACHC*) genetics, CFH antibody screening, Human immunodeficiency virus (HIV), hepatitis, malignant hypertension, and drug history; these yielded no causative agent in her. As part of the work up for her PCH she had genetic screening for known causes (Table 17) which revealed compound

heterozygous variant in *EXOSC3* c.92G>C (p.G31A) and c.395A>C (p.D132A), both known pathogenic variants (Wan *et al.*, 2012).

Child Two

A 7-month-old boy, with a background of severe neurodevelopmental delay, secondary to pontocerebellar hypoplasia (Figure 4-5) presented to the paediatric service with a short history of viral respiratory illness, he deteriorated rapidly and required ventilation for four days, investigations revealed microangiopathic haemolytic anaemia (raised Lactate Dehydrogenase (LDH) and schistocytes, however he had a normal reticulocyte count (88 reference range 50-100), thrombocytopenia and acute kidney injury. He was initially commenced on renal replacement therapy and eculizumab for presumed C-aHUS. However, there was no evidence of response. Due to his underlying neurological disorder it was decided that active treatment was not in his best interests, and he died shortly after (Figure 4-6). He underwent investigation for alternative causes of TMA including STEC testing, complement (*C3, CFH, CFI, CD46, CFHR1-5* copy number) and non-complement (*DGKε, INF2, MMACHC*) genetics, CFH antibody screening, HIV, Hepatitis, malignant hypertension, and drug history, no evidence of another cause was found. As part of the work up for his PCH he had genetic screening for known causes (Table 17) which revealed compound heterozygous variant in *EXOSC3* c.395A>C (p.D132A) and a novel in-frame three nucleotide deletion c.341_343del, this variant is in a highly conserved region that is predicted to affect splicing (Figure 4-7). In addition to the patients identified in this study, there are four cases of PCH1b reported with HUS (Table 4-3).

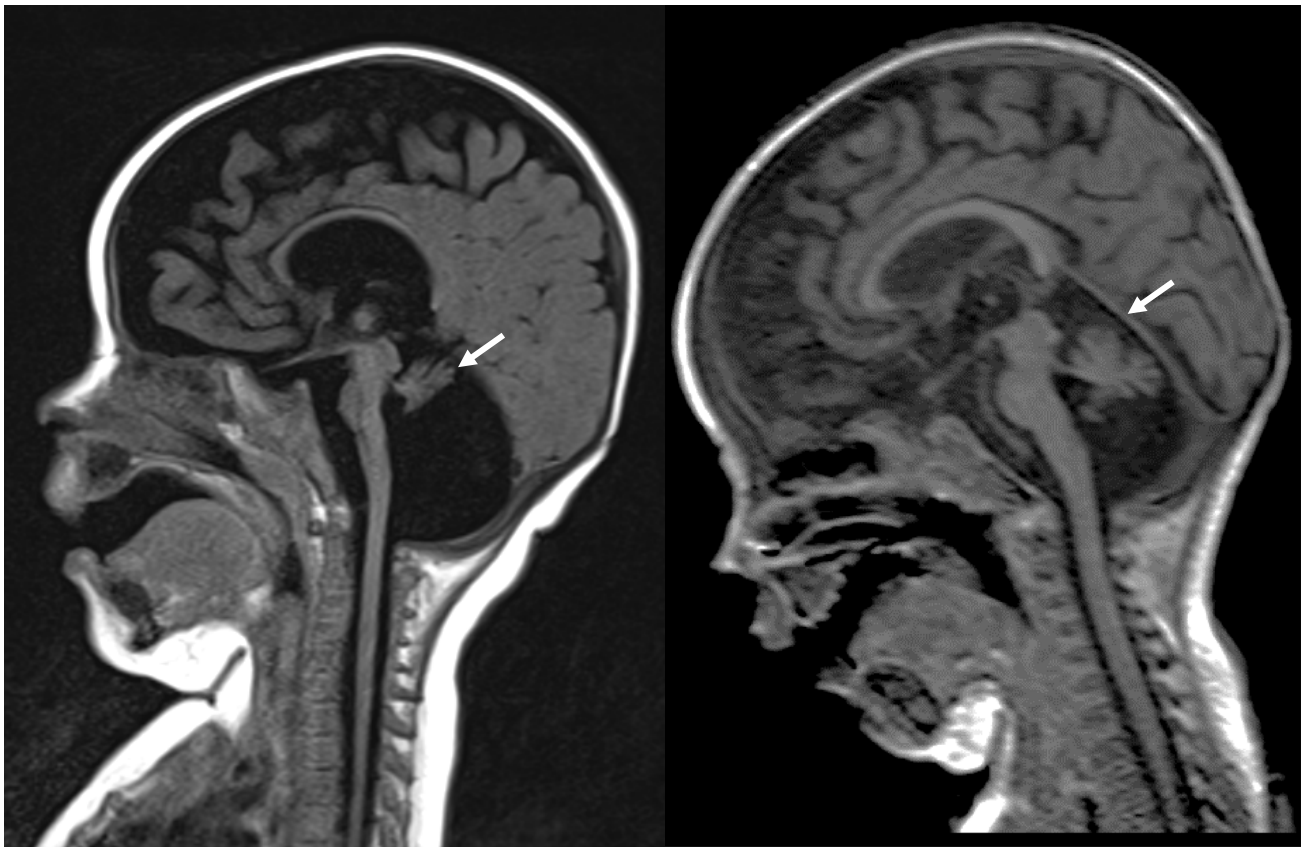

Figure 4-5: Magnetic Resonance Scans of two children with EXOSC3 variants.

Representative sagittal image, demonstrating hypoplasia of the pons and cerebellum (white arrow). Generalised white matter hypoplasia was evident throughout, as is common in PCH.

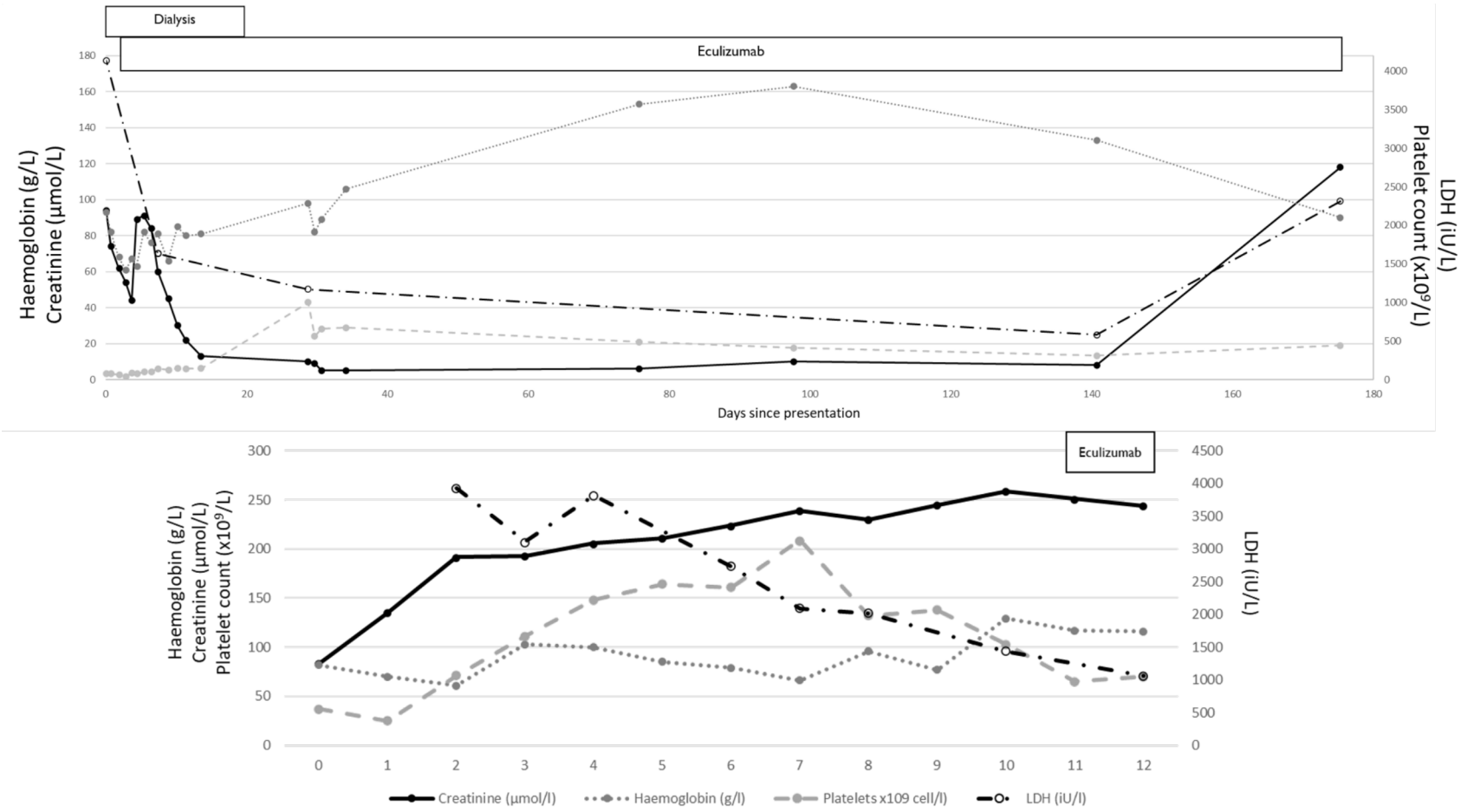

Figure 4-6: Haematological and biochemical data in two children presenting with HUS with EXOSC3 variants

Evidence of acute renal failure, thrombocytopenia and haemolytic anaemia. Child 1 had recovery in her kidney function and haematological parameters, however she represented whilst on eculizumab with recrudescence of her disease and died of HUS. Child 2 Presented with HUS, despite eculizumab he had no recovery in his biochemical or haematological parameters and died of HUS.

Patient	Variants in *EXOSC3*	Reference
1	c.395A>C (p.D132A), c.2226dupG (pD76fs)	(Rudnik-Schöneborn et al., 2013)
2	c.92G>C (p.G31A) (Homozygous)	(Van Quekelberghe et al., 2022)
3	c.92G>C (p.G31A) (Homozygous)	(Van Quekelberghe et al., 2022)
4	Not reported	(Ryan et al., 2000)
5	c.395A>C (p.D132A), c.92G>C (p.G31A)	This Study
6	c.395A>C (p.D132A), c.341_343del	This Study

Table 4-3: Patients identified with EXOSC3 variants and TMA

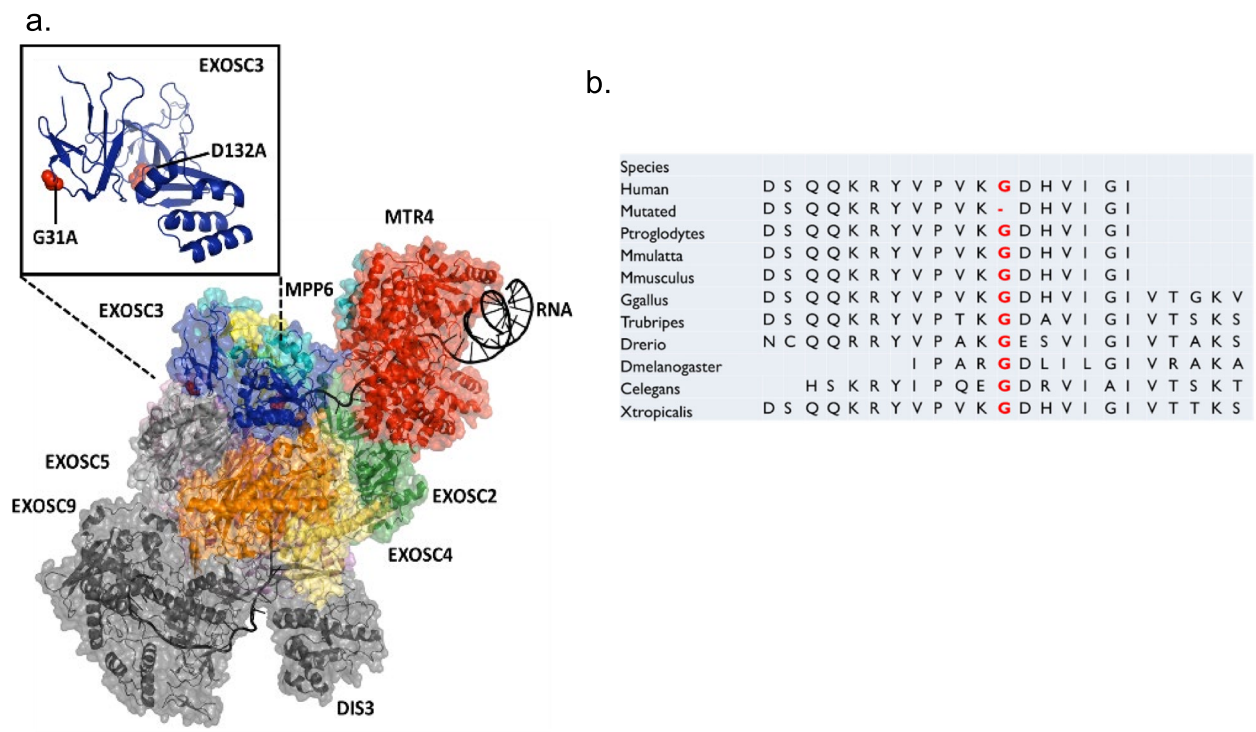

Figure 4-7: Position of variants identified in EXOSC3.

a. The Human RNA exosome with MTR4 delivering single stranded RNA bound, EXOSC3 highlighted in blue, with variants identified in this study highlighted on image inset. Generated on Pymol (PDB 6D6Q). b. Sequence alignment of c.341_343del showing preservation at this amino acid throughout evolution.

4.3.1.2. TSEN2

A 3 year old child, from a consangionous family, presented to the paediatric services with reduced oral intake, as part of her work up she underwent investigations that demonstrated microangiopathic haemolytic anaemia, thrombocytopenia and acute kidney injury. She was severely hypertensive at presentation, requiring multiple anti-hypertensive agents. A diagnosis of presumed C-aHUS was made and she was commenced on eculizumab. There was some improvement following eculizumab, however the effects of this were uncertain. She underwent renal biopsy that demonstrated chronic TMA despite eculizumab treatment. Investigation for a potential cause including known TMA gene (including *EXOSC3*), did not reveal any known cause. Following this she underwent exome screening that revealed a homozygous novel intronic variant in *TSEN2* c.-17-2A>C that is predicted to affect splicing. Following the identification of this patient Canpolat *et al.* reported four consngiounous families with six children with an intronic *TSEN2* variant c.914-5T>A who developed HUS, along with craniofacial and central nervous system abnormalities (Canpolat *et al.*, 2022). In addition to TMA, *TSEN2* variants are also associated with PCH2b, although neither the child within the NRCTC cohort or the six children previously reported have evidence of PCH2b.

4.3.1.3. POLR3

During the course of this project a review of children with neurological abnormalities, who did not have a variant in a known TMA genes, referred to the NRCTC was undertaken. This identifed three children who had been referred with a clinical diagnosis of TMA and a background of POLR3 related Hypomyelinating Leukodystrophy (POLR3-HLD). One of these patients had a variant in *POLR3H (RCP8),* one with *POLR3B* (*RCP2*) (Teoh *et al.*, 2018), and one child had a clinical

diagnosis of POLR3-HLD (the child's parents did not want POLR3-HLD genotyping for this child, although he had normal complement genetics).

4.3.1.4. RNU4ATAC

Within the NRCTC cohort whole exome sequencing in a family identified a *RNU4ATAC* biallelic variant in two affected siblings with a background of microcephalic osteodysplastic primordial dwarfism presenting with TMA, one of the children presented with a second episode of TMA at four years old.

4.4. RNA processing in the development of TMA

The cases identified within the NRCTC cohort (*EXOSC3, TSEN2 and POLR3,* and to a lesser extent *RNU4ATAC*) are all in genes involved in RNA processing, and surveillance resulting in an undescribed pathogenic process in TMA.

4.4.1. RNA species

To produce RNA from DNA it must be transcribed, this action is performed by three RNA polymerases (RNAP) in eukaryotes (I-III). RNAPI transcribes 45S rRNA, the large subunit of the ribosome; RNAPII is the only polymerase to produce coding RNA in the form of messenger RNA (mRNA), it is also responsible for producing non-coding RNA (ncRNA) such as Short nuclear (snRNA) and microRNA; RNAPIII transcribes tRNA, 5S rRNA and U6 spliceosome RNA (Carter and Drouin, 2009). Once transcribed extensive processing is required to produce the final mature RNA, the exact process depending on the RNA species. Most RNA species, including mRNA, tRNA and rRNA are produced with introns, which need to be removed, this may be done by the spliceosome in the case of mRNA (Nilsen, 2003), or by the tRNA splicing endonuclease complex in the case of tRNA (Hayne *et al.*, 2020). Once

fully mature RNA is able to carry out its required function, at the end of its life cycle RNA is removed from the cell by the RNA exosome.

4.5. The RNA exosome

4.5.1.1. Structure and function of the RNA exosome

The RNA exosome is a ubiquitous 3'→5' ribonuclease multi-subunit complex that degrades and processes virtually all forms of intracellular RNA (Januszyk and Lima, 2014). Its function and structure are highly conserved through evolution, with the recognisable RNA exosome in archaea, bacteria and eukaryotes. The mammalian RNA exosome is comprised of nine core proteins (EXOSC1-9, Exo9). Exo9 consists of a hexameric ring of six RNase PH-like proteins (EXOSC4-9) that is capped by three S1/KH domain proteins (EXOSC1-3). This results in a barrel shaped complex with a central channel that directs single stranded RNA (ssRNA) to a bound exonuclease.

Approximately 1.5% of the human genome code is protein coding, however an estimated 75% is transcribed (Jensen *et al.*, 2013). This results in a large pool of pervasive transcripts (non-coding RNAs), including tRNA, rRNA, snRNA, short nucleolar RNA (snoRNA), these function as scaffolds for Ribonucleoprotein as well as mediating the generation of polypeptides. In addition to these RNA species there are a growing number of short-lived RNA species that have poorly understood functions, these include transcription start site-associated RNA, promoter upstream transcripts (PROMPTs) and enhancer RNA (eRNA) (Jensen *et al.*, 2013) whether these RNA species truly have a physiological function in the cell is an area of debate, however what is clear is that uncontrolled production of these pervasive transcripts is detrimental to the cell (Jensen *et al.*, 2013). With an abundance of

pervasive transcripts there is an increased risk of disruption of normal cellular processes such as complementation with DNA sequences preventing the proper transcription of DNA, inappropriate translation of these non-coding transcripts or binding to limited RNA binding proteins within the cell, therefore reducing their availability for physiological RNAs.

One of the main functions of the RNA exosome is in RNA quality control (Houseley *et al.*, 2006); in the nucleus the exosome degrades defective tRNA, rRNA, mRNA and snRNA, whereas in the cytoplasm it is has only been identified in mRNA processing. In addition to this function in degrading abnormal RNA, the RNA exosome is required for the normal maturation of both rRNA and snRNA. In the absence of a functioning RNA exosome, there is a significant increase in pervasive RNA species across the genome indicating the requirement exosome degradation to maintain these species (Pefanis *et al.*, 2014; Pefanis *et al.*, 2015a).

In addition to its role in RNA quality control surveillance the RNA exosome has an emerging role in anti-viral response (Bartok and Hartmann, 2020). Specifically, the RNA exosome has been found to degrade viral RNA with the use of the co-factors SKIV2L (Aly *et al.*, 2016) and ZAP (Guo *et al.*, 2007). SKIV2L and ZAP are able to identify viral infection due to the differing viral RNA signatures compared to endogenous RNA, including sequence specific features such as unusual codon use, GC-Rich motifs and targeting by non-sense mediated decay proteins (Bartok and Hartmann, 2020). One of the regulatory functions of the RNA exosome is the degradation of mRNA containing AU-Rich Elements (AREs) in the 3’ untranslated region. Generally speaking, mRNAs containing AREs encode for proteins that control cell growth (e.g. p53, Bcl-2, VEGF, Cyclin A/B1/D1) or response to external stimuli such as infection or inflammation (TNF-α, Interferon-α/β, COX2, iNOS)

(Barreau *et al.*, 2005); In the normal cell, ARE-binding proteins (ARE-BP) bind to these mRNAs and target them for rapid degradation by the exosome. In response to an external stimulus, e.g. infection there is decoupling of the ARE-BP and the mRNA, meaning that it is rapidly free to be translated in to protein (Figure 4-9).

4.5.1.2. EXOSC3

EXOSC3 is an essential subunit of the non-catalytic component of the RNA exosome complex (Exo9, Figure 4-8). EXOSC3 is located in humans on chromosome 9 (Chromosome 4 in mouse). It is a four exon gene that contains NT, S1 and KH domains (Liu *et al.*, 2006), which facilitate the binding of EXOSC3 to the EXOSC5 and 9, to maintain the hexameric ring structure. Two of the variants identified in children with EXOSC3-mediated TMA have previously been identified in children with PCH1b, these include the c.395A>C (p.D132A) and c.92G>C (p.G31A) which are both highly conserved amino acid residue in the putative RNA binding S1 domain, these variants are predicted to affect the exosome interaction with specific co-factors and RNA binding (4.5.1.3) (Wan *et al.*, 2012).

4.5.1.3. Interaction between the RNA exosome and co-factors

Little is known about the exact interactions between the RNA exosome and associated co-factors. However there is recent studies using Cryo-EM have illuminated the interaction between the RNA exosome and one of the components of the nuclear exosome co-factors (Mtr4). (Weick *et al.*, 2018). For the first time the interaction between the RNA exosome and co-factors was visualised, this demonstrated the close association between the RNA co-factors and the ring of the RNA exosome, particularly highlighting the interaction between Mtr4 and EXOSC2 and 3. Further work is required to understand how mutations in the RNA exosome component impact the binding of co-factors, however this gives some insight in to

the reasoning behind the cell type specific nature of pathogenic variants in EXOSC3, conceivably hypofunctioning variants in the RNA exosome selectively inhibit the interactions between the RNA and specific co-factors resulting in the phenotype.

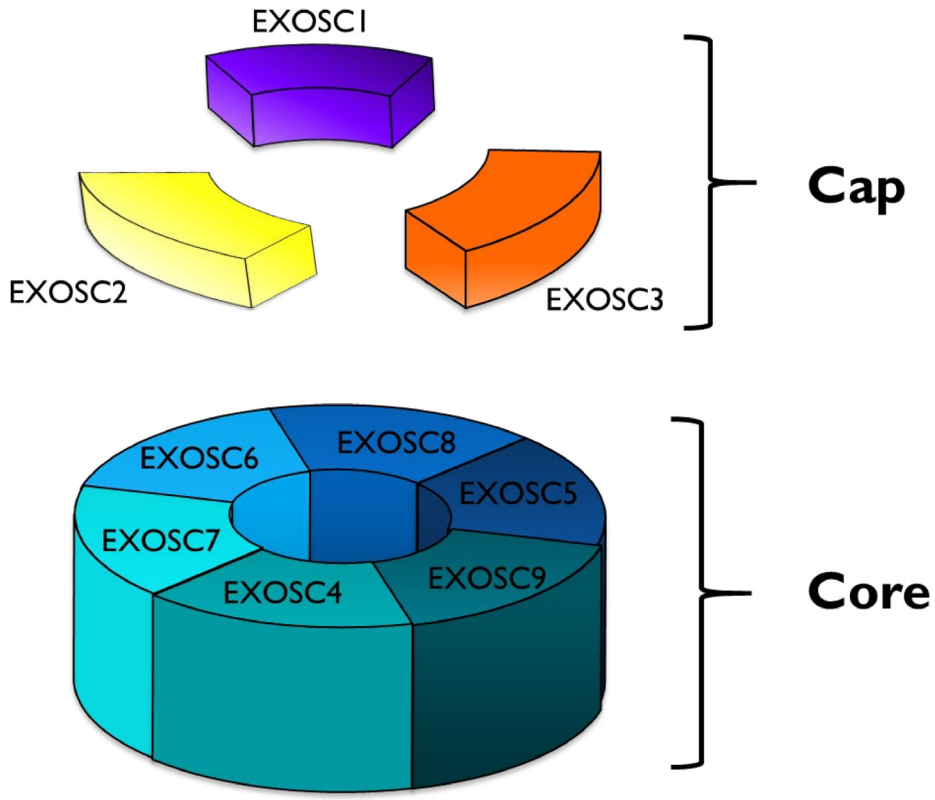

Figure 4-8: Representation of the RNA exosome complex.

Cap comprised of Exosc1-3 and the core comprising Exosc4-9, this forms a ring structure that allows single stranded RNA to be channelled through

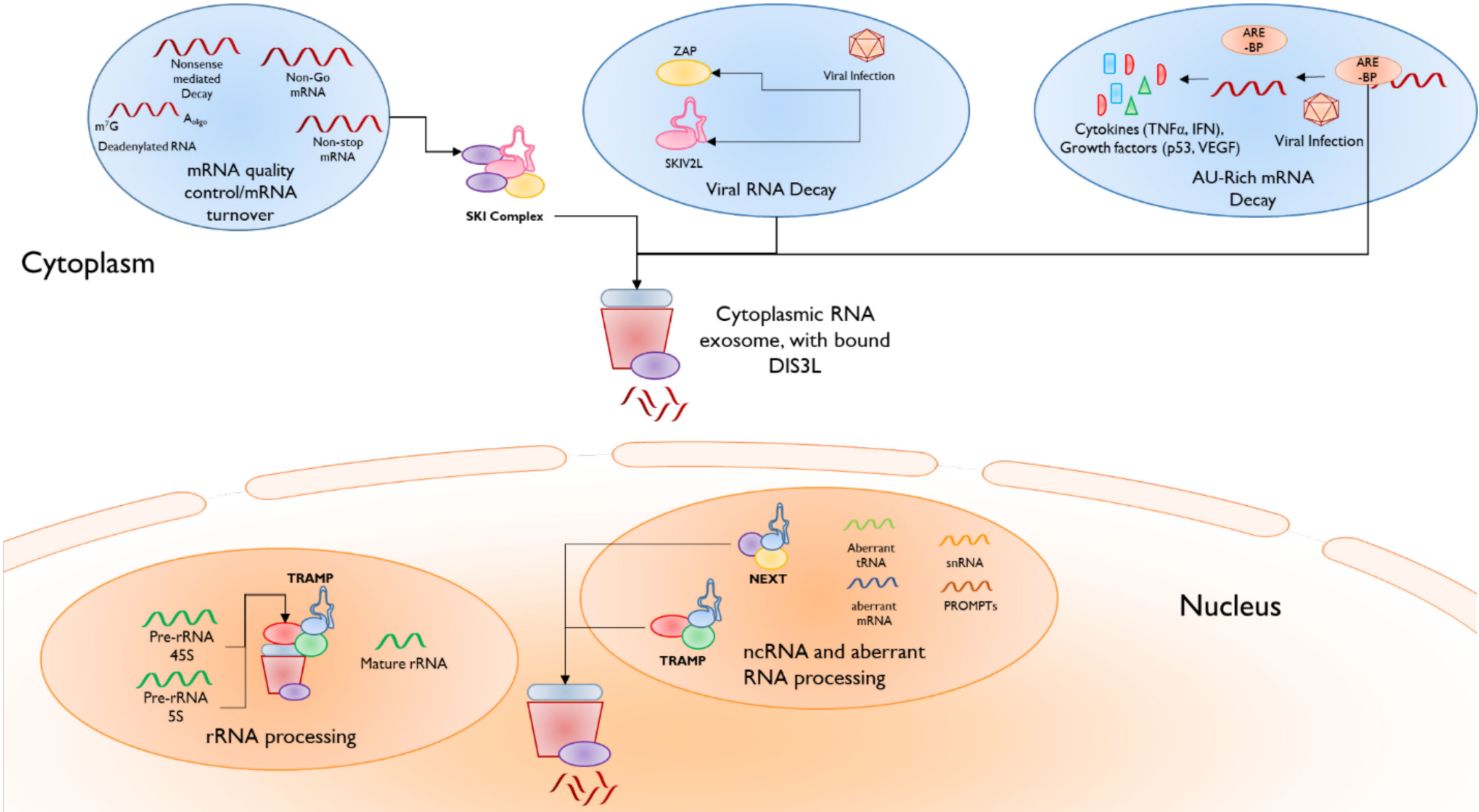
Nonsense mediated Decay
Non-Go mRNA
m7G
Aoligo
Deadenylated RNA
Non-stop mRNA
mRNA quality control/mRNA turnover
SKI Complex
ZAP
Viral Infection
SKIV2L
Viral RNA Decay
ARE -BP
ARE -BP
Cytokines (TNFα, IFN), Growth factors (p53, VEGF)
Viral Infection
AU-Rich mRNA Decay
Cytoplasm
Cytoplasmic RNA exosome, with bound DIS3L
TRAMP
Pre-rRNA 45S
Pre-rRNA 5S
Mature rRNA
rRNA processing
NEXT
Aberrant tRNA
snRNA
aberrant mRNA
PROMPTs
TRAMP
ncRNA and aberrant RNA processing
Nucleus

Figure 4-9: Simplified functions of the RNA exosome in the cell.

In the nucleus two of the RNA exosome functions are rRNA processing, and quality control of aberrant RNA species. The RNA exosome associates with the TRAMP complex within the nucleus to perform its functions. The RNA exosome has a vital role in RNA surveillance in the cytoplasm as well, here it is responsible for mRNA quality control, via interaction with the SKI complex. It also has roles in viral RNA decay, by associating with the anti-viral co-factors ZAP and SKIV2L. Finally it is essential for AU-Rich mRNA decay, in the resting cell state these mRNAs are rapidly degraded due to recognition of the AREs. Upon cell stress the ARE-binding protein releases from the ARE, the mRNA is no longer targeted for degradation and instead is transcribed by the ribosome. The RNA exosome is responsible for many other RNA interactions, including R-loop resolution and degradation of other ncRNAs, however the ones highlighted here are best understood, particularly with relevance to disease.

4.5.2. TSEN2

During this project, a child presented with TMA and was discovered to carry a novel intronic homozygous *TSEN2* variant (4.3.1.2). TSEN2 is a component of the tRNA splicing endonuclease complex, along with TSEN34, TSEN15 and TSEN54 (Hayne *et al.*, 2020). This complex along with CLP1 is responsible for processing pre-tRNA in to mature tRNA (Figure 4-10). Defects in components of the TSEN and CLP1 have been identified in patients with PCH. An intronic variant in *TSEN2* has been described in four families with TMA, craniofacial and central nervous system abnormalities (although not PCH) (Canpolat *et al.*, 2022). In these patients, bulk RNA analysis demonstrated abnormal tRNA transcripts indicating the pathogenicity of this variant. RNA pathway analysis highlighted upregulation of genes associated with cell cycle, ribosome function and shigellosis, potentially linking dysfunction of the tRNA biology with STEC-HUS.

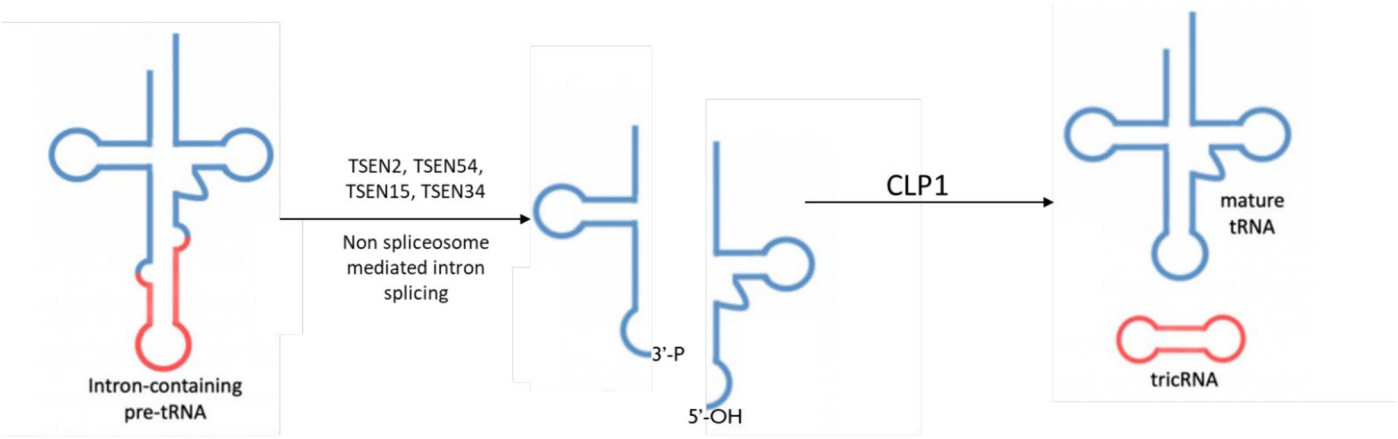

Figure 4-10: TSEN mediated tRNA splicing

Pre-tRNA is processed by the tRNA splicing endonuclease (TSEN). This results in removal of the intron, with the resulting free exons binding to CLP1 to ligate these two ends together. Finally, mature tRNA is produced with a tRNA intronic circular RNA formed from the intron (the function of the tricRNA is currently uncertain).

4.5.3. RNA polymerase III

The RNA polymerase III is responsible for the transcription of multiple forms of ncRNAs. Autosomal recessive pathogenic variants in components of the RNAPIII result in POLR3-HLD (OMIM 614381), a rare neurodegenerative disorder (Lata *et al.*, 2021). TMA has previously been reported in a patient with POLR3-HLD, secondary to *POLR3B* (*RCP2*) (Teoh *et al.*, 2018), however the pathogenesis of this is not understood. Review of patients in the NRCTC revealed one child with a clinical diagnosis of POLR3-HLD and one child with a biallelic pathogenic variants in *POLR3H* (RCP8). Additional evidence of the role of POLRIII in TMA comes from the finding of anti-RNAPIII antibodies in cases of TMA. Anti-RNAPIII antibodies have long been known to be a predictive risk factor for SRC (Penn *et al.*, 2007; MEYER *et al.*, 2010; Hudson *et al.*, 2014), however whether these antibodies are pathogenic or an epiphenomenon is unclear (Fritzler and Choi, 2016). In support of a pathogenic role for these antibodies is the finding that purified IgG from patients with anti-RNAPIII antibodies inhibit the effects of RNA polymerase *in vitro* (Kuwana

et al., 1993). Anti-RNAPIII are detectable years before the clinical manifestations of SRC, with a rapid rise in titres shortly before patients develop SRC (Burbelo *et al.*, 2019). Identification of pathogenic variants in RNAPIII suggests that these antibodies function to disrupt the normal function of RNAPIII.

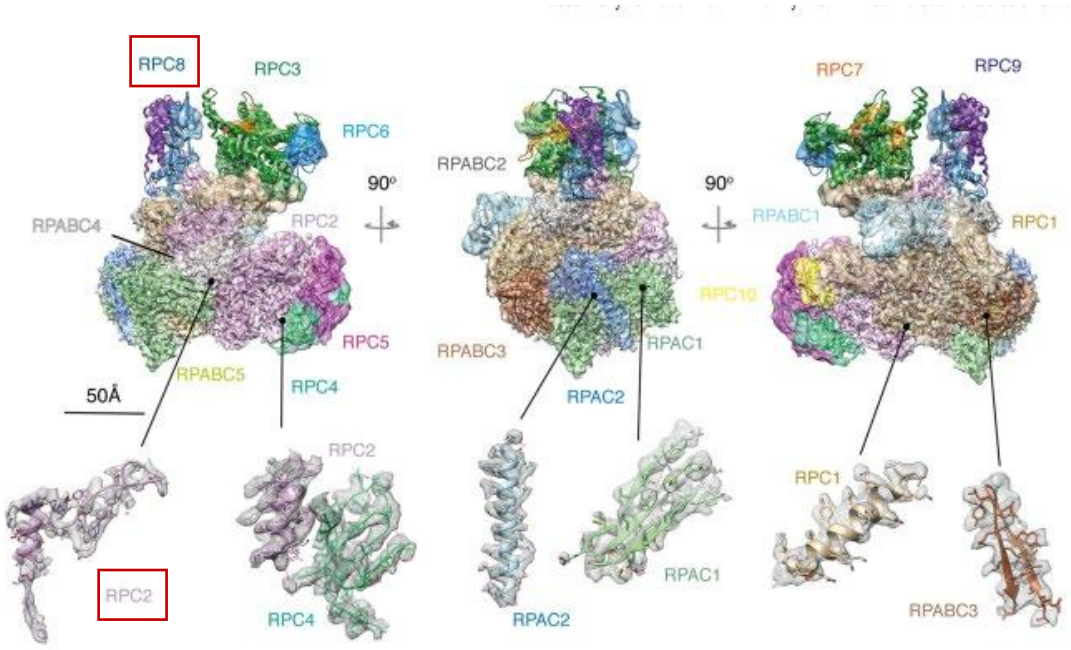

Figure 4-11: Pathogenic variants within RNAPIII in patients with HUS.

Red boxes denote the genes in which variants have been identified, adapted from Ramsey et al.(Naesens et al., 2022)

4.5.4. RNU4ATAC

RNU4ATAC is a snRNA that is incorporated in to the into the minor spliceosome component U4atac. The minor spliceosome is responsible for the removal of introns from a small number of mRNAs in humans (approximately 750/>20,000 genes) (Almentina Ramos Shidi et al., 2023). Biallelic variants in RNU4ATAC are known to cause MOPD1 (microcephaly, growth retardation, skeletal dysplasia and intellectual disability) (OMIM: 210710). However there is a wide spectrum of additional conditions identified in patients with *RNU4ATAC* variants including renal abnormalities (although TMA has not been recognised previously) (Adam *et al.*,

1993). In RNU4ATAC dysfunction there is accumulation of abnormal mRNA products with retained introns that interact with the Integrator complex, an RNA polymerase II associated complex that can regulate RNA polymerase II function (Skaar *et al.*, 2015; Almentina Ramos Shidi *et al.*, 2023). Ultimately this affects mRNA levels within the cell.

4.6. Summary

During this review of patients presenting the NRCTC with a diagnosis of aHUS, eight individuals were identified with pathogenic variants in RNA processing genes (Figure 4-12). The pathogenesis of this is unclear, however it is likely that the pathway is similar in these genetic conditions. EXOSC3 is the best understood of these genes and was the first to be identified in this project. The remainder of this project aimed to address how variants in EXOSC3 result in TMA, this was done by using an *Exosc3* knockout mouse.

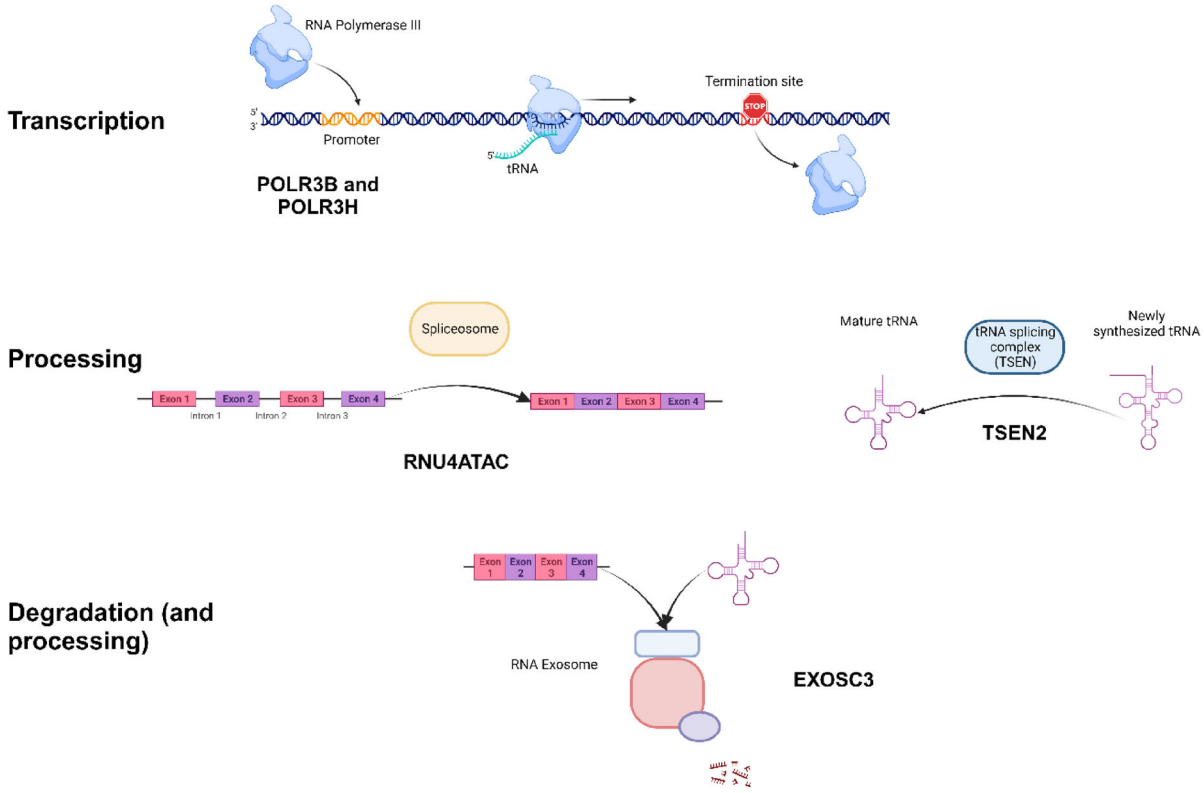

Figure 4-12: Summary of RNA processing proteins in TMA

Biallelic pathogenic variants detected in patients with complement non-responsive patients have been identified across the lifecycle of RNA. This includes patients with variants in two components of the RNA polymerase III, which is responsible for production of tRNA. Variants in genes responsible for processing pre-RNAs including both mRNA and tRNA have been identified. Finally, variants have been identified in EXOSC3 resulting in RNA exosome dysfunction and defects of RNA degradation.

4.6.1. Potential mechanism due to ectopic activation of nucleic acid sensors

It has previously been demonstrated that in the absence of a functioning RNA exosome there is accumulation of RNA species, predominantly pervasive transcripts (Jensen;Jacquier and Libri, 2013; Pefanis *et al.*, 2014). Defective nucleic acid surveillance has been shown to result in excessive interferon signalling. To prevent overwhelming viral infection, intracellular surveillance pathways are constitutively active. These pathways detect nucleic acid signatures (DNA and RNA) normally only present in viruses (Roers;Hiller and Hornung, 2016). Detection of intracellular viral RNA occurs through the RIG-I Like Regulators (RLR) pathway,

whilst TREX1 and the STING complex detect DNA (Takahasi *et al.*, 2008; Xiao and Fitzgerald, 2013). Activation of these pathways results in downstream events culminating in the production of type 1 interferon (Figure 4-13). Genetic variants in these pathways result in failure of nucleic acid sensing pathways and inappropriate activation of anti-viral pathways and interferon production, collectively these disorders are termed type 1 interferonopathies (Crow and Manel, 2015).

Type 1 interferonopathies are a heterogeneous group of conditions that can involve multiple organs. One of the key manifestations of type 1 interferonopathies is endothelial dysfunction. These include genetic variants in *TREX1* (SLE (OMIM:152700, aHUS/TMA and Retinal Vasculopathy with Cerebral Leukodystrophy (OMIM:192315) (Lee-Kirsch *et al.*, 2007; Richards *et al.*, 2007; Gulati *et al.*, 2018)); *IFIH1* (SLE (Cunninghame Graham et al., 2011)*; SKIV2L* (SLE (Fernando *et al.*, 2007)); *SAMHD1* (Cerebral vasculopathy and early-onset stroke (du Moulin *et al.*, 2011)); *TMEM173* (STING-associated vasculopathy (OMIM:*615934)* (Crow and Casanova, 2014))*.* Failure to degrade RNA by the RNA exosome results in accumulation of aberrant RNA species, not normally present in high concentration in host cell (Rigby and Rehwinkel, 2015). These RNA species may be misinterpreted by RLRs as viral infection, resulting in production of type 1 interferon (Wang and Colonna, 2014; Rigby and Rehwinkel, 2015). The idea of build-up of endogenous RNA that become immunostimulatory is demonstrated in SKIV2L deficiency cell models (Eckard *et al.*, 2014). SKIV2L is an essential component of the Ski complex, a cytoplasmic co-factor for the RNA exosome. In the absence of SKIV2L there is accumulation of aberrant mRNA species, presumably through failure to deliver these to the RNA exosome for degradation. These RNAs are sensed by the RLR pathway, resulting in interferon production. Additionally, *SKIV2L* mutations result in a rare disorder, Trichohepatoenteric syndrome, these

patients have been shown to have an increased interferon signature (Eckard *et al.*, 2014).

One potential mechanism for EXOSC3-mediated TMA is that a build-up of abnormal RNAs as a result of hypofunction RNA exosome are misinterpreted as viral infection (Figure 4-13) leading to ectopic activation of these anti-viral pathways and ultimately resulting in interferon expression. Children presenting with EXOSC3-mediated TMA had documented viral infection, the two patients in the NRCTC cohort had RSV and an unspecified respiratory virus. The two cases subsequently reported both presented following COVID-19 infection (Van Quekelberghe *et al.*, 2022). This could suggest that this increase in viral RNA overwhelms the cell and results in inappropriate activation of the anti-viral pathways, this also potentially explains why there is not a 100% penetrance in *EXOSC3* variants resulting in TMA, potentially highlighting the need for a trigger event to induce the phenotype.

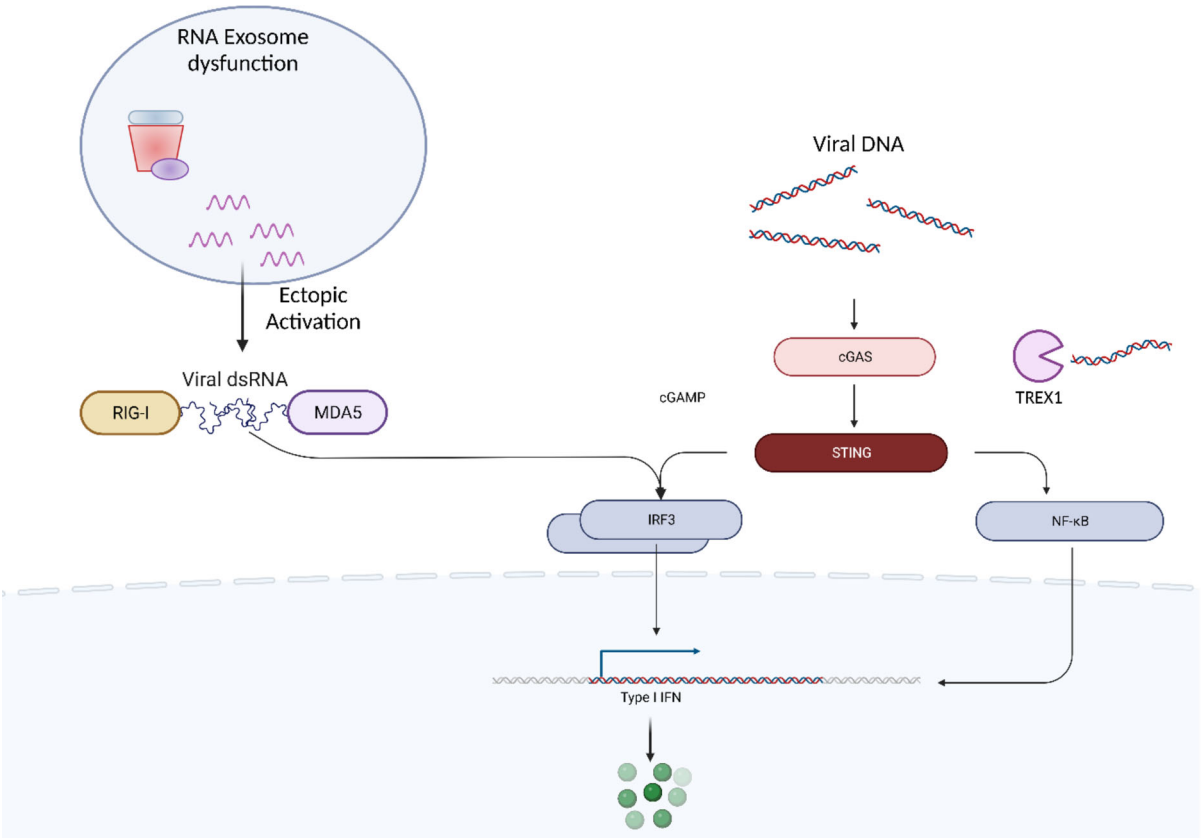

Figure 4-13: Intracellular nucleic acid sensing pathways.

Viral RNA and DNA species are detected by RIG-I/MDA5 and TREX1, respectively, triggering a series of downstream events resulting in activation of IRF3 and the production of interferon. Interferon is subsequently released from the cell and activates the interferon receptor (IFNAR). The cytoplasmic RNA exosome is responsible for degrading multiple endogenous RNA species, when this fails to function these RNA species accumulate. This could potentially be misinterpreted by RIG-I/MDA5 as viral infection and trigger the production of interferon. This is seen in SKIV2L deficiency, where generation of mRNA by the unfolded protein response (UPR) and IRE-1 results in abundance of mRNA that is not delivered to the RNA exosome for degradation and is capable of stimulating RIG-I (i.e. immunostimulatory).

4.6.2. Potential mechanism due to disruption of normal ribosomal function processes resulting in apoptosis

The accumulation of pervasive RNA species that occurs in the absence of a function RNA exosome interrupts normal cellular processes (4.5.1.1). Ribosomal function is sensitive to RNA disturbance due to the high energy requirements required for normal ribosomal function, therefore any disruption to cellular function can have catastrophic effects on the cell (Buttgereit and Brand, 1995). Following interruption

of ribosomal function there is activation of pro-apoptotic pathways including activation of p53 (Figure 4-14), animal models of EXOSC3 knockout have evidence of ribosomal dysfunction and apoptosis.

4.6.2.1. Zebrafish model

To investigate the role of the RNA exosome in the pathogenesis of disease a zebrafish model of *exosc8 and 9* has been developed (Müller *et al.*, 2020). This model highlighted the essential role of the RNA exosome in ribosomal processing. These zebrafish developed reduced head size, smaller brain, and cerebellum. qPCR in these fish demonstrated upregulation of pro-apoptotic genes including *tp53* and *mdm2*, as well as cell cycle arrest. These features suggest ribosomal dysfunction as the cause of the phenotype.

4.6.2.2. Mouse model

A mouse model of Exosc3 knockout has previous been developed to allow conditional knockout (Economides *et al.*, 2013a). This mouse model has been used interrogate the role of the RNA exosome in tissues, utilising tissue specific Cre^{ERT2} promoters.

<u>B Cells</u>

The RNA exosome has previously been shown to have an essential role in B cell development, specifically in class switching and somatic hypermutation, two processes required to generate the antibody diversity needed in life(Pefanis *et al.*, 2014). In *exosc3*-deficient cells, there was an increase in multiple forms of ncRNA, indicating the essential role the exosome in degrading the ncRNAs. Recently, an $Mb1^{cre}$ mouse was used to generate a B cell specific Exosc3 knockout. This mouse demonstrated a specific defect in progression of pro-B to pre-B cells, with accumulation in pervasive RNAs; ultimately, this results in upregulation of pro-

apoptotic genes including *Trp53, Bax* and *Cdkn1* leading to cell death (Laffleur *et al.*, 2022).

Erythropoiesis

The RNA exosome has been shown to be essential in normal erythropoiesis; previous models have demonstrated that downregulation of the RNA exosome in primary erythroid precursors results in apoptosis and down regulation of c-kit (Mehta *et al.*, 2021). A *in vivo* model of Exosc3 ablation in red cell progenitors (*Vav1*^{Cre}) demonstrated almost complete failure of erythroid progenitor activity and up regulation of p53-mediated apoptotic markers, including *Mdm2, Trp53inp1, Cdkn1a and Phlda3* (Fraga de Andrade *et al.*, 2022). Indicating increased apoptosis in the absence of the RNA exosome.

Neurological development

Pathogenic variants in the RNA exosome are linked to pontocerebellar hypoplasia (Wan *et al.*, 2012). To explore the role of the RNA exosome in neurodevelopment two brain specific cre expressers were used (*FoxG*$^{-Cre}$ and *Emx1*^{Cre})(Ulmke *et al.*, 2021). These demonstrated failure of normal neuronal development, secondary to overwhelming apoptosis. qPCR analysis of these cells demonstrated up-regulation of p53 mediators e.g. *Trp53inp1, Aen,* and *Bbc3.* Administration of PFTα, an experimental p53 antagonist, to these mice showed evidence of rescue, implying p53 mediated cell death as the primary driver of disease in this model.

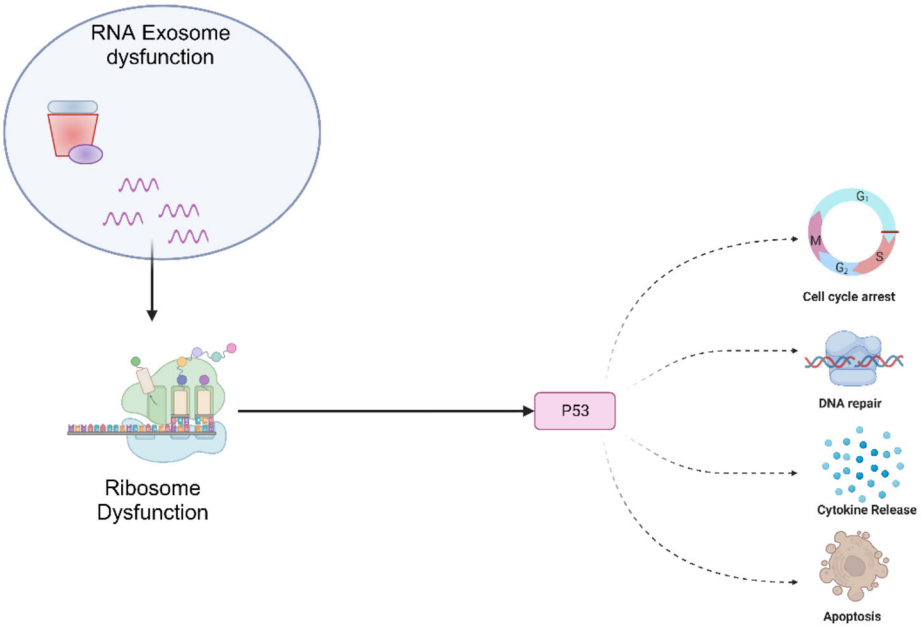

Figure 4-14: Ribosomal dysfunction in RNA exosome dysfunction

Build-up of aberrant RNA overwhelms the normal function of the ribosome, resulting in activation of P53, leading to downstream effects, including cell-cycle arrest, release of inflammatory cytokines, DNA repair pathway upregulation and ultimately activation of apoptotic pathways.

4.6.3. Summary of model organisms

The finding of up-regulation of p53-pathway genes and cell cycle arrest in these model organisms are hallmarks of ribosomal dysfunction (Kampen *et al.*, 2020). This is potentially of interest in the pathogenesis of TMA, due to the role of the ribosome and ribosomal dysfunction in STEC-HUS. As previously highlighted the children presenting with EXOSC3-mediated TMA had documented viral infection (4.6.1). The two patients in the NRCTC cohort had RSV and an unspecified respiratory virus. The two cases subsequently reported both presented following COVID-19 infection ((Van Quekelberghe *et al.*, 2022). This could suggest that this

increase in viral RNA overwhelms the cell and results in inappropriate activation of the anti-viral pathways, this also potentially explains why there is not a 100% penetrance in *EXOSC3* variants resulting in TMA, potentially highlighting the need for a trigger event to induce the phenotype, in a similar fashion to C-aHUS.

4.7. Hypothesis

I hypothesise that Exosc3 ablation in mice will result in TMA.

5. The Role of Complement Dysregulation in RNA Processing TMAs

5.1. Introduction

Following the identification of pathogenic variant in RNA processing genes resulting in TMA in humans, it was important to determine whether this represented a form of C-aHUS, or an entirely separate disease pathway.

5.2. Could EXOSC3 dysfunction result in complement activation

The clinical data from the patients presenting with EXOSC3-mediated TMA indicated this was an eculizumab non-responsive form of disease. This was determined due to lack of response seen in patient 2 and the representation of TMA in patient 1 despite adequate terminal complement blockade. In addition, both patients had undergone a full diagnostic pathway for C-aHUS (and other known forms of TMA), described above (3.1). Importantly this included the C5 eculizumab non-responsive SNP. No other complement variant or alternative cause of TMA was identified in either patient.

5.3. Could complement dysfunction result in activation of RNA surveillance pathways

The pathways that ultimately result in TMA in C-aHUS are still poorly understood. It is possible that EXOSC3 activation occurs as a result of complement dysregulation. To investigate this, bulk RNA sequencing was performed on $C3^{D1115N\ kidneys}$ (C-aHUS model) to determine if there was evidence of RNA processing dysfunction.

5.4. *RNA sequencing of $C3^{D1115N}$ mouse kidney*

To investigate gene regulation in $C3^{D1115N}$ compared to control, kidneys were isolated as described (3.8.2) and sent for RNA-Sequencing. Differential gene expression analysis in the kidney was undertaken on two pairs of mice, pair one was from Day 31 (disease and littermate control) and pair two was from Day 33 (Disease and control) mice, an additional sample pair at day 15 was sent but failed the quality control.

5.5. *Differentially expressed gene analysis*

Differentially expressed genes were analysed using Benjamini-Hochberg analysis. An adjusted p-value (false discovery rate) <0.05 and an absolute fold change of >2 was considered significant to ensure stringent analysis with a manageable number of differentially expressed genes.

A total of 378 genes were significantly differentially expressed (307 down regulated, 71 upregulated) using these conditions.

QIAGEN IPA core analyses were performed with significantly differentially expressed genes, as described (Krämer *et al.*, 2014).

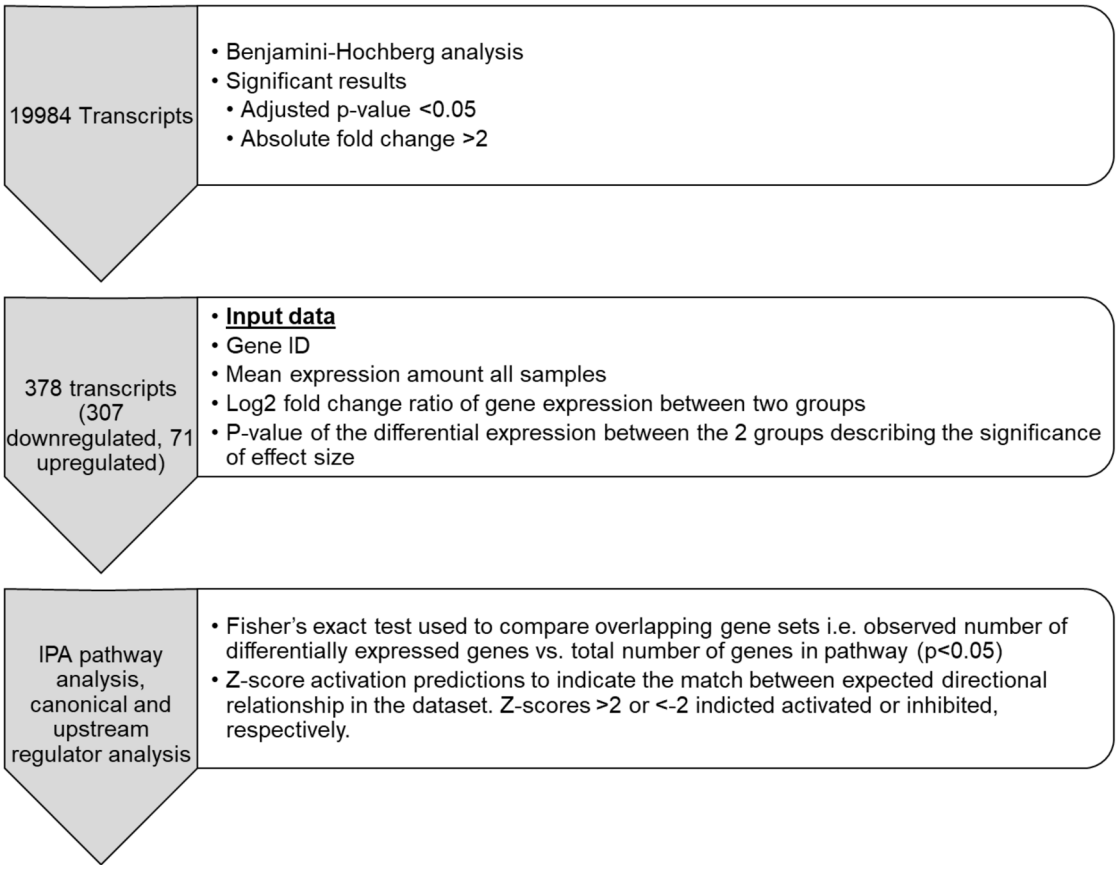

Figure 5-1: Differential gene expression analysis of $C3^{D1115N/\,D1115N}$ vs. Wild type.

A total of 378 transcripts were significantly differentially expressed between the two groups. IPA analysis was used to generate pathways that were significantly affected.

5.6. Canonical pathway analysis

5.6.1. RNA surveillance pathways

Following the discovery of *EXOSC3, POLR3, RNU4ATAC* and *TSEN2* variants in TMA, the differentially expressed genes data was examined to determine if there any evidence of changes in RNA surveillance genes in this mouse model of C-aHUS. In this data set there was no evidence of changes in any RNA surveillance genes, this with the clinical data that the patients did not respond to eculizumab suggests that the underlying mechanism of these TMAs is complement independent.

5.6.2. Significantly altered pathways

Canonical pathway analysis was performed on the samples to determine if there were any pathways that were significantly changed. This identified a number of overlapping pathways that were altered in the $C3^{D1115N}$ mouse compared to littermate controls (Figure 5-2). The pathways that were most upregulated were acute phase reactants, such as pathogen induced cytokine storm, acute phase response, Il-6 and IL-10 pathways. Additionally, there was significant upregulation of the coagulation pathway, in keeping with the phenotype observed. There were a number of pathways that showed down regulation including a number of metabolic pathways, including adipose and hepatic fibrosis pathways, the relevance of this on the whole body are unclear as mRNA was only generated from the kidney.

Analysis of individual pathways, specifically acute phase response and coagulation pathways revealed differential regulation of a number of genes that are involved in these pathways (Table 5-2).

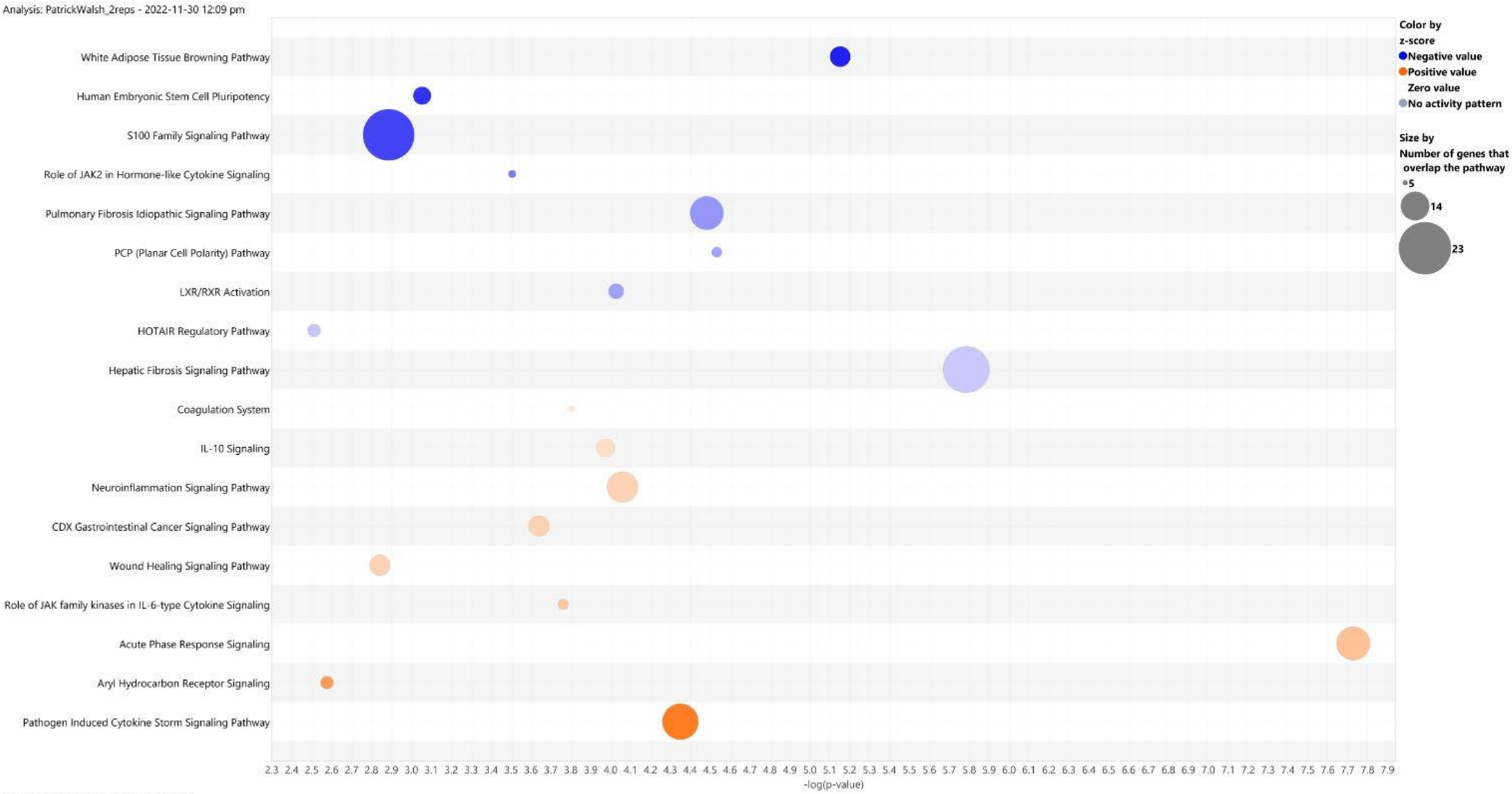

Figure 5-2: Bubble chart of differentially expressed gene pathways in $C3^{D1115N}$ mouse with HUS compared to littermate control.

X-axis Log score (p-value) calculated with Fisher exact analysis, $p<0.05$ considered significant. The Fisher's exact test tests whether the overlap between the two genes sets the observed gene set and the genes within a certain pathway is statistically significant. The size of the bubble indicates the number of genes differentially expressed. Finally, the colour represents the z-score activation indicates the match between the expected directional relationship and the observed gene expression in the dataset. Red represents activation and blue represents inhibition.

Gene	Gene Name	Log Ratio
CRABP2	cellular retinoic acid binding protein 2	-4.818
RBP4	retinol binding protein 4	-2.248
VWF	von Willebrand factor	-1.981
RBP7	retinol binding protein 7	-1.942
HP	Haptoglobin	-1.564
SERPINA3	serpin family A member 3	-1.242
TF	Transferrin	-1.191
FGA	fibrinogen alpha chain	1.381
JUN	Jun proto-oncogene, AP-1 transcription factor subunit	1.547
SERPINA1	serpin family A member 1	1.556
SOCS3	suppressor of cytokine signalling 3	1.718
HMOX1	heme oxygenase 1	1.987
SERPINE1	serpin family E member 1	2.243
IL1RN	interleukin 1 receptor antagonist	2.698
FOS	Fos proto-oncogene, AP-1 transcription factor subunit	2.895
IL36A	interleukin 36 alpha	4.302

Table 5-1: Differentially expressed genes within the acute phase response canonical pathway

Log ratio of change from control expression (Benjamini-Hochberg) negative values indicating downregulation, positive values indicate upregulation.

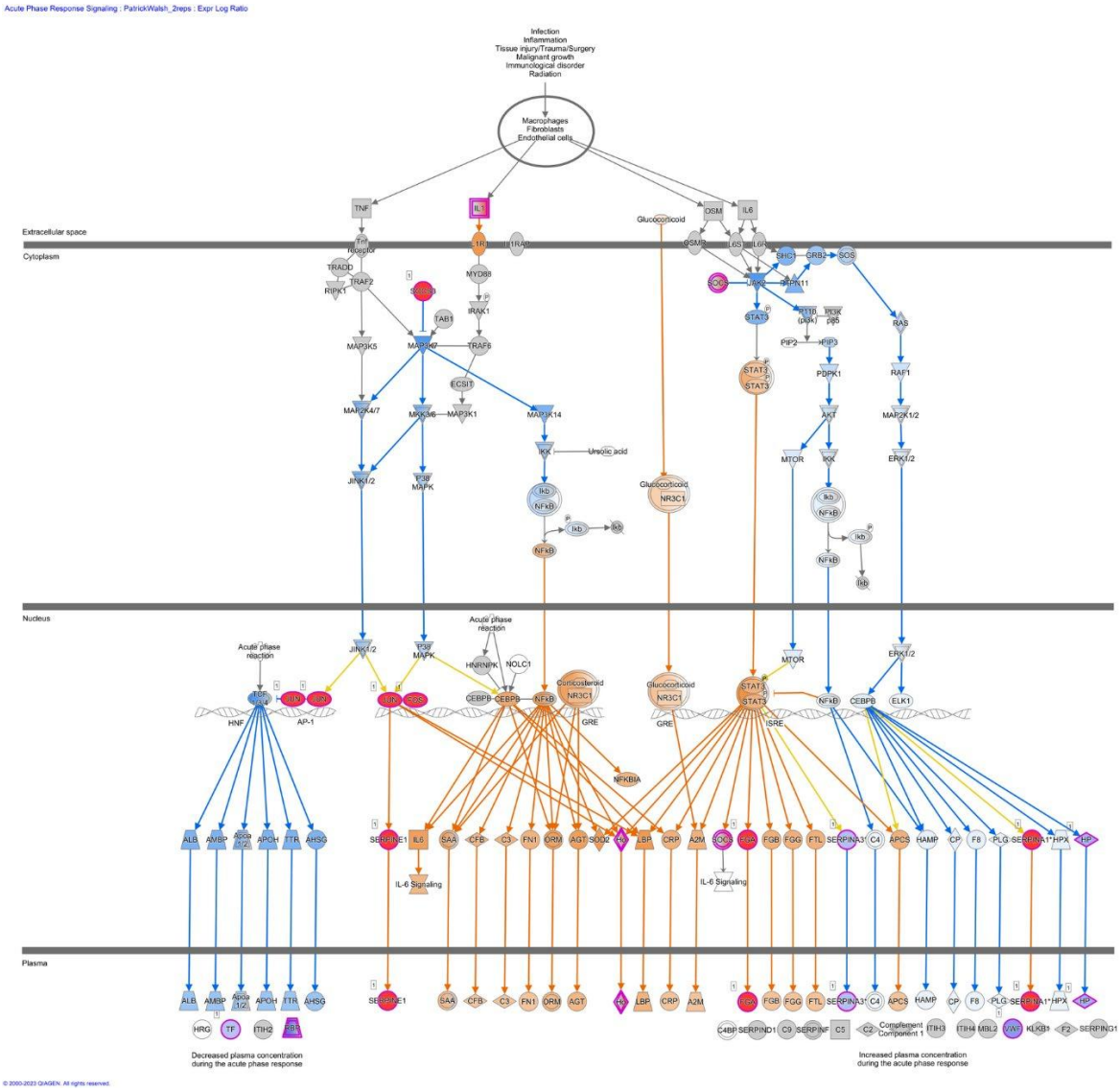

Figure 5-3: IPA of Acute Phase Response canonical pathway.

Dark red shading indicates genes that have been measured to increase, orange indicates genes that are predicted to increase due to the measured response. Orange arrows indicate upregulation of the downstream molecule as a result of the measured gene response. Blue with purple border indicates genes that have been measured to decrease. Pale blue indicates genes that are predicted to decrease due to the measured response. Blue arrows indicate downregulation of the downstream molecule as a result of the measured gene response. Yellow arrows indicate opposite regulation change compared to the expected change. Pathway indicates that the C3D1115N variant results in activation of IL1 signalling leading to Jun proto-oncogene, AP-1 transcription factor subunit and Fos proto-oncogene, AP-1 transcription factor subunit; and suppression of JAK2 due to activation of suppressor of cytokine signalling 3 (SOCS3), resulting in STAT phosphorylation, inhibition of NFκB and ERK1. These changes result in the observed acute phase response changes, specifically decreased levels of transferrin, serpin family A member 3, retinol binding protein 4 & 7, haptoglobin and von Willebrand factor. Increased acute phase genes including serpin family E member 1, fibrinogen alpha chain and serpin family A member 1.

Gene	Gene Name	Log Ratio
F5	coagulation factor V	1.534
FGA	fibrinogen alpha chain	1.381
SERPINA1	serpin family A member 1	1.556
SERPINE1	serpin family E member 1	2.243
VWF	von Willebrand factor	-1.981

Table 5-2: Differentially expressed genes within the coagulation canonical pathway

Log ratio of change from control expression (Benjamini-Hochberg) negative values indicating downregulation, positive values indicate upregulation.

5.7. Discussion

The differentially expressed gene analysis in the $C3^{D1115N}$ mouse demonstrated upregulation of acute phase proteins, including cytokines IL1 and IL36 as well as pro-coagulant genes FGA, Serpin genes and downregulation of vWf. Increased cytokine expression has previously been reported in STEC-HUS (including TNFα, IL1, IL6) (Litalien *et al.*, 1999; Ramos *et al.*, 2016; Exeni *et al.*, 2018; Pineda *et al.*, 2021). There is a well-documented link between complement activation and coagulation (Schmidt *et al.*, 2022), which is seen in TMA.

RNA-sequencing data is available from kidneys from a mouse model in which mouse C3 has been replaced with human C3, i.e. humanised C3 model ($C3^{Hu}$) (Devalaraja-Narashimha *et al.*, 2021). This model develops spontaneous complement activation resulting in C3 glomerulopathy, a disease in which there is extensive C3 deposition within the kidney leading to chronic kidney disease. RNA-sequencing data from this mouse showed similarities to the $C3^{D1115N}$ model. This model showed increase differential gene expression of genes in the IL-6, inflammation and coagulation pathways as was seen in the $C3^{D1115N}$ model. Both

the $C3^{Hu}$ and $C3^{D1115N}$ had downregulation in adipose metabolism pathways. It has been well documented that complement is intertwined with lipid metabolism, with C3 being central to this process reviewed in (Barbu *et al.*, 2015). Whilst exploration of this phenotype was outside the scope of this work it is of interest that both the $C3^{D1115N}$ and $C3^{Hu}$ models show significant downregulation in these metabolic pathways and potentially could be utilised to further investigate the contribution of C3 to lipid metabolism. The nature of the bulk sequencing performed on the $C3^{D1115N}$ mouse means it is not possible to be certain what cells are responsible for changes seen in the differential gene expression data. This may be relevant for the changes seen in vWf, the differential gene expression data demonstrates downregulation; however vWf deposition is increased in the $C3^{D1115N}$ mouse detected by immunofluorescence. The reason for this discrepancy is not entirely clear, it may be that local production of vWf is decreased in the $C3^{D1115N}$ glomerular endothelial cells, while systemically there is increase in vWf production that is then deposited on the endothelial surface. One way to answer questions about cellular contribution to differential gene expression would be to perform single cell RNA-Sequencing, or spatial transcriptomics to learn more about the contribution of cell types to the phenotype seen in these mice.

Previous total RNA sequencing data from RNA exosome deficient zebrafish (Müller *et al.*, 2020) has demonstrated upregulation of ncRNA, including snoRNA, snRNA and rRNA, RNA species that are involved in the ribosome biogenesis pathways. rRNA biogenesis defects result in upregulation of p53 mediated apoptosis and result in cell cycle arrest (Fumagalli *et al.*, 2012). These changes were seen in this zebrafish model, confirming the effects of rRNA biogenesis dysfunction as a result of RNA exosome knockout.

A cohort of children with aHUS due to hypomorphic *TSEN2* has recently been reported (Canpolat *et al.*, 2022). RNA sequencing data from one of these children demonstrated upregulation in cell cycle, ribosome and shigellosis pathways, potentially highlighting a link between RNA processing dysfunction and STEC-HUS (i.e. shigellosis) as previously eluded to (4.5.2).

Interestingly, neither the RNA exosome model nor the *TSEN2* data showed any differential change in complement expression and the $C3^{D1115N}$ data showed no changes in RNA processing, suggesting that these are two separate pathways resulting in TMA.

6. The Effects of Temporal Exosc3 Knock-down in a Mouse Model

6.1. *Exosc3$^{fl/fl}$.Rosa26Cre^{ERT2}*

To determine whether the observed TMA phenotype developed in mice following whole body Exosc3 knock-out mice were bred with the B6.129-Gt(ROSA)26Sor$^{tm1(cre/ERT2)Tyj}$/J (Rosa26Cre^{ERT2}). The first breeding round was performed to generate *Exosc3$^{fl/fl}$* mice and *Exosc3^{fl}* and *Rosa26Cre^{ERT2}* mice. These mice were bred to generate *Exosc3$^{fl/fl}$*.Rosa26Cre^{ERT2} mice that would enable Exosc3 knock-out following tamoxifen treatment (Figure 6-1). Previous work performed on *ex vivo* model of this mouse had demonstrated this was sufficient to cause Exosc3 knock-out in B cells (Pefanis *et al.*, 2014).

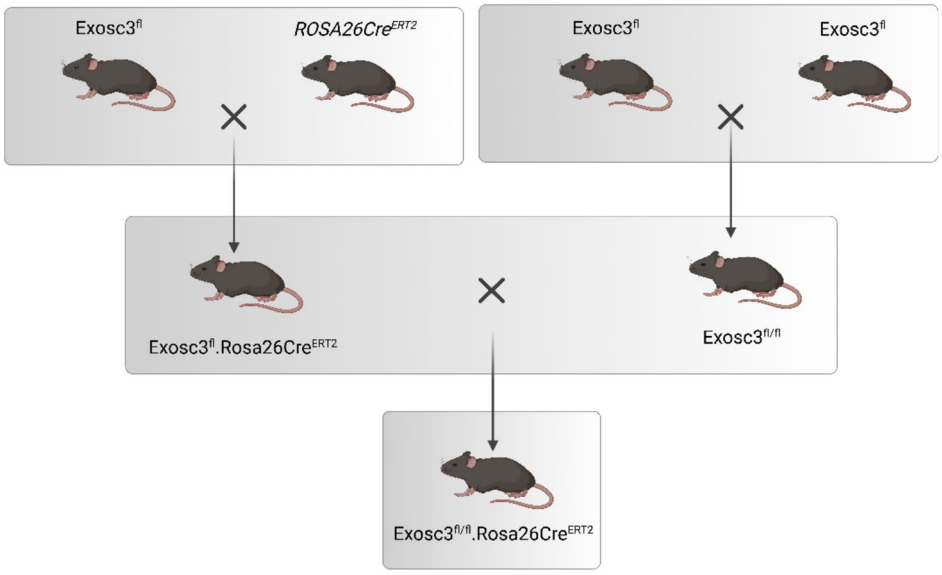

Figure 6-1: Exosc3$^{fl/fl.}$Rosa26Cre^{ERT2} Breeding strategy.

The first breeding round was performed to generate Exosc3^{fl}.Rosa26Cre^{ERT2} these mice were bred with Exosc3$^{fl/fl}$ mice, this breeding round generated Exosc3$^{fl/fl}$.Rosa26Cre^{ERT2} mice.

6.1.1. *Exosc3^{fl} Genotyping*

Genotyping of mice was performed on ear punch biopsies as described (3.7.2). This allowed discrimination and selection of wild-type, Exosc3^{fl} and Exosc3$^{fl/fl}$ mice to be performed.

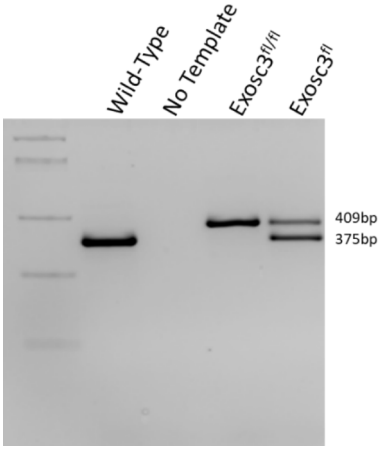

Figure 6-2: Exosc3 genotyping PCR

Genotyping was performed on ear punch biopsies and separated on 2% agarose TAE gel. Ladder Generuler 1Kb, Homozygous Exosc3$^{fl/fl}$ single band at 409bp, wild-type single band at 375bp, heterozygous bands at 409bp and 375bp.

6.1.2. *Rosa26Cre^{ERT2} Genotyping*

Genotyping of mice was performed on ear punch biopsies as described (3.7.2).

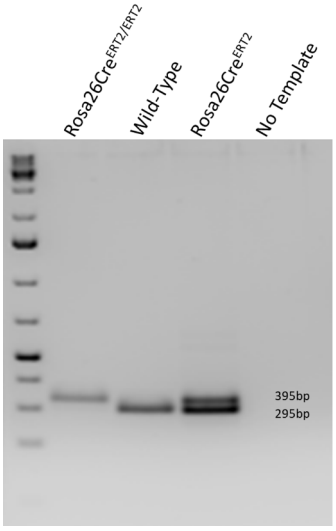

Figure 6-3: Rosa26Cre^{ERT2} genotyping PCR

Genotyping was performed on ear punch biopsies and separated on 2% agarose TAE gel. Ladder Generuler 1Kb plus, Homozygous Rosa26Cre^{ERT2} single band at 395bp, wild-type single band at 295bp, heterozygous bands at 295bp and 395bp.

6.1.3. Phenotype of *Exosc3*$^{gfp/gfp}$*.Rosa26Cre*^{ERT2}

Following standard tamoxifen induction (75mg/Kg/d I.P. for 4 days) mouse weights and condition score were recorded daily (3.3.5). Any mice recording a score of 15 or more on the clinical scoring matrix were considered to have reached maximal permitted harm and were euthanised. Following this standard tamoxifen protocol there was clear evidence of recombination, as measured by GFP positivity, but mice remained healthy without any evidence of disease at 1 month post recombination. *Rosa26Cre*$^{ERT2/ERT2}$ and *Exosc3*$^{fl/fl}$ mice were also treated with tamoxifen as controls, these showed no evidence of GFP positivity or a phenotype up to 1 month post treatment.

6.1.4. GFP positivity

Successful recombination was tracked utilising the GFP signal that was expressed in cells that had undergone inversion (Figure 6-4). Splenocytes were used as an easily accessible tissue to track recombination in cells. Following treatment with tamoxifen the GFP positivity in splenocytes in the *Exosc3*$^{gfp/gfp}$*.Rosa26Cre*^{ERT2} was 69.24%±1.6 (Figure 6-4). The absence of an obvious phenotype in these mice could be due to a lower level of cre in mice carrying a single copy of Rosa26 (Figure 6-8). Mice were bred to *Rosa*26*Cre*$^{ERT2/ERT2}$ to determine whether this was sufficient to generate a phenotype.

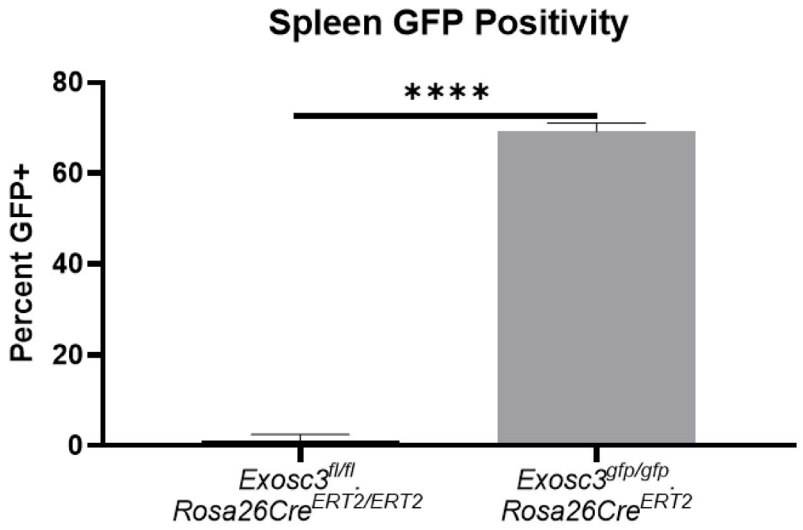

Figure 6-4 Splenocytes GFP positivity following 4 days tamoxifen treatment.

Single cell suspension was generated via mechanical disruption of spleen, followed by red cell lysis. 1x10^{6}cells were stained with viability dye. GFP positivity was detected via flow cytometry, after gating out debris, doublets and dead cells (n=3 in all groups). GFP positive cells, represent cells that have undergone recombination and inversion of the floxed region to put GFP in sense orientation. Unpaired t-test used to analyse.

6.2. *Exosc3$^{fl/fl}$.Rosa26Cre$^{ERT2/ERT2}$*

To generate mice homozygous for both *Exosc3$^{fl/fl}$* and *Rosa26Cre$^{ERT2/ERT2}$* the following breeding strategy was used (Figure 6-5). *Exosc3$^{fl/fl}$*.Rosa26Cre$^{ERT2/ERT2}$ mice were then inter-crossed to maintain homozygosity in subsequent breeding.

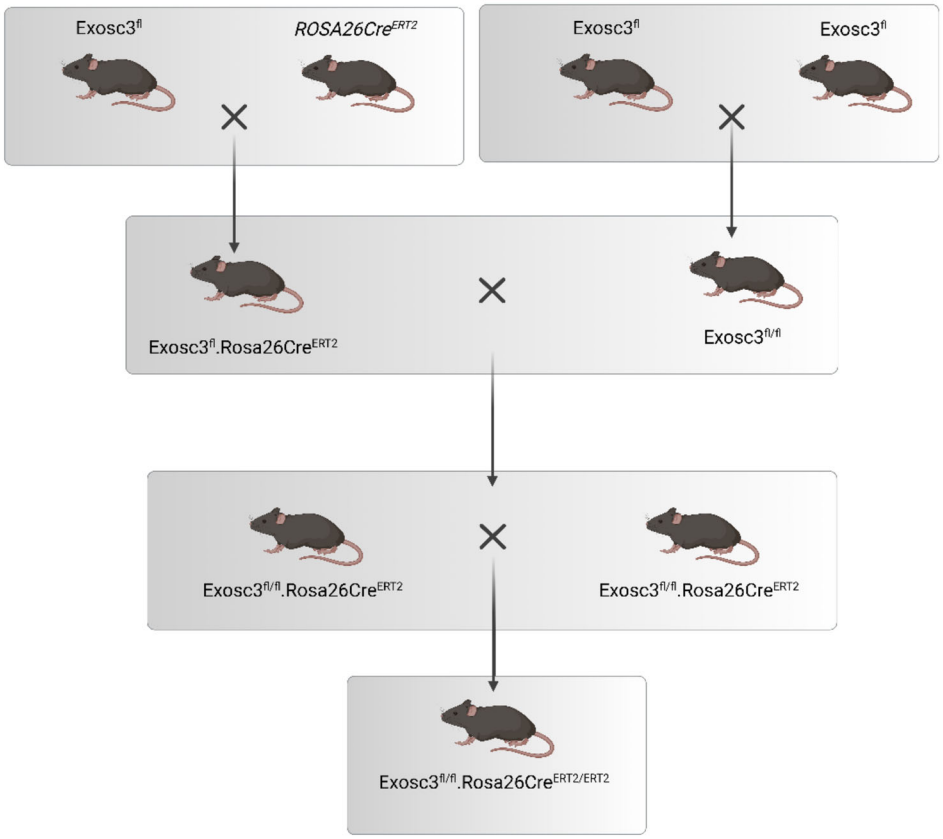

Figure 6-5 Breeding strategy for Exosc3$^{fl/fl}$.Rosa26Cre$^{ERT2/ERT2}$

The first breeding round was performed to generate Exosc3^{fl}.Rosa26Cre^{ERT2} these mice were bred with Exosc3$^{fl/f}$ mice, this breeding round generated Exosc3$^{fl/fl}$.Rosa26Cre^{ERT2}. Exosc3$^{fl/fl}$.Rosa26Cre^{ERT2} and Exosc3$^{fl/fl}$.Rosa26Cre^{ERT2} were bred together to generate Exosc3$^{fl/fl}$.Rosa26Cre$^{ERT2/ERT2}$ mice.

6.2.1. Phenotype of *Exosc3$^{gfp/gfp}$.Rosa26Cre$^{ERT2/ERT2}$*

Following standard tamoxifen treatment mice were tracked using the clinical monitoring scoring matrix (3.3.5). All mice lost weight, had a reduction in body condition score, had loose stools and reduced activity at 8 days ±2 following commencing treatment and had to be euthanised.

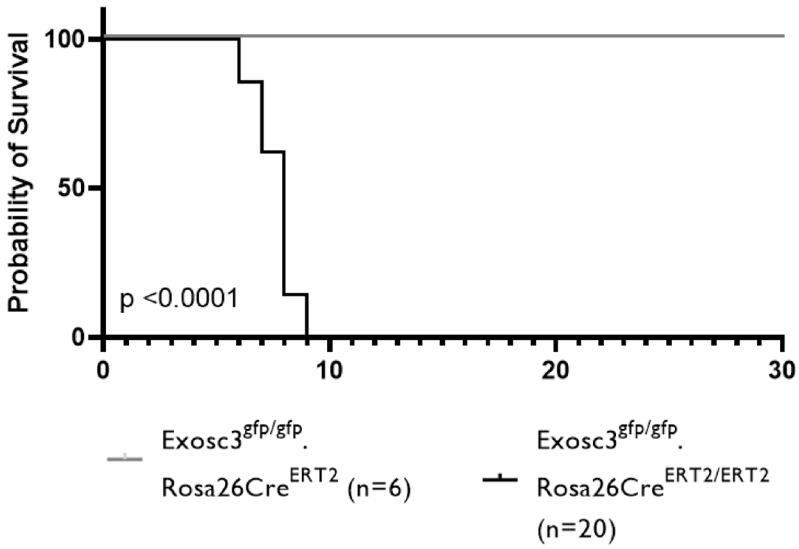

Figure 6-6: Survival analysis following standard tamoxifen treatment

Four days of I.P. tamoxifen at 75mg/Kg. All Exosc3$^{gfp/gfp}$.Rosa26Cre^{ERT2} mice survived out to one month following tamoxifen treatment. All Exosc3$^{gfp/gfp}$.Rosa26Cre$^{ERT2/ERT2}$ mice died or reached the predefined clinical score with a mean survival of 8 days following tamoxifen treatment. Mantel-Cox analysis was used to calculate difference between the groups.

6.2.2. GFP positivity in *Exosc3$^{gfp/gfp}$.Rosa26Cre$^{ERT2/ERT2}$*

Following tamoxifen treatment in *Exosc3$^{gfp/gfp}$.Rosa26Cre$^{ERT2/ERT2}$* mice the mean GFP positivity in splenocytes was 95.89%±0.995 (Figure 6-7). This compared to 69.24%±1.6 in *Exosc3$^{gfp/gfp}$.Rosa26Cre^{ERT2}* mice. These results indicate that the phenotype only became apparent once a certain proportion of cells had undergone recombination, this was further explored by varying the tamoxifen dosage to determine the level of recombination required to demonstrate a phenotype (6.2.3).

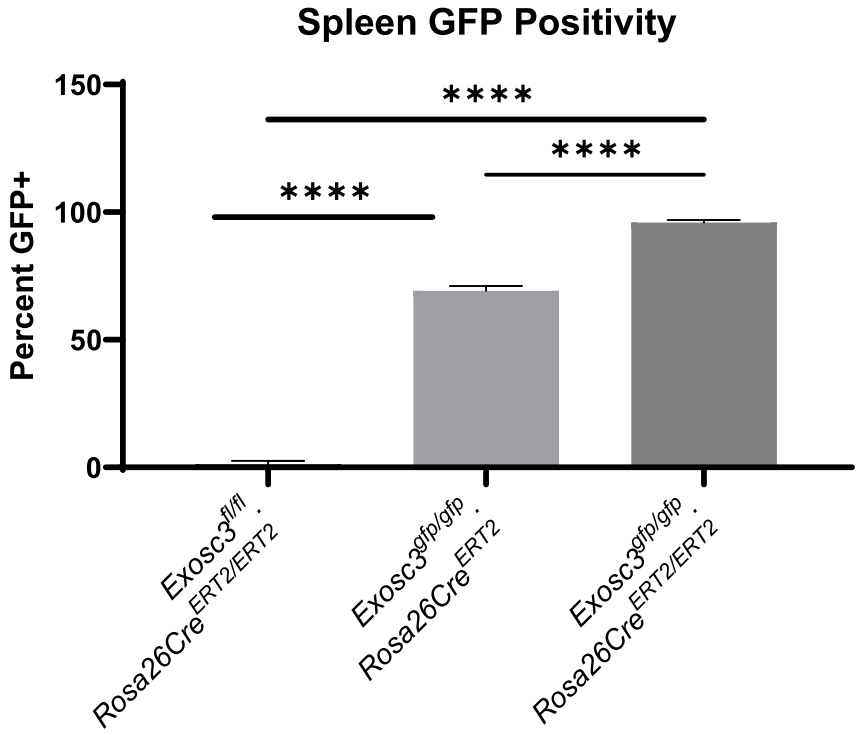

Figure 6-7 GFP positive Splenocytes

Single cell suspension was generated via mechanical disruption of spleen, followed by red cell lysis. 1x10^{6}cells were stained with viability dye. GFP positivity was detected via flow cytometry, after gating out debris, doublets and dead cells (n=3 in all groups). GFP positive cells, represent cells that have undergone recombination and inversion of the floxed region to put GFP in sense orientation. Unpaired t-test used to analyse

6.2.2.1. Cre qPCR

The *Exosc3*$^{gfp/gfp}$.*Rosa26Cre*^{ERT2} mice had lower levels of recombination than *Exosc3*$^{gfp/gfp}$.*Rosa26Cre*$^{ERT2/ERT2}$ mice as determined by GFP positivity (Figure 6-4), this explained the absence of a phenotype in these mice. One possible explanation for this is that a single Cre allele results in reduced mRNA (and therefore protein). To determine this RNA was isolated from kidney in *Exosc3*$^{fl/fl}$, *Exosc3*$^{gfp/gfp}$.*Rosa26Cre*^{ERT2}, *Exosc3*$^{gfp/gfp}$.*Rosa26Cre*$^{ERT2/ERT2}$ mice and RT-qPCR was performed. Higher *Cre* mRNA was detected in *Exosc3*$^{gfp/gfp}$.*Rosa26Cre*$^{ERT2/ERT2}$ compared to *Exosc3*$^{gfp/gfp}$.*Rosa26Cre*^{ERT} . Potentially explaining the difference in phenotype between the mice.

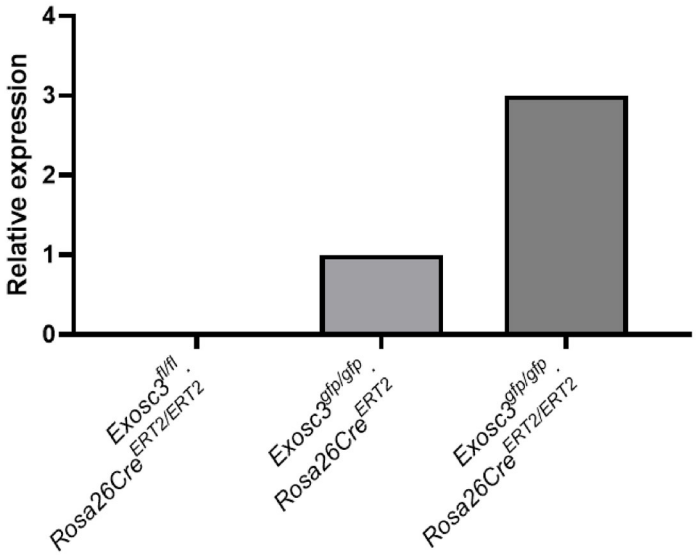

Figure 6-8: qPCR results for Cre mRNA from kidneys of mice (n=1).

Demonstrating increased levels of cre mRNA in mice with 2 copies of Rosa26CreERT2 alleles. RNA generated from flash frozen kidneys using Trizol. Following this RNA was treated with Turbo DNA-free kit to remove residual gDNA. cDNA generated using Superscript III. TaqMan RT-qPCR was performed using Cre specific primer and probes, with β-Actin used as housekeeper to normalise.

6.2.3. Exosc3 measurement

The inclusion of the anti-sense GFP in the *Exosc3^{fl}* mouse allows cells that have undergone recombination to be tracked. However, this is used as a surrogate marker for Exosc3 deletion. It is preferable to measure Exosc3 directly.

6.2.3.1. PCR to detect recombination

Standard PCR was design to detect Exosc3 recombination (3.7.2). The PCR was designed with an anti-sense primer in intron 2 and exon 4. Prior to recombination no product is produced, following recombination and inversion the reverse primer is inverted, allowing for a product

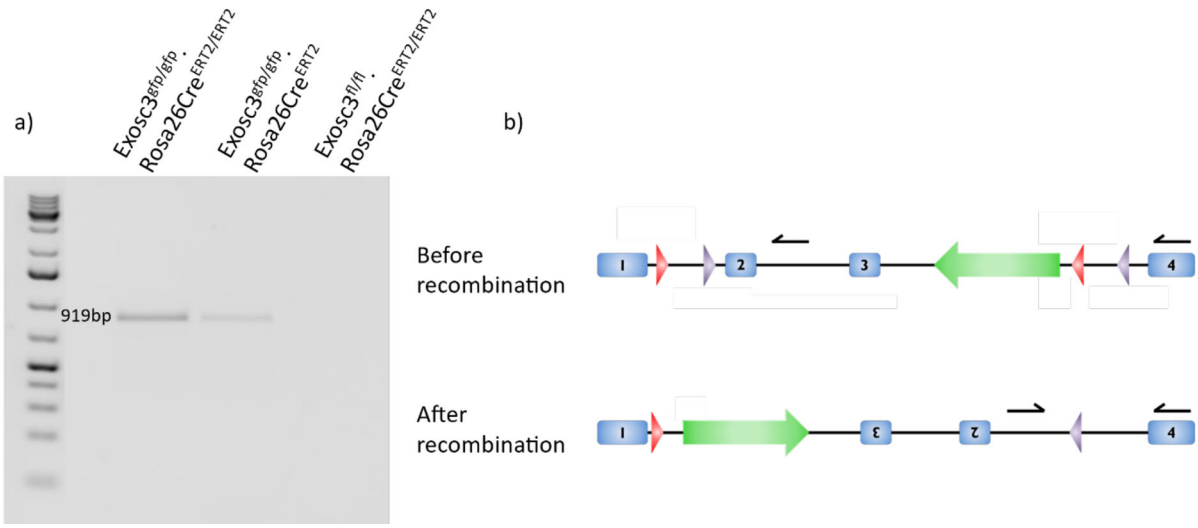

Figure 6-9: Exosc3 recombination PCR

a) Genotyping was performed on ear punch biopsies and separated on 2% agarose TAE gel. Ladder Generuler 1Kb plus, Exosc3$^{gfp/gfp}$.Rosa26Cre$^{ERT2/ERT2}$ single band at 919bp, Exosc3$^{gfp/gfp}$.Rosa26Cre^{ERT2} single band at 919bp, Exosc3$^{fl/fl}$.Rosa26Cre$^{ERT2/ERT2}$ no product produced. b) Primer design: prior to recombination both primers are in an anti-sense orientation with ~2.5Kb between the primers. Following cre-mediated recombination and inversion the primer pair are situated closer together and able to produce a product.

6.2.3.2. qPCR to detect Exosc3 mRNA levels

To determine whether the GFP signal observed in the *Exosc3$^{gfp/gfp}$.Rosa26Cre$^{ERT2/ERT2}$* mice resulted in disruption of Exosc3 mRNA RT-qPCR was performed. This demonstrated reduced Exosc3 in the kidney, brain and bone marrow (Figure 6-10). Given the nature of the whole tissue protein lysate used it is not possible to determine whether this reduction was across all cell types within the tissues tested or whether this represented biallelic disruption in cells or whether only a single allele had been affected. It is clear from this data that there is complete knockout is not seen in all tissues following recombination.

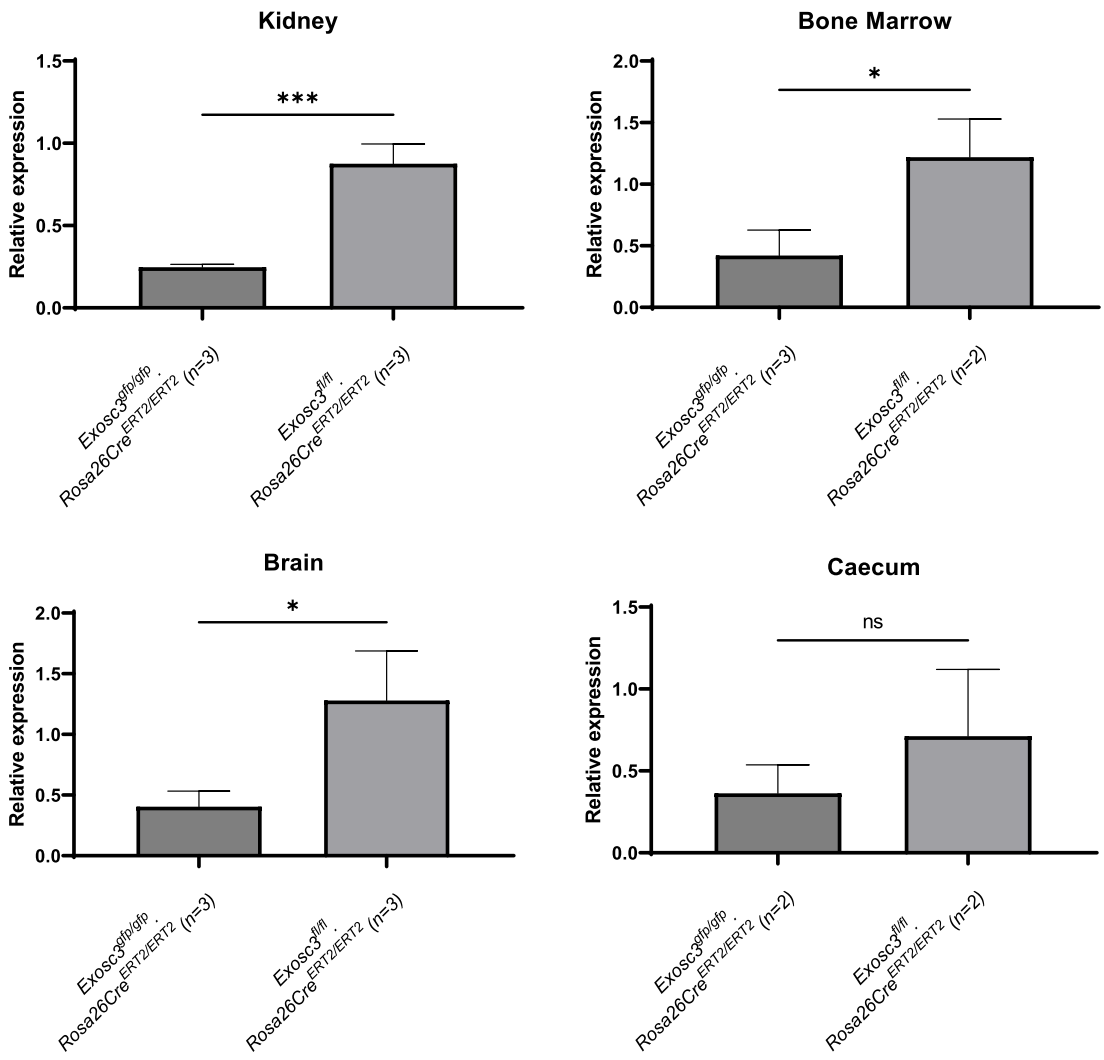

Figure 6-10: Exosc3 mRNA expression from various tissues

RNA was extracted from snap frozen tissue using Trizol and cDNA transcribed as per manufacturer's instructions. Taqman PCR was performed using the appropriate universal probe (Roche) and specific primers. Exosc3 mRNA was reduced in Exosc3$^{gfp/gfp}$.Rosa26Cre$^{ERT2/ERT2}$ kidney, brain, and bone marrow, confirming Exosc3 knockdown. Unpaired t-test used to analyse between groups

6.2.3.3. Western blot

Following the demonstration of reduced Exosc3 mRNA in the *Exosc3$^{gfp/gfp}$.Rosa26Cre$^{ERT2/ERT2}$* mouse, western blot was performed to determine whether there was evidence of reduced Exosc3 protein expression. Following generation of protein lysate from the kidney different conditions were trialled in an attempt to detect protein expression, including a monoclonal antibody (Abcam) and a polyclonal antibody (Proteintech) at varied concentrations (1/100 – 1/4000). Exosc3 expression could not be demonstrated in either *Exosc3$^{fl/fl}$Rosa26Cre$^{ERT2/ERT2}$ or Exosc3$^{gfp/gfp}$Rosa26Cre$^{ERT2/ERT2}$.*

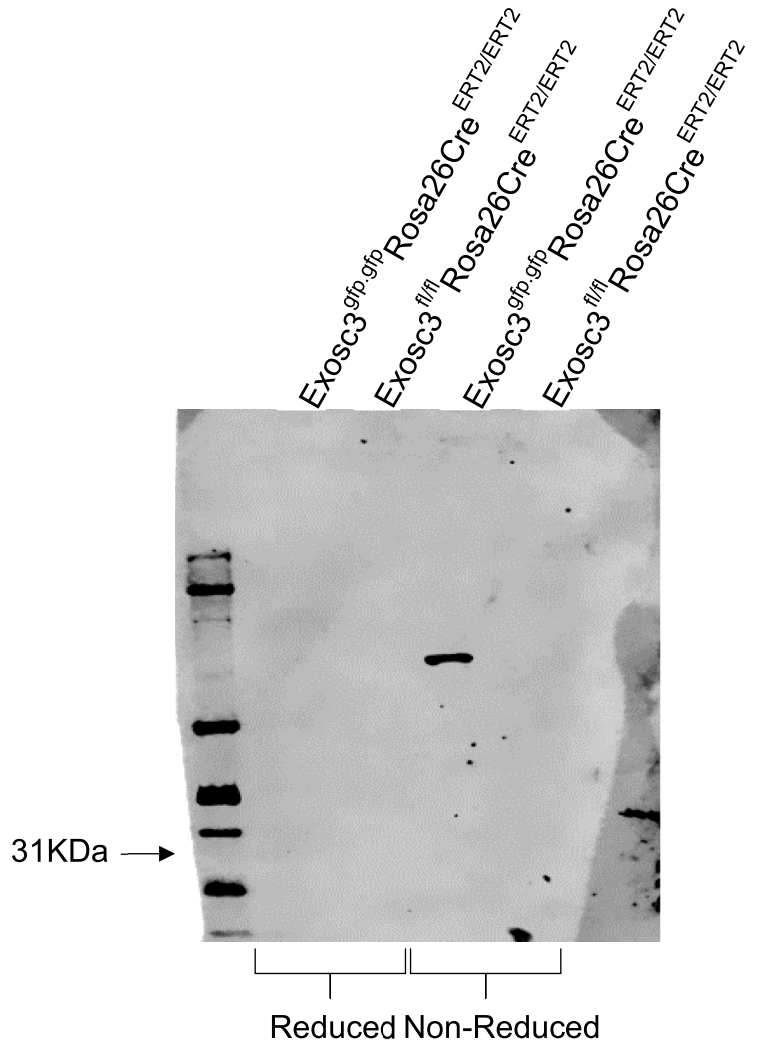

Figure 6-11: Western Blot using Polyclonal antibody

Whole kidney protein lysate from mice was generated using RIPA buffer. 30 µl of protein lysate was added to either reducing or non-reducing buffer at appropriate concentration and SDS-Page performed, following transfer the blot was washed and incubated with 1:1000 Exosc3 Polyclonal antibody in 5% milk TBST overnight at 4°C. Following further washes and incubation with Goat anti-Rabbit HRP for one hour at room temperature. The signal was developed with ECL and imaged using Licor OdysseyFc. No protein was detected at the predicted molecular weight of 31KDa in the $Exosc3^{fl/fl}Rosa26Cre^{ERT2/ERT2}$ *or* $Exosc3^{gfp/gfp}Rosa26Cre^{ERT2/ERT2}$ *in the reduced or non-reduced samples. In* $Exosc3^{gfp/gfp}Rosa26Cre^{ERT2/ERT2}$ *non-reduced sample a band was evident at ~75KDa, this potentially represents non-specific immunoglobulin, rather than specific Exosc3 binding*

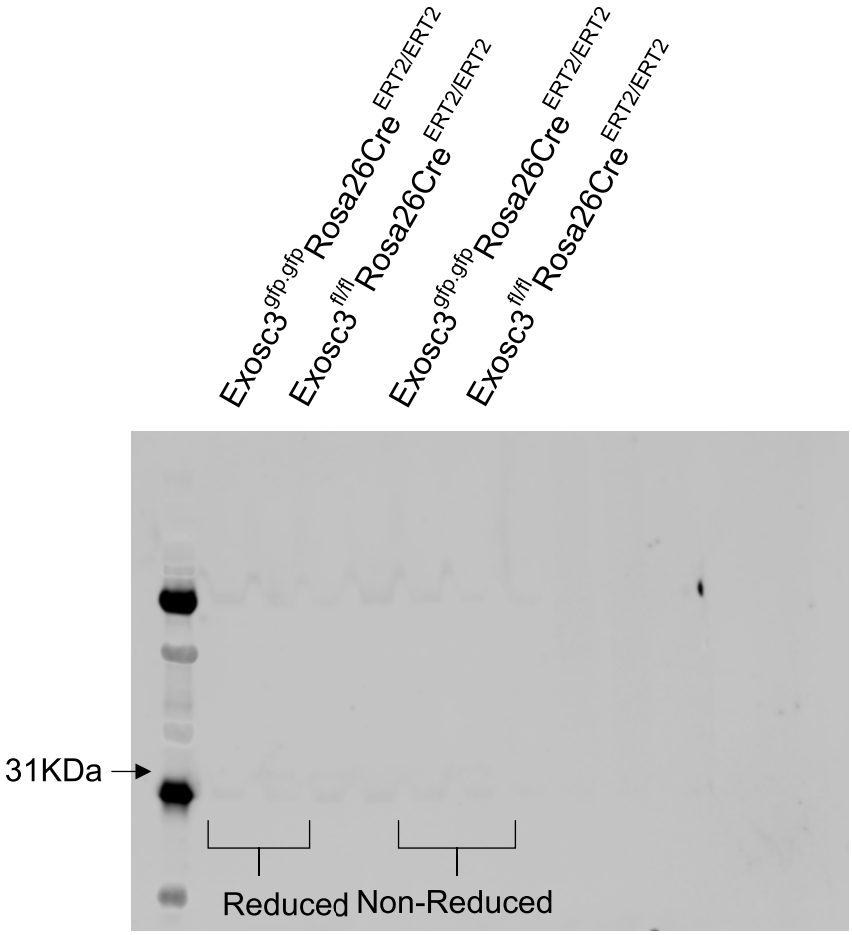

Figure 6-12: Western Blot using Monoclonal antibody

Whole kidney protein lysate from mice was generated using RIPA buffer. 30 µl of protein lysate was added to either reducing or non-reducing buffer at appropriate concentration and SDS-Page performed, following transfer the blot was washed and incubated with 1:1000 Exosc3 Monoclonal antibody in 5% milk TBST overnight at 4°C. Following further washes and incubation with Goat anti-Rabbit HRP for one hour at room temperature. The signal was developed with ECL and imaged using Licor OdysseyFc. No protein was detected at the predicted molecular weight of 31KDa in the Exosc3$^{fl/fl}$Rosa26Cre$^{ERT2/ERT2}$ or Exosc3$^{gfp/gfp}$Rosa26Cre$^{ERT2/ERT2}$ in the reduced or non-reduced samples.

6.2.3.4. Summary of methods of Exosc3 detection

The data presented above demonstrate successful recombination as detected by detection using standard PCR and reduced expression of Exosc3 mRNA. However, it was not possible to demonstrate protein expression, this was despite trying multiple different conditions and concentrations of the primary antibody (including 10 times the recommended concentrations). Both antibodies used have previously been demonstrated to detect Exosc3 by Western blot. This needs further optimisation to detect Exosc3 protein. However, during this project tracking with GFP was performed as a surrogate for Exosc3 depletion due to the fact that mice developed a phenotype associated with Exosc3 ablation and *Exosc3* disruption was demonstrated on a gRNA and mRNA level.

6.2.4. Optimisation of tamoxifen dosing

Previous data on tamoxifen induced cre-recombination has demonstrated that five days of tamoxifen at a dosage of 75mg/Kg I.P. is sufficient to achieve recombination. To determine whether it was possible to regulate the number of cells undergoing recombination and therefore allow a milder phenotype and therefore investigate a more chronic Exosc3 deficiency, the duration/dose of tamoxifen treatment was investigated. Mice were treated for 1 – 5 days. Mice treated for 1 or 2 days showed reduced level of recombination, with no observable phenotype. Mice treated for 4 and 5 days demonstrated no discernible difference between their phenotype (Figure 6-36). 75% (9/12) mice that were treated with 3 days of tamoxifen survived beyond 10 days (Figure 6-35). Some of these mice were aged to one year post treatment (6.2.14). Based on these results, 4 days of tamoxifen was used to ensure efficient recombination, whilst limiting the potential side effects of excessive tamoxifen.

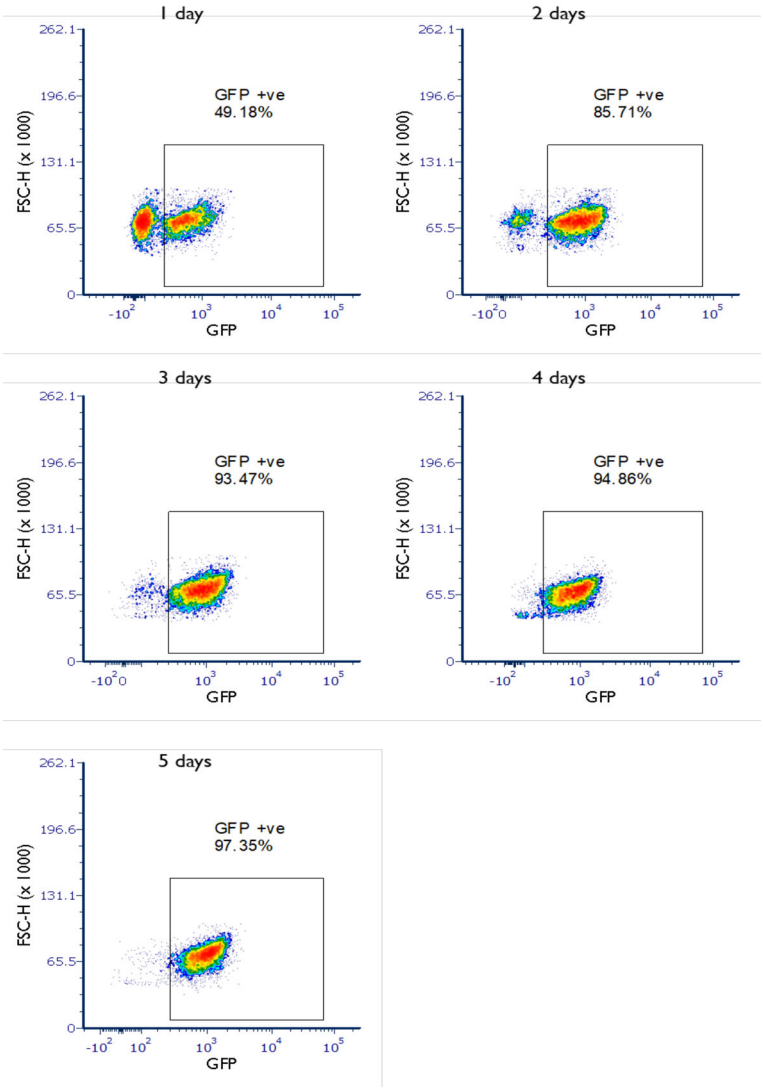

Figure 6-13: GFP positivity in Exosc3$^{gfp/gfp}$.Rosa26Cre$^{ERT2/ERT2}$ splenocytes treated with 75mg/Kg Tamoxifen I.P. for 1-5 days.

Splenocytes were isolated via mechanical disruption, following red cell lysis and washing, cells were stained with viability marker. Flow cytometry was performed on 1x10^6 cells, gating strategy was performed to exclude cellular debris, dead cells and doublets. Total GFP was calculated. Following eight days of treatment there was GFP expression in all samples, with an increase in the proportion of GFP positive cells with increasing duration of treatment.

6.2.5. Gross histological examination

To understand the phenotype in *Exosc3*$^{gfp/gfp}$*.Rosa26Cre*$^{ERT2/ERT2}$ mice histological examination on the mice was performed. Following Exosc3 ablation, these mice developed pathology in the intestine, bone marrow and thymus (i.e. cells with a fast turnover time), within the bone marrow and thymus there was evidence of reduced

cellularity, and the intestine showed evidence of proliferative colitis, with loss of villi (Figure 6-14). Kidneys were examined to determine whether the findings in humans were recapitulated in this mouse model, there were no remarkable findings in the kidney following Exosc3 ablation.

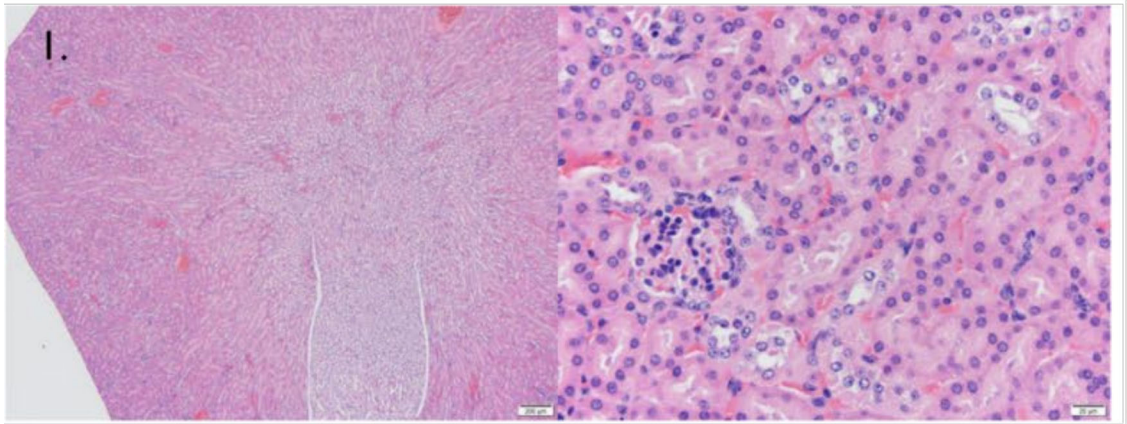
1.

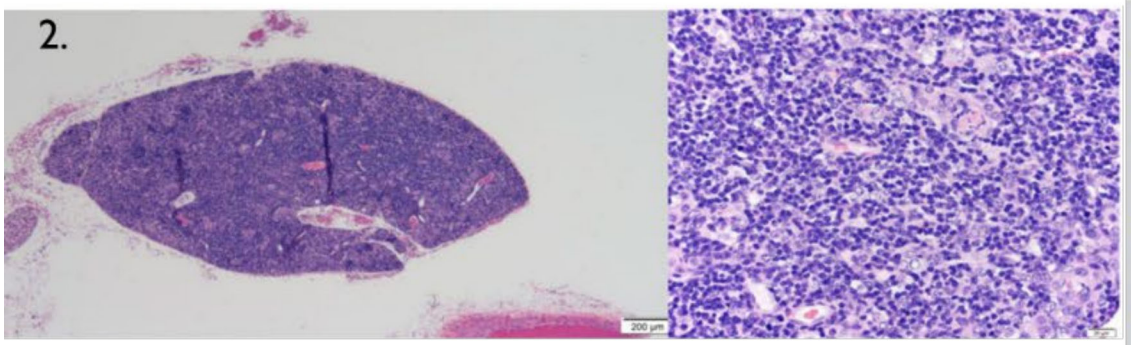
2.

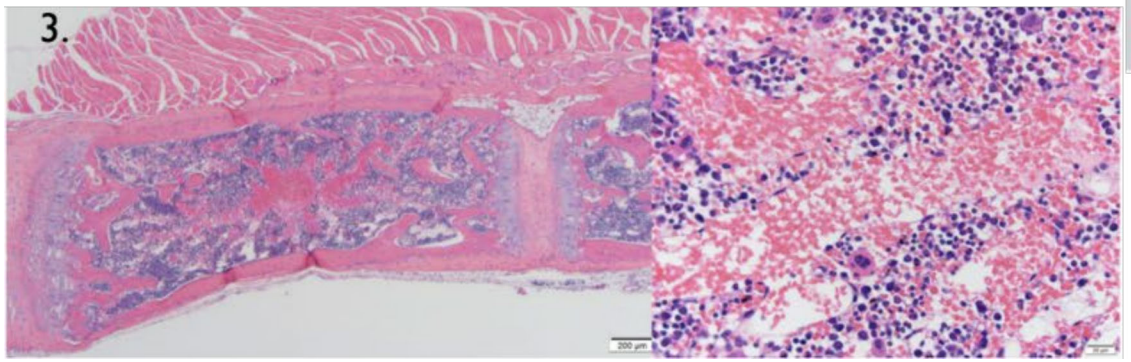
3.

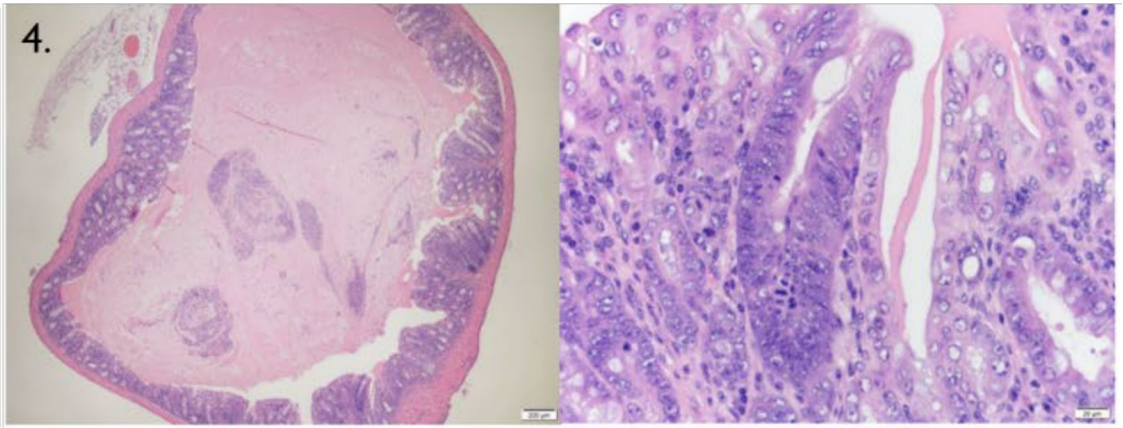
4.

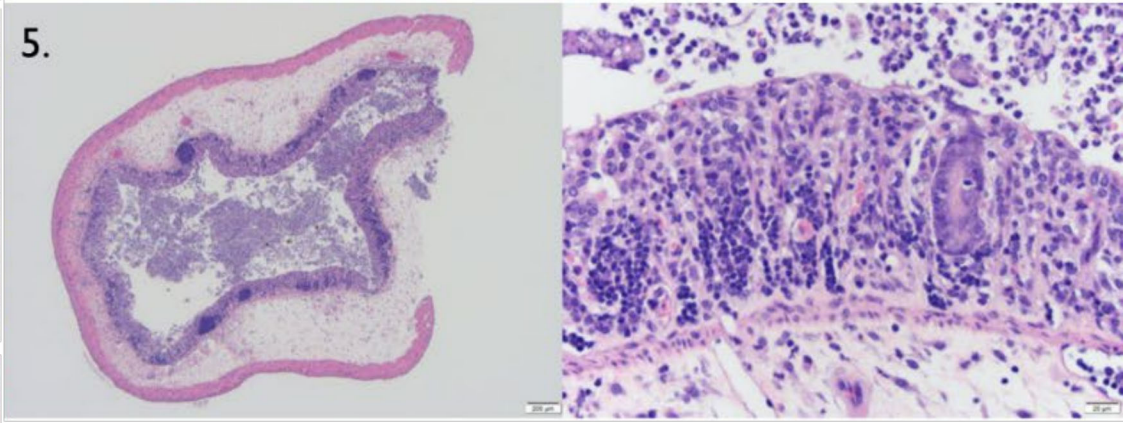
5.

Figure 6-14: H&E staining of selected organs in Exosc3$^{gfp/gfp}$.Rosa26Cre$^{ERT2/ERT2}$ mice

40x (left) and 400x (Right). 1. Kidney demonstrating normal morphology. 2. Thymus, Atrophy of the thymus with loss of cortical and medullary architecture. 3. Bone marrow, Hypocellularity. 4. Large intestine, Proliferative colitis with eosinophilic material and sloughed cells in the lumen. 5. Caecum, Neutrophilic and oedematous typhlitis.

6.2.6. Kidney histology

To further investigate for evidence of TMA in the kidney two additional stains were used Periodic Acid-Schiff, which enables closer examination of the glomerular basement membrane for evidence of double contouring. Secondly, Martius Scarlet Blue, which allows visualisation of fibrin clots (pink), collagen (blue) and erythrocytes (yellow), these stains were performed by Newcastle-Upon-Tyne hospital pathology. Both stains showed no evidence of abnormality in *Exosc3*$^{gfp/gfp}$.*Rosa26Cre*$^{ERT2/ERT2}$ mice following recombination.

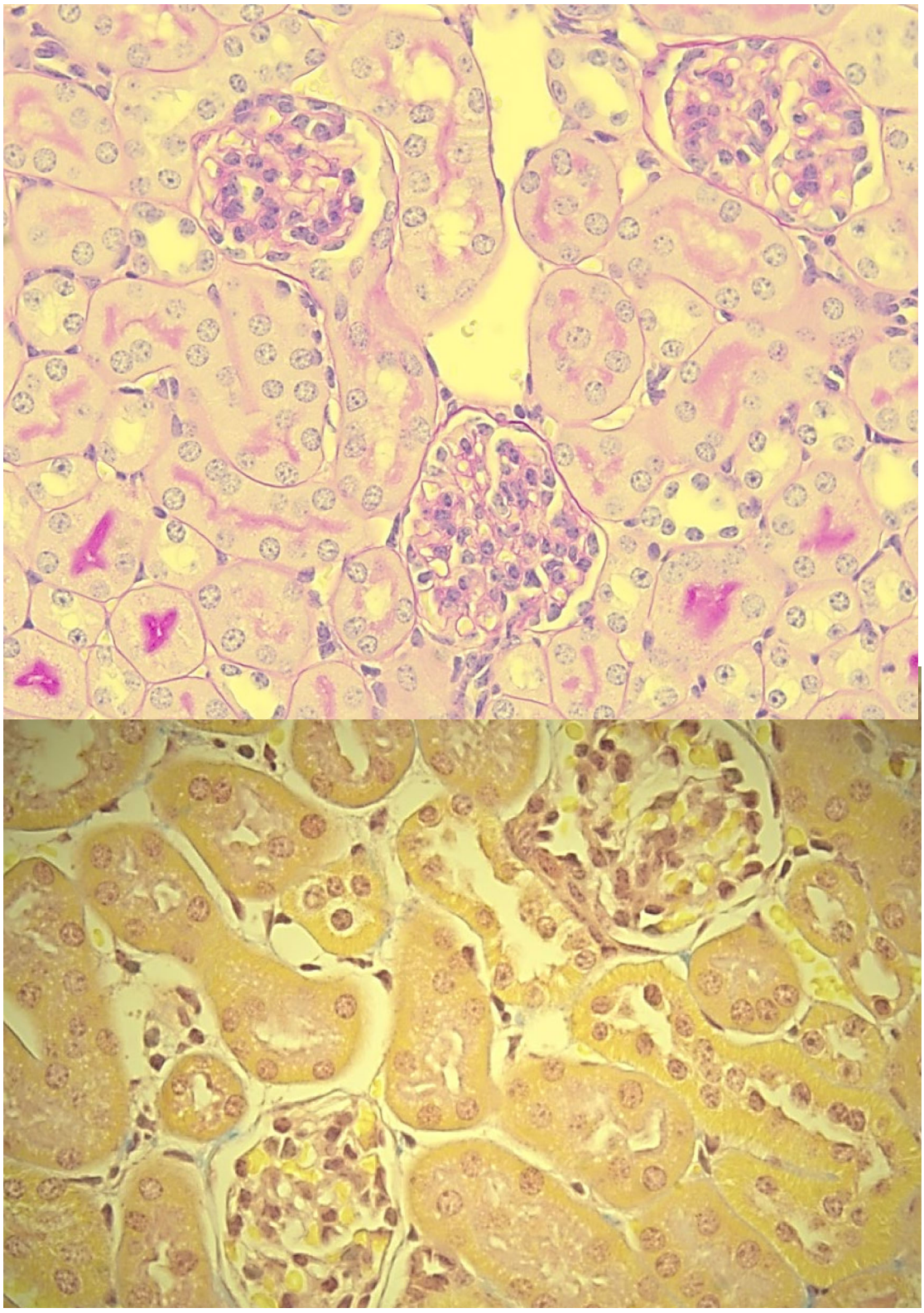

Figure 6-15: Exosc3$^{gfp/gfp}$.Rosa26Cre$^{ERT2/ERT2}$ mouse kidney following treatment with tamoxifen (x400).

Top panel PAS staining, demonstrating normal appearance of glomerular basement membrane, with no evidence of increased cellularity, no double contouring, no mesangiolysis. Bottom panel MSB staining with normal appearance of glomeruli, Collagen staining (blue) showing normal distribution, red blood cells (yellow) seen throughout the glomerular capillaries and no evidence of any fibrin clots (pink).

6.2.7. Transmission electron microscopy

To determine if there was any evidence of TMA on electron microscopy, Transmission electron microscopy was performed on *Exosc3*$^{gfp/gfp}$.*Rosa26Cre*$^{ERT2/ERT2}$ mice. This did not demonstrate any evidence of TMA.

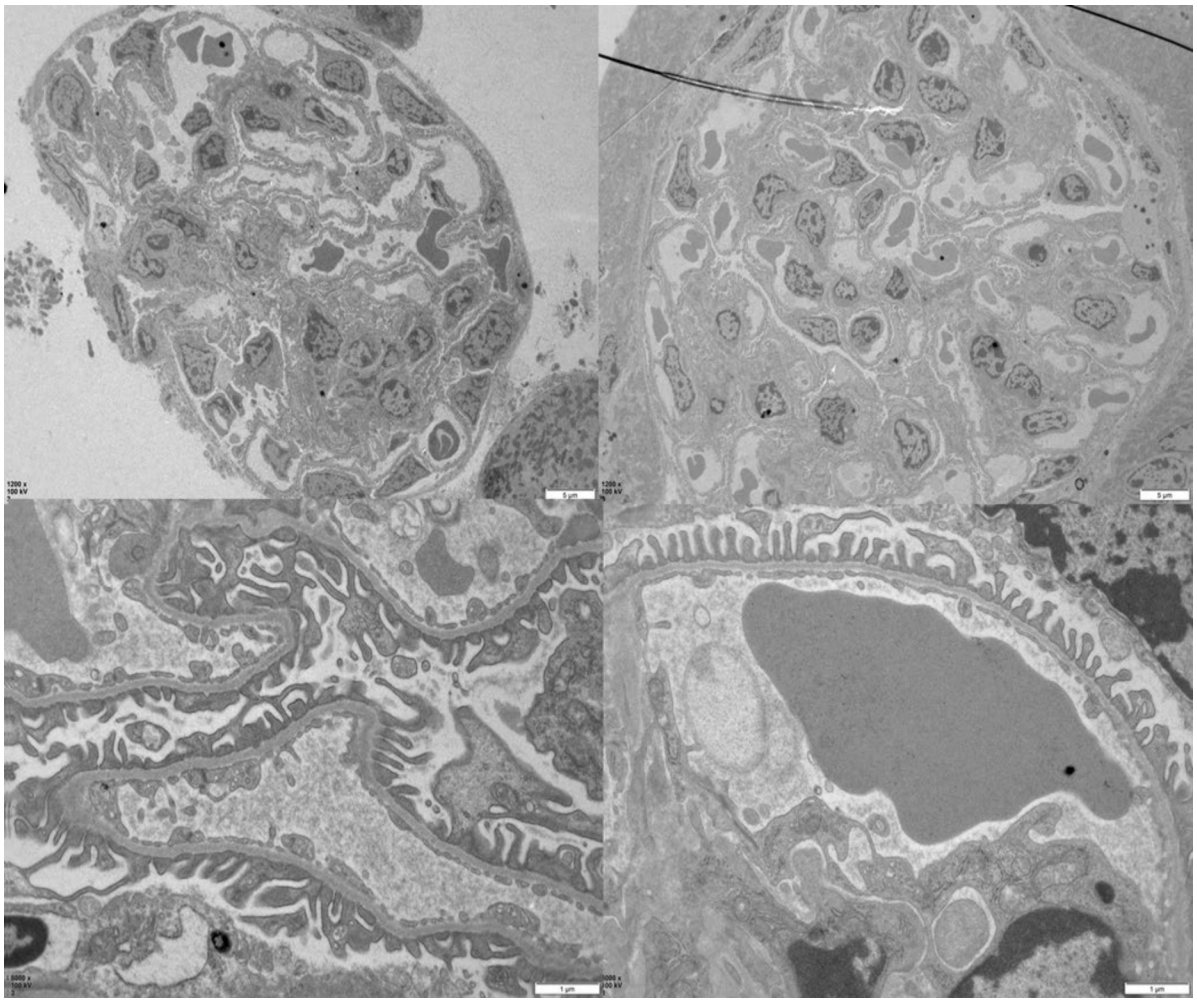

Figure 6-16: Transmission Electron Microscopy of Exosc3$^{gfp/gfp}$*.Rosa26Cre*$^{ERT2/ERT2}$ *mouse kidneys*

Kidneys were cut in to 1mmx1mm cubes and stored in glutaraldehyde solution. Transmission microscopy was performed by the Newcastle University Electron Microscopy Research Service using the Hitachi HT7800 120kV TEM (n=3 mice). No evidence of significant pathology was found.

6.2.8. Flow cytometry of mouse kidney

To determine whether the lack of phenotype in the kidney was due to inefficient recombination within the kidney single cell suspension from the kidney was generated using enzymatic digestion and flow cytometry was used to examine GFP expression. This demonstrated GFP expression in both the leukocytes and endothelial cells, although due to higher autofluorescence within the kidney it was more challenging to demonstrate this (Figure 6-19).

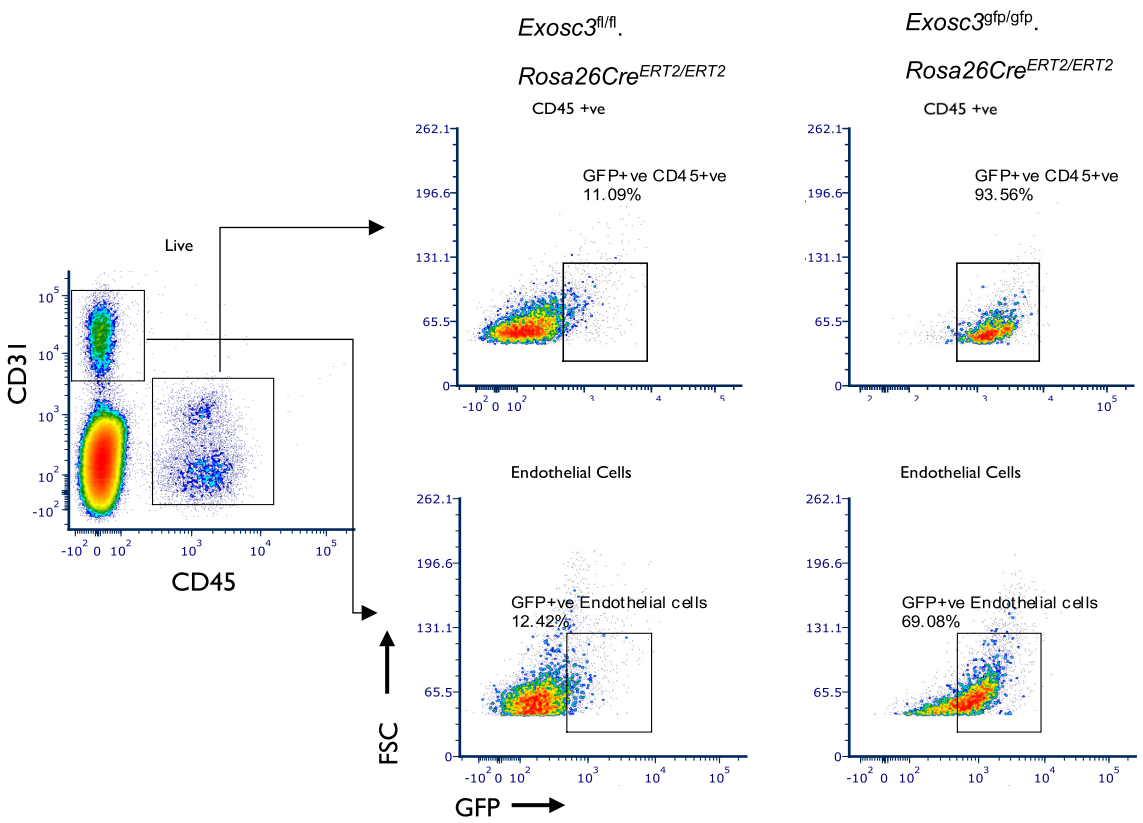

Figure 6-17: Representative example of GFP expression in kidney of Exosc3$^{gfp/gfp}$.Rosa26Cre$^{ERT2/ERT2}$ mice

GFP expression in both endothelial and leukocytes (n=3). Following isolation of kidney into ice-cold dPBS, kidneys were chopped up and digested in 2ml digestion buffer, 2mg/ml collagenase/dipase, 0.2mg/ml DNase I in RPMI at 37ºC for 1 hour. Following digestion kidneys were sieved with a 100µm sieve to remove large cell clumps. Red cell lysis was performed and then cells were washed. 1x10^6 cells were incubated with FcBlock and viability dye for 30 minutes, cells were then stained with a leukocyte marker (CD45 PE-Cy7, BD biosciences) and an endothelial cell marker (CD31 APC, Miltenyi). Following a final wash cells were run on the flow cytometer. Cells were gated to exclude cellular debris, doublets and dead cells. Endothelial cells were identified as CD31$^+$ CD45$^-$ cells. GFP positivity was recorded to determine the degree of homology. A total of 3 mice were examined demonstrating the same pattern.

6.2.9. Haematological analysis

Exosc3$^{gfp/gfp}$*.Rosa26Cre*$^{ERT2/ERT2}$ mice were anaemic, as measured by iSTAT following tamoxifen treatment. To determine whether this was secondary to TMA blood films were produced alongside platelet counts. Reticulocyte counts were performed as well to determine whether there was evidence of haemolysis (raised reticulocyte count). Finally white cell analysis was performed to determine whether there was any effect on this cell line.

6.2.9.1. Red cell analysis

Exosc3$^{gfp/gfp}$*.Rosa26Cre*$^{ERT2/ERT2}$ were anaemic following tamoxifen treatment with an average haemoglobin of (89g/L vs. 126g/L) (Figure 6-21). To determine whether anaemia was haemolytic or aplastic in nature, reticulocyte enumeration was performed. This demonstrated significant suppression in reticulocyte count in *Exosc3*$^{gfp/gfp}$*.Rosa26Cre*$^{ERT2/ERT2}$ mice following tamoxifen (0.45% vs. 3.48%), indicating bone marrow suppression as the underlying cause of anaemia in these mice. Blood films were reviewed, which did not show evidence of schistocytes (*Figure 1-2*).

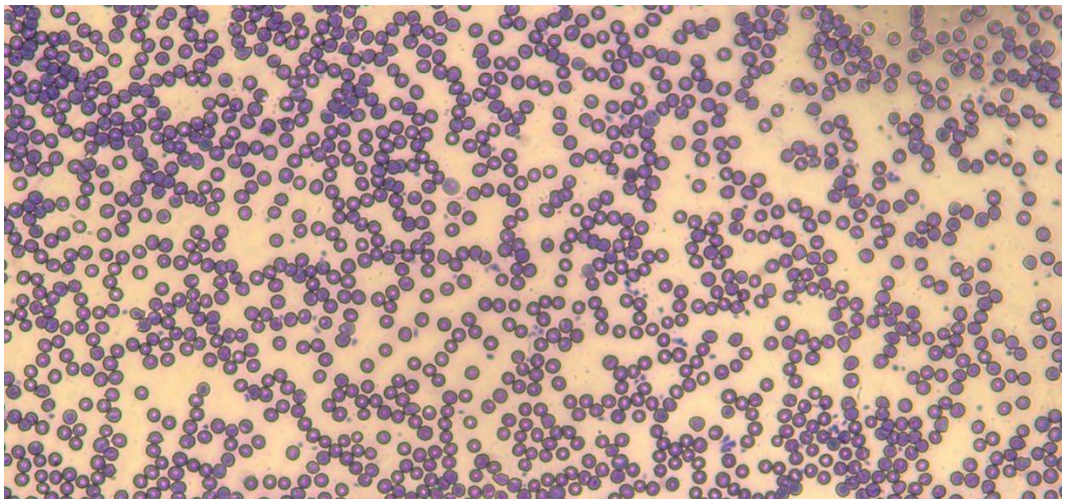

Figure 6-18: Blood film from terminal exsanguination of Exosc3$^{gfp/gfp}$*.Rosa26Cre*$^{ERT2/ERT2}$ *mouse*

Blood film stained with Rapi-Diff II Stain. No evidence of haemolysis was seen on this blood smear, no obvious platelet clumps were seen (which would lead to a falsely low platelet count)

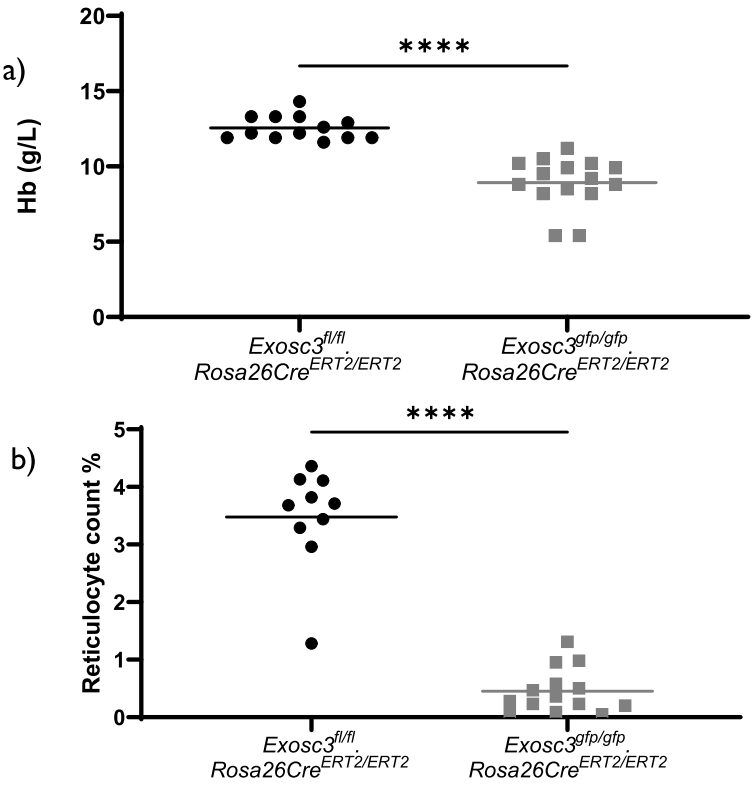

Figure 6-19: Haematology results from Exosc3$^{gfp/gfp}$.Rosa26Cre$^{ERT2/ERT2}$ mice following tamoxifen treatment.

a) Haemoglobin was measured using Heparinised blood with the iSTAT machine. This demonstrated in significant anaemia in Exosc3$^{gfp/gfp}$.Rosa26Cre$^{ERT2/ERT2}$ mice compared to litter-mate controls. b) Reticulocyte percentage determined by flow cytometry, using Retic-Count (BD Biosciences), 10µl of blood was added to Retic-Count and incubated for 30 minutes. Positive cells were identified and calculated as a percentage of the total erythrocytes. This demonstrated significantly reduced reticulocyte percentage in treated mice, indicating aplastic cause of anaemia in mice. (n= 12 for Exosc3$^{fl/fl}$.Rosa26Cre$^{ERT2/ERT2}$ mice and =14 for Exosc3$^{gfp/gfp}$.Rosa26Cre$^{ERT2/ERT2}$ Unpaired t-test used to analyse between groups

6.2.9.2. *Platelet count*

As part of the investigation for TMA, a platelet count was performed to look for evidence of thrombocytopenia. This demonstrated significantly lower platelet count in *Exosc3*$^{gfp/gfp}$.*Rosa26Cre*$^{ERT2/ERT2}$ mice compared to control (1.36x10^{9} vs. 6.12x10^{8} cells/ml) (Figure 6-20).

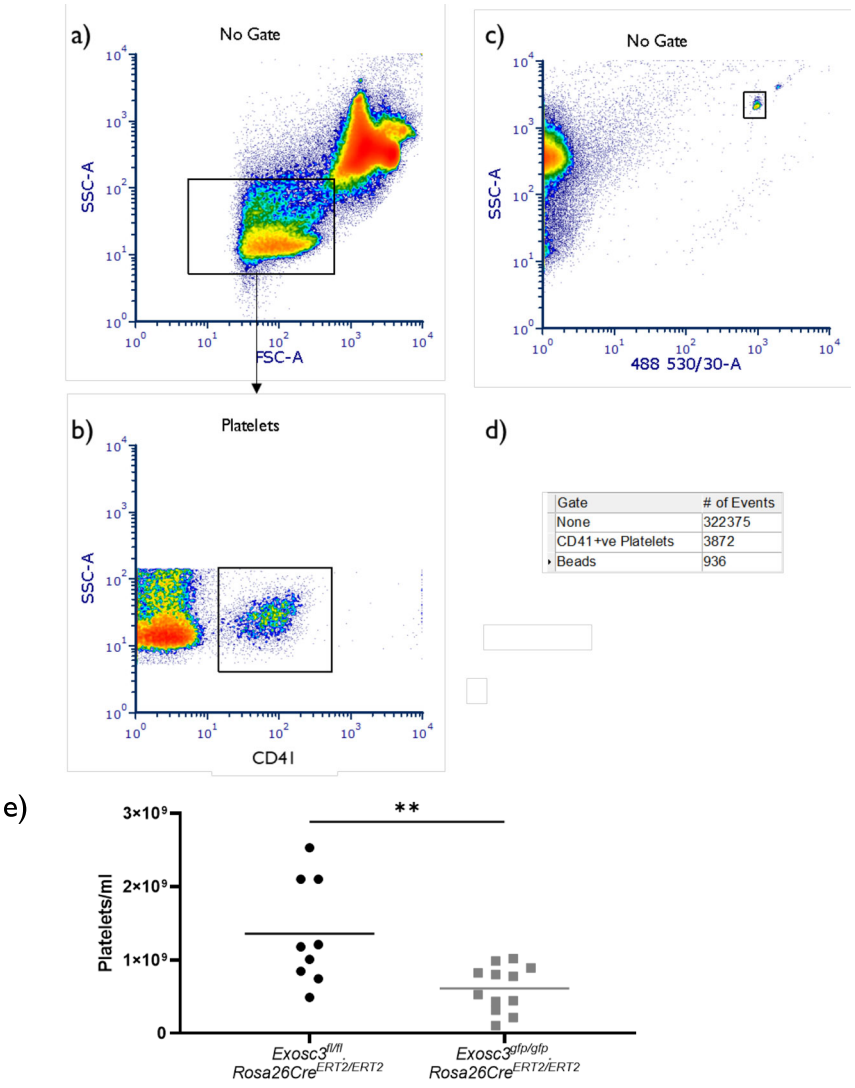

Figure 6-20 Representative flow cytometry of blood sample to determine platelet count.

Blood samples were diluted at 1 in 40 in platelet flow buffer. 5µl of diluted blood was added to 200µl of flow buffer containing 1:400 anti-CD41 and incubated on ice for 30 minutes, 50µl of Absolute Counting beads were added to prior to flow cytometry to allow for cell count to be worked out. a) FSC-A vs. SSC-A (log-scale) used to identify platelet containing fraction b) SSC-A vs 561 586/15, anti-CD41 (PE) used to identify platelets within platelet fraction c) SSC-A vs. 488 530/30 used to identify counting beads d) Gate statistics e) Total platelet count in Exosc3$^{gfp/gfp}$*.Rosa26Cre*$^{ERT2/ERT2}$ *mice following tamoxifen treatment, litter-mate untreated mice used as controls, demonstrating*

thrombocytopenia following tamoxifen treatment. (n= 9 for Exosc3$^{fl/fl}$.Rosa26Cre$^{ERT2/ERT2}$ and =12 for Exosc3$^{gfp/gfp}$.Rosa26Cre$^{ERT2/ERT2}$) Unpaired t-test used to analyse between groups

.

6.2.9.3. White Cell Count

Following the identification of thrombocytopenia and anaemia in *Exosc3*$^{gfp/gfp}$.*Rosa26Cre*$^{ERT2/ERT2}$ mice a white cell count was performed to determine whether there was evidence of pancytopenia, due to the hypocellularity seen in the bone marrow, or whether there was isolated anaemia and thrombocytopenia, which would be in keeping with TMA. *Exosc3*$^{gfp/gfp}$.*Rosa26Cre*$^{ERT2/ERT2}$ mice had significantly lower white cell counts, in all cell types analysed including total white cell count, neutrophils, T-cells and B-cells. The most severely affected line was neutrophils (Figure 6-23).

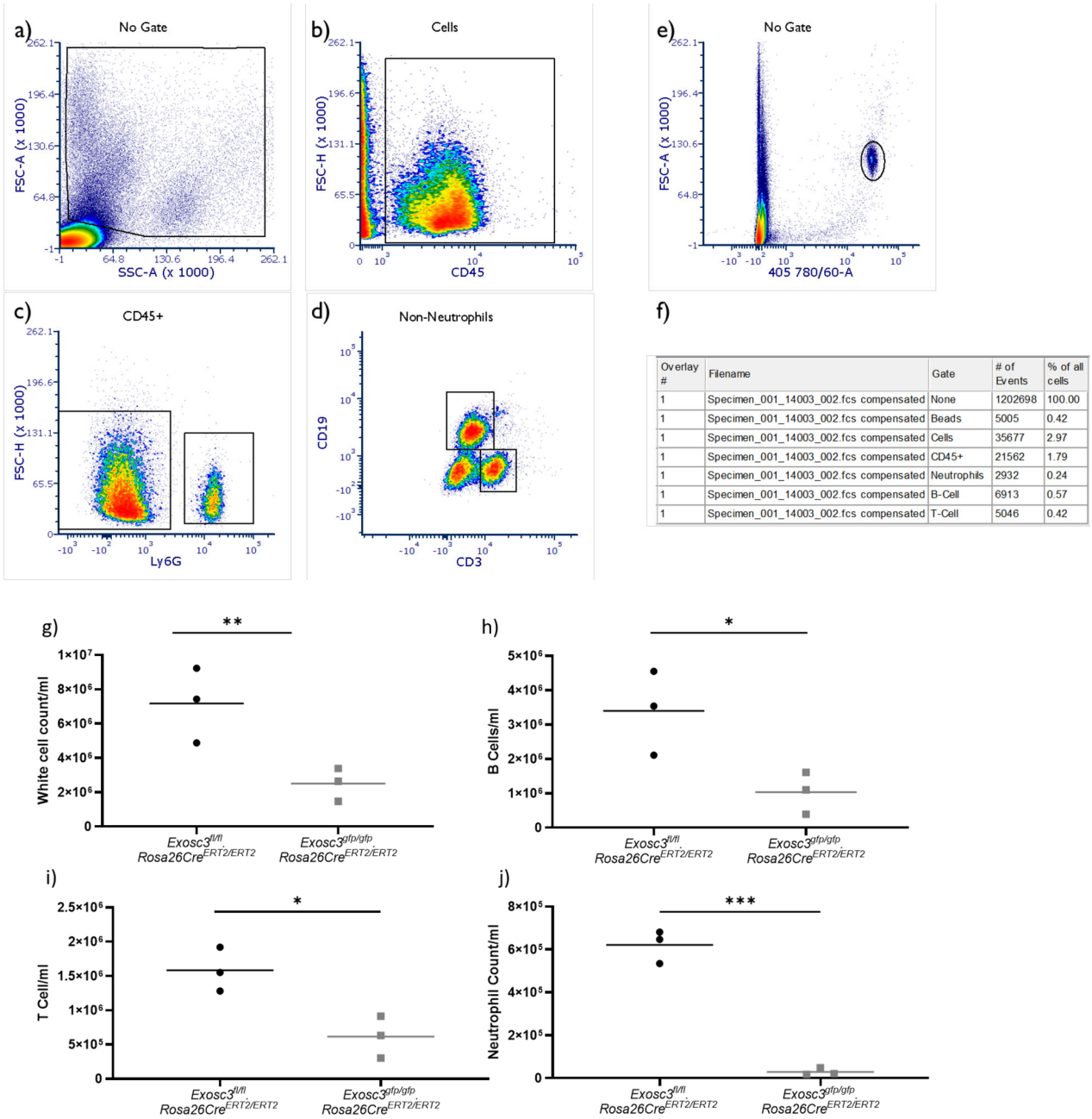

Figure 6-21 Representative example of white cell counting performed via flow cytometry (n=3).

50µl of heparinised blood was stained with 1µl of Anti-CD45, Ly6G, CD19 and CD3 antibodies and incubated on ice for 30 minutes, 450µl of red cell lysis fixation buffer was added and incubated for 10 minutes at room temperature, finally 50µl of Absolute Counting beads were added to allow cell count to be determined. a) FSC-A vs. SCC-A used to identify differentiate cells from debris. b) Anti-CD45 (PE-Cy7) used to identify total leucocytes. c) Anti-Ly6G (APC) used to identify Neutrophils, within the CD45 positive population d) Anti-CD3 (PerCP-Vio700) and Anti-CD19 (PE) used to identify T and B cells respectively. e) Beads identified using 405 780/60 positivity and used to count cells using Equation 1. f) Summary statistics of cell and bead counts. g-j) Total cells per ml in Exosc3$^{gfp/gfp}$.Rosa26Cre$^{ERT2/ERT2}$ mice following recombination, Exosc3$^{fl/fl}$.Rosa26Cre$^{ERT2/ERT2}$ littermates used as controls. Significantly lower cell counts in all cell types tested were seen following recombination, with the most significant reduction in neutrophils. (n=3 in both groups) Unpaired t-test used to analyse between groups

6.2.9.4. Peripheral cell count interpretation

Following Exosc3 ablation there was evidence of pancytopenia in the *Exosc3*$^{gfp/gfp}$.*Rosa26Cre*$^{ERT2/ERT2}$ mice. This contrasts with mice that develop TMA (C3^{D1115N}), in which there is anaemia and thrombocytopenia, without effect on the white cell line. These results, in addition to the finding that the anaemia was aplastic in nature suggest an effect on the normal development of haemopoetic cells. This was further examined by investigating the effects on the bone marrow.

6.2.10. Bone marrow analysis

Given the demonstration of pancytopenia bone marrow analysis was performed to determine whether there was a common stage at which cell development was affected following Exosc3 ablation.

6.2.10.1. Histology

To determine the effects of Exosc3 knockout on the structure of the bone marrow H&E staining was performed on mice following recombination this demonstrated decreased cellularity in bone marrow (Figure 6-14).

6.2.10.2. Cell count

To confirm the reduced cellularity seen in these mice, a cell count was performed using the Anvajo cell counter, following extraction of the bone marrow and red cell lysis. This confirmed a reduction in cells in *Exosc3*$^{gfp/gfp}$.*Rosa26Cre*$^{ERT2/ERT2}$ mice (Figure 6-22).

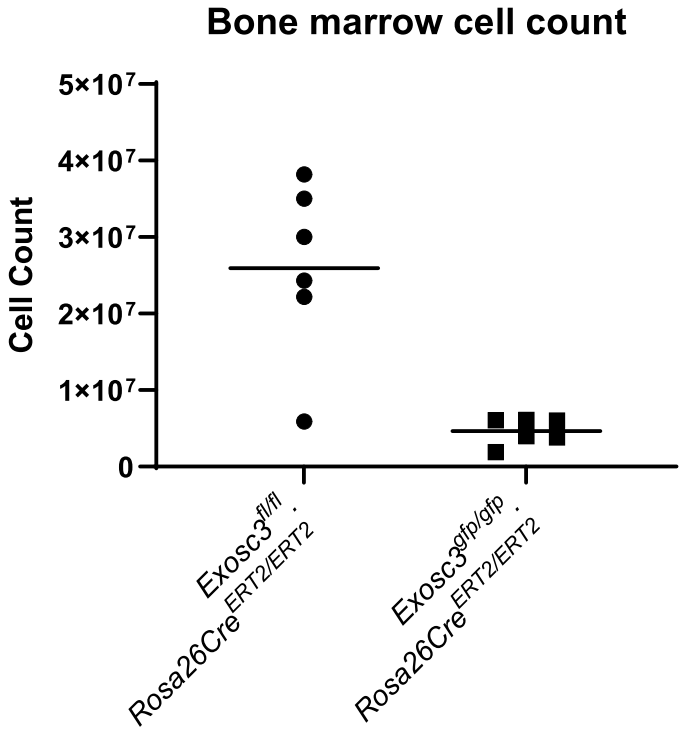

Figure 6-22: Total bone marrow cell count, following extraction of the bone marrow from 3 limbs

Cells were treated with red cell lysis buffer and washed, cells were then counted using the Anvajo cell counter. (n=6 in both groups) Unpaired t-test used to analyse between groups

6.2.10.3. Stem cell analysis

Stem cell analysis was performed to determine whether the observed reduction in cell count (both peripherally and within the bone marrow) was secondary to a global reduction in cells or whether there was a specific block in development. A flow cytometry panel was designed to determine the effects on the earliest haematopoietic stem cells (HSCs). To look at early HSC development a combination of cell surface markers were used c-Kit, Sca-1, CD127, CD34, CD135 and the lineage committed markers CD3, Ter119 and GR-1, CD11b and B220 (Figure 6-25)(Challen *et al.*, 2009). To determine changes following Exosc3 ablation, flow cytometry was performed on bone marrow aspirates (Figure 6-26).

Analysis of the lineage depleted population in *Exosc3*$^{gfp/gfp}$*.Rosa26Cre*$^{ERT2/ERT2}$ mice demonstrated a clear change in the cell population with a loss of c-kit cells and a relative increase in Sca1^{+} cells. When total cell number was calculated from this there was a significant reduction in c-kit positive cells (Figure 6-27). Analysis of Sca1^{+} cells demonstrated no difference between total cell number in untreated and *Exosc3*$^{gfp/gfp}$*.Rosa26Cre*$^{ERT2/ERT2}$ mice.

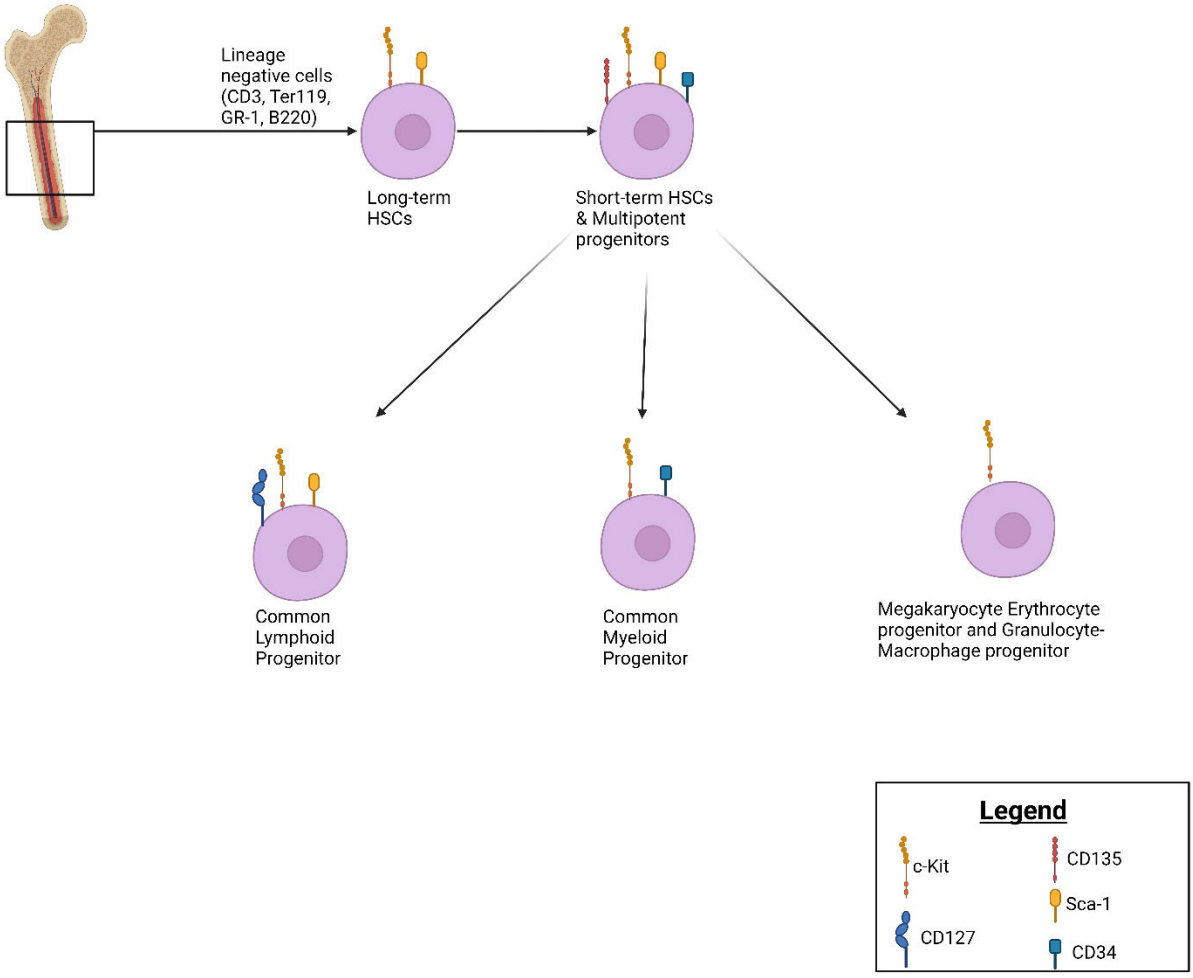

Figure 6-23: Stem cell investigations in mice.

Lineage committed cells are first excluded using a combination of CD3ε, B220, GR-1, Ter119 and CD11b. This results in only uncommitted cells, stem cells can then be identified using c-kit and Sca1 antibodies, further progenitors can be identified using CD127, CD34 and CD135

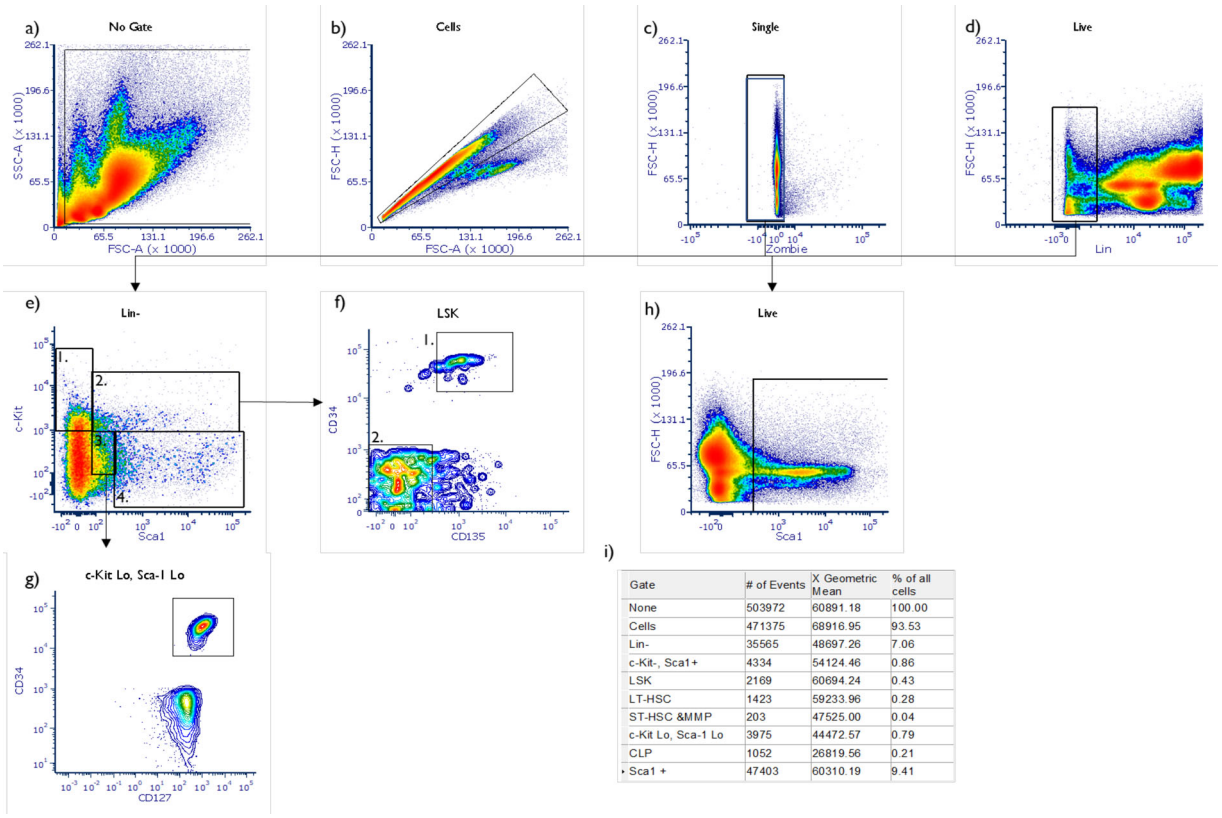

Gate	# of Events	X Geometric Mean	% of all cells
None	503972	60891.18	100.00
Cells	471375	68916.95	93.53
Lin-	35565	48697.26	7.06
c-Kit-, Sca1+	4334	54124.46	0.86
LSK	2169	60694.24	0.43
LT-HSC	1423	59233.96	0.28
ST-HSC &MMP	203	47525.00	0.04
c-Kit Lo, Sca-1 Lo	3975	44472.57	0.79
CLP	1052	26819.56	0.21
Sca1 +	47403	60310.19	9.41

Figure 6-24 Representative example of early haematopoietic development in an untreated mouse.

Bone marrow was extracted from 3 limbs, this was treated with red cell lysis buffer and then washed, cells were counted and 1x10^6 cells were stained with viability dye and FcBlock for 30 minutes on ice. Cells were then stained with lineage cocktail (Ter119, CD3ε, CD11b, GR-1 and B220 APC) CD135 (PE), CD34 (Streptavidin), c-Kit (Pacific blue), Sca1 (PE-Dazzle) and CD127 (BV605), cells were incubated for 30 minutes on ice, following washing, Biotinylated BV711 was added and incubated for 30 minutes. This was then then run on the flow cytometer to determine cell number. a)FSC-A vs. SSC-A used to exclude debris. b) FSC-H vs. FSC-A used to exclude doublets and ensure that only single cells are analysed. c) Dead cells excluded using Zombie NIR™ (Biolegend, USA). d) Linage depletion using anti-CD3, B220, GR-1, Ter-119, CD11b to isolate uncommitted cells only. e) Lin$^-$ cells stained with c-kit vs. Sca1 to identify cell populations. 1. Lin$^-$ c-kit$^+$ 2. Stem cell population Lin$^-$ Sca1$^+$c-Kit$^+$ (LSK) 3. Lin$^-$ Sca1^{lo}c-Kit^{lo} containing common lymphoid progenitor population. 4. c-kit$^-$Lin$^-$ Sca1$^+$ population. f) CD135 vs CD34 on LSK population to identify 1. Multipotent progenitors and 2. Long-term haematopoietic stem cells. g) Common lymphoid progenitors isolated using CD127 in the Lin$^-$ Sca1^{lo}c-Kit^{lo} population. h) Total Sca-1 positivity in live cells. i) Gate statistics used to determine absolute number of cells.

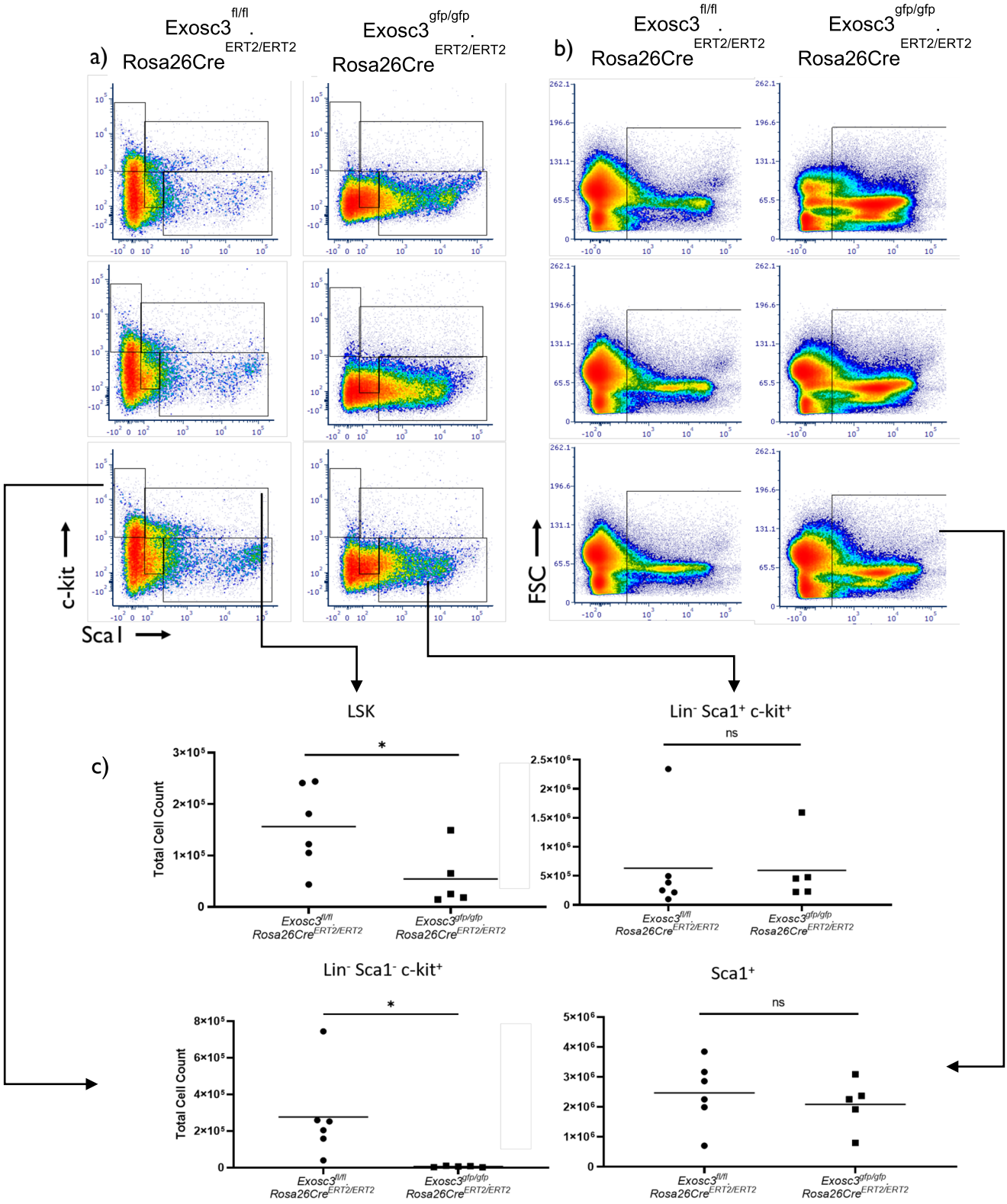

Figure 6-25: Stem cell analysis in Exosc3$^{gfp/gfp}$.Rosa26Cre$^{ERT2/ERT2}$ mice

a) Lineage negative cells. 1. c-kit$^+$ Sca1$^-$ cells, 2. c-kit$^+$Sca1$^+$ cells (LSK), within which stem cells reside 3. c-kit$^-$Sca1$^+$ cells. b) Total Sca1$^+$ cells following gating on live cells. c) Total cell counts within these populations, demonstrating a significant reduction in c-kit positive cells, both LSK and c-kit$^+$ Sca1$^-$ cells, relative preservation of Sca1$^+$ populations. (n=6 in Exosc3$^{fl/fl}$.Rosa26Cre$^{ERT2/ERT2}$ group and =5 in Exosc3$^{gfp/gfp}$.Rosa26Cre$^{ERT2/ERT2}$) Unpaired t-test used to analyse between groups

6.2.10.4. Cell cycle analysis and apoptosis

There were two potential explanations for the reduced HSC number in the bone marrow. Firstly, increased cell death and failure to replenish the cells could have resulted in a reduction in the viable cell count. Secondly, cell cycle arrest during a specific stage of replication could have occurred, this has been previously demonstrated in both zebrafish and drosophila models of *Exosc3* knock-out (Morton *et al.*, 2020; Müller *et al.*, 2020). It was possible that it was a combination of both of these. To determine which of these was the case cell cycle analysis was performed using annexin V and Propidium Iodide (PI). This demonstrated a significant increase in the number of apoptotic cells in *Exosc3*$^{gfp/gfp}$*.Rosa26Cre*$^{ERT2/ERT2}$ mice, with an increase in both early and late apoptotic cells (Figure 6-26). Cell cycle analysis was undertaken with BrdU to determine the number of actively cycling cells. Following Exosc3 ablation there was a reduction in cycling cells (BrdU positive cells) with evidence of G1/G0 cell cycle arrest and an increase in the proportion of apoptotic cells, indicating a reduction in actively cycling cells and an increase in cell death following Exosc3 ablation.

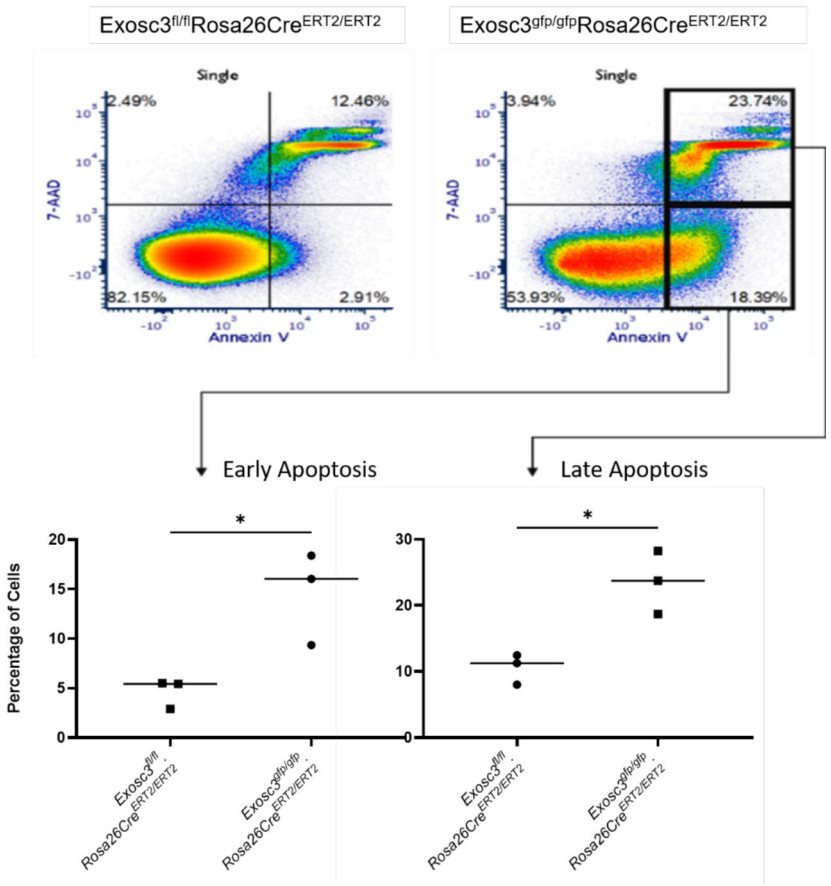

Figure 6-26: Apoptosis following recombination in bone marrow cells.

Bone marrow cells were isolated from 3 limbs. 1x10^6 cells were incubated with Annexin V (APC) in Annexin V flow buffer and incubated for 30 minutes, 7-AAD was added prior to flow cytometry to allow late and early apoptotic cells to be differentiated. This demonstrated increase in both early (Annexin V positive, 7-AAD negative) and late (Annexin V positive, 7-AAD positive) apoptotic cells following Exosc3 knock-out. (n=3 Exosc3$^{gfp/gfp}$.Rosa26Cre$^{ERT2/ERT2}$ and Exosc3$^{fl/fl}$.Rosa26Cre$^{ERT2/ERT2}$) Unpaired t-test used to analyse between groups

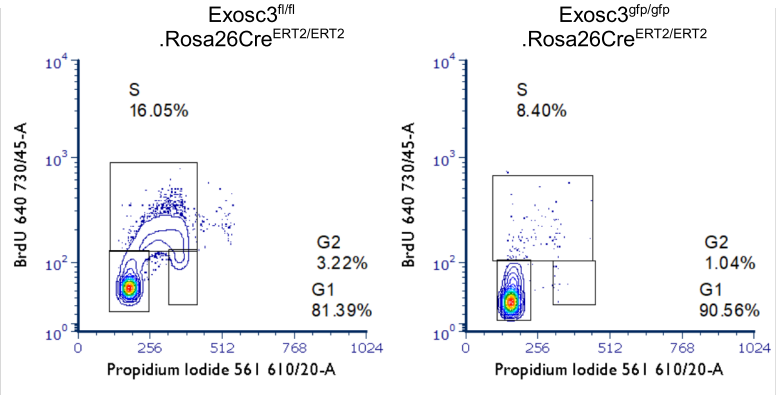

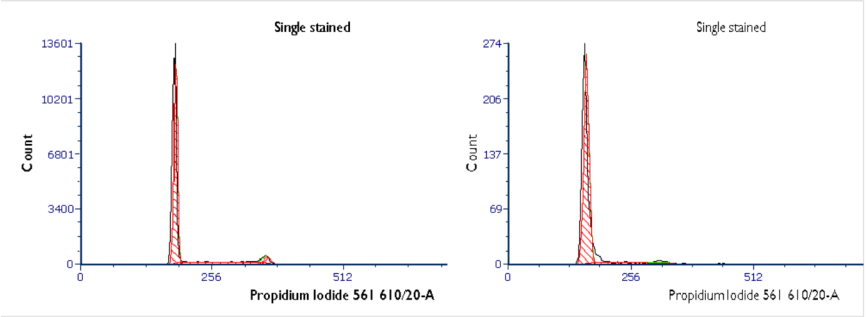

Interpretation
MultiCycle suggestions (a guideline only):
No abnormal DNA content is observed.
The diploid %S=17.3, %G2=5.01
The S Phase confidence is good

Experiment Statistics
Chi sq: 6.46
BAD: 0.00
Number of cells: 37288.00
Number of cycles: 1.00
Cycle fit model: 1 Cycle

Interpretation
MultiCycle suggestions (a guideline only):
No abnormal DNA content is observed.
The diploid %S=7.5, %G2=1.66
The S Phase confidence is fair
Note: intra-model error,

Experiment Statistics
Chi sq: 2.52
BAD: 0.00
Number of cells: 1059.00
Number of cycles: 1.00
Cycle fit model: 1 Cycle

Figure 6-27: Representative example of cell cycle dynamics in Exosc3$^{gfp/gfp}$.Rosa26Cre$^{ERT2/ERT2}$ and Exosc3$^{fl/fl}$.Rosa26Cre$^{ERT2/ERT2}$ littermate controls.

Mice were treated with 100µl of BrdU I.P. 1 hour prior to euthanasia. Bone marrow cells were then isolated from three limbs. Following red cell lysis and washing, 1x10^7 cells were resuspended in ice-cold 70% ethanol added in drop-wise fashion to fix cells. Cells were stored at -20ºC for at least 24 hours. To detect BrdU 1x10^6 cells were incubated with 2M HCl for 20 minutes and washed three times with PBS. Cells were then stained with anti-BrdU antibody (APC) for 30 minutes on ice, prior to analysis PI was added to enable DNA content to be calculated. Flow cytometry was undertaken on these cells to determine the proportion cells actively cycling. FCS express cell cycle model was used to determine cell cycle statistics. In untreated mice cells are actively cycling as measured by BrdU positive cells in S phase. Following recombination there is a marked reduction in cell cycle, with fewer cells in S phase and greater number of cells residing in G_0/G_1.

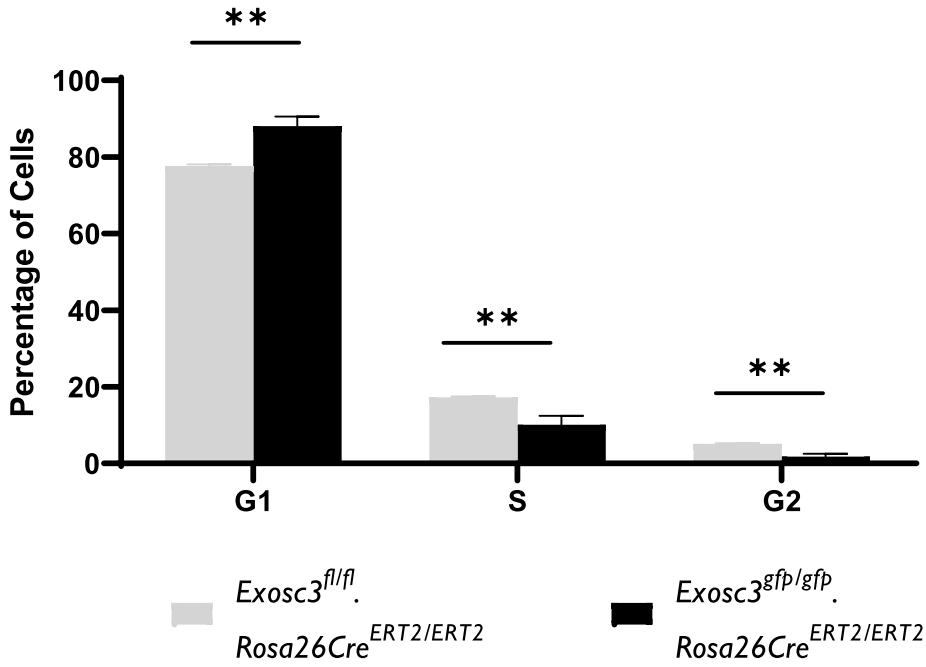

Figure 6-28: Cell cycle analysis of Exosc3$^{gfp/gfp}$.Rosa26Cre$^{ERT2/ERT2}$ bone marrow cells.

Evidence of cell cycle arrest at G_1, with a reduction in actively cycling cells in both S and G_2 phase. Calculated using FCS express cell cycle analysis. (n=3 Exosc3$^{gfp/gfp}$.Rosa26Cre$^{ERT2/ERT2}$ and Exosc3$^{fl/fl}$.Rosa26Cre$^{ERT2/ERT2}$). Unpaired t-test used to analyse between groups

6.2.10.5. Interpretation of bone marrow analysis

The bone marrow analysis undertaken on the Exosc3$^{gfp/gfp}$.Rosa26Cre$^{ERT2/ERT2}$ mouse demonstrated reduced bone marrow cell number, secondary to cell cycle arrest and apoptosis. In depth analysis of the phenotype revealed loss of early stem cells

6.2.11. Cytokine profile

The phenotype observed in *Exosc3$^{gfp/gfp}$.Rosa26Cre$^{ERT2/ERT2}$* mice is similar to that seen in mice that develop acute radiation syndrome and ribosomopathy (Schaue and McBride, 2019; Singh;Seed and Olabisi, 2019). In both these conditions TNF-α expression is increased, to determine whether there was similar cytokine activity

a TNF-α ELISA was performed. This demonstrated significantly increased serum TNF-α concentration in mice following Exosc3 ablation. Suggesting a similar disease mechanism

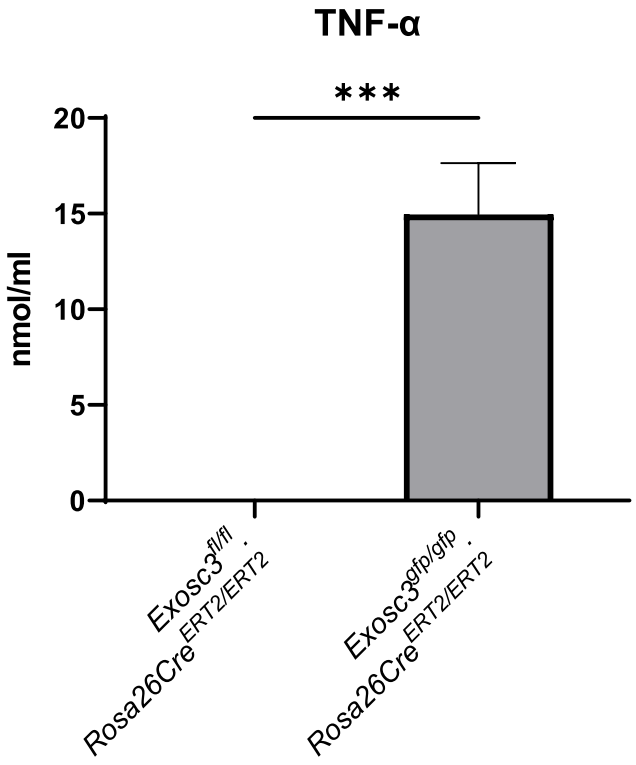

Figure 6-29: Serum TNF-α concentration in Exosc3$^{gfp/gfp}$.Rosa26Cre$^{ERT2/ERT2}$ mice compared to Exosc3$^{fl/fl}$.Rosa26Cre$^{ERT2/ERT2}$.

Undetectable levels in untreated control mice. Blood was collected in lithium heparin and plasma separated by centrifugation. TNF-α concentration was determined using the Quantikine TNF-α ELISA. Optical density was calculated using the plate reader at 450nm. All samples were run in triplicate. Regression analysis was used to develop a standard curve. (n=3 Exosc3$^{gfp/gfp}$.Rosa26Cre$^{ERT2/ERT2}$ and Exosc3$^{fl/fl}$.Rosa26Cre$^{ERT2/ERT2}$) Unpaired t-test used to analyse between groups

6.2.12. Interferon expression

As highlighted above one of the initial hypotheses was that increased levels of RNA within the cell could result in ectopic activation of intracellular viral RNA sensors (4.6.1). To examine this hypothesis cDNA was generated from kidney, affected

bone marrow and caecum. To determine interferon expression three interferon stimulated genes (ISGs) (OAS1a, RSAD22 and IFI44) were measured. The measurement of ISGs is the preferred measurement for interferon upregulation (Duncan *et al.*, 2019b). This demonstrated no difference in both the bone marrow and kidney, there was however an increase in ISGs in the caecum following recombination. This could represent either increased local interferon expression due to stimulation resulting from Exosc3 knockout, or non-specific increase secondary to widespread cell death. This was explored by investigating the interferon receptor knockout (7.1).

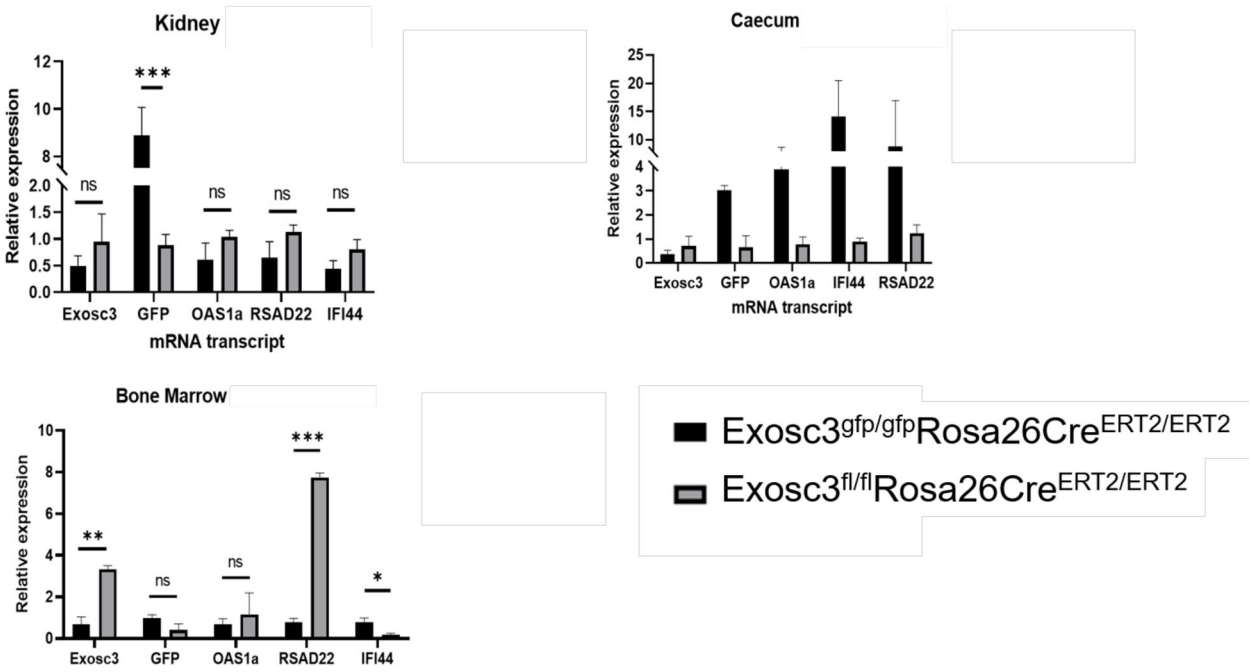

Figure 6-30: mRNA levels from Exosc3$^{gfp/gfp}$.Rosa26Cre$^{ERT2/ERT2}$ mice and untreated littermate controls.

RNA was extracted from snap frozen tissue using Trizol and cDNA transcribed as per manufacturer's instructions. Taqman PCR was performed using the appropriate universal probe (Roche) and specific primers. Exosc3 mRNA was reduced following tamoxifen recombination, there was evidence of increased GFP mRNA at the same time, confirming the recombination. Three commonly used ISGs were investigated: OAS1a, RSAD22 and IFI44. There was no evidence of increased interferon signal in the kidney or bone marrow. In the caecum there was evidence of increased ISG expression, although this is potentially a representation of cell death rather than increased interferon expression. (n=3 Exosc3$^{gfp/gfp}$.Rosa26Cre$^{ERT2/ERT2}$ and Exosc3$^{fl/fl}$.Rosa26Cre$^{ERT2/ERT2}$) Unpaired t-test used to analyse between groups

6.2.13. *Rosa26Cre$^{ERT2/ERT2}$ and Exosc3$^{fl/fl}$ controls*

Tamoxifen is known to have side-effects when used to induce recombination in tamoxifen-sensitive Cre models (Zhong *et al.*, 2015; Donocoff *et al.*, 2020). To determine whether there was an effect on survival *Exosc3*$^{fl/fl}$ and Rosa26Cre$^{ERT2/ERT2}$ were treated with four days of tamoxifen. These mice showed no evidence of disease at 8 days post treatment (the median time to disease in *Exosc3$^{gfp/gfp}$.Rosa26Cre$^{ERT2/ERT2}$* mice), at this point there was no evidence of anaemia (Figure 6-31), and there was no GFP expression detectable and HSC analysis was the same as wild type. These results indicate that the effects seen in the *Exosc3$^{gfp/gfp}$.Rosa26Cre$^{ERT2/ERT2}$* mice were not secondary to tamoxifen treatment.

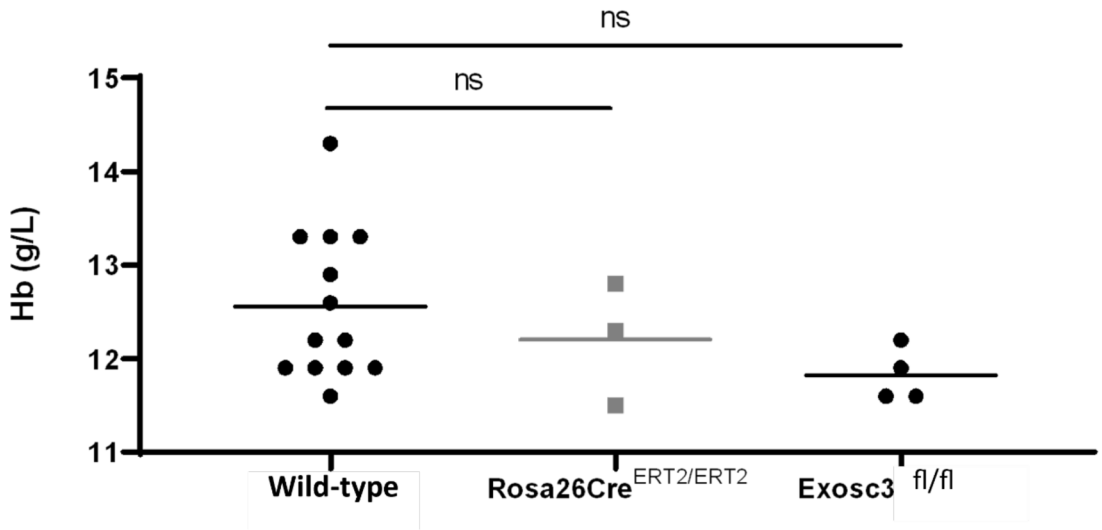

Figure 6-31: Haemoglobin as measured by iSTAT, using Chem8+ cartridges.

Exosc3$^{fl/fl}$ and Rosa26Cre$^{ERT2/ERT2}$ mice treated with the standard I.P. tamoxifen dosage (four days at 75mg/Kg). No significant difference detected between untreated mice and Exosc3$^{fl/fl}$ or Rosa26Cre$^{ERT2/ERT2}$. (n=13 in untreated group and =3 in Rosa26Cre$^{ERT2/ERT2}$ and =4 in Exosc3$^{fl/fl}$) Unpaired t-test used to analyse between groups

6.2.14. Aged cohort

Mice that were treated for 3 days with tamoxifen were monitored until 1 year post treatment. 8/12 mice survived beyond 10 days. Within these remaining mice, 2 mice developed darkening of their ears followed by decrease in their body condition score that required them to be euthanised approximately two months following treatment. Examination of their tissues revealed chronic ulcerative dermatitis, which may account for their deterioration (Figure 6-34).

6/12 mice were aged to one year post treatment. GFP expression was examined in these mice, this demonstrated persistent GFP expression in spleen, bone marrow, white cells and endothelial cells (within the kidney).

Examination of the LSK ($Lin^- Sca1^+c\text{-}Kit^+$) in this cohort demonstrated no difference in distribution at one year compared to wild-type cells, despite 76.28% ±9.7 GFP positivity in the splenocytes.

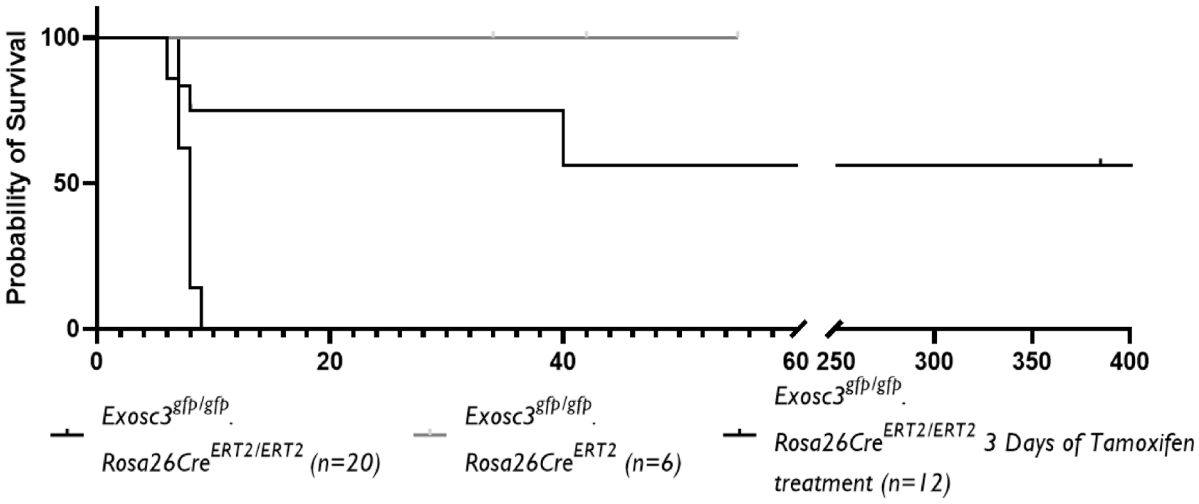

Figure 6-32: Survival analysis of mice following treatment with tamoxifen for 3 days.

$Exosc3^{gfp/gfp}.Rosa26Cre^{ERT2/ERT2}$ and $Exosc3^{R/WT}$ mice treated with standard four-day tamoxifen shown for reference.

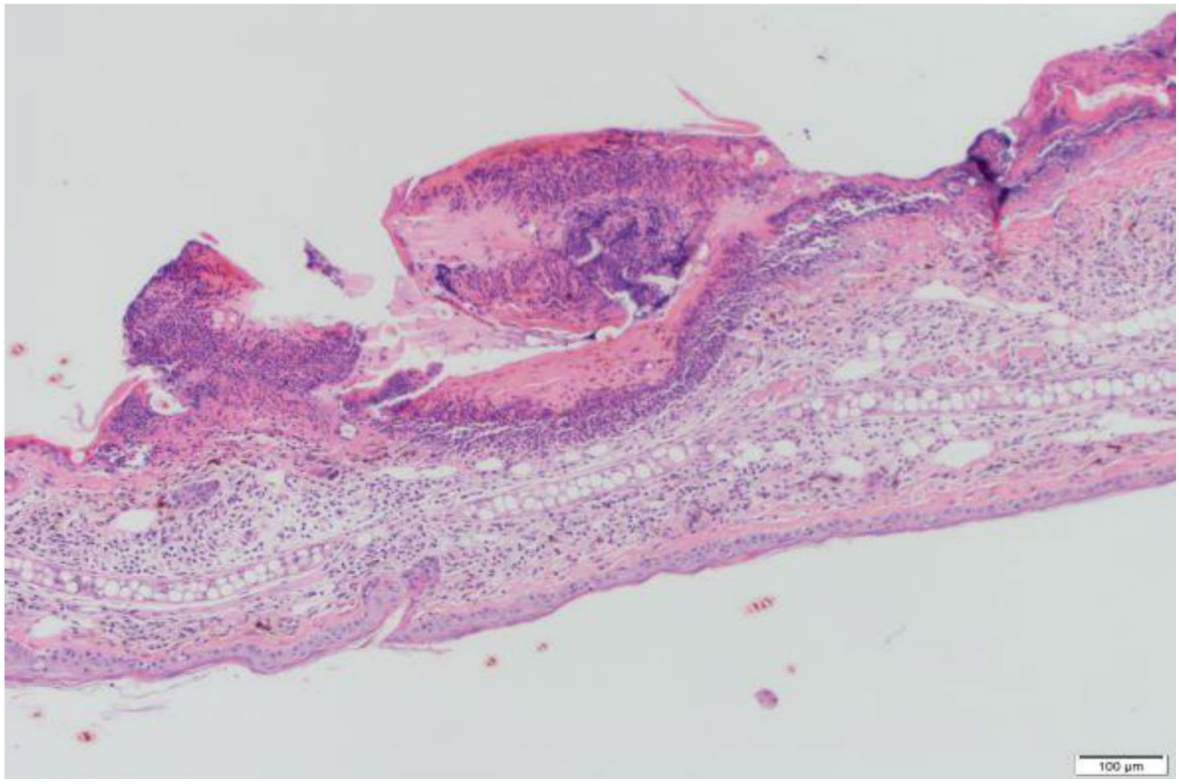

Figure 6-33: H&E stained pinna from Exosc3$^{gfp/gfp}$.Rosa26Cre$^{ERT2/ERT2}$ mouse

This mouse was treated with tamoxifen for three days in a mouse that developed darkening of ears and weight loss at eight weeks post treatment. Demonstrating chronic ulcerative dermatitis.

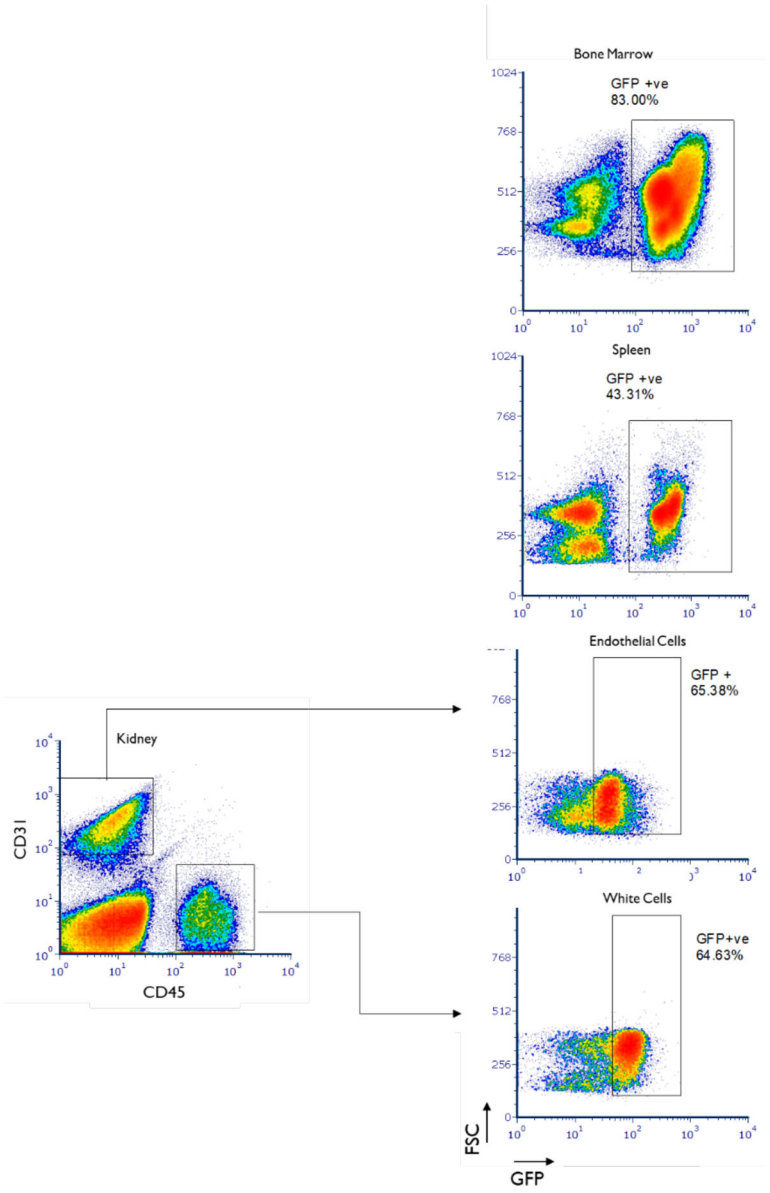

Figure 6-34: Representative flow cytometry from Exosc3$^{gfp/gfp}$.Rosa26Cre$^{ERT2/ERT2}$ mice treated with tamoxifen for three days that survived to one year.

Single cell suspensions from kidney, via enzymatic disruption, spleen, via mechanical disruption, and bone marrow via centrifugation were generated. Cells were treated with red cell lysis and incubated with FcBlock and viability dye. Cells were stained for surface antibodies, for kidney this was CD45 and CD31, for spleen no further antibodies were used and for bone marrow this was lineage cocktail (B220, Ter119, GR-1, CD11b and B220), c-kit, Sca1 and CD127. Samples were then analysed via flow cytometry to determine the GFP positivity, following exclusion of cell debris, dead cells and doublets.

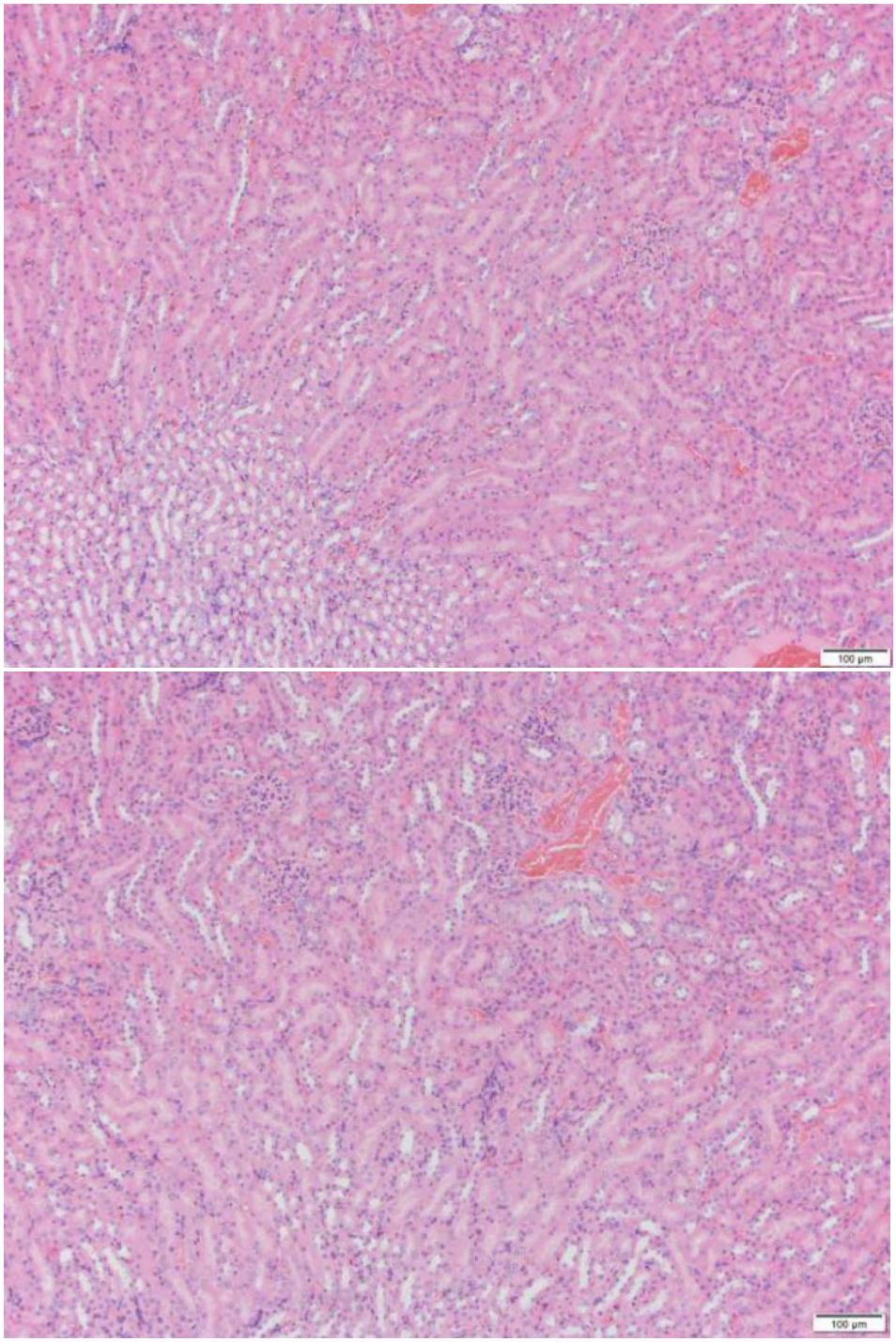

Figure 6-35: H&E staining from Exosc3$^{gfp/gfp}$.Rosa26Cre$^{ERT2/ERT2}$ mouse kidney treated for three days

These mice developed darkening of ears and weight loss at eight weeks post treatment. No evidence of pathology in kidneys from these mice.

6.3. Discussion

6.3.1. Rationale of Rosa26Cre^{ERT2} selection

6.3.1.1. Inducible gene expression system

In order to achieve temporal control of Cre-mediated knock-out an inducible system was required. There are two well described, the Tamoxifen-inducible and the Tetracycline-inducible systems. The tetracycline system can be designed as a Tet-Off, in which tetracycline (or derivatives, doxycycline) prevents binding of the tetracycline-responsive transactivator to the Tet operon, thus preventing expression of the gene following the Tet operon. Following cessation of tetracycline conformational change in tetracycline-responsive transactivator results in binding to the Tet operon. This result in expression of the gene of interest. The second option for the tetracycline system is a Tet-On design, in which reverse tetracycline-responsive transactivator only binds to the Tet operon in the presence of tetracycline.

The second commonly employed system, and the one used in this study, is the tamoxifen-inducible system. In this system a modified oestrogen receptor is fused to Cre. In an inactive state the ER is bound to heat shock protein 90 (Hsp90) and is excluded from the nucleus. Treatment with tamoxifen results in decoupling of Hsp90 to the oestrogen receptor Cre fusion protein. This is then able to enter the nucleus, where it is able to induce recombination.

In this project the Tamoxifen-inducible system was utilised. This decision was influenced by a number of factors. Firstly, Tamoxifen can be delivered by a number of routes (including both IP and oral) allowing for accurate dosing of mice, this allowed a variable dosing strategy to be explored. Tetracycline is restricted to oral dosing and therefore delivered via drinking water. This would have made

modulating the dose delivered impossible. Secondly, the Tamoxifen-induced cre system has been used previously to induced Exosc3 ablation in the *Exosc3$^{fl/fl}$* mouse, therefore it was more likely that employing this system in this model would work. Finally, there is a higher number of tissues specific tamoxifen systems, which would allow easier comparison of different tissue specific models in the future.

6.3.1.2. Ubiquitous Cre^{ERT2} selection

There are several options for ubiquitous Cre^{ERT2} expression available including the B6.Cg-Tg(CAG-cre/Esr1*)5Amc/J, B6.Cg-Ndor1Tg(UBC-cre/ERT2)1Ejb/1J and B6.129-Gt(ROSA)26Sortm1(cre/ERT2)Tyj/J. The Rosa26Cre^{ERT2} was utilised in this project, this had a number of advantages over the other available systems, firstly this system had been shown to result in effective recombination in the *Exosc3$^{fl/fl}$* mouse, secondly the Rosa26Cre^{ERT2} mouse is the most commonly uses and therefore best reported ubiquitous cre system, and unlike other models the Rosa26Cre^{ERT2} mouse can be bred in homozygosity, which enabled an easier breeding strategy and potentially enabled higher cre expression.

6.3.2. Efficient recombination

Previous data on the Exosc3^{fl} mouse in an *ex vivo* model had demonstrated a phenotype in mice that were *Exosc3$^{gfp/gfp}$.Rosa26Cre^{ERT2}*(Pefanis *et al.*, 2014). The *Exosc3$^{gfp/gfp}$.Rosa26Cre^{ERT2}* mouse was initially used in this project. Despite evidence of recombination in 69.24%±1.6 of splenocytes there was no observable phenotype up to 1 month after treatment. When mice were generated that were homozygous for the Exosc3^{fl} and Rosa26Cre^{ERT2} alleles (*Exosc3$^{gfp/gfp}$.Rosa26Cre$^{ERT2/ERT2}$*) there was evidence of increased recombination and development of a phenotype. The efficiency of Rosa26Cre^{ERT2} has previously been reported as 30-80% when maintained in hemizygous state (Zheng *et al.*, 2000;

Sohal *et al.*, 2001; Muzumdar *et al.*, 2007; Kristianto *et al.*, 2017; Sandlesh *et al.*, 2018). This level of efficiency is sufficient for most knockout models, however it is clear that this level of knockout was not sufficient to produce a phenotype in the *Exosc3*$^{gfp/gfp}$*.Rosa26Cre*^{ERT2} mice. There are few studies that have examined the effect of Rosa26Cre^{ERT2} copy number on recombination, one study that failed to demonstrate efficient recombination in the hemizygote mouse demonstrated complete excision when mice were bred to a homozygous state (Sandlesh *et al.*, 2018). It is clear from the data on the *Exosc3*$^{gfp/gfp}$*.Rosa26Cre*^{ERT2} and *Exosc3*$^{gfp/gfp}$*.Rosa26Cre*$^{ERT2/ERT2}$ mice that cre-mediated recombination was significantly improved in the presence of a second copy of the Rosa26Cre^{ERT2} allele. The explanation for this is likely that the reduced level of Cre produced in mice with a single copy of Rosa26Cre^{ERT2} results in less efficient recombination (Figure 6-8).

The work done to optimise tamoxifen dosing demonstrates that there is a critical number of cells that need to have undergone recombination for a phenotype to develop. This appeared to be between 85 – 95%, as mice that were treated with tamoxifen for 2 days showed 85% GFP positivity without signs of disease, however 100% of the mice that achieved over 95% GFP positivity died. Previous studies have attempted to determine whether adjusting the dosage of tamoxifen results in different levels of recombination. These studies concurred with the findings displayed here that increased duration of tamoxifen results in an increase level of recombination (Jahn *et al.*; Donocoff *et al.*, 2020). The finding that three days of tamoxifen was able to induce recombination with variable effects may have implications for examining the effects of chronic knockout in genes that are otherwise fatal in the acute setting.

6.3.3. Phenotype observed in Exosc3$^{gfp/gfp}$.Rosa26Cre$^{ERT2/ERT2}$ mice

Following treatment with 75mg/Kg I.P. for 4 days mice developed a predictable and repeatable phenotype that included weight loss and anaemia clinically. These mice reached the pre-defined maximum acceptable harm within 10 days of commencing treatment. These mice all developed gut and bone marrow failure that led to death (or euthanasia). This phenotype is similar to Acute Radiation Syndrome (ARS) (Schaue and McBride, 2019; Singh;Seed and Olabisi, 2019). Previous research on ARS has demonstrated a phenotype composed of neurological (n-ARS), gastrointestinal (GI-ARS) and bone marrow (H-ARS) failure. In ARS, ionising radiation results in irreparable DNA damage that results in apoptotic and necrotic cell death. Exposure to high levels of radiation have previously occurred due to nuclear accidents, famously in Chernobyl and Fukushima, and during the fallout of a nuclear weapon. Developing animal models that recapitulate this phenotype has proved useful to understand the pathophysiology of ARS (Gurley *et al.*; Merritt *et al.*, 1994; Singh;Seed and Olabisi, 2019; Yashavarddhan *et al.*, 2021).

6.3.4. Bone marrow effects

Following Exosc3 knock-out there was a marked loss in total cell count, which was in keeping with the changes seen peripherally with the development of pancytopenia. Deeper investigation of the bone marrow demonstrated almost couple loss of c-kit expression. There was an increase in the percentage of cells that were $Sca1^+$, however when total cell counts was determined there was no difference between the number of $Sca1^+$ cells in *Exosc3$^{gfp/gfp}$.Rosa26Cre$^{ERT2/ERT2}$* compared to *Exosc3$^{fl/fl}$.Rosa26Cre$^{ERT2/ERT2}$* mice.

These findings are similar to changes seen in mice that develop H-ARS; mice with H-ARS demonstrate a predictable pattern of both peripheral and bone marrow

changes. Peripherally, neutropenia and thrombocytopenia are the most pronounced, possibly due to the shorter half-life of these cells in mice, 10 hours and 5 days respectively, compared to 38-52 days of erythrocytes (O'Connell *et al.*, 2015). *Exosc3*$^{gfp/gfp}$*.Rosa26Cre*$^{ERT2/ERT2}$ displayed was profound pancytopenia, with the largest difference in neutrophils and platelets in keeping with H-ARS phenotype, however there was a reduction total white cell count, T- and B-cell and haemoglobin. The observation of this at 10 days is less than the half-life of these cell types indicating that differentiated cells are affected as well. This may be due to the ubiquitous expression of Exosc3, resulting in these cells undergoing cell death following Exosc3 knock-out. It is less clear why the haemoglobin in these mice is affected as erythrocytes lack RNA. There is clear evidence of reduced erythropoiesis, as demonstrated in the reduced reticulocyte percentage, this finding is supported by the demonstration that the RNA exosome is crucial for red cell development (McIver *et al.*, 2016; Mehta *et al.*, 2021; Fraga de Andrade *et al.*, 2022). It has been demonstrated *in vivo* that disruption of the exosome complex during development (using a *Vav-1* cre model) results in failure to produced erythroid precursors (at the Burst forming unit (BFU) stage) and leads to reduced c-kit surface expression. Within red cell development c-kit is essential for signalling to drive proliferation and maturation. Along with the reduction in the BFU there was an increase in apoptotic markers and increase in TNF receptor transcripts (Fraga de Andrade *et al.*, 2022). These are findings that were seen in the *Exosc3*$^{gfp/gfp}$*.Rosa26Cre*$^{ERT2/ERT2}$. There was a reduction in c-kit expression in the lin$^-$ cells from $2.76x10^5$ to $5.76x10^3$. TNF-α was measured to determine whether this was increased in the *Exosc3*$^{gfp/gfp}$*.Rosa26Cre*$^{ERT2/ERT2}$ mice, this was raised indicating activation of death cell pathways. Cell cycle and apoptosis analysis also indicated an increase in the proportion of cells that had undergone apoptosis, with

a blockage of cell cycle at G_0/G_1 stage. Together these data indicate that *Exosc3*$^{gfp/gfp}$*.Rosa26Cre*$^{ERT2/ERT2}$ mice had bone marrow failure secondary to aplastic causes, similar to H-ARS. The exact pathogenesis of ARS is not understood, one of the effects of ARS is depletion of metabolic precursors and cell stress (Huang *et al.*, 2019).

6.3.4.1. Sca-1 positivity

Sca-1 is widely used, in conjunction with other antibodies, to isolate murine stem cells (Figure 6-25) (Holmes and Stanford, 2007); despite this the exact function of Sca-1 has yet to be elucidated. It has been shown that Sca-1 is essential for normal HSC proliferation (Morcos *et al.*, 2017) in response to interferon or polyinosinic-polycytidylic acid (double stranded RNA that is known to simulate viral infection and therefore induce interferon) HSCs upregulate Sca-1 and are pushed from a quiescent G_0 state in to active proliferation (Essers *et al.*). Following Exosc3 ablation there was a preservation of $Sca1^+$ cells following Exosc3 knock-out (Figure 6-26). Due to the bone marrow stress induced by Exosc3 ablation it is possible that this represents an attempt to replace the stem cell pool by driving increased proliferation within the diminished pool of viable HSCs. An alternative explanation is that $Sca1^+$ cells are inherently radiation resistant (Chen *et al.*, 2007).

In the absence of a functioning RNA exosome there is an increase in the total RNA, due failure to degrade RNA species (Pefanis *et al.*, 2014). One possible consequence of this increased RNA is inappropriate activation of interferon pathways. This has previously been demonstrated in other genetic disease of nucleic acid surveillance, collectively known as type 1 interferonopathies, this increased interferon results in upregulation of Sca1 within the bone marrow. This is further explored by utilising interferon receptor knock-out mice (7.1).

6.3.4.2. Bowel phenotype

Following Exosc3 knock-out there was evidence of diarrhoea and anorexia in the mice. In keeping with this clinical finding there was histological evidence of typhlitis and neutrophilic infiltration in the large bowel and caecum, with evidence of villous blunting. These changes are in keeping with the changes seen in patients who sustain irradiation injury as part of ARS (GI-ARS) (Gurley *et al.*). GI-ARS is known to occur following high levels of radiation damage, in humans this is a dose >10Gy, compared to 0.7Gy that can result in H-ARS (CDC data). GI-ARS is almost universally fatal in humans, with death occurring secondary to dehydration and bacterial translocation (Booth *et al.*, 2012). The changes seen in GI-ARS occur due to widespread apoptosis in the radiosensitive fast dividing cells intestinal epithelium; this epithelial breakdown pre-disposes to the dehydration, electrolyte imbalance and bacteraemia, which with the addition of marrow suppression of H-ARS result in overwhelming sepsis. These changes are identical to those seen in *Exosc3*$^{gfp/gfp}$*.Rosa26Cre*$^{ERT2/ERT2}$ mice treated with 4 days of tamoxifen. The damage seen in GI-ARS has been shown to be caused by upregulation of pro-apoptotic factors, specifically p53 and Bcl-2 (Merritt *et al.*, 1994).

6.3.4.3. Differences between patients and mouse model

Humans with *EXOSC3*-related disease develop pontocerebellar hypoplasia 1b (Wan *et al.*, 2012). Using whole exosome sequencing in patients with aHUS *EXOSC3* variants were identified as a cause of non-complement mediated TMA (4.3.1). Previously identified patients with EXOSC3-mediated disease have all been found to have hypomorphic variants, with no reports of human patients with null variants (Karczewski *et al.*, 2020). Data on constitutive Exosc3 knock-out in mouse has demonstrated embryonic lethality at E14.5 (Personal communication, Uttiya Basu). These data all demonstrate the essential nature of the RNA exosome in

development and potentially explain why Exosc3 knock-out mice do not recapitulate the human phenotype. It is now clear that the intricate interaction between the EXOSC3 and specific co-factors are essential for normal function (4.5.1.3), it is possible that complete knockout of the RNA exosome is not Interaction between the RNA exosome and co-factors an accurate recapitulation of the human phenotype as it will obliterate the RNA exosome, whereas it may be that subtle changes in the interaction between the RNA exosome and co-factors are responsible for the human phenotype. This could be addressed in future by developing a patient specific mouse knock-in.

TMA is a disease of endothelial dysfunction; these cells are slow dividing and fully differentiated cells. This may be why whole body Exosc3 knockout mice did not develop an endothelial phenotype as fast cycling cells (the bone marrow and gastrointestinal tract) were dying before an endothelial cell phenotype developed. To further investigate this, an attempt at an endothelial specific Cre^{ERT2} mouse was developed (8).

Treating mice with a sub-lethal dose of tamoxifen (three days) and allowing these mice to age to one year post treatment was a way to investigate the effects of chronic Exosc3 knock down. This demonstrate GFP expression in all tissues investigated 1 year after treatment, however only 65% of endothelial cells within the kidney demonstrated GFP expression. The work done in mice treated for 4 days it was demonstrated that >85% of cells needed to have undergone recombination for a phenotype to develop (Figure 6-15). Additionally, it is not possible to determine whether both *Exosc3* alleles have undergone recombination using GFP positivity, despite attempts to investigate Exosc3 protein levels in these mice it proved challenging with no convincing antibody available to determine Exosc3 levels. To

determine whether one or both alleles was knocked out in the cell single cell RNA sequencing could be used in the future to investigate the endothelium.

6.3.4.4. Potential role in TMA

The discovery that *Exosc3*$^{gfp/gfp}$*.Rosa26Cre*$^{ERT2/ERT2}$ mice developed a phenotype consistent with a ribosomopathy (cell cycle arrest, apoptosis and TNFα expression in fast dividing and highly metabolically active tissues) offers potential insight into the development of TMA in patients. This identification of ribosomal dysfunction is comparable to the data from other model organisms of Exosc3 knock-out; these models develop P53 mediated apoptosis and cell cycle arrest attributed to ribosomal dysfunction (Morton *et al.*, 2020; Müller *et al.*, 2020).

STEC-HUS is the most common form of TMA in children. As outlined previously (*Figure 1-2*) the underlying pathogenesis of this disease is ribosomal dysfunction secondary to Stx. production; this toxin is a member of the ribosome-inactivating protein family. Following binding to the Gb_3 receptor Stx. is internalised and processed through the Golgi and ultimately binds to and inactivates ribosomes. This ribosomal dysfunction results in ribosomal stress response, protein synthesis arrest and upregulation of pro-inflammatory and pro-apoptotic pathways, including TNF-α expression (Melton-Celsa, 2014). This is the phenotype seen in the *Exosc3*$^{gfp/gfp}$*.Rosa26Cre*$^{ERT2/ERT2}$ mice, in which cell cycle arrest, apoptosis and TNF-α expression were all seen. Unfortunately these changes were not seen in the endothelium in this model likely due to the slow turn-over time of the endothelium.

6.3.4.5. Summary

The data presented on the whole body *Exosc3* knockout mouse demonstrates a phenotype similar to that of overwhelming ribosomal dysfunction. This data demonstrates the essential nature of the RNA exosome in rapidly dividing cells.

Whilst there was no evidence of a TMA in this model, the observed ribosomal dysfunction phenotype of increase in apoptosis, cell cycle arrest and pro-inflammatory cytokine production are features of both STEC-HUS and Exosc3-mediated TMA.

The similarity between ARS and Exosc3 knock-out means that $Exosc3^{fl}$ mice may be valuable for the investigation of potential treatments in ARS. Research into treatments in ARS is challenging due to the predictable pattern of damage, e.g. the emergence of H-ARS at lower doses than GI-ARS and N-ARS. $Exosc3^{fl}$ mice could be bred with specific Cre^{ERT2} expressers to enable investigation of ARS in specific cell types and allow investigation of various treatments.

6.4. Hypothesis

1. I hypothesis that the cause of the observed phenotype in these mice is due to either:
    a. Ectopic activation of interferon pathways due to the accumulation of aberrant RNA (Figure 4-13) or
    b. The induction of apoptosis through p53 mediated pathways (Figure 4-14)
2. I hypothesis that that absence of TMA in this mouse model was due to the rapidity of the bone marrow and gut failure. To examine the effects on the endothelium, Exosc3 knockout could be restricted to this cell type.

7. Attempts to Improve the Survival of the *Exosc3$^{gfp/gfp}$.Rosa26Cre$^{ERT2/ERT2}$* mouse

7.1. Development of the Exosc3$^{fl/fl.}$Rosa26Cre$^{ERT2/ERT2}$Ifnar$^{-/-}$ mouse

To examine the hypothesis that Exosc3-mediated TMA is a form of interferonopathy due to ectopic activation of RNA sensing pathways in the cell, secondary to accumulation of abnormal RNA species in the presences of a non-functioning exosome (Figure 4-13) interferon signalling in the mouse was knocked out. There is evidence that chronic exposure to or expression of interferon causes TMA (Hunt *et al.*, 2014; Kavanagh *et al.*, 2016; Duncan *et al.*, 2019b). To determine whether interferon knock-out could rescue the phenotype, an *Exosc3$^{fl/fl}$.Rosa26Cre$^{ERT2/ERT2}$* (type-I interferon-α/β receptor knock-out) was generated.

7.1.1. Generation of the Exosc3$^{fl/fl.}$Rosa26Cre$^{ERT2/ERT2}$Ifnar$^{-/-}$mouse

Exosc3$^{fl/fl}$.Rosa26Cre$^{ERT2/ERT2}$ mice were bred with Ifnar$^{-/-}$ to generate a triple transgenic *Exosc3$^{fl/fl}$.Rosa26Cre$^{ERT2/ERT2}$.Ifnar$^{-/-}$* mouse, due to the large lead team required to generate a triple transgenic model this work was commenced at the very beginning of the project in tandem with the generation of the *Exosc3$^{fl/fl}$.Rosa26Cre$^{ERT2/ERT2}$*. This mouse enabled Exosc3 ablation following tamoxifen treatment. Mice were difficult to breed to the triple transgenic homozygote status, as litters were frequently lost within the first five days of life, possibly due to increased susceptibility to infection in the *Ifnar$^{-/-}$* mice. Only four experimental mice were available to generate results, therefore some data sets are incomplete.

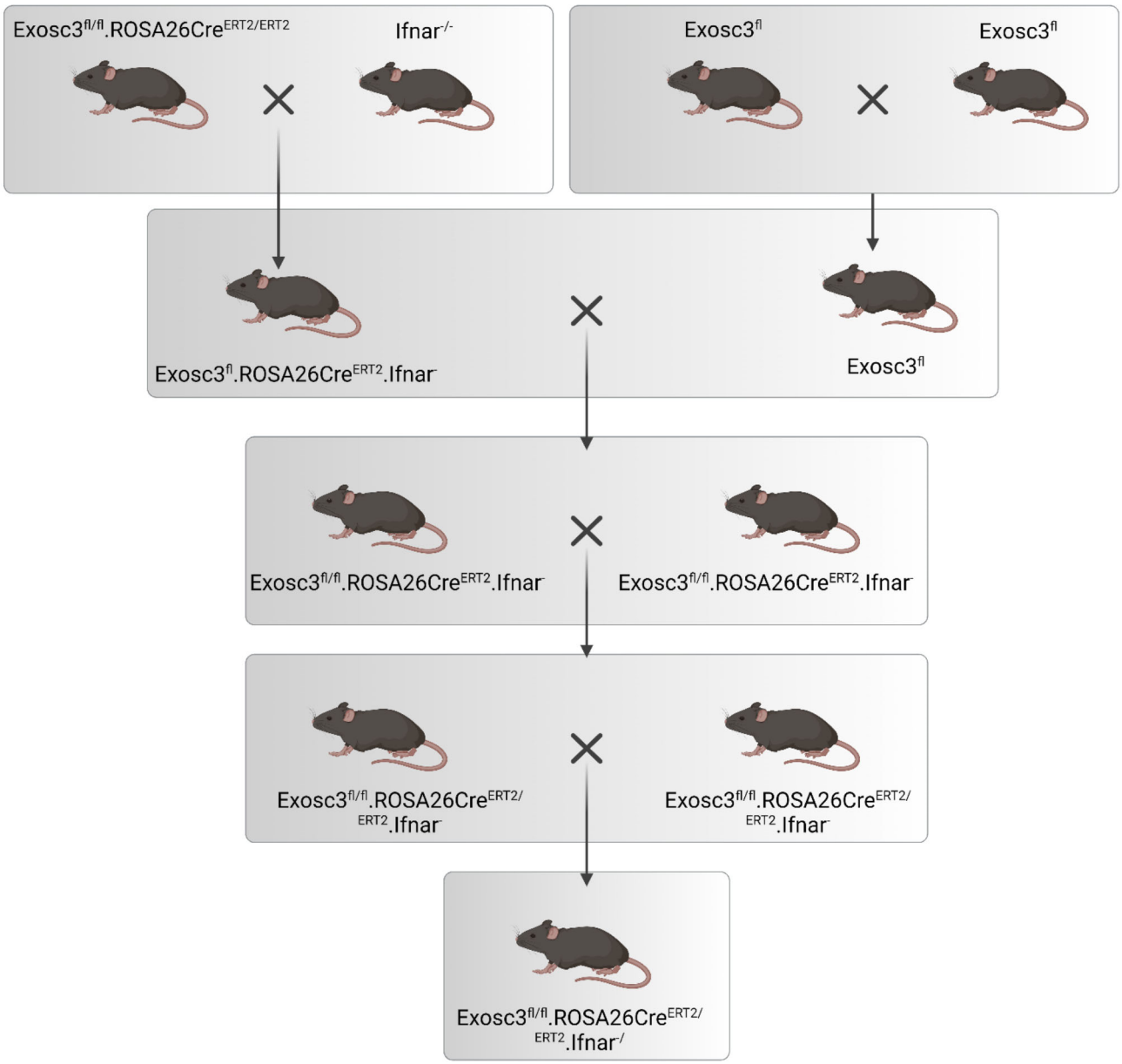

Figure 7-1: Exosc3$^{fl/fl}$.Rosa26Cre$^{ERT2/ERT2}$.Ifnar$^{-/-}$ breeding strategy.

Exosc3$^{fl/fl}$.Rosa26Cre$^{ERT2/ERT2}$ mice were bred with Ifnar$^{-/-}$ mice to generate mice that were heterozygous at each allele, these were bred with Exosc3$^{fl/fl}$. Mice were selected that were homozygous for the Exosc3$^{fl/fl}$ and Rosa26Cre$^{ERT2/ERT2}$ alleles, finally these mice were bred together to generate Exosc3$^{fl/fl}$.Rosa26Cre$^{ERT2/ERT2}$.Ifnar$^{-/-}$

7.1.2. Ifnar Genotyping

Genotyping of mice was performed on ear punch biopsies as described.

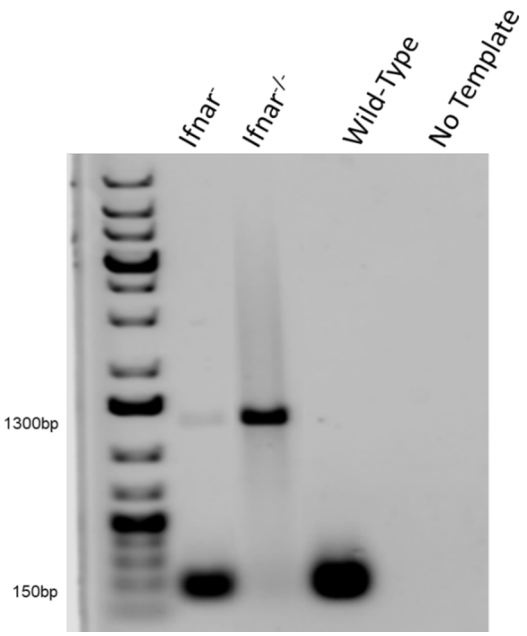

Figure 7-2: Ifnar$^{-/-}$ genotyping PCR

Genotyping was performed on ear punch biopsies and separated on 1.5% agarose TAE gel. Ladder Generuler 1Kb plus, Homozygous Ifnar$^{-/-}$ single band at 1300bp, wild-type single band at 150bp, heterozygous bands at 1300bp and 150bp.

7.1.3. Mouse survival

To determine if there was evidence of effect on the mouse phenotype in the *Exosc3$^{fl/fl}$.Rosa26Cre$^{ERT2/ERT2}$.Ifnar$^{-/-}$* mice were treated with standard tamoxifen protocol (75mg/Kg/d I.P. for 4 days); mouse weights and condition score was recorded daily. Any mice recording a score of 15 were considered to have breached the pre-arranged score were euthanised. Following recombination using the standard tamoxifen protocol there was no difference in the percentage of GFP positive splenocytes in *Exosc3$^{gfp/gfp}$.Rosa26Cre$^{ERT2/ERT2}$.Ifnar$^{-/-}$* compared to the *Exosc3$^{gfp/gfp}$.Rosa26Cre$^{ERT2/ERT2}$* (Figure 7-3). Survival analysis in these mice demonstrated a significantly reduced time to death in *Exosc3$^{gfp/gfp}$.Rosa26Cre$^{ERT2/ERT2}$.Ifnar$^{-/-}$* mice compared to

Exosc3$^{gfp/gfp}$*.Rosa26Cre*$^{ERT2/ERT2}$ (median survival 6 days vs. 8 days) (Figure 7-4), suggesting a more severe phenotype in *Exosc3*$^{gfp/gfp}$*.Rosa26Cre*$^{ERT2/ERT2}$*.Ifnar*$^{-/-}$ mice.

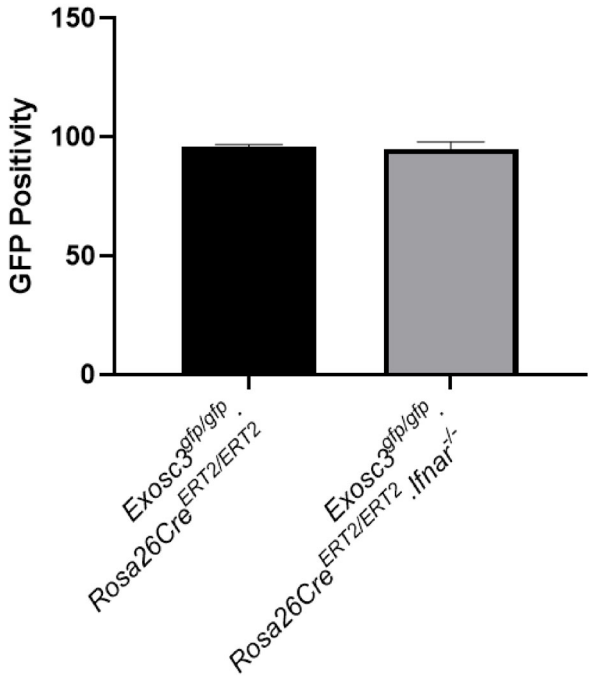

Figure 7-3: Splenocytes GFP positivity following 4 days tamoxifen treatment

Single cell suspension generated via mechanical disruption of spleen, followed by red cell lysis. 1x10^6*cells stained with viability dye. GFP positivity detected via flow cytometry, after gating out debris, doublets and dead cells. (n=3 for Exosc3*$^{gfp/gfp}$*.Rosa26Cre*$^{ERT2/ERT2}$*, =2 for Exosc3*$^{gfp/gfp}$*.Rosa26Cre*$^{ERT2/ERT2}$*.Ifnar*$^{-/-}$*)*

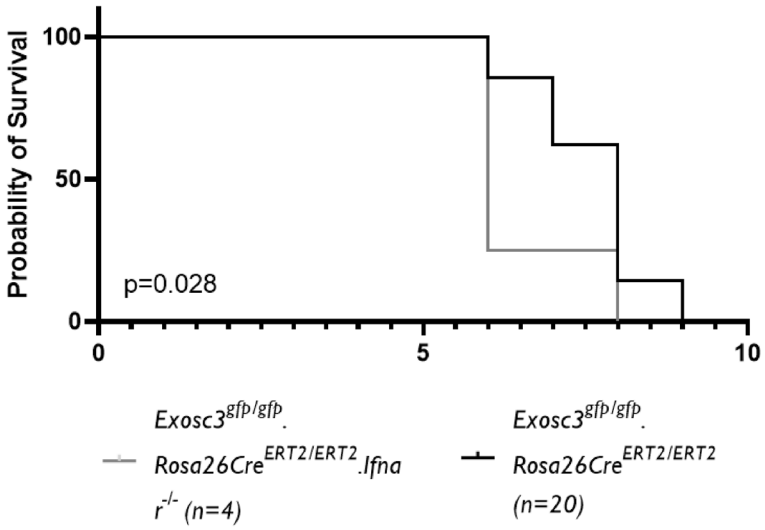

Figure 7-4: Survival analysis in Exosc3$^{gfp/gfp}$.Rosa26Cre$^{ERT2/ERT2}$.Ifnar$^{-/-}$and Exosc3$^{gfp/gfp}$.Rosa26Cre$^{ERT2/ERT2}$ mice

Decreased survival in Exosc3$^{gfp/gfp}$.Rosa26Cre$^{ERT2/ERT2}$.Ifnar$^{-/-}$ mice compared to Exosc3$^{gfp/gfp}$.Rosa26Cre$^{ERT2/ERT2}$ mice. Mantel-Cox analysis used to determine differences between the groups.

7.1.4. Haematological analysis

7.1.4.1. Red cell analysis

As there was no difference between the phenotype of *Exosc3$^{gfp/gfp}$.Rosa26Cre$^{ERT2/ERT2}$.Ifnar$^{-/-}$* and *Exosc3$^{gfp/gfp}$.Rosa26Cre$^{ERT2/ERT2}$* mice, investigations were undertaken to determine whether the haematological phenotype had been altered as a result of *Ifnar$^{-/-}$*. Following tamoxifen treatment *Exosc3$^{gfp/gfp}$.Rosa26Cre$^{ERT2/ERT2}$.Ifnar$^{-/-}$* mice were anaemic with suppressed reticulocyte count (Figure 6-21). There was no significant difference between *Exosc3$^{gfp/gfp}$.Rosa26Cre$^{ERT2/ERT2}$.Ifnar$^{-/-}$* compared to *Exosc3$^{gfp/gfp}$. Rosa26Cre$^{ERT2/ERT2}$* mice (haemoglobin 7.1g/L vs. 8.9g/L and reticulocyte percentage 0.84% vs. 0.45%)

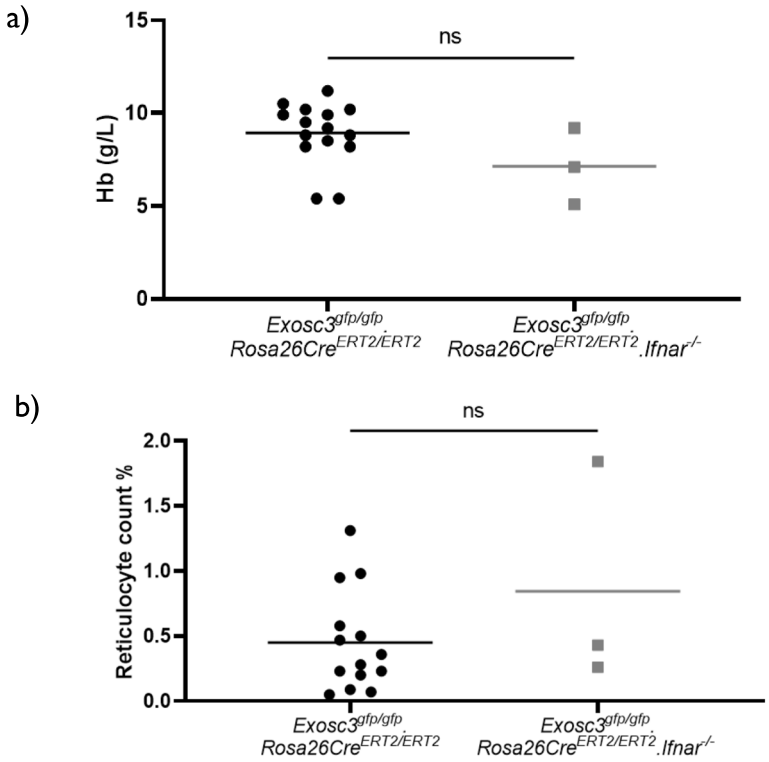

Figure 7-5: Haematological parameters following tamoxifen treatment in Exosc3$^{gfp/gfp}$.Rosa26Cre$^{ERT2/ERT2}$.Ifnar$^{-/-}$ and Exosc3$^{gfp/gfp}$.Rosa26Cre$^{ERT2/ERT2}$ mice

Haemoglobin as measured by iSTAT in Exosc3$^{gfp/gfp}$.Rosa26Cre$^{ERT2/ERT2}$.Ifnar$^{-/-}$ and Exosc3$^{gfp/gfp}$.Rosa26Cre$^{ERT2/ERT2}$ mice following tamoxifen treatment, demonstrating no significant difference in degree of anaemia between Exosc3$^{gfp/gfp}$.Rosa26Cre$^{ERT2/ERT2}$.Ifnar$^{-/-}$ and Exosc3$^{gfp/gfp}$.Rosa26Cre$^{ERT2/ERT2}$ mice following tamoxifen treatment. b) Reticulocyte percentage determined by flow cytometry, demonstrating no significant difference between Exosc3$^{gfp/gfp}$.Rosa26Cre$^{ERT2/ERT2}$.Ifnar$^{-/-}$ and Exosc3$^{gfp/gfp}$.Rosa26Cre$^{ERT2/ERT2}$ mice indicating aplastic cause of anaemia in mice. (n=14 in Exosc3$^{gfp/gfp}$.Rosa26Cre$^{ERT2/ERT2}$ group and =3 in Exosc3$^{gfp/gfp}$.Rosa26Cre$^{ERT2/ERT2}$.Ifnar$^{-/-}$) Unpaired t-test used to analyse between groups

7.1.4.2. Platelet count

Platelet count was only available for 2 *Exosc3$^{gfp/gfp}$.Rosa26Cre$^{ERT2/ERT2}$.Ifnar$^{-/-}$* mice, due to clots in other samples. This demonstrated no significant difference between the *Exosc3$^{gfp/gfp}$.Rosa26Cre$^{ERT2/ERT2}$* and *Exosc3$^{gfp/gfp}$.Rosa26Cre$^{ERT2/ERT2}$.Ifnar$^{-/-}$* mice (Figure 7-5).

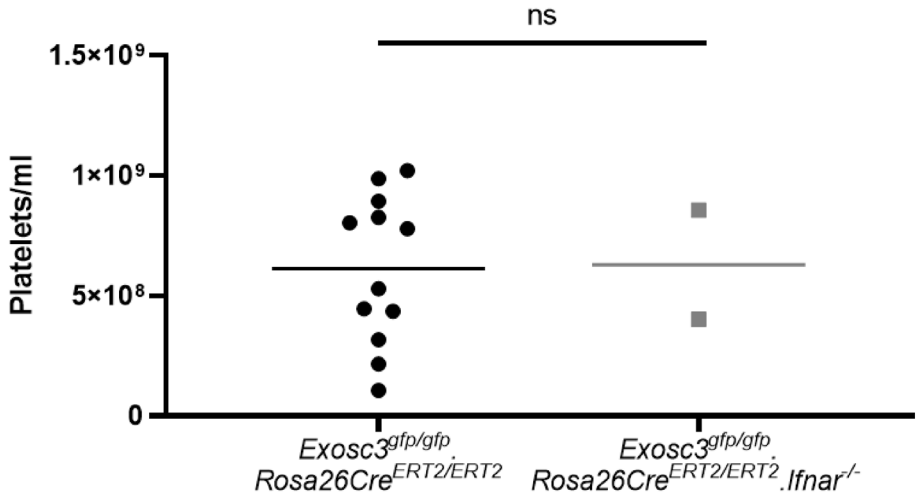

Figure 7-6: Total platelet count in Exosc3$^{gfp/gfp}$.Rosa26Cre$^{ERT2/ERT2}$.Ifnar$^{-/-}$ and Exosc3$^{gfp/gfp}$.Rosa26Cre$^{ERT2/ERT2}$ mice following tamoxifen treatment

Measured by flow cytometry, as previously described. No significant difference was seen between Exosc3$^{gfp/gfp}$.Rosa26Cre$^{ERT2/ERT2}$.Ifnar$^{-/-}$ and Exosc3$^{gfp/gfp}$.Rosa26Cre$^{ERT2/ERT2}$ mice. (n=12 in Exosc3$^{gfp/gfp}$.Rosa26Cre$^{ERT2/ERT2}$ group and =2 in Exosc3$^{gfp/gfp}$.Rosa26Cre$^{ERT2/ERT2}$.Ifnar$^{-/-}$) Unpaired t-test used to analyse between groups.

7.1.4.3. White Cell Count

A white cell count was performed on the *Exosc3$^{gfp/gfp}$.Rosa26Cre$^{ERT2/ERT2}$.Ifnar$^{-/-}$* mice to determine whether there was any evidence of bone marrow suppression, decreased white cell count, or infection, due to interferon signalling deficiency, increased white cell count. There was no significant difference between

Exosc3$^{gfp/gfp}$*.Rosa26Cre*$^{ERT2/ERT2}$ and *Exosc3*$^{gfp/gfp}$*.Rosa26Cre*$^{ERT2/ERT2}$*.Ifnar*$^{-/-}$ mice (Figure 7-7).

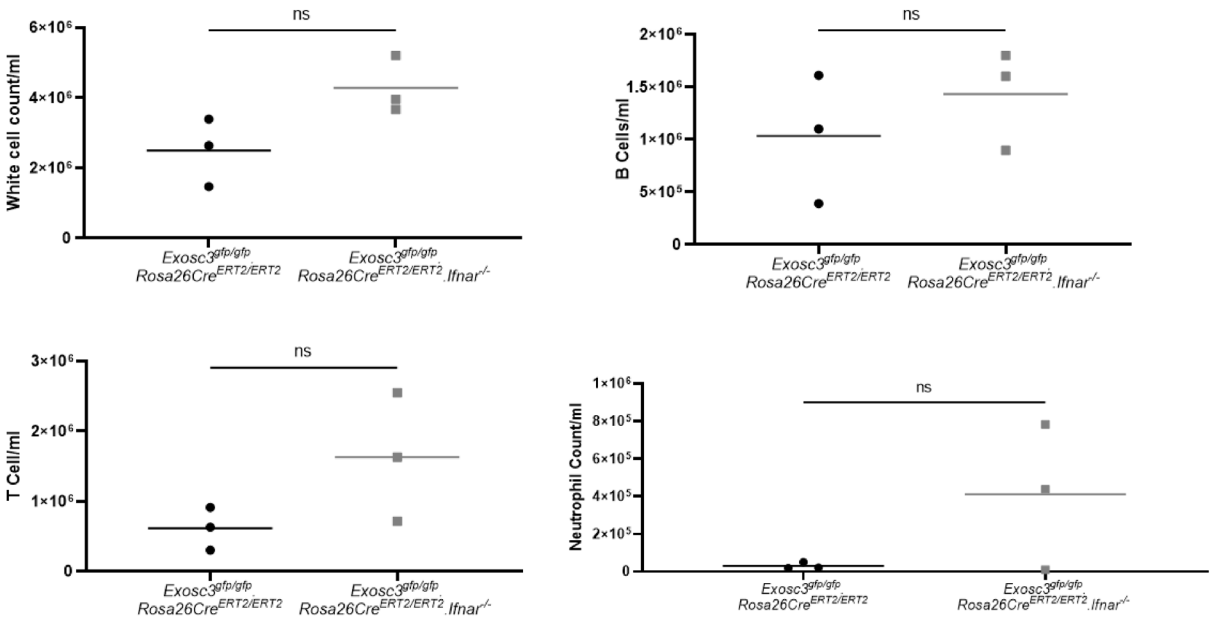

Figure 7-7 Total cells per ml in Exosc3$^{gfp/gfp}$*.Rosa26Cre*$^{ERT2/ERT2}$ *and Exosc3*$^{gfp/gfp}$*.Rosa26Cre*$^{ERT2/ERT2}$*.Ifnar*$^{-/-}$ *mice following tamoxifen treatment.*

There was no significant difference between Exosc3$^{gfp/gfp}$*.Rosa26Cre*$^{ERT2/ERT2}$ *and Exosc3*$^{gfp/gfp}$*.Rosa26Cre*$^{ERT2/ERT2}$*.Ifnar*$^{-/-}$ *mice (n=3 in Exosc3*$^{gfp/gfp}$*.Rosa26Cre*$^{ERT2/ERT2}$ *group and =3 in Exosc3*$^{gfp/gfp}$*.Rosa26Cre*$^{ERT2/ERT2}$*.Ifnar*$^{-/-}$*) Unpaired t-test used to analyse between groups*

7.1.5. Bone marrow analysis

7.1.5.1. Cell count

To determine whether the bone marrow phenotype seen in the *Exosc3*$^{gfp/gfp}$*.Rosa26Cre*$^{ERT2/ERT2}$*.Ifnar*$^{-/-}$ was similar to *Exosc3*$^{gfp/gfp}$*.Rosa26Cre*$^{ERT2/ERT2}$ bone marrow count was determined using the Anvajo cell counter following extraction of the bone marrow and red cell lysis. This demonstrated a significantly lower bone marrow cell count in

Exosc3$^{gfp/gfp}$*.Rosa26Cre*$^{ERT2/ERT2}$*.Ifnar*$^{-/-}$compared to *Exosc3*$^{gfp/gfp}$*.Rosa26Cre*$^{ERT2/ERT2}$*.Ifnar*$^{-/-}$mice (Figure 7-8).

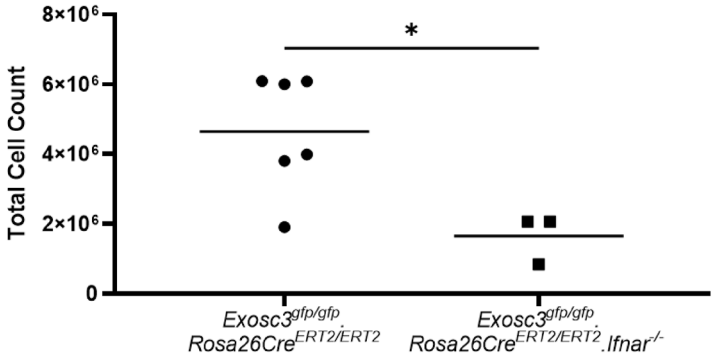

Figure 7-8 Total bone marrow cell count, following red cell lysis treatment

Measured on Anvajo cell counter. (n=6 in Exosc3$^{gfp/gfp}$*.Rosa26Cre*$^{ERT2/ERT2}$ *group and =3 in Exosc3*$^{gfp/gfp}$*.Rosa26Cre*$^{ERT2/ERT2}$*.Ifnar*$^{-/-}$*) Unpaired t-test used to analyse between groups*

7.1.5.2. Stem cell analysis

Analysis of the bone marrow demonstrated a significantly reduced number of Sca1 positive cells in the *Exosc3*$^{gfp/gfp}$*.Rosa26Cre*$^{ERT2/ERT2}$*.Ifnar*$^{-/-}$ mouse, potentially indicating a failure to upregulate Sca1 in this cell population. Sca1 has been shown to be upregulated in response to interferon (23, 24).

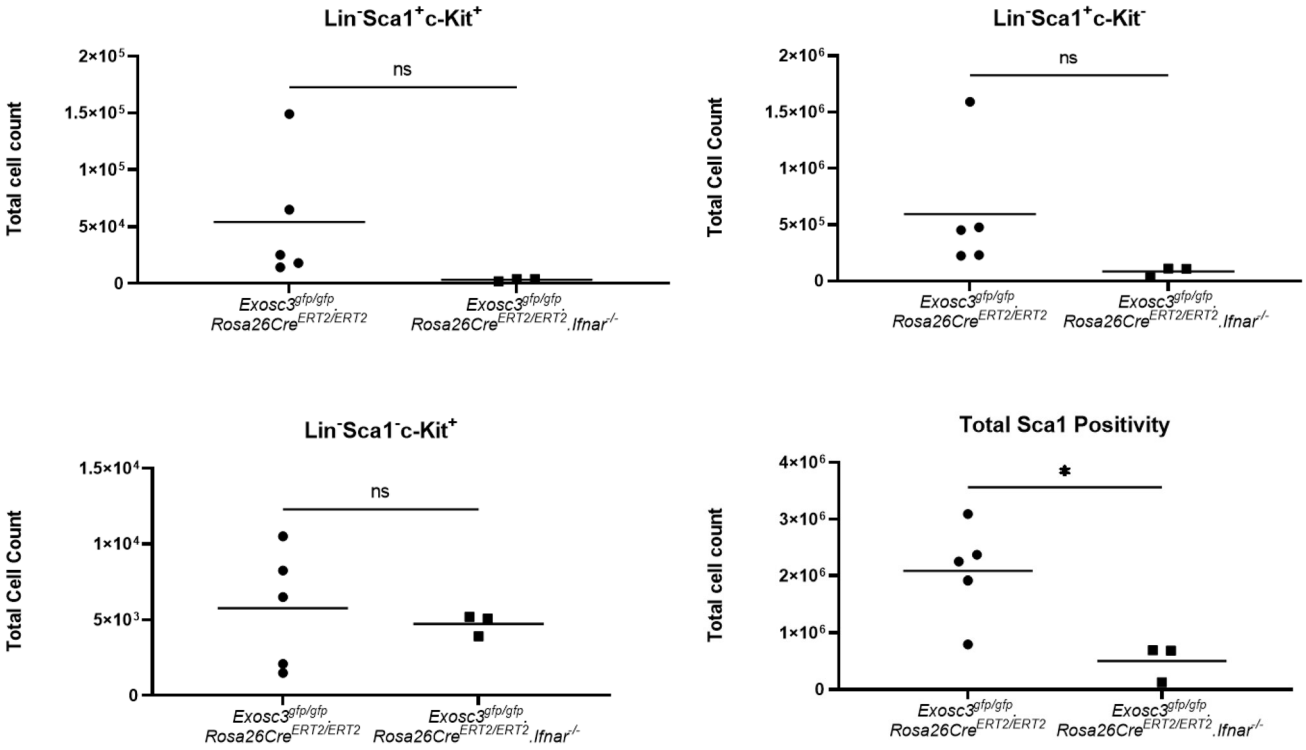

Figure 9: Stem cell analysis in Exosc3gfp/gfp.Rosa26CreERT2/ERT2.Ifnar-/- compared to Exosc3gfp/gfp.Rosa26CreERT2/ERT2 mice.

Total Sca1 positive cells demonstrated reduced Sca1 positive cell in Exosc3$^{gfp/gfp}$.Rosa26Cre$^{ERT2/ERT2}$.Ifnar$^{-/-}$mice. Lineage negative cells were isolated as described and subtypes analysed no significant difference in these cell types were seen in Exosc3$^{gfp/gfp}$.Rosa26Cre$^{ERT2/ERT2}$.Ifnar$^{-/-}$ mice compared to Exosc3$^{gfp/gfp}$.Rosa26Cre$^{ERT2/ERT2}$ mice. (n=5 in Exosc3$^{gfp/gfp}$.Rosa26Cre$^{ERT2/ERT2}$ group and =3 in Exosc3$^{gfp/gfp}$.Rosa26Cre$^{ERT2/ERT2}$.Ifnar$^{-/-}$) Unpaired t-test used to analyse between groups

7.2. Attempts to Improve Survival using P53 Inhibition

One of the other potential causes of the TMA phenotype seen in the patients is ribosomal dysfunction resulting in p53 upregulation. The results of the whole body knock out demonstrate these are features of ribosomal dysfunction (6.2.10.4).

To determine whether p53 modulation would affect the phenotype The *Exosc3*$^{gfp/gfp}$*.Rosa26Cre*$^{ERT2/ERT2}$ *were* treated with PFTα, a p53 antagonist that has been shown to protect mice from acute radiation syndrome (Komarov *et al.*, 1999). The results of this treatment are preliminary and as so data is only available for some parameters.

7.2.1. Mouse survival following treatment with PFTα

To determine if there was evidence of survival effect following PFTα treatment, mice were treated with a single dose of PFTα (2.2mg/Kg I.P.) 24 hours before followed by every 48 hours and treated with standard tamoxifen protocol (75mg/Kg/d I.P. for 4 days). Mouse weights and condition score was recorded daily (3.3.3). Any mice recording a score of 15 were considered to have breached the pre-arranged score were euthanised. Survival analysis in mice following PFTα demonstrated a significant benefit from PFTα treatment (median survival from 8 days to 9 days), indicating a survival benefit from PFTα treatment and suggesting P53 activation is responsible for the phenotype seen in *Exosc3*$^{gfp/gfp}$*.Rosa26Cre*$^{ERT2/ERT2}$ mice (Figure 7-9).

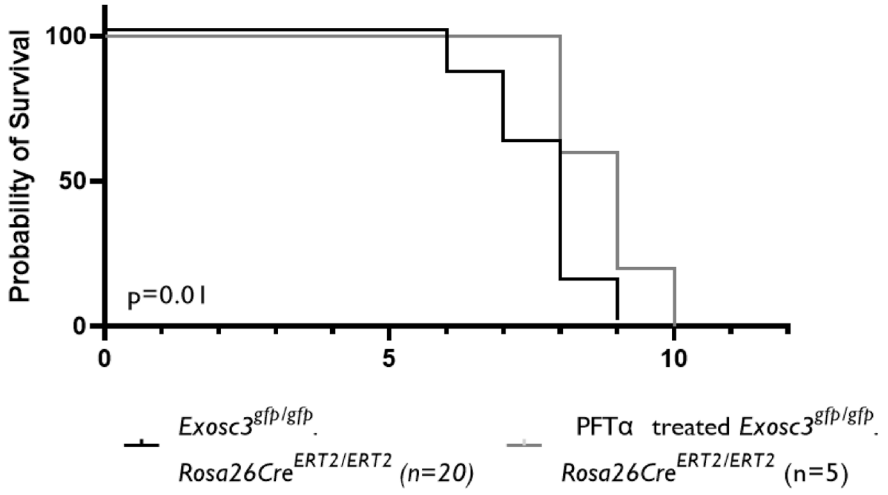

Figure 7-9: Survival analysis in Exosc3$^{gfp/gfp}$.Rosa26Cre$^{ERT2/ERT2}$ mice compared to Exosc3$^{gfp/gfp}$.Rosa26Cre$^{ERT2/ERT2}$ treated with PFTα

Mice were treated with PFTα starting 24 hours before tamoxifen treatment and then every 48 hours, there was a significant increase in survival following PFTα treatment ^{Mantel}-Cox analysis was used to analyse the difference between the two groups.

7.2.2. Haematological analysis

To determine whether the haematological phenotype seen in the *Exosc3$^{gfp/gfp}$.Rosa26Cre$^{ERT2/ERT2}$* was affected by PFTα treatment haemoglobin, platelet and white cell counts were performed.

7.2.2.1. Red cell analysis

To determine if there was any effect on the haematological phenotype following PFTα treatment haemoglobin and reticulocytes were performed. PFTα treatment had no effect on haemoglobin or reticulocyte count compared to *Exosc3$^{gfp/gfp}$.Rosa26Cre$^{ERT2/ERT2}$* mice at time of death (Figure 7-10)

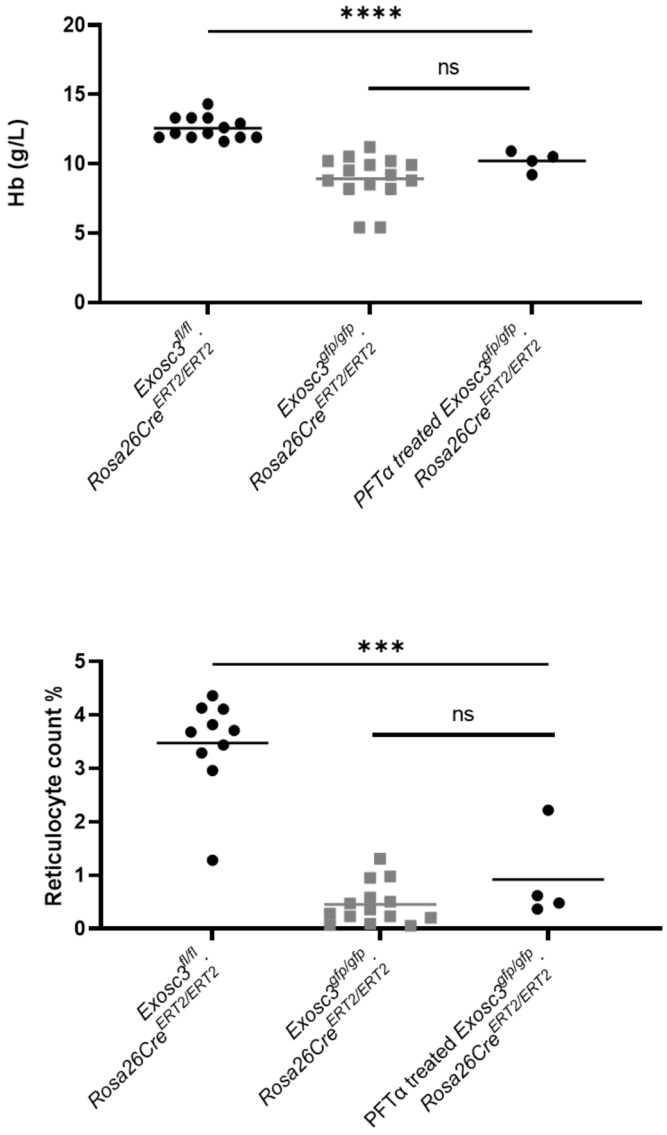

Figure 7-10: Haemoglobin as measured by iSTAT in Exosc3$^{gfp/gfp}$.Rosa26Cre$^{ERT2/ERT2}$ treated with PFTα, Exosc3$^{gfp/gfp}$.Rosa26Cre$^{ERT2/ERT2}$ and Exosc3$^{fl/fl}$.Rosa26Cre$^{ERT2/ERT2}$.

No significant difference in degree of anaemia between PFTα treated and Exosc3$^{gfp/gfp}$.Rosa26Cre$^{ERT2/ERT2}$ mice. Reticulocyte percentage determined via flow cytometry demonstrating no difference between PFTα treated and Exosc3$^{gfp/gfp}$.Rosa26Cre$^{ERT2/ERT2}$ mice. (n=10 in Exosc3$^{fl/fl}$.Rosa26Cre$^{ERT2/ERT2}$ group =15 in Exosc3$^{gfp/gfp}$.Rosa26Cre$^{ERT2/ERT2}$ group and =4 in Exosc3$^{gfp/gfp}$.Rosa26Cre$^{ERT2/ERT2}$ treated with PFTα) Unpaired t-test used to analyse between groups

7.2.2.2. Platelet count

There was an improvement in the platelet count following PFTα treatment in *Exosc3$^{gfp/gfp}$.Rosa26Cre$^{ERT2/ERT2}$* mice and normalisation to baseline, adding further evidence that PFTα treatment is resulting in improvement in the phenotype.

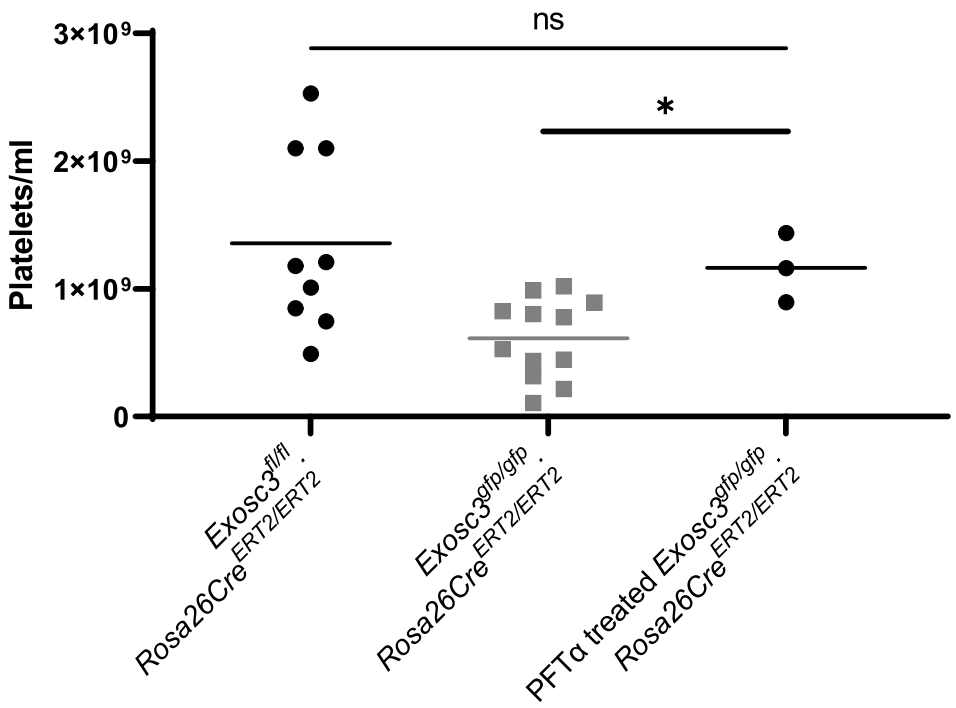

Figure 7-11: Total platelet count in Exosc3$^{gfp/gfp}$.Rosa26Cre$^{ERT2/ERT2}$ treated with PFTα, Exosc3$^{gfp/gfp}$.Rosa26Cre$^{ERT2/ERT2}$ and Exosc3$^{fl/fl}$.Rosa26Cre$^{ERT2/ERT2}$ mice.

Significant improvement in platelet count was seen following treatment with PFT-α in the Exosc3$^{gfp/gfp}$.Rosa26Cre$^{ERT2/ERT2}$ mice. The platelet count was normalised following PFT- α compared to the Exosc3$^{fl/fl}$.Rosa26Cre$^{ERT2/ERT2}$ (n=10 in untreated group =15 in Exosc3$^{gfp/gfp}$.Rosa26Cre$^{ERT2/ERT2}$ group and =4 in PFTα treated Exosc3$^{gfp/gfp}$.Rosa26Cre$^{ERT2/ERT2}$) Unpaired t-test used to analyse between groups

7.2.2.3. White cell count

A white cell count was performed following PFTα treatment to determine whether there was any evidence of a difference between the PFTα treated *Exosc3$^{gfp/gfp}$.Rosa26Cre$^{ERT2/ERT2}$* and *Exosc3$^{gfp/gfp}$.Rosa26Cre$^{ERT2/ERT2}$* mice. This demonstrated no difference between these mice following PFTα treatment.

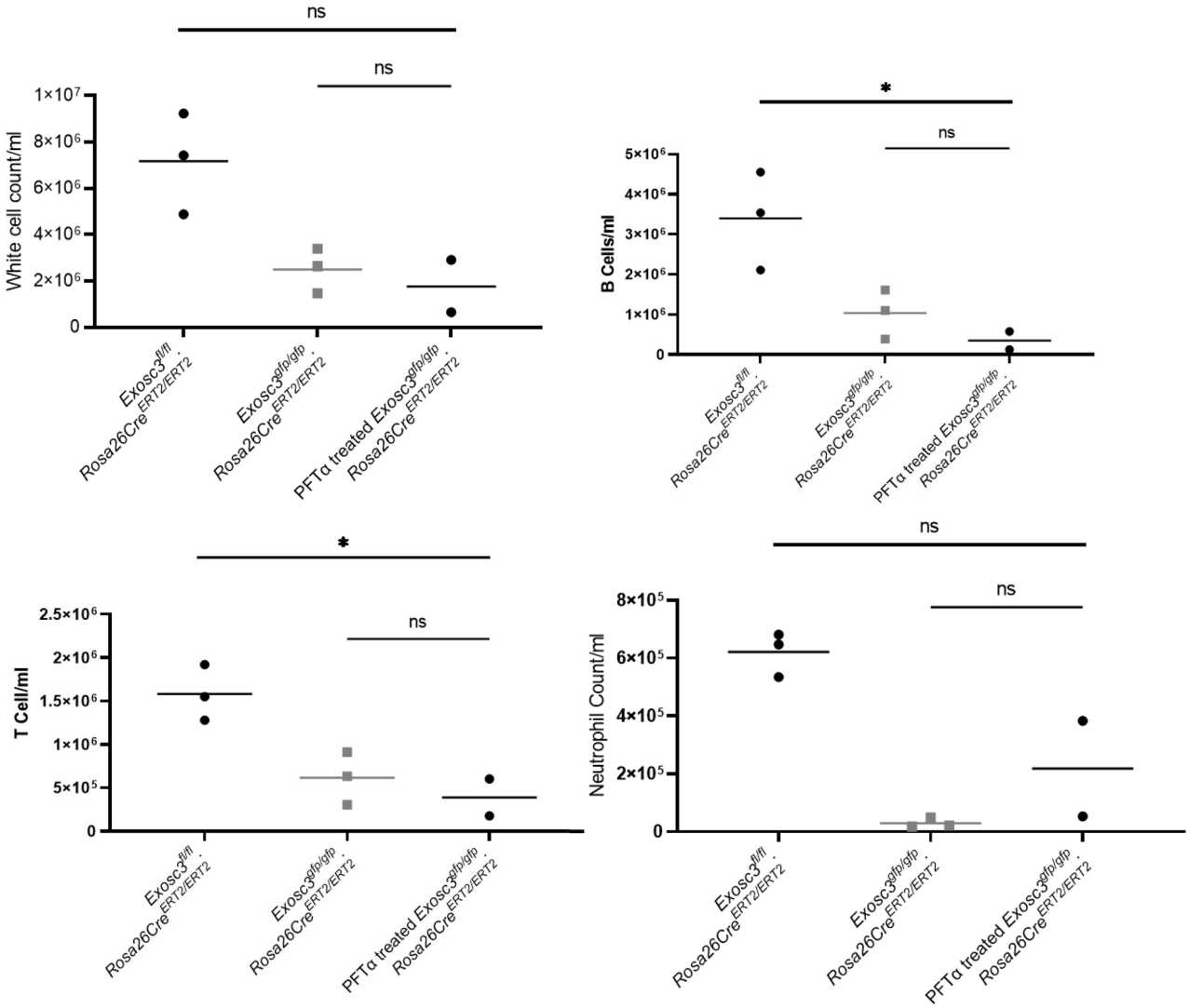

Figure 7-12:Total cells per ml in PFTα treated Exosc3$^{gfp/gfp}$.Rosa26Cre$^{ERT2/ERT2}$ and Exosc3$^{gfp/gfp}$.Rosa26Cre$^{ERT2/ERT2}$ and Exosc3$^{fl/fl}$.Rosa26Cre$^{ERT2/ERT2}$ mice,

As determined by flow cytometry using CD45, CD19, CD3 and Ly6G to enable counting of total white cell, B cell, T cell and neutrophils, respectively. Counting beads were added as previously described to enable cell count. There was no significant difference between Exosc3$^{gfp/gfp}$.Rosa26Cre$^{ERT2/ERT2}$ and Exosc3$^{gfp/gfp}$.Rosa26Cre$^{ERT2/ERT2}$.Ifnar$^{-/-}$ mice, there was evidence of a reduction in B and T cell count, and however there were only two mice available for analysis. (n=3 in Exosc3$^{fl/fl}$.Rosa26Cre$^{ERT2/ERT2}$ group =3 in Exosc3$^{gfp/gfp}$.Rosa26Cre$^{ERT2/ERT2}$ group and =2 in PFTα treated Exosc3$^{gfp/gfp}$.Rosa26Cre$^{ERT2/ERT2}$) Unpaired t-test used to analyse between groups

7.3. Discussion

7.3.1. Interferon receptor knockout

One of the original hypotheses for the TMA phenotype seen in patients with Exosc3-related TMA was that accumulation of aberrant RNA species in the absence of a functioning RNA exosome resulted in ectopic activation of intracellular RNA pattern recognition receptors (PRR). To investigate this the Ifnar$^{-/-}$ mouse was utilised. Interferon acts through binding to Ifnar. This results in activation of JAK/STAT pathways resulting in upregulation of ISGs. ISGs function to inhibit viral infection, including increasing viral sensing proteins, inhibiting viral shedding and promoting Toll-like receptor signalling (Duncan;Randall and Hambleton, 2021). The Ifnar$^{-/-}$ mouse displays increased susceptibility to viral infection due to blunted response to interferon.

Interferonopathies are characterised by chronic neuroinflammation, chilblains, autoimmune disease and in some cases vasculopathy (Crow, 2011). Recently TMA has been reported as the predominant vasculopathy in two separate genetic forms of interferonopathy (Duncan *et al.*, 2019a; Naesens *et al.*, 2022). In addition to genetic forms of interferon dysregulation, there is evidence that iatrogenic chronic interferon exposure results in TMA; patients treated with interferon for multiple sclerosis develop TMA (Hunt *et al.*, 2014) . Additionally, an interferon over expressing mouse model develops TMA lesions (Kavanagh *et al.*, 2016). In these cases, interferon exposure was chronic, in humans more TMA only occurred in patients treated for more than 5 years, in mice lesions were seen at 2-3 months. Together these data suggest that chronic interferon exposure to the endothelium results in TMA. The mechanism underlying this is currently unknown.

In the *Exosc3*$^{gfp/gfp}$*.Rosa26Cre*$^{ERT2/ERT2}$*.Ifnar*$^{-/-}$ mice death occurred in a median of six days, this is too fast for an interferon mediated TMA to develop. There was evidence of a more severe phenotype in the *Exosc3*$^{gfp/gfp}$*.Rosa26Cre*$^{ERT2/ERT2}$*.Ifnar*$^{-/-}$ mouse; one explanation for this would be that in the absence of interferon signalling these mice are more susceptible to infection, secondary to bacterial translocation, could compound the immunosuppression secondary to Exosc3 ablation.

During this project one child with TMA and a *TSEN2* (4.3.1.2) variant, which is within the RNA processing pathway, presented and had ISGs investigated this showed no evidence of increased activity, albeit whilst she was in remission.

7.3.2. Sca1 positivity

Interferon has previously been shown to upregulate Sca1 in the bone marrow, driving cells from a quiescent to a proliferative state (Morcos *et al.*, 2017) . In the *Exosc3*$^{gfp/gfp}$*.Rosa26Cre*$^{ERT2/ERT2}$*.Ifnar*$^{-/-}$ there was a significant reduction in the both the total bone marrow cell count Sca1 positivity cells, this may be due to an inability to activate dormant HSCs in interferon mediated manner, in the absence of the interferon receptor. This could be an additional stress on the animal resulting in the accelerated death of these animals.

7.3.3. Conclusion

The evidence presented from the *Exosc3*$^{gfp/gfp}$*.Rosa26Cre*$^{ERT2/ERT2}$*.Ifnar*$^{-/-}$ mouse suggest that interferon is not causing the observed phenotype in the mice.

7.3.4. P53 inhibition

Previous research utilising the *Exosc3*^{fl} mouse and other model organisms (Müller *et al.*, 2020; Fraga de Andrade *et al.*, 2022; Laffleur *et al.*, 2022) have demonstrated upregulation of p53 as the central pathogenic process in driving apoptosis as a

result of Exosc3 ablation. This phenotype was seen in the *Exosc3*$^{gfp/gfp}$*.Rosa26Cre*$^{ERT2/ERT2}$ mice, the mice developed cell cycle arrest, pro-inflammatory cytokine release and apoptosis. To determine whether the phenotype could be modulated by p53 inhibition, treatment with PFT-α was given to the mice. PFT-α is a small molecule p53 antagonist (Komarov *et al.*, 1999) that alters the post-translational modification of p53 (Zhu *et al.*, 2020) preventing translocation to the nucleus and therefore the p53 mediated gene regulation. There was a significant increase in survival in the *Exosc3*$^{gfp/gfp}$*.Rosa26Cre*$^{ERT2/ERT2}$ mice following PFTα treatment. These data, with the data provided from model organisms (Müller *et al.*, 2020) indicate that the phenotype seen in Exosc3gfp$^{/gfp}$*.Rosa26Cre*$^{ERT2/ERT2}$ is secondary to ribosomal dysfunction, and that p53 inhibition is able to partially rescue these mice. Further optimisation of the experimental conditions are required to confirm this improved survival and demonstrate an effect on other parameters (haematological, gastrointestinal). Firstly PFTα dosing could be optimised, whilst the dosage schedule used in these mice has previously been shown to effect P53-mediated death (Komarov *et al.*, 1999) it is possible that the overwhelming severity of the *Exosc3*$^{gfp/gfp}$*.Rosa26Cre*$^{ERT2/ERT2}$ resulted in rapid cell death prior to the ability to modulate P53. There are a number of new P53 inhibitors that could be used as an alternative to PFTα, including NiCur (Lodi *et al.*, 2022), PFTβ (Christodoulou *et al.*, 2011) and RG7112 (Vu *et al.*, 2013).

8. Attempts to Develop a Conditionally Inducible Endothelial Specific Exosc3 Knock-down Mouse

The results of the whole-body knockout model, *Exosc3$^{gfp/gfp}$.Rosa26Cre$^{ERT2/ERT2}$* demonstrated that mice developed a rapid severe phenotype, mimicking a ribosomopathy (1.1)

TMA is largely a disease of endothelial dysfunction, therefore the role of Exosc3 dysfunction in the endothelium in the mouse was investigated. The Tie2Cre^{ERT2} mouse was used as this has previously been shown to restrict tamoxifen sensitive cre recombination to the endothelium, and a minority (0.2%) of white blood cells (Forde *et al.*, 2002).

8.1.1. Generation of the Exosc3$^{fl/fl}$.Tie2Cre^{ERT2}

Exosc3$^{fl/fl}$.Rosa26Cre$^{ERT2/ERT2}$ mice were bred with Tie2Cre^{ERT2} to generate mice that were homozygous for both the Exosc3^{fl} and Tie2Cre^{ERT2} alleles, the *Exosc3$^{fl/fl}$.Tie2Cre$^{ERT2/ERT2}$* mouse. This mouse should have enabled Exosc3 knockout following tamoxifen treatment restricted to the endothelium.

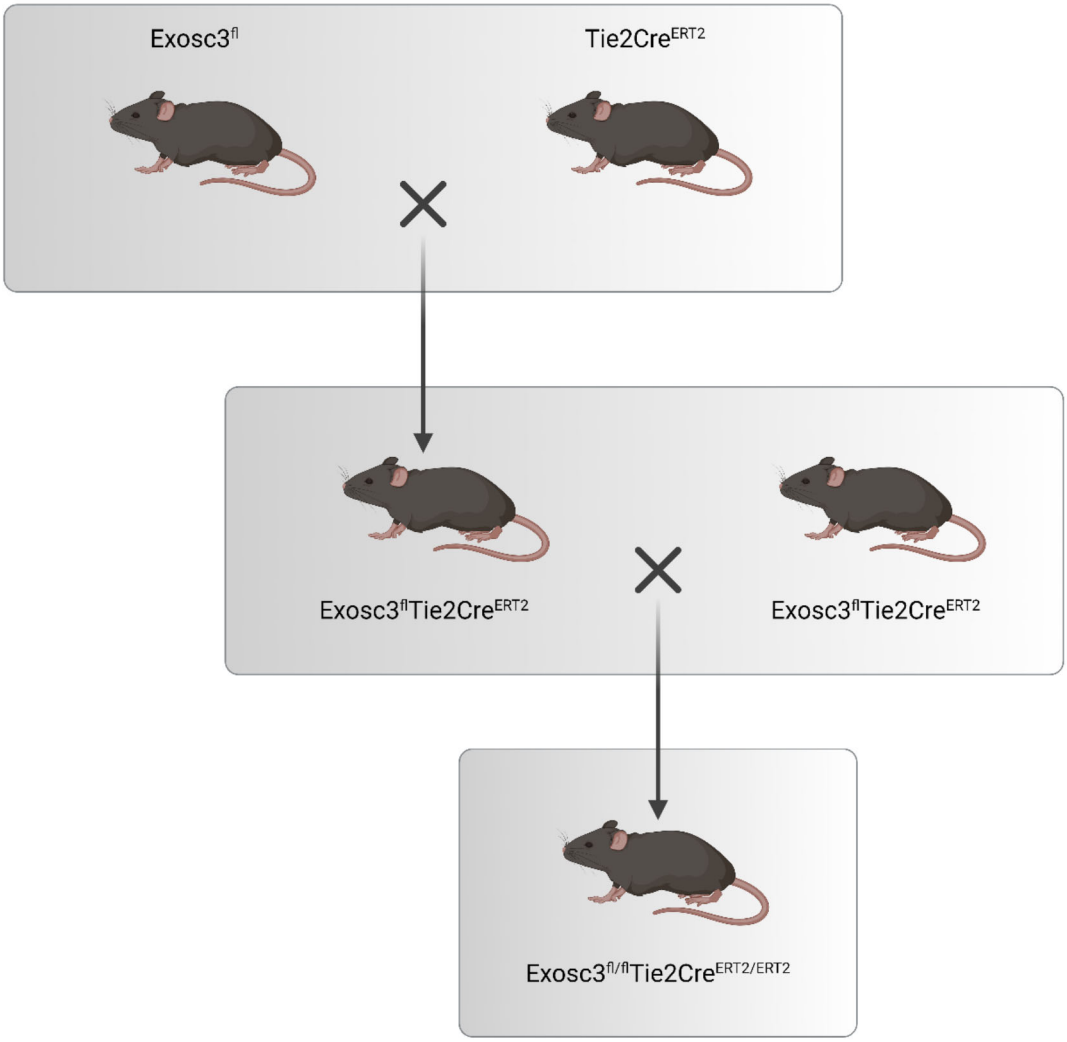

Figure 8-1 Breeding strategy for Exosc3$^{fl/fl}$.Tie2Cre$^{ERT2/ERT2}$ mice

The first breeding round was performed to generate Exosc3^{fl}.Tie2Cre^{ERT2}. These mice were bred together to generate Exosc3$^{fl/fl}$Tie2Cre$^{ERT2/ERT2}$ mice.

8.1.2. Cre Genotyping

Genotyping of mice was performed on ear punch biopsies as described, due to the original design of the mouse, the Tie2Cre^{ERT2} cassette had been introduced as a Bacterial Artificial Chromosome (BAC), which results in random integration, and it was not known where the integration has occurred. To genotype the mice qPCR for the Cre allele was used. This enabled discrimination between wild-type, Tie2Cre^{ERT2} and Tie2Cre$^{ERT2/ERT2}$ mice.

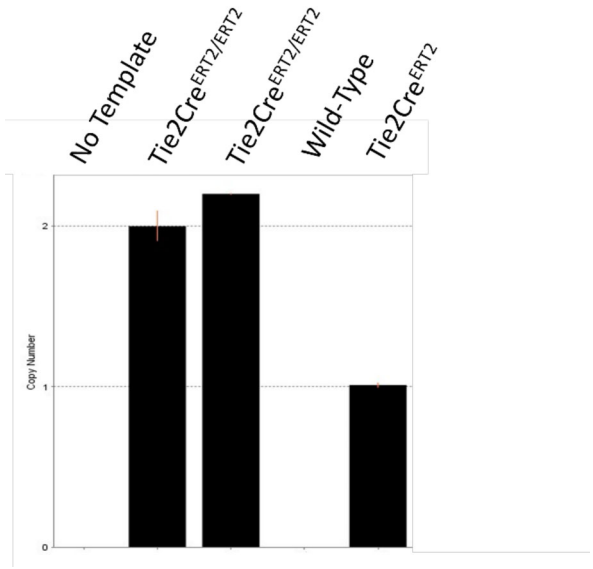

Figure 8-2: Tie2Cre^{ERT2} genotyping qPCR results.

DNA was isolated from mouse ear punch using TaqMan® Sample-to-SNP™. RT-qPCR was then undertaken in duplicate. CopyCaller (Applied biosciences) was used to determine the Cre copy number.

8.1.3. Optimisation of tamoxifen administration

Exosc3$^{fl/fl}$.Tie2Cre$^{ERT2/ERT2}$ mice were treated with standard tamoxifen protocol (75mg/Kg/d I.P. for 4 days); mouse weights and condition score were recorded daily (3.3.5). Any mice recording a score of 15 were considered to have breached the pre-arranged score were euthanised. There was no evidence of a phenotype up to one month following treatment. Mice were euthanised at this point, to determine the

effects of tamoxifen treatment on these mice. As expected, there was no evidence of recombination in splenocytes, however there was no evidence of GFP signal in endothelial cells from kidney or spleen after treatment with I.P. tamoxifen.

8.1.4. Tamoxifen oral administration

The initial description of the B6.Cg-Tg(Tek-cre/ERT2)1Arnd/ArndCnrm demonstrated no recombination following standard I.P. tamoxifen treatment (Forde *et al.*, 2002). In this model mice required five weeks of oral tamoxifen, delivered as 250mg/kg tamoxifen in the chow to achieve recombination. To achieve prolonged oral administration tamoxifen containing chow was used (400mg/kg tamoxifen citrate, equivalent to 250mg/Kg tamoxifen base, Envigo, TD.130860). Upon commencing this diet mice lost an average of 17.5% (range 14-22%, n=8) within 48 hours and stopped eating. This necessitated the re-introduction of normal diet. Gradual introduction of escalating percentage of tamoxifen containing diet (e.g. 30% tamoxifen chow, 50% regular chow, increasing to 55% tamoxifen chow, 25% regular chow) and addition of peanut butter (20%) improved consumption. However, mice lost often lost weight when the percentage of tamoxifen chow was increased, resulting in de-escalation of the tamoxifen chow; resulting in unpredictable dosing.

To determine the efficiency of the tamoxifen containing diet *Exosc3*$^{fl/fl}$*.Rosa26Cre*$^{ERT2/ERT2}$ mice were treated. As discussed in Chapter 6 100% of *Exosc3*$^{gfp/gfp}$*.Tie2Cre*$^{ERT2/ERT2}$ mice breached the pre-defined clinical score within nine days (Figure 8-3). *Exosc3*$^{fl/fl}$*.Tie2Cre*$^{ERT2/ERT2}$ mice treated with the tamoxifen diet did not develop the same phenotype, these mice survived for 5 weeks after starting tamoxifen, however they developed a similar phenotype of anaemia, diarrhoea, and weight loss at five weeks. As tamoxifen is a pro-drug and requires hepatic metabolism to produce biologically active 4-Hydroxytamoxifen (4-OHT) oral

administration should produce an identical phenotype to I.P. administration (as I.P. administration is absorbed via mesenteric vessels that drain into the liver) (Al Shoyaib;Archie and Karamyan, 2019). To determine whether oral administration would achieve the same phenotype as I.P. *Exosc3*$^{fl/fl}$*. Rosa26Cre*$^{ERT2/ERT2}$ mice were treated with oral gavage of 75mg/Kg tamoxifen dissolved in corn oil (the same vehicle as used for I.P. administration), these mice demonstrated weight loss from day one of treatment, with reduced oral intake of chow, this was potentially due to the oral administration of corn oil with tamoxifen, rather than induction of recombination as mice were otherwise well, until day eight when mice developed the same phenotype of anaemia and diarrhoea as the *Exosc3*$^{gfp/gfp}$*.Rosa26Cre*$^{ERT2/ERT2}$ mice treated with I.P. tamoxifen. To prevent weight loss associated with corn oil, tamoxifen was instead dissolved in Kolliphor HS (Sigma), a non-ionic surfactant that is a capable solubiliser and emulsifying agent. Tamoxifen was dissolved at 10mg/ml in Kolliphor HS, this was well tolerated, without evidence of gavage associated weight loss. Following treatment, the phenotype was identical to I.P. treated *Exosc3*$^{gfp/gfp}$*. Rosa26Cre*$^{ERT2/ERT2}$. Tamoxifen Kolliphor HS was used in further studies as it was the best tolerated.

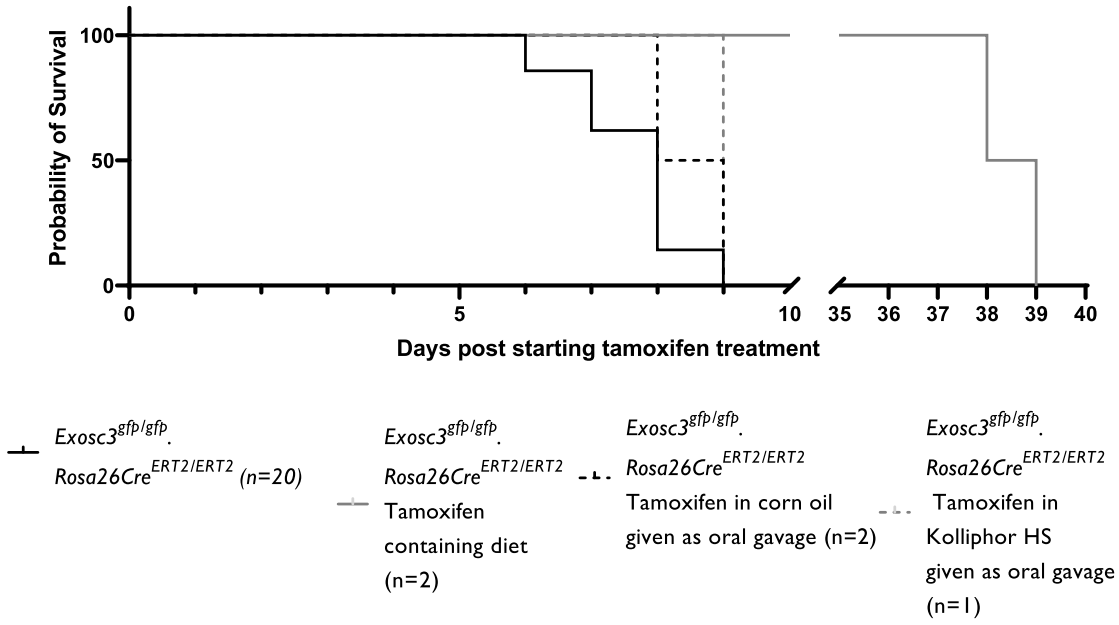

Figure 8-3: Survival analysis in Exosc3$^{gfp/gfp}$.Rosa26Cre$^{ERT2/ERT2}$ mice treated with oral tamoxifen, I.P. treated Exosc3$^{gfp/gfp}$.Rosa26Cre$^{ERT2/ERT2}$ mice used as the control.

Following tamoxifen diet there was a significant increase in survival, however the phenotype was the same when mice developed disease. Mice that received tamoxifen via oral gavage (both dissolved in corn oil and Kolliphor HS) both developed a phenotype identical to mice that received I.P. tamoxifen. Survival analysis calculated via Mantel-Cox.

8.1.5. Survival analysis

Following tamoxifen treatment with oral gavage, mice were monitored according to the clinical scoring tool (Figure 3-4). Mice recording a score of 15 were considered to have breached the pre-arranged score were euthanised.

Two *Exosc3$^{gfp/gfp}$.Tie2Cre$^{ERT2/ERT2}$* breached the clinical threshold and needed to be euthanised, one mouse was euthanised at 8 weeks after commencing tamoxifen treatment, this mouse had evidence of a renal cyst on post-mortem, with normal haematological parameters, histology performed on this mouse showed no obvious abnormality in the kidney. A second mouse was euthanised at 5 weeks, this mouse

had no evidence of TMA, histology demonstrated severe hepatic lipidosis with vacuolation (Staining and interpretation performed by Charles River Research Animal Diagnostic Services, USA), a recognised complication of prolonged tamoxifen treatment (Donocoff *et al.*, 2020).

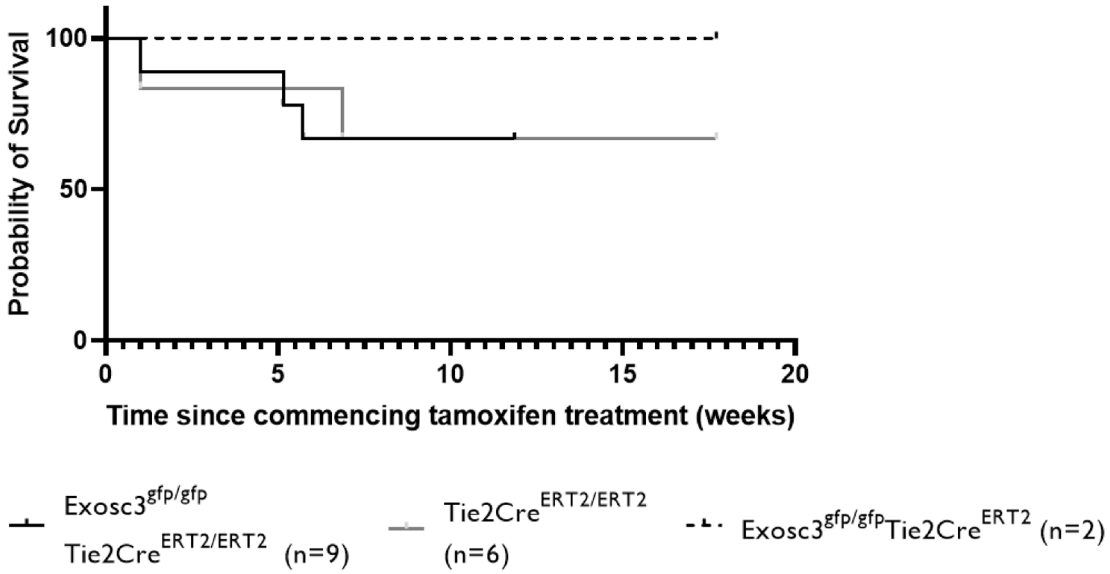

Figure 8-4 : Survival following tamoxifen treatment Exosc3$^{gfp/gfp}$.Tie2Cre$^{ERT2/ERT2}$, Exosc3$^{gfp/gfp}$.Tie2Cre^{ERT2} and Tie2Cre$^{ERT2/ERT2}$

There was no significant difference between these groups.

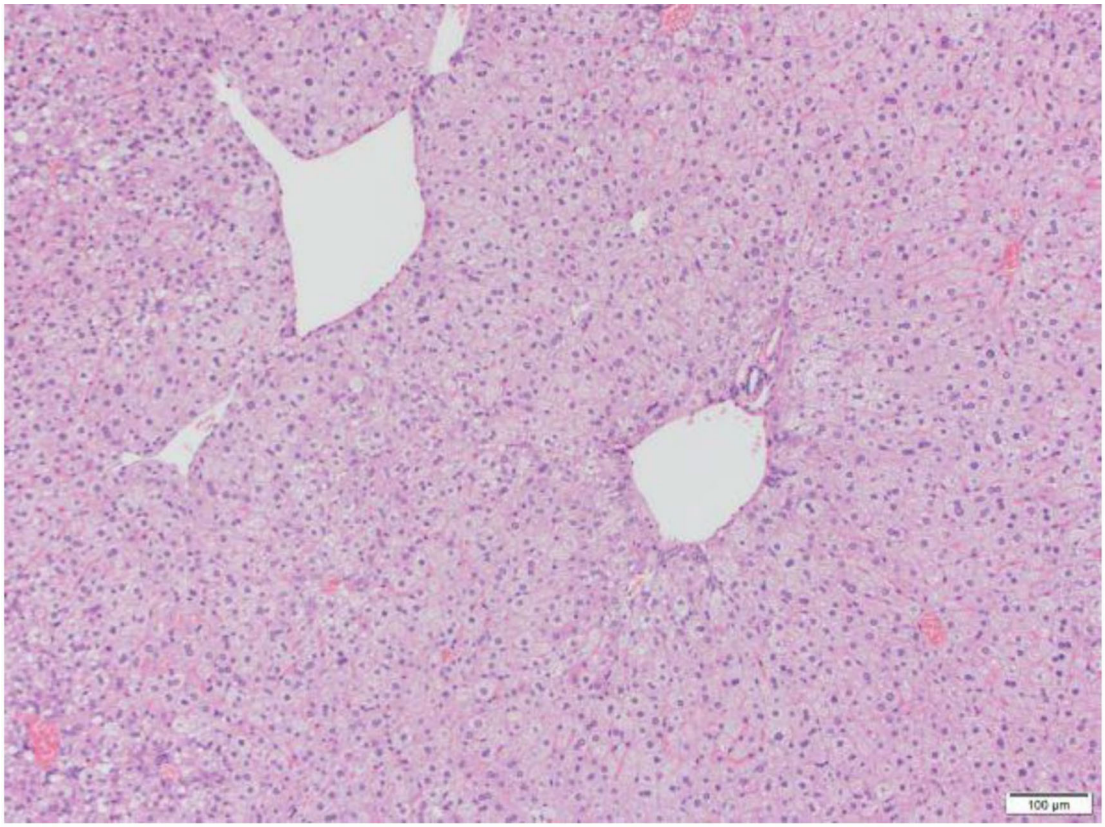

Figure 8-5: H&E stained liver from Exosc3$^{gfp/gfp}$.Tie2Cre$^{ERT2/ERT2}$ mouse

Treated with oral tamoxifen for five weeks. Staining demonstrates severe hepatic lipidosis with vacuolation, a recognised side effect of tamoxifen treatment.

8.1.6. Evidence of Successful Recombination in the mouse endothelial cells

One possibility was that there was no recombination in the endothelial cells following prolonged treatment with tamoxifen. To investigate this, spleens were isolated from mice and single cell suspension generated as described. The spleen was then stained with anti-CD45 and anti-CD31 to isolate endothelial cells. There was evidence of GFP expression in only 2/9 mice. In these mice there was evidence of restriction to endothelium, however the GFP expression was only evident is approximately 60% of endothelial cells, evidence from the whole-body knockout model had already demonstrated that more than 85% GFP recombination was required to develop a phenotype in this model (6.2.3). This lack of a predictable and

sufficiently efficient response to tamoxifen means that this mouse model is not able to accurately recapitulate the human phenotype.

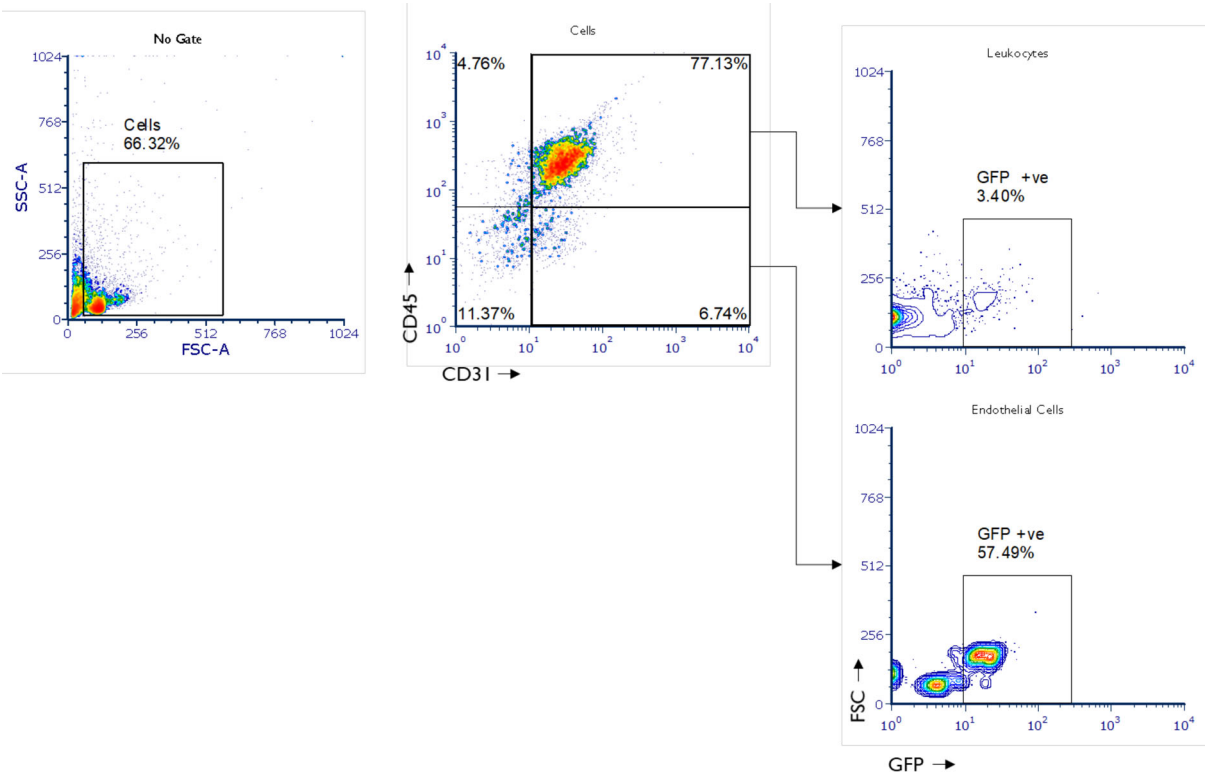

Figure 8-6: Representative flow cytometry from one mouse that demonstrated evidence of endothelial recombination.

Single cell suspension was generated from the spleen of the mouse as described. This was stained with anti-CD45 and anti-CD31. Flow cytometry was performed and subsequent gating isolate leukocytes (CD45 positive, CD31 positive) and endothelial cells (CD31 CD45 negative). In this mouse 57.49% of the endothelial cells expressed GFP, compared to only 3.4% of the leukocytes.

8.2. Discussion

The *Exosc3*$^{gfp/gfp}$*.Tie2Cre*$^{ERT2/ERT2}$ did not demonstrate reliable endothelial recombination, despite prolonged high dose exposure to tamoxifen. Unfortunately, this means that it was not possible to determine the role of Exosc3 ablation in the endothelium using this model.

8.2.1. Selection of the B6.Cg-Tg(Tek-cre/ERT2)1Arnd/ArndCnrm

The Tie2Cre^{ERT2} mouse was selected for endothelial cell specificity as it is one of the mostly widely used of the endothelial cell tamoxifen sensitive Cre expressers (Payne;De Val and Neal, 2018). It is also described as being relatively well restricted to the endothelium; most tissue specific cre models display "off-target" recombination events, i.e. recombination events in tissues other than the tissue of interest. The Tie2 promoter is known to be active in developing haematopoietic cells in addition to endothelial cells (Forde *et al.*, 2002). However, the Tie2Cre^{ERT2} model was initially described as being restricted to the endothelium, with only 0.2% of B and T cells undergoing cre mediated recombination. One issue with this model is the requirement to treat these mice with prolonged tamoxifen to achieve recombination, in the original description of this mouse, recombination was only seen after 5 weeks of oral tamoxifen dosing (Forde *et al.*, 2002). However, recombination has been successfully reported in this mouse model more than 90 times, with some reporting efficient recombination following two I.P. doses (Haidey *et al.*, 2021). In the Exosc3gfp$^{/gfp}$.*Tie2Cre*$^{ERT2/ERT2}$ mouse treated with the standard tamoxifen protocol (75mg/Kg I.P. for four days) there was no evidence of recombination. In an attempt to induce recombination mice were exposed to prolonged tamoxifen administration (8 weeks oral gavage), unfortunately this failed to induce reliable recombination in endothelial cells. The reason for the lack of recombination following tamoxifen treatment is not entirely clear.

The Tie2Cre^{ERT2} model was developed using a Bacterial Artificial Chromosome (BAC), whilst this is a reliable method of producing tissue specific Cre models, it can result in issues due to the random integration of the BAC (Becher *et al.*, 2018). Firstly, there is no way of limiting the number of BACs that integrate, which can result in significant gene number variations, and resulting in varied expression. The

nature of the random integration of the BAC can also result in disruption of endogenous genes, leading to phenotype not attributed to the Cre-lox system, finally the random integration may result in epigenetic modification such as methylation, resulting in unpredictable effects (Song and Palmiter, 2018).

The stochastic nature of recombination seen in the *Exosc3*$^{gfp/gfp}$*.Tie2Cre*$^{ERT2/ERT2}$ mice is a recognised complication of using tissue specific cre-expressing lines (Song and Palmiter, 2018). This may have contributed to the lack of consistent recombination in the endothelial cells in the *Exosc3*$^{gfp/gfp}$*.Tie2Cre*$^{ERT2/ERT2}$ mouse. Previous reports using the Tie2Cre^{ERT2}, may have a mosaic nature to the recombination, i.e. only a variable number of endothelial cells, but not 100%, undergoing recombination. It may be that in these models, this is sufficient to generate a phenotype. Data from the *Exosc3*$^{gfp/gfp}$*.Rosa26Cre*$^{ERT2/ERT2}$mice (6.2.3) demonstrated that more than 85% of cells needed to have undergone recombination for a phenotype to appear, therefore it may be that only a small number of cells are undergoing recombination, and therefore the mice are not displaying a phenotype. It is well documented that different loci have varied recombination efficiency in different cell types (Becher *et al.*, 2018), possibly due to chromatin structure preventing Cre access to Lox sites (Vooijs;Jonkers and Berns, 2001). It is possible that in the *Exosc3*$^{gfp/gfp}$*.Tie2Cre*$^{ERT2/ERT2}$ mouse, Cre recombinase is unable to access the Exosc3 loci, resulting in an absence of recombination. This does not entirely explain the lack of endothelial expression as the *Exosc3*$^{gfp/gfp}$*.Rosa26Cre*$^{ERT2/ERT2}$ mouse demonstrated endothelial GFP positivity up to one year after tamoxifen treatment (6.2.14). Different promoters used for cre expression can have different levels of cre activity, the Rosa26Cre^{ERT2} is known to have a high level of cre activity(Soriano, 1999). The lack of detectable cre recombination following up to three weeks of tamoxifen in the original report of this

model, suggests that the cre activity in this model is not particularly high, although it has never been quantified (Forde *et al.*, 2002). It was not possible to quantify the difference between the cre activity in the *Exosc3$^{gfp/gfp}$.Rosa26Cre$^{ERT2/ERT2}$* and *Exosc3$^{gfp/gfp}$.Tie2Cre$^{ERT2/ERT2}$* mice, this would have required isolation of endothelial cells form the two mice and either protein or mRNA quantification.

Unfortunately, there are a limited options to achieve endothelial specific cre expression and all have issues with off target expression and/or expression in only a subtype of endothelial cells (Table 8-1).

The other tamoxifen sensitive cre model considered was the Cadherin 5 model (Cdh5-Cre^{ERT2}), however this has been reported to have lower levels of cre activity compared to the Rosa26Cre^{ERT2}; the degree of mosaicism in this model is considerable, following five days of I.P. tamoxifen only 65% of endothelial cells examined in this model had evidence of recombination (Monvoisin *et al.*, 2006). This would be unlikely to result in the TMA phenotype in the Exosc3 mice, as greater than 85% recombination was required to demonstrate a phenotype in this model (6.2.2)

One potential solution to increase the level of recombination is to develop a hemizygote Exosc3 mouse, this could be generated using a constitutive cre expresser in the germline, this is a method that is used to enable more efficient cre recombination (Becher *et al.*, 2018). This mouse is unlikely to display a phenotype, in the unrecombined state, as there are reports of patients carrying null EXOSC3 variants (although no reports of homozygous null variants) suggesting that a single copy of EXOSC3 is sufficient for normal exosome function (Karczewski *et al.*, 2020).

It is unlikely that further optimisation of the tamoxifen regime is likely to increase recombination, the eight week oral tamoxifen treatment that was used in this study

resulted in a large overall dosage (112mg vs. 8mg for the standard I.P. dosage) and resulted in significant side effects, including the death of three control (Tie2Cre$^{ERT2/ERT2}$) mice due to tamoxifen side effects and one *Exosc3$^{gfp/gfp}$.Tie2Cre$^{ERT2/ERT2}$* mouse that developed severe hepatic lipidosis with vacuolation, a well-documented side effect of tamoxifen treatment (Donocoff *et al.*, 2020).

It is difficult to explain the reason the *Exosc3$^{gfp/gfp}$.Tie2Cre$^{ERT2/ERT2}$* mouse model did not display evidence of reliable recombination, however it is clear that the *Exosc3$^{gfp/gfp}$.Tie2Cre$^{ERT2/ERT2}$* model is not a useful model of TMA in its current form.

Mouse Line	Regulation of Cre Activity	Expression	Non-EC Expression
Tg(Tie2-cre/ERT2)1Arnd	10 kb enhancer and 2.1 kb promoter	Pan-Endothelial cell	None reported
Tg(Cdh5-cre/ERT2)#Ykub	Endogenous locus, Cre/ERT2 inserted at start codon within BAC	Pan-Endothelial cell	None reported
Tg(Pdgfb-icre/ERT2)1Frut	Endogenous locus, Cre/ERT2 inserted at start codon in PAC	Capillary and arterial endothelial cells	Keratinocytes, megakaryocytes
Tg(Bmx-cre/ERT2)1Rha	Endogenous locus, Cre/ERT2 inserted at start codon within PAC	Some arterial endothelial cells	None reported
Tg(Esm1-cre/ERT2)1Rha	Endogenous locus, Cre/ERT2 inserted at start codon within BAC	Tip Endothelial cells	None reported
Aplntm1.1(cre/ERT2)Bz	Endogenous locus, targeted knock-in of CreERT2 cDNA into gene deleting exon 1	Sprouting Endothelial cells	None reported
Tg(Aplnr-cre/ERT2)#Krh	Endogenous locus, Cre/ERT2 inserted at start codon of BAC	sinus venosus, coronary , Capillary, vein endothelial cells	None reported
Tg(Fabp4-cre/ERT2)1Ipc	5.4 kb promoter fragment	Coronary endothelial cells	Adipocytes and macrophages
Nfatc1tm1.1(cre/ERT2)Bzsh	Endogenous locus, targeted knock-in of CreERT2 cDNA into gene deleting exon 1	Endocardial and sinus venous endothelial cells	None reported
Nfatc1em1(cre/ERT2)Bzsh	Endogenous locus, targeted knock-in of Cre/ERT2 cDNA into 3′ UTR	Endocardial and sinus venous endothelial cells	None reported

Npr3tm1.1(cre/ERT2)Bzsh	Endogenous locus, targeted knock-in of Cre/ERT2 cDNA into translational start codon	Endocardial endothelial cells	Some epicardial cells

Table 8-1: Endothelial specific tamoxifen sensitive Cre models currently available, of the available options only Tie2 and cadherin 5 show pan-endothelial cell expression. Adapted for Payne et al.(Payne;De Val and Neal, 2018)

9. Summary and Future Work

The role of complement dysregulation, in particular C5 in the pathogenesis of C-aHUS is well established (Legendre *et al.*, 2013; Licht *et al.*, 2015). This disease has been revolutionised by the introduction of anti-C5 treatment. However, it is clear that some patients do not respond to treatment. During this project I initially described the current genetic causes of C-aHUS in the NRCTC cohort (4) and demonstrated the role of genomic rearrangements in the RCA leading to C-aHUS. These copy number variants are of particular importance as these would be missed with both Sanger sequencing and whole exome sequencing techniques. At the start of this project CFH::CFHR1 crossovers and gene conversion events had been described (Abarrategui-Garrido *et al.*, 2009) However, reviewing the MLPA data has uncovered patients who do not have these gene conversions or cross-over events and instead have double crossovers (or very large gene conversions), whilst these produce functionally similar proteins they are genetically distinct processes, it is not currently possible to determine where this occurs. To answer this question ultra-long DNA sequencing technology can be used in the future, such as Nanopore technology (Oxford Nanopore, UK). This allows ultra-long lengths of DNA, up to 4Mb to be sequenced, this will identify the region in which this second cross-over event has occurred. Developing this technology in RCA cluster will allow for better understanding of genomic events that lead to fusion genes.

A review of the genetic data from the NRCTC identified eight patients with pathogenic variants in RNA surveillance genes, this included two children with *EXOSC3* mediated TMA (4.3.1.1). This has been described as an association before (Van Quekelberghe *et al.*, 2022) however the underlying pathogenesis is unclear. In this project I utilised a conditionally inducible Exosc3 knockout that

resulted in Exosc3 ablation following treatment with tamoxifen. For the first time this allowed the role of the RNA exosome in a whole body mammalian system to be examined. This has highlighted the essential role the RNA exosome performs in maintaining the normal cellular function in rapidly dividing cells (including the bone marrow, intestine and thymus). In the absence of a function RNA exosome, due to Exosc3 ablation mice developed cell cycle arrest and cell death, recapitulating an ARS phenotype.

The data from the *Exosc3*$^{gfp/gfp}$*.Rosa26Cre*$^{ERT2/ERT2}$ mouse indicates that EXOSC3-mediated TMA occurs secondary to ribosomal dysfunction. Preliminary data from the use of the p53 antagonist, PFTα, demonstrated improved survival, further supporting the role of the EXOSC3 dysfunction in ribosomopathies. This demonstrates a common pathogenic process in EXOSC3-mediated TMA and STEC-HUS and potentially offer a new model to investigate the pathogenesis of STEC-HUS.

9.1. Future work

TMA is a disease of endothelial dysfunction. This has proved challenging due to the severity of the phenotype in the *Exosc3*$^{gfp/gfp}$*.Rosa26Cre*$^{ERT2/ERT2}$ mouse and the lack of a phenotype in the *Exosc3*$^{gfp/gfp}$*.Tie2Cre*$^{ERT2/ERT2}$. To look specifically at the endothelium using the currently available models in Newcastle, ^{an} alternative solution is to induce Exosc3 recombination *ex vivo*. This strategy has been shown to be possible using the Exosc3^{COIN} mouse (Pefanis *et al.*, 2014; Fraga de Andrade *et al.*, 2022). To investigate the role of the RNA exosome, specifically Exosc3, endothelial cells could be isolated from an *Exosc3*$^{gfp/gfp}$*.Rosa26Cre*$^{ERT2/ERT2}$ mouse. This could be done using the protocol described by (Dumas *et al.*, 2021) in which mice are infused with digestion media via transcardiac infusion to release the

endothelial cells. The endothelial cells can then be isolated by further enzymatic digestion and filtration. To isolate an enriched endothelial cell population anti-CD31 magnetic beads and positive selection would be performed, followed by Fluorescence-activated cell sorting (FACS) using an endothelial cell marker (e.g. CD102, CD31). The isolated primary endothelial cells could then be treated with 4-OHT (the active metabolite of tamoxifen) to induce recombination. The cells could then be tracked for cell survival, apoptosis, and RNA analysis for markers of apoptosis, specifically p53 pathway genes, as all previous models of Exosc3 knockout, including zebrafish, drosophila and the $Exosc3^{COIN}$ mouse models have demonstrated upregulation of p53. The GFP expression would allow for selection of cells, via FACS, that have undergone recombination. This method could be used to perform single cell RNA-sequencing, which could then be compared to data from the $C3^{D1115N}$ model to determine if there is any common final pathway leading to TMA in these models. Performing RNA sequencing was considered on *Exosc3*$^{gfp/gfp}$*.Rosa26Cre*$^{ERT2/ERT2}$ mouse kidney to allow comparison with the $C3^{D1115N}$ model, however in the absence of a phenotype in the kidney it was felt that planning to undertake *in vitro* work would be more likely to produce results.

A second option to investigate is the role of Exosc3 in the pathogenesis of TMA is to develop a patient specific knock-in mouse model. Both patients with EXOSC3-mediated TMA in the NRCTC cohort carried the p.D132A (p.D131A in mouse) variant. This model could be generated to allow examination of the patient specific variant, in a similar way to the $C3^{D1115N}$ mouse (Smith-Jackson *et al.*, 2019). EXOSC3 forms an essential component of the RNA exosome cap, it is currently not clear how different variants affect the RNA exosome function, but it is unlikely that pathogenic variants lead to complete EXOSC3 inactivation, as there are no documented reports of patients with null *EXOSC3* variants (Karczewski *et al.*, 2020)

and exosc3 is essential for survival (Mitchell *et al.*, 1997). It is likely that known variants in *EXOSC3* result in hypofunctioning variants that could result in global reduction in RNA exosome function, or a subset of the RNA functions, for example altering the interaction with specific co-factors in different cell compartments. One interesting possibility that could link *POLR3*, *TSEN2*, *EXOSC3*-mediated, and to a lesser extent *RNU4ATAC* TMA is tRNA dysfunction. It has been demonstrated, in yeast that missense variants identified in *EXOSC3* (yeast equivalent *rrp40*) result in defects in RNA exosome-mediated degradation of tRNAs specifically. The RNA exosome degrades both mature, unstable tRNAs (Wichtowska *et al.*, 2013) and misprocessed precursors of initiator tRNAs (Kadaba *et al.*, 2004). Ultimately in the absence of normal tRNA metabolism there is depletion of the tRNA pool, which results in ribosomal stalling (Orellana;Siegal and Gregory, 2022) and the downstream effects of ribosomal dysfunction, including upregulation of p53 mediated apoptosis. This mechanism links genetic variants in RNA processing identified in TMA (EXOSC3, POLR3, TSEN2), with STEC-HUS. Further understanding of the role of RNA surveillance in TMA generation will enable better understanding of the pathogenesis of STEC-HUS. The preliminary findings detailed that PFTα is able to modulate the effects of Exosc3 knockout suggests a potential treatment avenue.

Ultimately, this project has uncovered a new group of genetic diseases that result in TMA. The work presented within has begun to uncover the pathogenesis of RNA-surveillance dysfunction in the TMA, more work is needed to fully elucidate the cause of TMA in this group of disorders.

9.2. Summary of work and future plans

Chapter	Aim of chapter	Techniques used	Summary of results obtained	Limitations/challenges of work	Future plans/experiments to address aim.
Genetic Analysis of the NRCTC aHUS Cohort	To describe genomic rearrangement events in the RCA cluster	MLPA and Sanger sequencing	This work identified and described gene conversions, cross-over events and described double cross-over events for the first time.	This was unable to identify the position of the second cross-over event using these mechanisms	long-range PCR techniques, such as the Oxford Nanopore will be used to identify the second breakpoint
	To identify novel genetic causes of TMA	Whole Exome and Sanger sequencing	Biallelic pathogenic variants in five RNA processing genes were described for the first time		Further genetic analysis in unexplained TMA will be carried out to investigate for other RNA processing genes resulting in TMA.
Complement Dysregulation in RNA processing TMAs	To investigate whether EXOSC3-mediated TMA is a form of C-aHUS	Complement diagnostics and bulk mRNA sequencing	The mRNA Seq data showed no changes in RNA processing genes in the C-aHUS model. The clinical data in the EXOSC3-mediated TMA patients did not demonstrate response to complement inhibition	Data was available form only 2 pairs of mice, due to QC failures in one of the pairs. RNA seq. data was not available for the $Exosc3^{gfp/gfp}.Rosa26Cre^{ERT2/ERT2}$	RNA seq. could be performed on the $Exosc3^{gfp/gfp}.Rosa26Cre^{ERT2/ERT2}$ mouse to determine evidence of complement dysregulation
The effect of whole body Exosc3 ablation in a mouse model	To develop a conditional inducible whole body Exosc3 knock-down and investigate the effects	Cre recombination, qPCR, ELISA, Flow cytometry and Histology	Mice developed typical features of ribosomal dysfunction, including cell cycle arrest, apoptosis and TNF-alpha	These mice did not develop TMA, with limited evidence of endothelial cell Exosc3 knock-down	Endothelial cells will be isolated from these mice and cre-mediated recombination will be performed to determine the effects of Exosc3 knock-down

Exosc3$^{fl/fl}$.Rosa26 Cre$^{ERT2/ERT2}$Ifnar$^{-/-}$	The role of type 1 interferon dysregulation following Exosc3 ablation in the mouse	Cre recombination, Flow cytometry	A more severe effect was seen following type 1 interferon signalling knockout	These mice were very challenging to breed so data was lacking	No further experiments are planned with this model at present
P53 Inhibition	The role of P53 inhibition following Exosc3 ablation in the mouse	Cre recombination, Flow cytometry	There was a significant improvement in survival following P53 inhibition	These were preliminary results and there were only a small number of mice treated	Further work including the use of different p53 modulators and *ex vivo* work is planned to determine whether p53 inhibition improves survival
Attempts to develop a conditionally inducible endothelial specific Exosc3 ablation	To develop an endothelial specific Cre-expresser to restrict Exosc3 ablation to the endothelium	Cre recombination, Flow cytometry	There was no reproducible Exosc3 ablation in the endothelium	There was no consistent evidence of Exosc3 ablation in the endothelium in this model	No further work is planned with this model, instead an ex vivo approach of Exosc3 ablation in the endothelium is planned.

10. References

Abarrategui-Garrido, C., Martínez-Barricarte, R., López-Trascasa, M., Rodríguez De Córdoba, S. and Sánchez-Corral, P. (2009) 'Characterization of complement factor H-related (CFHR) proteins in plasma reveals novel genetic variations of CFHR1 associated with atypical hemolytic uremic syndrome', Blood, 114, pp. 4261-4271.

Adam, M.P., Everman, D.B., Mirzaa, G.M., Pagon, R.A., Wallace, S.E., Bean, L.J.H., Gripp, K.W. and Amemiya, A. (1993) 'GeneReviews', in.

Adams, N., Byrne, L., Edge, J., Hoban, A., Jenkins, C. and Larkin, L. (2019a) 'Gastrointestinal infections caused by consumption of raw drinking milk in England & Wales, 1992-2017', Epidemiol Infect, 147, p. e281.

Adams, N., Byrne, L., Rose, T., Adak, B., Jenkins, C., Charlett, A., Violato, M., O'Brien, S., Whitehead, M., Barr, B., Taylor-Robinson, D. and Hawker, J. (2019b) 'Sociodemographic and clinical risk factors for paediatric typical haemolytic uraemic syndrome: retrospective cohort study', BMJ Paediatr Open, 3(1), p. e000465.

Al Shoyaib, A., Archie, S.R. and Karamyan, V.T. (2019) 'Intraperitoneal Route of Drug Administration: Should it Be Used in Experimental Animal Studies?', Pharm Res, 37(1), p. 12.

Al-Nouri, Z.L., Reese, J.A., Terrell, D.R., Vesely, S.K. and George, J.N. (2015) 'Drug-induced thrombotic microangiopathy: a systematic review of published reports', Blood, 125(4), pp. 616-618.

Almentina Ramos Shidi, F., Cologne, A., Delous, M., Besson, A., Putoux, A., Leutenegger, A.L., Lacroix, V., Edery, P., Mazoyer, S. and Bordonné, R. (2023) 'Mutations in the non-coding RNU4ATAC gene affect the homeostasis and function of the Integrator complex', Nucleic Acids Res, 51(2), pp. 712-727.

Aly, H.H., Suzuki, J., Watashi, K., Chayama, K., Hoshino, S., Hijikata, M., Kato, T. and Wakita, T. (2016) 'RNA Exosome Complex Regulates Stability of the Hepatitis B Virus X-mRNA Transcript in a Non-stop-mediated (NSD) RNA Quality Control Mechanism', J Biol Chem, 291(31), pp. 15958-74.

André, P. (2004) 'P-selectin in haemostasis', British journal of haematology, 126(3), pp. 298-306.

Ardissino, G., Tel, F., Possenti, I., Testa, S., Consonni, D., Paglialonga, F., Salardi, S., Borsa-Ghiringhelli, N., Salice, P., Tedeschi, S., Castorina, P., Colombo, R.M., Arghittu, M., Daprai, L., Monzani, A., Tozzoli, R., Brigotti, M. and Torresani, E. (2015) 'Early Volume Expansion and Outcomes of Hemolytic Uremic Syndrome.', Pediatrics, 137, pp. e20152153-.

Arvidsson, I., Stahl, A.L., Hedstrom, M.M., Kristoffersson, A.C., Rylander, C., Westman, J.S., Storry, J.R., Olsson, M.L. and Karpman, D. (2015) 'Shiga toxin-induced complement-mediated hemolysis and release of complement-coated red blood cell-derived microvesicles in hemolytic uremic syndrome', J Immunol, 194(5), pp. 2309-18.

Barbu, A., Hamad, O.A., Lind, L., Ekdahl, K.N. and Nilsson, B. (2015) 'The role of complement factor C3 in lipid metabolism', Molecular Immunology, 67(1), pp. 101-107.

Barreau, C., Paillard, L. and Osborne, H.B. (2005) 'AU-rich elements and associated factors: are there unifying principles?', Nucleic Acids Res, 33(22), pp. 7138-50.

Bartok, E. and Hartmann, G. (2020) 'Immune Sensing Mechanisms that Discriminate Self from Altered Self and Foreign Nucleic Acids', Immunity, 53(1), pp. 54-77.

Becher, B., Waisman, A. and Lu, L.F. (2018) 'Conditional Gene-Targeting in Mice: Problems and Solutions', Immunity, 48(5), pp. 835-836.

Beck, B.B., van Spronsen, F., Diepstra, A., Berger, R.M. and Kömhoff, M. (2017) 'Renal thrombotic microangiopathy in patients with cblC defect: review of an under-recognized entity', Pediatr Nephrol, 32(5), pp. 733-741.

Bielaszewska, M., Idelevich, E.A., Zhang, W., Bauwens, A., Schaumburg, F., Mellmann, A., Peters, G. and Karch, H. (2012) 'Effects of Antibiotics on Shiga Toxin 2 Production and Bacteriophage Induction by Epidemic Escherichia coli O104:H4 Strain', Antimicrobial Agents and Chemotherapy, 56, pp. 3277-3282.

Blaum, B.S., Hannan, J.P., Herbert, A.P., Kavanagh, D., Uhrín, D. and Stehle, T. (2015) 'Structural basis for sialic acid-mediated self-recognition by complement factor H', Nat Chem Biol, 11(1), pp. 77-82.

Bonifacino, J.S. and Rojas, R. (2006) 'Retrograde transport from endosomes to the trans-Golgi network', Nat Rev Mol Cell Biol, 7(8), pp. 568-79.

Booth, C., Tudor, G., Tudor, J., Katz, B.P. and MacVittie, T.J. (2012) 'Acute gastrointestinal syndrome in high-dose irradiated mice', Health Phys, 103(4), pp. 383-99.

Boyer, O., Benoit, G., Gribouval, O., Nevo, F., Tête, M.J., Dantal, J., Gilbert-Dussardier, B., Touchard, G., Karras, A., Presne, C., Grunfeld, J.P., Legendre, C., Joly, D., Rieu, P., Mohsin, N., Hannedouche, T., Moal, V., Gubler, M.C., Broutin, I., Mollet, G. and Antignac, C. (2011a) 'Mutations in INF2 are a major cause of autosomal dominant focal segmental glomerulosclerosis', J Am Soc Nephrol, 22(2), pp. 239-45.

Boyer, O., Nevo, F., Plaisier, E., Funalot, B., Gribouval, O., Benoit, G., Huynh Cong, E., Arrondel, C., Tête, M.J., Montjean, R., Richard, L., Karras, A., Pouteil-Noble, C., Balafrej, L., Bonnardeaux, A., Canaud, G., Charasse, C., Dantal, J., Deschenes, G., Deteix, P., Dubourg, O., Petiot, P., Pouthier, D., Leguern, E., Guiochon-Mantel, A., Broutin, I., Gubler, M.C., Saunier, S., Ronco, P., Vallat, J.M., Alonso, M.A., Antignac, C. and Mollet, G. (2011b) 'INF2 mutations in Charcot-Marie-Tooth disease with glomerulopathy', N Engl J Med, 365(25), pp. 2377-88.

Brocklebank, V., Johnson, S., Sheerin, T.P., Marks, S.D., Gilbert, R.D., Tyerman, K., Kinoshita, M., Awan, A., Kaur, A. and Webb, N. (2017) 'Factor H autoantibody is associated with atypical hemolytic uremic syndrome in children in the United Kingdom and Ireland', Kidney international, 92(5), pp. 1261-1271.

Brocklebank, V., Kumar, G., Howie, A.J., Chandar, J., Milford, D.V., Craze, J., Evans, J., Finlay, E., Freundlich, M., Gale, D.P., Inward, C., Mraz, M., Jones, C., Wong, W., Marks, S.D., Connolly, J., Corner, B.M., Smith-Jackson, K., Walsh, P.R., Marchbank, K.J., Harris, C.L., Wilson, V., Wong, E.K.S., Malina, M., Johnson, S., Sheerin, N.S. and Kavanagh, D. (2020) 'Long-term outcomes and response to treatment in diacylglycerol kinase epsilon nephropathy', Kidney Int.

Brocklebank, V., Walsh, P.R., Smith-Jackson, K., Hallam, T.M., Marchbank, K.J., Wilson, V., Bigirumurame, T., Dutt, T., Montgomery, E.K., Malina, M., Wong, E.K., Johnson, S., Sheerin, N. and Kavanagh, D. (2023) 'Atypical haemolytic uraemic syndrome in the era of terminal complement inhibition- An observational cohort study', Blood.

Brocklebank, V., Wood, K.M. and Kavanagh, D. (2018) 'Thrombotic Microangiopathy and the Kidney', Clin J Am Soc Nephrol, 13(2), pp. 300-317.

Brown, E.J., Schlöndorff, J.S., Becker, D.J., Tsukaguchi, H., Tonna, S.J., Uscinski, A.L., Higgs, H.N., Henderson, J.M. and Pollak, M.R. (2010) 'Mutations in the formin gene INF2 cause focal segmental glomerulosclerosis', Nat Genet, 42(1), pp. 72-6.
Bruel, A., Kavanagh, D., Noris, M., Delmas, Y., Wong, E.K.S., Bresin, E., Provot, F., Brocklebank, V., Mele, C., Remuzzi, G., Loirat, C., Fremeaux-Bacchi, V. and Fakhouri, F. (2017) 'Hemolytic Uremic Syndrome in Pregnancy and Postpartum', Clin J Am Soc Nephrol, 12(8), pp. 1237-1247.
Buchholz, U., Bernard, H., Werber, D., Böhmer, M.M., Remschmidt, C., Wilking, H., Deleré, Y., an der Heiden, M., Adlhoch, C., Dreesman, J., Ehlers, J., Ethelberg, S., Faber, M., Frank, C., Fricke, G., Greiner, M., Höhle, M., Ivarsson, S., Jark, U., Kirchner, M., Koch, J., Krause, G., Luber, P., Rosner, B., Stark, K. and Kühne, M. (2011) 'German Outbreak of Escherichia coli O104:H4 Associated with Sprouts', New England Journal of Medicine, 365, pp. 1763-1770.
Burbelo, P.D., Gordon, S.M., Waldman, M., Edison, J.D., Little, D.J., Stitt, R.S., Bailey, W.T., Hughes, J.B. and Olson, S.W. (2019) 'Autoantibodies are present before the clinical diagnosis of systemic sclerosis', PLoS One, 14(3), p. e0214202.
Bussone, G., Bérezné, A., Pestre, V., Guillevin, L. and Mouthon, L. (2011) 'The Scleroderma Kidney: Progress in Risk Factors, Therapy, and Prevention', Current Rheumatology Reports, 13(1), pp. 37-43.
Buttgereit, F. and Brand, M.D. (1995) 'A hierarchy of ATP-consuming processes in mammalian cells', Biochem J, 312 (Pt 1)(Pt 1), pp. 163-7.
Callaway, T.R., Carr, M.a., Edrington, T.S., Anderson, R.C., Nisbet, D.J., Safety, F. and Ag-, S.P. (2007) 'Diet , Escherichia coli O157 : H7 , and Cattle : A Review After 10 Years', Curr. Issues Mol. Biol, 1, pp. 67-80.
Canpolat, N., Liu, D., Atayar, E., Saygili, S., Kara, N.S., Westfall, T.A., Ding, Q., Brown, B.J., Braun, T.A., Slusarski, D., Karli Oguz, K., Ozluk, Y., Tuysuz, B., Tastemel Ozturk, T., Sever, L., Sezerman, O.U., Topaloglu, R., Caliskan, S., Attanasio, M. and Ozaltin, F. (2022) 'A splice site mutation in the TSEN2 causes a new syndrome with craniofacial and central nervous system malformations, and atypical hemolytic uremic syndrome', Clin Genet, 101(3), pp. 346-358.
Caprioli, J., Noris, M., Brioschi, S., Pianetti, G., Castelletti, F., Bettinaglio, P., Mele, C., Bresin, E., Cassis, L., Gamba, S., Porrati, F., Bucchioni, S., Monteferrante, G., Fang, C.J., Liszewski, M.K., Kavanagh, D., Atkinson, J.P. and Remuzzi, G. (2006)

'Genetics of HUS: The impact of MCP, CFH, and IF mutations on clinical presentation, response to treatment, and outcome', Blood, 108, pp. 1267-1279.
Carrillo-Carrasco, N. and Venditti, C.P. (2012) 'Combined methylmalonic acidemia and homocystinuria, cblC type. II. Complications, pathophysiology, and outcomes', J Inherit Metab Dis, 35(1), pp. 103-14.
Carter, R. and Drouin, G. (2009) 'Structural differentiation of the three eukaryotic RNA polymerases', Genomics, 94(6), pp. 388-96.
Challen, G.A., Boles, N., Lin, K.K. and Goodell, M.A. (2009) 'Mouse hematopoietic stem cell identification and analysis', Cytometry A, 75(1), pp. 14-24.
Challis, R.C., Araujo, G.S., Wong, E.K., Anderson, H.E., Awan, A., Dorman, A.M., Waldron, M., Wilson, V., Brocklebank, V., Strain, L., Morgan, B.P., Harris, C.L., Marchbank, K.J., Goodship, T.H. and Kavanagh, D. (2016) 'A De Novo Deletion in the Regulators of Complement Activation Cluster Producing a Hybrid Complement Factor H/Complement Factor H-Related 3 Gene in Atypical Hemolytic Uremic Syndrome', J Am Soc Nephrol, 27(6), pp. 1617-24.
Challis, R.C., Ring, T., Xu, Y., Wong, E.K., Flossmann, O., Roberts, I.S., Ahmed, S., Wetherall, M., Salkus, G., Brocklebank, V., Fester, J., Strain, L., Wilson, V., Wood, K.M., Marchbank, K.J., Santibanez-Koref, M., Goodship, T.H. and Kavanagh, D. (2017) 'Thrombotic Microangiopathy in Inverted Formin 2-Mediated Renal Disease', J Am Soc Nephrol, 28(4), pp. 1084-1091.
Chan, Y.S. and Ng, T.B. (2016) 'Shiga toxins: from structure and mechanism to applications', Applied Microbiology and Biotechnology, 100(4), pp. 1597-1610.
Chen, M.S., Woodward, W.A., Behbod, F., Peddibhotla, S., Alfaro, M.P., Buchholz, T.A. and Rosen, J.M. (2007) 'Wnt/beta-catenin mediates radiation resistance of Sca1+ progenitors in an immortalized mammary gland cell line', J Cell Sci, 120(Pt 3), pp. 468-77.
Chiasakul, T. and Cuker, A. (2018) 'Clinical and laboratory diagnosis of TTP: an integrated approach', Hematology Am Soc Hematol Educ Program, 2018(1), pp. 530-538.
Christodoulou, M.S., Colombo, F., Passarella, D., Ieronimo, G., Zuco, V., De Cesare, M. and Zunino, F. (2011) 'Synthesis and biological evaluation of imidazolo[2,1-b]benzothiazole derivatives, as potential p53 inhibitors', Bioorg Med Chem, 19(5), pp. 1649-57.

Colic, E., Dieperink, H., Titlestad, K. and Tepel, M. (2011) 'Management of an acute outbreak of diarrhoea-associated haemolytic uraemic syndrome with early plasma exchange in adults from southern Denmark: an observational study', The Lancet, 378, pp. 1089-1093.
Copelovitch, L. and Kaplan, B.S. (2008) 'Streptococcus pneumoniae-associated hemolytic uremic syndrome', Pediatric Nephrology, 23, pp. 1951-1956.
Cornec-Le Gall, E., Delmas, Y., De Parscau, L., Doucet, L., Ogier, H., Benoist, J.F., Fremeaux-Bacchi, V. and Le Meur, Y. (2014) 'Adult-onset eculizumab-resistant hemolytic uremic syndrome associated with cobalamin C deficiency', Am J Kidney Dis, 63(1), pp. 119-23.
Crow, Y.J. (2011) 'Type I interferonopathies: a novel set of inborn errors of immunity', Ann N Y Acad Sci, 1238, pp. 91-8.
Crow, Y.J. and Casanova, J.L. (2014) 'STING-associated vasculopathy with onset in infancy--a new interferonopathy', N Engl J Med, 371(6), pp. 568-71.
Crow, Y.J. and Manel, N. (2015) 'Aicardi-Goutieres syndrome and the type I interferonopathies', Nat Rev Immunol, 15(7), pp. 429-40.
Cunninghame Graham, D.S., Morris, D.L., Bhangale, T.R., Criswell, L.A., Syvanen, A.C., Ronnblom, L., Behrens, T.W., Graham, R.R. and Vyse, T.J. (2011) 'Association of NCF2, IKZF1, IRF8, IFIH1, and TYK2 with systemic lupus erythematosus', PLoS Genet, 7(10), p. e1002341.
Dallman, T.J., Jalava, K., Verlander, N.Q., Gally, D., Jenkins, C., Godbole, G. and Gharbia, S. (2022) 'Identification of domestic reservoirs and common exposures in an emerging lineage of Shiga toxin-producing Escherichia coli O157:H7 in England: a genomic epidemiological analysis', Lancet Microbe, 3(8), pp. e606-e615.
Devalaraja-Narashimha, K., Meagher, K., Luo, Y., Huang, C., Kaplan, T., Muthuswamy, A., Halasz, G., Casanova, S., O'Brien, J., Peyser Boiarsky, R., McWhirter, J., Gartner, H., Bai, Y., MacDonnell, S., Liu, C., Hu, Y., Latuszek, A., Wei, Y., Prasad, S., Huang, T., Yancopoulos, G., Murphy, A., Olson, W., Zambrowicz, B., Macdonald, L. and Morton, L.G. (2021) 'Humanized C3 Mouse: A Novel Accelerated Model of C3 Glomerulopathy', Journal of the American Society of Nephrology, 32(1), pp. 99-114.
Donocoff, R.S., Teteloshvili, N., Chung, H., Shoulson, R. and Creusot, R.J. (2020) 'Optimization of tamoxifen-induced Cre activity and its effect on immune cell populations', Sci Rep, 10(1), p. 15244.

du Moulin, M., Nurnberg, P., Crow, Y.J. and Rutsch, F. (2011) 'Cerebral vasculopathy is a common feature in Aicardi-Goutieres syndrome associated with SAMHD1 mutations', Proc Natl Acad Sci U S A, 108(26), p. E232; author reply E233.
Dumas, S.J., Meta, E., Conchinha, N.V., Sokol, L., Chen, R., Borri, M., Teuwen, L.A., Veys, K., García-Caballero, M., Geldhof, V., Treps, L., de Zeeuw, P., Falkenberg, K.D., Dubois, C., Parys, M., de Rooij, L.P.M.H., Rohlenova, K., Goveia, J., Schoonjans, L., Dewerchin, M., Eelen, G., Li, X., Kalucka, J. and Carmeliet, P. (2021) 'Protocols for endothelial cell isolation from mouse tissues: kidney, spleen, and testis', STAR Protoc, 2(3), p. 100523.
Duncan, C.J.A., Randall, R.E. and Hambleton, S. (2021) 'Genetic Lesions of Type I Interferon Signalling in Human Antiviral Immunity', Trends Genet, 37(1), pp. 46-58.
Duncan, C.J.A., Thompson, B.J., Chen, R., Rice, G.I., Gothe, F., Young, D.F., Lovell, S.C., Shuttleworth, V.G., Brocklebank, V., Corner, B., Skelton, A.J., Bondet, V., Coxhead, J., Duffy, D., Fourrage, C., Livingston, J.H., Pavaine, J., Cheesman, E., Bitetti, S., Grainger, A., Acres, M., Innes, B.A., Mikulasova, A., Sun, R., Hussain, R., Wright, R., Wynn, R., Zarhrate, M., Zeef, L.A.H., Wood, K., Hughes, S.M., Harris, C.L., Engelhardt, K.R., Crow, Y.J., Randall, R.E., Kavanagh, D., Hambleton, S. and Briggs, T.A. (2019a) 'Severe type I interferonopathy and unrestrained interferon signaling due to a homozygous germline mutation in STAT2', Science Immunology, 4(42), p. eaav7501.
Duncan, C.J.A., Thompson, B.J., Chen, R., Rice, G.I., Gothe, F., Young, D.F., Lovell, S.C., Shuttleworth, V.G., Brocklebank, V., Corner, B., Skelton, A.J., Bondet, V., Coxhead, J., Duffy, D., Fourrage, C., Livingston, J.H., Pavaine, J., Cheesman, E., Bitetti, S., Grainger, A., Acres, M., Innes, B.A., Mikulasova, A., Sun, R., Hussain, R., Wright, R., Wynn, R., Zarhrate, M., Zeef, L.A.H., Wood, K., Hughes, S.M., Harris, C.L., Engelhardt, K.R., Crow, Y.J., Randall, R.E., Kavanagh, D., Hambleton, S. and Briggs, T.A. (2019b) 'Severe type I interferonopathy and unrestrained interferon signaling due to a homozygous germline mutation in STAT2', Sci Immunol, 4(42).
Eaton, K., Fontaine, C., Friedman, D., Conti, N. and Alteri, C. (2017) 'Pathogenesis of colitis in germ-free mice infected with EHEC O157: H7', Veterinary pathology, 54(4), pp. 710-719.
Eckard, S.C., Rice, G.I., Fabre, A., Badens, C., Gray, E.E., Hartley, J.L., Crow, Y.J. and Stetson, D.B. (2014) 'The SKIV2L RNA exosome limits activation of the RIG-I-like receptors', Nat Immunol, 15(9), pp. 839-45.

Economides, A.N., Frendewey, D., Yang, P., Dominguez, M.G., Dore, A.T., Lobov, I.B., Persaud, T., Rojas, J., McClain, J., Lengyel, P., Droguett, G., Chernomorsky, R., Stevens, S., Auerbach, W., DeChiara, T.M., Pouyemirou, W., Cruz, J.M., Feeley, K., Mellis, I.A., Yasenchack, J., Hatsell, S.J., Xie, L., Latres, E., Huang, L., Zhang, Y., Pefanis, E., Skokos, D., Deckelbaum, R.A., Croll, S.D., Davis, S., Valenzuela, D.M., Gale, N.W., Murphy, A.J. and Yancopoulos, G.D. (2013a) 'Conditionals by inversion provide a universal method for the generation of conditional alleles', Proceedings of the National Academy of Sciences, 110(34), pp. E3179-E3188.
Economides, A.N., Frendewey, D., Yang, P., Dominguez, M.G., Dore, A.T., Lobov, I.B., Persaud, T., Rojas, J., McClain, J., Lengyel, P., Droguett, G., Chernomorsky, R., Stevens, S., Auerbach, W., Dechiara, T.M., Pouyemirou, W., Cruz, J.M., Feeley, K., Mellis, I.A., Yasenchack, J., Hatsell, S.J., Xie, L., Latres, E., Huang, L., Zhang, Y., Pefanis, E., Skokos, D., Deckelbaum, R.A., Croll, S.D., Davis, S., Valenzuela, D.M., Gale, N.W., Murphy, A.J. and Yancopoulos, G.D. (2013b) 'Conditionals by inversion provide a universal method for the generation of conditional alleles', Proc Natl Acad Sci U S A, 110(34), pp. E3179-88.
Elfeky, R., Lucchini, G., Lum, S.H., Ottaviano, G., Builes, N., Nademi, Z., Battersby, A., Flood, T., Owens, S., Cant, A.J., Young, H., Greener, S., Walsh, P., Kavanagh, D., Annavarapu, S., Rao, K., Amrolia, P., Chiesa, R., Worth, A., Booth, C., Skinner, R., Doncheva, B., Standing, J., Gennery, A.R., Qasim, W., Slatter, M. and Veys, P. (2020) 'New insights into risk factors for transplant-associated thrombotic microangiopathy in pediatric HSCT', Blood Adv, 4(11), pp. 2418-2429.
Elliott, S.J., Wainwright, L.A., McDaniel, T.K., Jarvis, K.G., Deng, Y.K., Lai, L.C., McNamara, B.P., Donnenberg, M.S. and Kaper, J.B. (1998) 'The complete sequence of the locus of enterocyte effacement (LEE) from enteropathogenic Escherichia coli E2348/69', Mol Microbiol, 28(1), pp. 1-4.
Essers, M.A.G., Offner, S., Blanco-Bose, W.E., Waibler, Z., Kalinke, U., Duchosal, M.A. and Trumpp, A. 'IFNα activates dormant haematopoietic stem cells in vivo'.
Exeni, R.A., Fernandez-Brando, R.J., Santiago, A.P., Fiorentino, G.A., Exeni, A.M., Ramos, M.V. and Palermo, M.S. (2018) 'Pathogenic role of inflammatory response during Shiga toxin-associated hemolytic uremic syndrome (HUS)', Pediatr Nephrol, 33(11), pp. 2057-2071.

Falguières, T., Römer, W., Amessou, M., Afonso, C., Wolf, C., Tabet, J.C., Lamaze, C. and Johannes, L. (2006) 'Functionally different pools of Shiga toxin receptor, globotriaosyl ceramide, in HeLa cells', FEBS J, 273(22), pp. 5205-18.
Ferens, W.A. and Hovde, C.J. (2011) 'Escherichia coli O157:H7: Animal Reservoir and Sources of Human Infection', Foodborne Pathogens and Disease, 8, pp. 465-487.
Fernando, M.M.A., Stevens, C.R., Sabeti, P.C., Walsh, E.C., McWhinnie, A.J.M., Shah, A., Green, T., Rioux, J.D. and Vyse, T.J. (2007) 'Identification of Two Independent Risk Factors for Lupus within the MHC in United Kingdom Families', PLOS Genetics, 3(11), p. e192.
Fernández, D., Rodríguez, E.M., Arroyo, G.H., Padola, N.L. and Parma, A.E. (2009) 'Seasonal variation of Shiga toxin-encoding genes (stx) and detection of E. coli O157 in dairy cattle from Argentina', J Appl Microbiol, 106(4), pp. 1260-7.
Ferraris, J.R., Ferraris, V., Acquier, A.B., Sorroche, P.B., Saez, M.S., Ginaca, A. and Mendez, C.F. (2015) 'Activation of the alternative pathway of complement during the acute phase of typical haemolytic uraemic syndrome', Clinical & Experimental Immunology, 181(1), pp. 118-125.
Ferreira, M.R., Freitas Filho, E.G., Pinto, J.F., Dias, M. and Moreira, C.N. (2014) 'Isolation, prevalence, and risk factors for infection by shiga toxin-producing Escherichia coli (STEC) in dairy cattle', Trop Anim Health Prod, 46(4), pp. 635-9.
Ferreira, V.P., Pangburn, M.K. and Cortés, C. (2010) 'Complement control protein factor H: the good, the bad, and the inadequate', Molecular immunology, 47(13), pp. 2187-2197.
Forde, A., Constien, R., Gröne, H.J., Hämmerling, G. and Arnold, B. (2002) 'Temporal Cre-mediated recombination exclusively in endothelial cells using Tie2 regulatory elements', Genesis, 33(4), pp. 191-7.
Fraga de Andrade, I., Johnson, K.D., Mehta, C., Dewey, C., Basu, U. and Bresnick, E.H. (2022) 'RNA-Regulatory Exosome Complex Suppresses an Apoptotic Program to Confer Erythroid Progenitor Cell Survival In Vivo', Blood Adv.
Franz, E. and van Bruggen, A.H.C. (2008) 'Ecology of E. coli O157:H7 and Salmonella enterica in the Primary Vegetable Production Chain', Critical Reviews in Microbiology, 34, pp. 143-161.
Fritzler, M.J. and Choi, M.Y. (2016) 'Editorial: Are Autoantibodies Involved in the Pathogenesis of Systemic Sclerosis?', Arthritis Rheumatol, 68(9), pp. 2067-70.

Fumagalli, S., Ivanenkov, V.V., Teng, T. and Thomas, G. (2012) 'Suprainduction of p53 by disruption of 40S and 60S ribosome biogenesis leads to the activation of a novel G2/M checkpoint', Genes Dev, 26(10), pp. 1028-40.
Furutani, M., Kashiwagi, K., Ito, K., Endo, Y. and Igarashi, K. (1992) 'Comparison of the modes of action of a Vero toxin (a Shiga-like toxin) from Escherichia coli, of ricin, and of alpha-sarcin', Arch Biochem Biophys, 293(1), pp. 140-6.
Garnier, A., Brochard, K., Kwon, T., Sellier-Leclerc, A.L., Lahoche, A., Launay, E.A., Nobili, F., Caillez, M., Taque, S., Harambat, J., Michel-Bourdat, G., Guigonis, V., Fila, M., Cloarec, S., Djamal-Dine, D., de Parscaux, L., Allard, L., Salomon, R., Ulinski, T., Frémeaux-Bacchi, V., Morin, C., Olivier-Abbal, P., Colineaux, H., Auriol, F., Arnaud, C., Kieffer, I. and Brusq, C. (2023) 'Efficacy and Safety of Eculizumab in Pediatric Patients Affected by Shiga Toxin-Related Hemolytic and Uremic Syndrome: A Randomized, Placebo-Controlled Trial', J Am Soc Nephrol, 34(9), pp. 1561-1573.
Garred, O., van Deurs, B. and Sandvig, K. (1995) 'Furin-induced cleavage and activation of Shiga toxin', J Biol Chem, 270(18), pp. 10817-21.
Gaytán, M.O., Martínez-Santos, V.I., Soto, E. and González-Pedrajo, B. (2016) 'Type Three Secretion System in Attaching and Effacing Pathogens', Front Cell Infect Microbiol, 6, p. 129.
Gbadegesin, R.A., Lavin, P.J., Hall, G., Bartkowiak, B., Homstad, A., Jiang, R., Wu, G., Byrd, A., Lynn, K., Wolfish, N., Ottati, C., Stevens, P., Howell, D., Conlon, P. and Winn, M.P. (2012) 'Inverted formin 2 mutations with variable expression in patients with sporadic and hereditary focal and segmental glomerulosclerosis', Kidney Int, 81(1), pp. 94-9.
Glover, E.K., Smith-Jackson, K., Brocklebank, V., Wilson, V., Walsh, P.R., Montgomery, E.K., Wong, E.K.S., Johnson, S., Malina, M., Kavanagh, D. and Sheerin, N.S. (2022) 'Assessing the Impact of Prophylactic Eculizumab on Renal Graft Survival in Atypical Hemolytic Uremic Syndrome', Transplantation.
Goodship, T.H.J., Cook, H.T., Fakhouri, F., Fervenza, F.C., Frémeaux-Bacchi, V., Kavanagh, D., Nester, C.M., Noris, M., Pickering, M.C., Rodríguez de Córdoba, S., Roumenina, L.T., Sethi, S., Smith, R.J.H., Alpers, C.E., Appel, G.B., Ardissino, G., Ariceta, G., Arici, M., Bagga, A., Bajema, I.M., Blasco, M., Burke, L., Cairns, T.D., Carratala, M., D'Agati, V.D., Daha, M.R., De Vriese, A.S., Dragon-Durey, M.-A., Fogo, A.B., Galbusera, M., Gale, D.P., Haller, H., Johnson, S., Józsi, M., Karpman,

D., Lanning, L., Le Quintrec, M., Licht, C., Loirat, C., Monfort, F., Morgan, B.P., Noël, L.-H., O'Shaughnessy, M.M., Rabant, M., Rondeau, E., Ruggenenti, P., Sheerin, N.S., Smith, J., Spoleti, F., Thurman, J.M., van de Kar, N.C.A.J., Vivarelli, M. and Zipfel, P.F. (2017) 'Atypical hemolytic uremic syndrome and C3 glomerulopathy: conclusions from a “Kidney Disease: Improving Global Outcomes” (KDIGO) Controversies Conference', Kidney International, 91(3), pp. 539-551.

Gravel, R.A., Mahoney, M.J., Ruddle, F.H. and Rosenberg, L.E. (1975) 'Genetic complementation in heterokaryons of human fibroblasts defective in cobalamin metabolism', Proc Natl Acad Sci U S A, 72(8), pp. 3181-5.

Greenbaum, L.A., Fila, M., Ardissino, G., Al-Akash, S.I., Evans, J., Henning, P., Lieberman, K.V., Maringhini, S., Pape, L., Rees, L., van de Kar, N.C.A.J., Vande Walle, J., Ogawa, M., Bedrosian, C.L. and Licht, C. (2016) 'Eculizumab is a safe and effective treatment in pediatric patients with atypical hemolytic uremic syndrome', Kidney International, 89, pp. 701-711.

Gulati, A., Bale, A.E., Dykas, D.J., Bia, M.J., Danovitch, G.M., Moeckel, G.W., Somlo, S. and Dahl, N.K. (2018) 'TREX1 Mutation Causing Autosomal Dominant Thrombotic Microangiopathy and CKD-A Novel Presentation', Am J Kidney Dis.

Guo, X., Ma, J., Sun, J. and Gao, G. (2007) 'The zinc-finger antiviral protein recruits the RNA processing exosome to degrade the target mRNA', Proc Natl Acad Sci U S A, 104(1), pp. 151-6.

Gurley, K.E., Ashley, A.K., Moser, R.D. and Kemp, C.J. 'Synergy between Prkdc and Trp53 regulates stem cell proliferation and GI-ARS after irradiation'.

Haidey, J.N., Peringod, G., Institoris, A., Gorzo, K.A., Nicola, W., Vandal, M., Ito, K., Liu, S., Fielding, C., Visser, F., Nguyen, M.D. and Gordon, G.R. (2021) 'Astrocytes regulate ultra-slow arteriole oscillations via stretch-mediated TRPV4-COX-1 feedback', Cell Rep, 36(5), p. 109405.

Hayne, C.K., Schmidt, C.A., Haque, M.I., Matera, A.G. and Stanley, R.E. (2020) 'Reconstitution of the human tRNA splicing endonuclease complex: insight into the regulation of pre-tRNA cleavage', Nucleic Acids Res, 48(14), pp. 7609-7622.

Hiriart, Y., Pardo, R.P., Bukata, L., Lauché, C.E., Muñoz, L., Berengeno, A.L., Colonna, M., Ortega, H.H., Goldbaum, F.A. and Sanguineti, S. (2019) 'Preclinical Studies of NEAST (Neutralizing Equine Anti-Shiga Toxin): A Potential Treatment for Prevention of Stec-Hus'.

Holcik, M. and Sonenberg, N. (2005) 'Translational control in stress and apoptosis', Nature Reviews Molecular Cell Biology, 6(4), pp. 318-327.
Holmes, C. and Stanford, W.L. (2007) 'Concise review: stem cell antigen-1: expression, function, and enigma', Stem Cells, 25(6), pp. 1339-47.
Holter, J.C., Pischke, S.E., de Boer, E., Lind, A., Jenum, S., Holten, A.R., Tonby, K., Barratt-Due, A., Sokolova, M. and Schjalm, C. (2020) 'Systemic complement activation is associated with respiratory failure in COVID-19 hospitalized patients', Proceedings of the National Academy of Sciences, 117(40), pp. 25018-25025.
Hourcade, D., Garcia, A.D., Post, T.W., Taillon-Miller, P., Holers, V.M., Wagner, L.M., Bora, N.S. and Atkinson, J.P. (1992) 'Analysis of the human regulators of complement activation (RCA) gene cluster with yeast artificial chromosomes (YACs)', Genomics, 12(2), pp. 289-300.
Houseley, J., LaCava, J. and Tollervey, D. (2006) 'RNA-quality control by the exosome', Nat Rev Mol Cell Biol, 7(7), pp. 529-39.
Huang, W., Yu, J., Jones, J.W., Carter, C.L., Pierzchalski, K., Tudor, G., Booth, C., MacVittie, T.J. and Kane, M.A. (2019) 'Proteomic Evaluation of the Acute Radiation Syndrome of the Gastrointestinal Tract in a Murine Total-body Irradiation Model', Health Phys, 116(4), pp. 516-528.
Hudson, M., Baron, M., Tatibouet, S., Furst, D.E. and Khanna, D. (2014) 'Exposure to ACE inhibitors prior to the onset of scleroderma renal crisis—Results from the International Scleroderma Renal Crisis Survey', Seminars in Arthritis and Rheumatism, 43(5), pp. 666-672.
Hughes, M., Prescott, C., Elliott, N. and Adler, A.I. (2021) 'NICE guidance on caplacizumab for treating acute acquired thrombotic thrombocytopenia purpura', The Lancet Haematology, 8(1), pp. e14-e15.
Hunt, D., Kavanagh, D., Drummond, I., Weller, B., Bellamy, C., Overell, J., Evans, S., Jackson, A. and Chandran, S. (2014) 'Thrombotic Microangiopathy Associated with Interferon Beta', New England Journal of Medicine, 370(13), pp. 1270-1271.
Iordanov, M.S., Pribnow, D., Magun, J.L., Dinh, T.H., Pearson, J.A., Chen, S.L. and Magun, B.E. (1997) 'Ribotoxic stress response: activation of the stress-activated protein kinase JNK1 by inhibitors of the peptidyl transferase reaction and by sequence-specific RNA damage to the alpha-sarcin/ricin loop in the 28S rRNA', Mol Cell Biol, 17(6), pp. 3373-81.

Jahn, H.M., Kasakow, C.V., Helfer, A., Michely, J., Verkhratsky, A., Maurer, H.H., Scheller, A. and Kirchhoff, F. 'Refined protocols of tamoxifen injection for inducible DNA recombination in mouse astroglia'.

Januszyk, K. and Lima, C.D. (2014) 'The eukaryotic RNA exosome', Curr Opin Struct Biol, 24, pp. 132-40.

Java, A., Apicelli, A.J., Liszewski, M.K., Coler-Reilly, A., Atkinson, J.P., Kim, A.H. and Kulkarni, H.S. (2020) 'The complement system in COVID-19: friend and foe?', JCI insight, 5(15).

Jenkins, C., Bird, P.K., Wensley, A., Wilkinson, J., Aird, H., Mackintosh, A., Greig, D.R., Simpson, A., Byrne, L., Wilkinson, R., Godbole, G., Arunachalam, N., Hughes, G.J. and Team, I.M. (2022) 'Outbreak of STEC O157:H7 linked to a milk pasteurisation failure at a dairy farm in England, 2019', Epidemiol Infect, 150, p. e114.

Jensen, Torben H., Jacquier, A. and Libri, D. (2013) 'Dealing with Pervasive Transcription', Molecular Cell, 52(4), pp. 473-484.

Jobst, K.A., Klenov, A., Neller, K.C.M. and Hudak, K.A. (2016) 'Effect of Depurination on Cellular and Viral RNA', in Jurga, S., Erdmann, V.A. and Barciszewski, J. (eds.) Modified Nucleic Acids in Biology and Medicine. Cham: Springer International Publishing, pp. 273-297.

Jodele, S., Davies, S.M., Lane, A., Khoury, J., Dandoy, C., Goebel, J., Myers, K., Grimley, M., Bleesing, J., El-Bietar, J., Wallace, G., Chima, R.S., Paff, Z. and Laskin, B.L. (2014a) 'Diagnostic and risk criteria for HSCT-associated thrombotic microangiopathy: a study in children and young adults', Blood, 124(4), pp. 645-653.

Jodele, S., Fukuda, T., Vinks, A., Mizuno, K., Laskin, B.L., Goebel, J., Dixon, B.P., Teusink, A., Pluthero, F.G., Lu, L., Licht, C. and Davies, S.M. (2014b) 'Eculizumab Therapy in Children with Severe Hematopoietic Stem Cell Transplantation–Associated Thrombotic Microangiopathy', Biology of Blood and Marrow Transplantation, 20(4), pp. 518-525.

Jodele, S., Licht, C., Goebel, J., Dixon, B.P., Zhang, K., Sivakumaran, T.A., Davies, S.M., Pluthero, F.G., Lu, L. and Laskin, B.L. (2013) 'Abnormalities in the alternative pathway of complement in children with hematopoietic stem cell transplant-associated thrombotic microangiopathy', Blood, 122(12), pp. 2003-2007.

Kadaba, S., Krueger, A., Trice, T., Krecic, A.M., Hinnebusch, A.G. and Anderson, J. (2004) 'Nuclear surveillance and degradation of hypomodified initiator tRNAMet in S. cerevisiae', Genes Dev, 18(11), pp. 1227-40.
Kamitsuji, H., Nonami, K., Ishikawa, N., Murakami, T., Nakayama, A., Umeki, Y. and Nakajima, M. (1999) 'PLASMA P-SELECTIN IN CHILDREN WITH HEMOLYTIC UREMIC SYN-DROME CAUSED BY ESCHERICHIA COLI O157: H7'.
Kampen, K.R., Sulima, S.O., Vereecke, S. and De Keersmaecker, K. (2020) 'Hallmarks of ribosomopathies', Nucleic Acids Res, 48(3), pp. 1013-1028.
Karczewski, K.J., Francioli, L.C., Tiao, G., Cummings, B.B., Alföldi, J., Wang, Q., Collins, R.L., Laricchia, K.M., Ganna, A., Birnbaum, D.P., Gauthier, L.D., Brand, H., Solomonson, M., Watts, N.A., Rhodes, D., Singer-Berk, M., England, E.M., Seaby, E.G., Kosmicki, J.A., Walters, R.K., Tashman, K., Farjoun, Y., Banks, E., Poterba, T., Wang, A., Seed, C., Whiffin, N., Chong, J.X., Samocha, K.E., Pierce-Hoffman, E., Zappala, Z., O'Donnell-Luria, A.H., Minikel, E.V., Weisburd, B., Lek, M., Ware, J.S., Vittal, C., Armean, I.M., Bergelson, L., Cibulskis, K., Connolly, K.M., Covarrubias, M., Donnelly, S., Ferriera, S., Gabriel, S., Gentry, J., Gupta, N., Jeandet, T., Kaplan, D., Llanwarne, C., Munshi, R., Novod, S., Petrillo, N., Roazen, D., Ruano-Rubio, V., Saltzman, A., Schleicher, M., Soto, J., Tibbetts, K., Tolonen, C., Wade, G., Talkowski, M.E., Neale, B.M., Daly, M.J., MacArthur, D.G. and Consortium, G.A.D. (2020) 'The mutational constraint spectrum quantified from variation in 141,456 humans', Nature, 581(7809), pp. 434-443.
Kassenborg, H.D., Hedberg, C.W., Hoekstra, M., Evans, M.C., Chin, A.E., Marcus, R., Vugia, D.J., Smith, K., Ahuja, S.D., Slutsker, L., Griffin, P.M. and Group, f.t.E.I.P.F.W. (2004) 'Farm Visits and Undercooked Hamburgers as Major Risk Factors for Sporadic Escherichia coli O157:H7 Infection: Data from a Case-Control Study in 5 FoodNet Sites', Clinical Infectious Diseases, 38, pp. S271-S278.
Kavanagh, D., Goodship, T.H. and Richards, A. (2013) 'Atypical Hemolytic Uremic Syndrome', Seminars in Nephrology, 33(6), pp. 508-530.
Kavanagh, D., McGlasson, S., Jury, A., Williams, J., Scolding, N., Bellamy, C., Gunther, C., Ritchie, D., Gale, D.P., Kanwar, Y.S., Challis, R., Buist, H., Overell, J., Weller, B., Flossmann, O., Blunden, M., Meyer, E.P., Krucker, T., Evans, S.J.W., Campbell, I.L., Jackson, A.P., Chandran, S. and Hunt, D.P.J. (2016) 'Type I interferon causes thrombotic microangiopathy by a dose-dependent toxic effect on the microvasculature', Blood.

Khalid, M. and Andreoli, S. (2019) 'Extrarenal manifestations of the hemolytic uremic syndrome associated with Shiga toxin-producing Escherichia coli (STEC HUS)', Pediatr Nephrol, 34(12), pp. 2495-2507.
Khalil, R.A. (2013) 'Protein Kinase C Inhibitors as Modulators of Vascular Function and their Application in Vascular Disease', Pharmaceuticals (Basel), 6(3), pp. 407-39.
Kielstein, J.T., Beutel, G., Fleig, S., Steinhoff, J., Meyer, T.N., Hafer, C., Kuhlmann, U., Bramstedt, J., Panzer, U., Vischedyk, M., Busch, V., Ries, W., Mitzner, S., Mees, S., Stracke, S., Nürnberger, J., Gerke, P., Wiesner, M., Sucke, B., Abu-Tair, M., Kribben, A., Klause, N., Schindler, R., Merkel, F., Schnatter, S., Dorresteijn, E.M., Samuelsson, O. and Brunkhorst, R. (2012) 'Best supportive care and therapeutic plasma exchange with or without eculizumab in Shiga-toxin-producing E. coli O104:H4 induced haemolytic–uraemic syndrome: an analysis of the German STEC-HUS registry', Nephrology Dialysis Transplantation, 27, pp. 3807-3815.
Kintz, E., Byrne, L., Jenkins, C., McCARTHY, N., Vivancos, R. and Hunter, P. (2019) 'Outbreaks of Shiga Toxin-Producing', J Food Prot, 82(11), pp. 1950-1958.
Kitov, P.I., Sadowska, J.M., Mulvey, G., Armstrong, G.D., Ling, H., Pannu, N.S., Read, R.J. and Bundle, D.R. (2000) 'Shiga-like toxins are neutralized by tailored multivalent carbohydrate ligands', Nature, 403(6770), pp. 669-72.
Komarov, P.G., Komarova, E.A., Kondratov, R.V., Christov-Tselkov, K., Coon, J.S., Chernov, M.V. and Gudkov, A.V. (1999) 'A chemical inhibitor of p53 that protects mice from the side effects of cancer therapy', Science, 285(5434), pp. 1733-7.
Konowalchuk, J., Speirs, J.I. and Stavric, S. (1977) 'Vero response to a cytotoxin of Escherichia coli', Infect Immun, 18(3), pp. 775-9.
Kothary, M.H. and Babu, U.S. (2001) 'Infective Dose of Foodborne Pathogens In Volunteers: a Review', Journal of Food Safety, 21(1), pp. 49-68.
Kristianto, J., Johnson, M.G., Zastrow, R.K., Radcliff, A.B. and Blank, R.D. (2017) 'Spontaneous recombinase activity of Cre-ERT2 in vivo', Transgenic Res, 26(3), pp. 411-417.
Krämer, A., Green, J., Pollard, J. and Tugendreich, S. (2014) 'Causal analysis approaches in Ingenuity Pathway Analysis', Bioinformatics, 30(4), pp. 523-30.
Kuang, S.Q., Medina-Martinez, O., Guo, D.C., Gong, L., Regalado, E.S., Reynolds, C.L., Boileau, C., Jondeau, G., Prakash, S.K., Kwartler, C.S., Zhu, L.Y., Peters, A.M., Duan, X.Y., Bamshad, M.J., Shendure, J., Nickerson, D.A., Santos-Cortez,

R.L., Dong, X., Leal, S.M., Majesky, M.W., Swindell, E.C., Jamrich, M. and Milewicz, D.M. (2016) 'FOXE3 mutations predispose to thoracic aortic aneurysms and dissections', J Clin Invest, 126(3), pp. 948-61.

Kuwana, M., Kaburaki, J., Mimori, T., Tojo, T. and Homma, M. (1993) 'Autoantibody reactive with three classes of RNA polymerases in sera from patients with systemic sclerosis', The Journal of Clinical Investigation, 91(4), pp. 1399-1404.

Laffleur, B., Batista, C.R., Zhang, W., Lim, J., Yang, B., Rossille, D., Wu, L., Estrella, J., Rothschild, G., Pefanis, E. and Basu, U. (2022) 'RNA exosome drives early B cell development via noncoding RNA processing mechanisms', Sci Immunol, 7(72), p. eabn2738.

Lai, Y., Rosenshine, I., Leong, J.M. and Frankel, G. (2013) 'Intimate host attachment: enteropathogenic and enterohaemorrhagic Escherichia coli', Cell Microbiol, 15(11), pp. 1796-808.

Lapeyraque, A.L., Malina, M., Fremeaux-Bacchi, V., Boppel, T., Kirschfink, M., Oualha, M., Proulx, F., Clermont, M.J., Le Deist, F., Niaudet, P. and Schaefer, F. (2011) 'Eculizumab in severe Shiga-toxin-associated HUS', N Engl J Med, 364(26), pp. 2561-3.

Lata, E., Choquet, K., Sagliocco, F., Brais, B., Bernard, G. and Teichmann, M. (2021) 'RNA Polymerase III Subunit Mutations in Genetic Diseases', Front Mol Biosci, 8, p. 696438.

Lee-Kirsch, M.A., Gong, M., Chowdhury, D., Senenko, L., Engel, K., Lee, Y.A., de Silva, U., Bailey, S.L., Witte, T., Vyse, T.J., Kere, J., Pfeiffer, C., Harvey, S., Wong, A., Koskenmies, S., Hummel, O., Rohde, K., Schmidt, R.E., Dominiczak, A.F., Gahr, M., Hollis, T., Perrino, F.W., Lieberman, J. and Hubner, N. (2007) 'Mutations in the gene encoding the 3'-5' DNA exonuclease TREX1 are associated with systemic lupus erythematosus', Nat Genet, 39(9), pp. 1065-7.

Legendre, C.M., Licht, C., Muus, P., Greenbaum, L.a., Babu, S., Bedrosian, C., Bingham, C., Cohen, D.J., Delmas, Y., Douglas, K., Eitner, F., Feldkamp, T., Fouque, D., Furman, R.R., Gaber, O., Herthelius, M., Hourmant, M., Karpman, D., Lebranchu, Y., Mariat, C., Menne, J., Moulin, B., Nürnberger, J., Ogawa, M., Remuzzi, G., Richard, T., Sberro-Soussan, R., Severino, B., Sheerin, N.S., Trivelli, A., Zimmerhackl, L.B., Goodship, T. and Loirat, C. (2013) 'Terminal complement inhibitor eculizumab in atypical hemolytic-uremic syndrome.', The New England journal of medicine, 368, pp. 2169-81.

Lemaire, M., Frémeaux-Bacchi, V., Schaefer, F., Choi, M., Tang, W.H., Le Quintrec, M., Fakhouri, F., Taque, S., Nobili, F., Martinez, F., Ji, W., Overton, J.D., Mane, S.M., Nürnberg, G., Altmüller, J., Thiele, H., Morin, D., Deschenes, G., Baudouin, V., Llanas, B., Collard, L., Majid, M.A., Simkova, E., Nürnberg, P., Rioux-Leclerc, N., Moeckel, G.W., Gubler, M.C., Hwa, J., Loirat, C., Lifton, R.P., Fremeaux-Bacchi, V., Quintrec, M.L., Nurnberg, G., Altmuller, J. and Nurnberg, P. (2013) 'Recessive mutations in DGKE cause atypical hemolytic-uremic syndrome.', Nature Genetics, 45, pp. 531-536.

Lerner-Ellis, J.P., Anastasio, N., Liu, J., Coelho, D., Suormala, T., Stucki, M., Loewy, A.D., Gurd, S., Grundberg, E., Morel, C.F., Watkins, D., Baumgartner, M.R., Pastinen, T., Rosenblatt, D.S. and Fowler, B. (2009) 'Spectrum of mutations in MMACHC, allelic expression, and evidence for genotype-phenotype correlations', Hum Mutat, 30(7), pp. 1072-81.

Licht, C., Greenbaum, L.A., Muus, P., Babu, S., Bedrosian, C.L., Cohen, D.J., Delmas, Y., Douglas, K., Furman, R.R., Gaber, O.A., Goodship, T., Herthelius, M., Hourmant, M., Legendre, C.M., Remuzzi, G., Sheerin, N., Trivelli, A. and Loirat, C. (2015) 'Efficacy and safety of eculizumab in atypical hemolytic uremic syndrome from 2-year extensions of phase 2 studies', Kidney International, 87, pp. 1061-1073.

Lieber, M.R. (2010) 'The mechanism of double-strand DNA break repair by the nonhomologous DNA end-joining pathway', Annu Rev Biochem, 79, pp. 181-211.

Litalien, C., Proulx, F., Mariscalco, M.M., Robitaille, P., Turgeon, J.P., Orrbine, E., Rowe, P.C., McLaine, P.N. and Seidman, E. (1999) 'Circulating inflammatory cytokine levels in hemolytic uremic syndrome', Pediatr Nephrol, 13(9), pp. 840-5.

Liu, D., Ding, Q., Dai, D.F., Padhy, B., Nayak, M.K., Li, C., Purvis, M., Jin, H., Shu, C., Chauhan, A.K., Huang, C.L. and Attanasio, M. (2021) 'Loss of diacylglycerol kinase ε causes thrombotic microangiopathy by impairing endothelial VEGFA signaling', JCI Insight, 6(9).

Liu, Q., Greimann, J.C. and Lima, C.D. (2006) 'Reconstitution, Activities, and Structure of the Eukaryotic RNA Exosome', Cell, 127(6), pp. 1223-1237.

Livak, K.J. and Schmittgen, T.D. (2001) 'Analysis of relative gene expression data using real-time quantitative PCR and the 2(-Delta Delta C(T)) Method', Methods, 25(4), pp. 402-8.

Lodi, G., Gentili, V., Casciano, F., Romani, A., Zauli, G., Secchiero, P., Zauli, E., Simioni, C., Beltrami, S., Fernandez, M., Rizzo, R. and Voltan, R. (2022) 'Cell cycle

block by p53 activation reduces SARS-CoV-2 release in infected alveolar basal epithelial A549-hACE2 cells', Front Pharmacol, 13, p. 1018761.
Lusco, M.A., Fogo, A.B., Najafian, B. and Alpers, C.E. 'Atlas of Renal Pathology: Thrombotic Microangiopathy', American Journal of Kidney Diseases, 68(6), pp. e33-e34.
Lynn, R.M., O'Brien, S.J., Taylor, C.M., Adak, G.K., Chart, H., Cheasty, T., Coia, J.E., Gillespie, I.A., Locking, M.E., Reilly, W.J., Smith, H.R., Waters, A. and Willshaw, G.A. (2005) 'Childhood hemolytic uremic syndrome, United Kingdom and Ireland', Emerging Infectious Diseases, 11, pp. 590-596.
M K Liszewski, T W Post, a. and Atkinson, J.P. (1991) 'Membrane Cofactor Protein (MCP or CD46): Newest Member of the Regulators of Complement Activation Gene Cluster', Annual Review of Immunology, 9(1), pp. 431-455.
Matthews, L., Reeve, R., Gally, D.L., Low, J.C., Woolhouse, M.E.J., McAteer, S.P., Locking, M.E., Chase-Topping, M.E., Haydon, D.T., Allison, L.J., Hanson, M.F., Gunn, G.J. and Reid, S.W.J. (2013) 'Predicting the public health benefit of vaccinating cattle against Escherichia coli O157.', Proceedings of the National Academy of Sciences of the United States of America, 110, pp. 16265-70.
McDaniel, T.K. and Kaper, J.B. (1997) 'A cloned pathogenicity island from enteropathogenic Escherichia coli confers the attaching and effacing phenotype on E. coli K-12', Mol Microbiol, 23(2), pp. 399-407.
McIver, S.C., Katsumura, K.R., Davids, E., Liu, P., Kang, Y.A., Yang, D. and Bresnick, E.H. (2016) 'Exosome complex orchestrates developmental signaling to balance proliferation and differentiation during erythropoiesis', Elife, 5.
McNamara, L.A., Topaz, N., Wang, X., Hariri, S., Fox, L. and MacNeil, J.R. (2017) 'High Risk for Invasive Meningococcal Disease Among Patients Receiving Eculizumab (Soliris) Despite Receipt of Meningococcal Vaccine', Am J Transplant, 17(9), pp. 2481-2484.
Mehta, C., Fraga de Andrade, I., Matson, D.R., Dewey, C.N. and Bresnick, E.H. (2021) 'RNA-regulatory exosome complex confers cellular survival to promote erythropoiesis', Nucleic Acids Res, 49(16), pp. 9007-9025.
Mellor, G.E., Fegan, N., Duffy, L.L., McMILLAN, K.E., Jordan, D. and Barlow, R.S. (2016) 'National Survey of Shiga Toxin-Producing Escherichia coli Serotypes O26, O45, O103, O111, O121, O145, and O157 in Australian Beef Cattle Feces', J Food Prot, 79(11), pp. 1868-1874.

Melton-Celsa, A.R. (2014) 'Shiga Toxin (Stx) Classification, Structure, and Function', Microbiology spectrum, 2(2), pp. 10.1128/microbiolspec.EHEC-0024-2013.

Menne, J., Delmas, Y., Fakhouri, F., Licht, C., Lommelé, Å., Minetti, E.E., Provôt, F., Rondeau, E., Sheerin, N.S., Wang, J., Weekers, L.E. and Greenbaum, L.A. (2019) 'Outcomes in patients with atypical hemolytic uremic syndrome treated with eculizumab in a long-term observational study', BMC Nephrology, 20(1), p. 125.

Menne, J., Nitschke, M., Stingele, R., Abu-Tair, M., Beneke, J., Bramstedt, J., Bremer, J.P., Brunkhorst, R., Busch, V., Dengler, R., Deuschl, G., Fellermann, K., Fickenscher, H., Gerigk, C., Goettsche, A., Greeve, J., Hafer, C., Hagenmuller, F., Haller, H., Herget-Rosenthal, S., Hertenstein, B., Hofmann, C., Lang, M., Kielstein, J.T., Klostermeier, U.C., Knobloch, J., Kuehbacher, M., Kunzendorf, U., Lehnert, H., Manns, M.P., Menne, T.F., Meyer, T.N., Michael, C., Munte, T., Neumann-Grutzeck, C., Nuernberger, J., Pavenstaedt, H., Ramazan, L., Renders, L., Repenthin, J., Ries, W., Rohr, A., Rump, L.C., Samuelsson, O., Sayk, F., Schmidt, B.M.W., Schnatter, S., Schocklmann, H., Schreiber, S., von Seydewitz, C.U., Steinhoff, J., Stracke, S., Suerbaum, S., van de Loo, A., Vischedyk, M., Weissenborn, K., Wellhoner, P., Wiesner, M., Zeissig, S., Buning, J., Schiffer, M. and Kuehbacher, T. (2012) 'Validation of treatment strategies for enterohaemorrhagic Escherichia coli O104:H4 induced haemolytic uraemic syndrome: case-control study', Bmj, 345, pp. 1-13.

Merle, N.S., Church, S.E., Fremeaux-Bacchi, V. and Roumenina, L.T. (2015) 'Complement System Part I – Molecular Mechanisms of Activation and Regulation', Frontiers in Immunology, 6.

Merritt, A.J., Potten, C.S., Kemp, C.J., Hickman, J.A., Balmain, A., Lane, D.P. and Hall, P.A. (1994) 'The role of p53 in spontaneous and radiation-induced apoptosis in the gastrointestinal tract of normal and p53-deficient mice', Cancer Res, 54(3), pp. 614-7.

MEYER, O., DE CHAISEMARTIN, L., NICAISE-ROLAND, P., CABANE, J., TUBACH, F., DIEUDE, P., HAYEM, G., PALAZZO, E., CHOLLET-MARTIN, S., KAHAN, A. and ALLANORE, Y. (2010) 'Anti-RNA Polymerase III Antibody Prevalence and Associated Clinical Manifestations in a Large Series of French Patients with Systemic Sclerosis: A Cross-sectional Study', The Journal of Rheumatology, 37(1), pp. 125-130.

Michael, M., Bagga, A., Sartain, S.E. and Smith, R.J.H. (2022) 'Haemolytic uraemic syndrome', Lancet, 400(10364), pp. 1722-1740.
Mitchell, P., Petfalski, E., Shevchenko, A., Mann, M. and Tollervey, D. (1997) 'The exosome: a conserved eukaryotic RNA processing complex containing multiple 3'-->5' exoribonucleases', Cell, 91(4), pp. 457-66.
Moake, J.L. (2002) 'Thrombotic Microangiopathies', New England Journal of Medicine, 347(8), pp. 589-600.
Monvoisin, A., Alva, J.A., Hofmann, J.J., Zovein, A.C., Lane, T.F. and Iruela-Arispe, M.L. (2006) 'VE-cadherin-CreERT2 transgenic mouse: a model for inducible recombination in the endothelium', Dev Dyn, 235(12), pp. 3413-22.
Morace, I., Pilz, R., Federico, G., Jennemann, R., Krunic, D., Nordström, V., von Gerichten, J., Marsching, C., Schießl, I.M. and Müthing, J. (2019) 'Renal globotriaosylceramide facilitates tubular albumin absorption and its inhibition protects against acute kidney injury', Kidney international, 96(2), pp. 327-341.
Morcos, M.N.F., Schoedel, K.B., Hoppe, A., Behrendt, R., Basak, O., Clevers, H.C., Roers, A. and Gerbaulet, A. (2017) 'SCA-1 Expression Level Identifies Quiescent Hematopoietic Stem and Progenitor Cells', Stem Cell Reports, 8(6), pp. 1472-1478.
Morigi, M., Galbusera, M., Gastoldi, S., Locatelli, M., Buelli, S., Pezzotta, A., Pagani, C., Noris, M., Gobbi, M., Stravalaci, M., Rottoli, D., Tedesco, F., Remuzzi, G. and Zoja, C. (2011) 'Alternative Pathway Activation of Complement by Shiga Toxin Promotes Exuberant C3a Formation That Triggers Microvascular Thrombosis', The Journal of Immunology, 187, pp. 172-180.
Morton, D.J., Jalloh, B., Kim, L., Kremsky, I., Nair, R.J., Nguyen, K.B., Rounds, J.C., Sterrett, M.C., Brown, B., Le, T., Karkare, M.C., McGaughey, K.D., Sheng, S., Leung, S.W., Fasken, M.B., Moberg, K.H. and Corbett, A.H. (2020) 'A Drosophila model of Pontocerebellar Hypoplasia reveals a critical role for the RNA exosome in neurons', PLoS Genet, 16(7), p. e1008901.
Moxley, R.A., Francis, D.H., Tamura, M., Marx, D.B., Santiago-Mateo, K. and Zhao, M. (2017) 'Efficacy of Urtoxazumab (TMA-15 Humanized Monoclonal Antibody Specific for Shiga Toxin 2) Against Post-Diarrheal Neurological Sequelae Caused by Escherichia coli O157:H7 Infection in the Neonatal Gnotobiotic Piglet Model', Toxins (Basel), 9(2).

Muller, J.S., Burns, D.T., Griffin, H., Wells, G.R., Zendah, R.A., Munro, B., Schneider, C. and Horvath, R. (2020) 'RNA exosome mutations in pontocerebellar hypoplasia alter ribosome biogenesis and p53 levels', Life Sci Alliance, 3(8).
Muzumdar, M.D., Tasic, B., Miyamichi, K., Li, L. and Luo, L. (2007) 'A global double-fluorescent Cre reporter mouse', Genesis, 45(9), pp. 593-605.
Müller, J.S., Burns, D.T., Griffin, H., Wells, G.R., Zendah, R.A., Munro, B., Schneider, C. and Horvath, R. (2020) 'RNA exosome mutations in pontocerebellar hypoplasia alter ribosome biogenesis and p53 levels', Life Sci Alliance, 3(8).
Naesens, L., Nemegeer, J., Roelens, F., Vallaeys, L., Meuwissen, M., Janssens, K., Verloo, P., Ogunjimi, B., Hemelsoet, D., Hoste, L., Roels, L., De Bruyne, M., De Baere, E., Van Dorpe, J., Dendooven, A., Sieben, A., Rice, G.I., Kerre, T., Beyaert, R., Uggenti, C., Crow, Y.J., Tavernier, S.J., Maelfait, J., Haerynck, F. and (UD-PrOZA), P.f.U.R.D. (2022) 'Mutations in RNU7-1 Weaken Secondary RNA Structure, Induce MCP-1 and CXCL10 in CSF, and Result in Aicardi-Goutières Syndrome with Severe End-Organ Involvement', J Clin Immunol, 42(5), pp. 962-974.
Nilsen, T.W. (2003) 'The spliceosome: the most complex macromolecular machine in the cell?', Bioessays, 25(12), pp. 1147-9.
Nishimura, J.-i., Yamamoto, M., Hayashi, S., Ohyashiki, K., Ando, K., Brodsky, A.L., Noji, H., Kitamura, K., Eto, T., Takahashi, T., Masuko, M., Matsumoto, T., Wano, Y., Shichishima, T., Shibayama, H., Hase, M., Li, L., Johnson, K., Lazarowski, A., Tamburini, P., Inazawa, J., Kinoshita, T. and Kanakura, Y. (2014) 'Genetic Variants in C5 and Poor Response to Eculizumab', New England Journal of Medicine, 370(7), pp. 632-639.
Noris, M., Benigni, A. and Remuzzi, G. (2020) 'The case of complement activation in COVID-19 multiorgan impact', Kidney international, 98(2), pp. 314-322.
Noris, M., Caprioli, J., Bresin, E., Mossali, C., Pianetti, G., Gamba, S., Daina, E., Fenili, C., Castelletti, F., Sorosina, A., Piras, R., Donadelli, R., Maranta, R., van der Meer, I., Conway, E.M., Zipfel, P.F., Goodship, T.H. and Remuzzi, G. (2010) 'Relative role of genetic complement abnormalities in sporadic and familial aHUS and their impact on clinical phenotype.', Clinical journal of the American Society of Nephrology : CJASN, 5, pp. 1844-1859.
O'Connell, K.E., Mikkola, A.M., Stepanek, A.M., Vernet, A., Hall, C.D., Sun, C.C., Yildirim, E., Staropoli, J.F., Lee, J.T. and Brown, D.E. (2015) 'Practical murine

hematopathology: a comparative review and implications for research', Comp Med, 65(2), pp. 96-113.
Oakes, R.S., Siegler, R.L., McReynolds, M.A., Pysher, T. and Pavia, A.T. (2006) 'Predictors of fatality in postdiarrheal hemolytic uremic syndrome', Pediatrics, 117(5), pp. 1656-62.
Ohara, T., Kojio, S., Taneike, I., Nakagawa, S., Gondaira, F., Tamura, Y., Gejyo, F., Zhang, H.M. and Yamamoto, T. (2002) 'Effects of azithromycin on shiga toxin production by Escherichia coli and subsequent host inflammatory response', Antimicrob Agents Chemother, 46(11), pp. 3478-83.
Orellana, E.A., Siegal, E. and Gregory, R.I. (2022) 'tRNA dysregulation and disease', Nat Rev Genet, 23(11), pp. 651-664.
Orth, D., Khan, A.B., Naim, A., Grif, K., Brockmeyer, J., Karch, H., Joannidis, M., Clark, S.J., Day, A.J., Fidanzi, S., Stoiber, H., Dierich, M.P., Zimmerhackl, L.B. and Würzner, R. (2009) 'Shiga Toxin Activates Complement and Binds Factor H: Evidence for an Active Role of Complement in Hemolytic Uremic Syndrome', The Journal of Immunology, 182, pp. 6394-6400.
Page, E.E., Kremer Hovinga, J.A., Terrell, D.R., Vesely, S.K. and George, J.N. (2017) 'Thrombotic thrombocytopenic purpura: diagnostic criteria, clinical features, and long-term outcomes from 1995 through 2015', Blood Adv, 1(10), pp. 590-600.
Palma, L.M.P., Sridharan, M. and Sethi, S. (2021) 'Complement in Secondary Thrombotic Microangiopathy', Kidney International Reports, 6(1), pp. 11-23.
Pan, X., Whitten, D.A., Wu, M., Chan, C., Wilkerson, C.G. and Pestka, J.J. (2013) 'Global protein phosphorylation dynamics during deoxynivalenol-induced ribotoxic stress response in the macrophage', Toxicol Appl Pharmacol, 268(2), pp. 201-11.
Pangburn, M.K., Schreiber, R.D. and Müller-Eberhard, H. (1981) 'Formation of the initial C3 convertase of the alternative complement pathway. Acquisition of C3b-like activities by spontaneous hydrolysis of the putative thioester in native C3', The Journal of experimental medicine, 154(3), pp. 856-867.
Payne, S., De Val, S. and Neal, A. (2018) 'Endothelial-Specific Cre Mouse Models', Arterioscler Thromb Vasc Biol, 38(11), pp. 2550-2561.
Pefanis, E., Wang, J., Rothschild, G., Lim, J., Chao, J., Rabadan, R., Economides, A.N. and Basu, U. (2014) 'Noncoding RNA transcription targets AID to divergently transcribed loci in B cells', Nature, 514(7522), pp. 389-393.

Pefanis, E., Wang, J., Rothschild, G., Lim, J., Kazadi, D., Sun, J., Federation, A., Chao, J., Elliott, O., Liu, Z.-P., Economides, Aris N., Bradner, James E., Rabadan, R. and Basu, U. (2015a) 'RNA Exosome-Regulated Long Non-Coding RNA Transcription Controls Super-Enhancer Activity', Cell, 161(4), pp. 774-789.

Pefanis, E., Wang, J., Rothschild, G., Lim, J., Kazadi, D., Sun, J., Federation, A., Chao, J., Elliott, O., Liu, Z.P., Economides, A.N., Bradner, J.E., Rabadan, R. and Basu, U. (2015b) 'RNA exosome-regulated long non-coding RNA transcription controls super-enhancer activity', Cell, 161(4), pp. 774-89.

Penn, H., Howie, A.J., Kingdon, E.J., Bunn, C.C., Stratton, R.J., Black, C.M., Burns, A. and Denton, C.P. (2007) 'Scleroderma renal crisis: patient characteristics and long-term outcomes', QJM: An International Journal of Medicine, 100(8), pp. 485-494.

Peumans, W.J., Hao, Q. and Van Damme, E.J. (2001) 'Ribosome-inactivating proteins from plants: more than RNA N-glycosidases?', The FASEB Journal, 15(9), pp. 1493-1506.

Phillips, E., Westwood, J., Brocklebank, V., Wong, E., Tellez, J., Marchbank, K., McGuckin, S., Gale, D., Connolly, J. and Goodship, T. (2016) 'The role of ADAMTS-13 activity and complement mutational analysis in differentiating acute thrombotic microangiopathies', Journal of Thrombosis and Haemostasis, 14(1), pp. 175-185.

Pickering, M.C., de Jorge, E.G., Martinez-Barricarte, R., Recalde, S., Garcia-Layana, A., Rose, K.L., Moss, J., Walport, M.J., Cook, H.T., de Córdoba, S.R. and Botto, M. (2007) 'Spontaneous hemolytic uremic syndrome triggered by complement factor H lacking surface recognition domains', J Exp Med, 204(6), pp. 1249-56.

Pineda, G.E., Rearte, B., Todero, M.F., Bruballa, A.C., Bernal, A.M., Fernandez-Brando, R.J., Isturiz, M.A., Zotta, E., Alba-Soto, C.D., Palermo, M.S. and Ramos, M.V. (2021) 'Absence of interleukin-10 reduces progression of shiga toxin-induced hemolytic uremic syndrome', Clin Sci (Lond), 135(3), pp. 575-588.

Ponticelli, C. and Banfi, G. (2006) 'Thrombotic microangiopathy after kidney transplantation', Transplant international, 19(10), pp. 789-794.

Quaggin, S.E. (2013) 'DGKE and atypical HUS', Nat Genet, 45(5), pp. 475-6.

Ramos, M.V., Mejias, M.P., Sabbione, F., Fernandez-Brando, R.J., Santiago, A.P., Amaral, M.M., Exeni, R., Trevani, A.S. and Palermo, M.S. (2016) 'Induction of

Neutrophil Extracellular Traps in Shiga Toxin-Associated Hemolytic Uremic Syndrome', J Innate Immun, 8(4), pp. 400-11.
Rangel, J.M., Sparling, P.H., Crowe, C., Griffin, P.M. and Swerdlow, D.L. (2005) 'Epidemiology of Escherichia coli O157:H7 outbreaks, United States, 1982-2002', Emerging Infectious Diseases, 11, pp. 603-609.
Richards, A. and Kavanagh, D. (2009) 'Pathogenesis of Thrombotic Microangiopathy: Insights from Animal Models', Nephron Experimental Nephrology, 113(4), pp. e97-e103.
Richards, A., van den Maagdenberg, A.M.J.M., Jen, J.C., Kavanagh, D., Bertram, P., Spitzer, D., Liszewski, M.K., Barilla-LaBarca, M.-L., Terwindt, G.M., Kasai, Y., McLellan, M., Grand, M.G., Vanmolkot, K.R.J., de Vries, B., Wan, J., Kane, M.J., Mamsa, H., Schafer, R., Stam, A.H., Haan, J., de Jong, P.T.V.M., Storimans, C.W., van Schooneveld, M.J., Oosterhuis, J.A., Gschwendter, A., Dichgans, M., Kotschet, K.E., Hodgkinson, S., Hardy, T.A., Delatycki, M.B., Hajj-Ali, R.A., Kothari, P.H., Nelson, S.F., Frants, R.R., Baloh, R.W., Ferrari, M.D. and Atkinson, J.P. (2007) 'C-terminal truncations in human 3[prime]-5[prime] DNA exonuclease TREX1 cause autosomal dominant retinal vasculopathy with cerebral leukodystrophy', Nat Genet, 39(9), pp. 1068-1070.
Rigby, R.E. and Rehwinkel, J. (2015) 'RNA degradation in antiviral immunity and autoimmunity', Trends Immunol, 36(3), pp. 179-88.
Roers, A., Hiller, B. and Hornung, V. (2016) 'Recognition of Endogenous Nucleic Acids by the Innate Immune System', Immunity, 44(4), pp. 739-54.
Rondeau, E., Scully, M., Ariceta, G., Barbour, T., Cataland, S., Heyne, N., Miyakawa, Y., Ortiz, S., Swenson, E., Vallee, M., Yoon, S.S., Kavanagh, D. and Haller, H. (2020) 'The long-acting C5 inhibitor, Ravulizumab, is effective and safe in adult patients with atypical hemolytic uremic syndrome naïve to complement inhibitor treatment', Kidney Int, 97(6), pp. 1287-1296.
Ross, C.M., Rapp, D., Cave, V.M. and Brightwell, G. (2019) 'Prevalence of Shiga toxin-producing Escherichia coli in pasture-based dairy herds', Lett Appl Microbiol, 68(2), pp. 112-119.
Rudnik-Schöneborn, S., Senderek, J., Jen, J.C., Houge, G., Seeman, P., Puchmajerová, A., Graul-Neumann, L., Seidel, U., Korinthenberg, R., Kirschner, J., Seeger, J., Ryan, M.M., Muntoni, F., Steinlin, M., Sztriha, L., Colomer, J., Hübner, C., Brockmann, K., Van Maldergem, L., Schiff, M., Holzinger, A., Barth, P., Reardon,

W., Yourshaw, M., Nelson, S.F., Eggermann, T. and Zerres, K. (2013) 'Pontocerebellar hypoplasia type 1: Clinical spectrum and relevance of EXOSC3 mutations', Neurology, 80(5), pp. 438-446.

Ryan, M.M., Cooke-Yarborough, C.M., Procopis, P.G. and Ouvrier, R.A. (2000) 'Anterior horn cell disease and olivopontocerebellar hypoplasia', Pediatric Neurology, 23(2), pp. 180-184.

Sandlesh, P., Juang, T., Safina, A., Higgins, M.J. and Gurova, K.V. (2018) 'Uncovering the fine print of the CreERT2-LoxP system while generating a conditional knockout mouse model of Ssrp1 gene', PLoS One, 13(6), p. e0199785.

Schaue, D. and McBride, W.H. (2019) 'Are animal models a necessity for acute radiation syndrome drug discovery?', Expert Opin Drug Discov, 14(6), pp. 511-515.

Schmid-Hempel, P. and Frank, S.A. (2007) 'Pathogenesis, Virulence, and Infective Dose', PLoS Pathogens, 3(10), p. e147.

Schmidt, C.Q., Schrezenmeier, H. and Kavanagh, D. (2022) 'Complement and the prothrombotic state', Blood, 139(13), pp. 1954-1972.

Scully, M., Yarranton, H., Liesner, R., Cavenagh, J., Hunt, B., Benjamin, S., Bevan, D., Mackie, I. and Machin, S. (2008) 'Regional UK TTP registry: correlation with laboratory ADAMTS 13 analysis and clinical features', British journal of haematology, 142(5), pp. 819-826.

Seifert, M.E. and Tarr, P.I. (2012) 'Azithromycin and decolonization after HUS', Nature Reviews Nephrology, 8(6), pp. 317-318.

Sharma, A.P., Greenberg, C.R., Prasad, A.N. and Prasad, C. 'Hemolytic uremic syndrome (HUS) secondary to cobalamin C (cblC) disorder'.

Sheth, K.J., Swick, H.M. and Haworth, N. (1986) 'Neurological involvement in hemolytic-uremic syndrome', Ann Neurol, 19(1), pp. 90-3.

Shiga, K. (1898) 'Über den Dysenteriebacillus (Bacillus dysenteriae)', Zentralbl Bakteriol Orig, 24, pp. 913-918.

Siegler, R.L., Brewer, E.D. and Pysher, T.J. (1989) 'Hemolytic uremic syndrome associated with glomerular disease', Am J Kidney Dis, 13(2), pp. 144-7.

Singh, V.K., Seed, T.M. and Olabisi, A.O. (2019) 'Drug discovery strategies for acute radiation syndrome', Expert Opin Drug Discov, 14(7), pp. 701-715.

Skaar, J.R., Ferris, A.L., Wu, X., Saraf, A., Khanna, K.K., Florens, L., Washburn, M.P., Hughes, S.H. and Pagano, M. (2015) 'The Integrator complex controls the

termination of transcription at diverse classes of gene targets', Cell Res, 25(3), pp. 288-305.
Smith-Jackson, K. and Harrison, R.A. (2023) 'Alternative pathway activation in pregnancy, a measured amount "complements" a successful pregnancy, too much results in adverse events', Immunol Rev, 313(1), pp. 298-319.
Smith-Jackson, K., Yang, Y., Denton, H., Pappworth, I.Y., Cooke, K., Barlow, P.N., Atkinson, J.P., Liszewski, M.K., Pickering, M.C., Kavanagh, D., Cook, H.T. and Marchbank, K.J. (2019) 'Hyperfunctional complement C3 promotes C5-dependent atypical hemolytic uremic syndrome in mice', The Journal of Clinical Investigation, 129(3), pp. 1061-1075.
Sohal, D.S., Nghiem, M., Crackower, M.A., Witt, S.A., Kimball, T.R., Tymitz, K.M., Penninger, J.M. and Molkentin, J.D. (2001) 'Temporally regulated and tissue-specific gene manipulations in the adult and embryonic heart using a tamoxifen-inducible Cre protein', Circ Res, 89(1), pp. 20-5.
Song, A.J. and Palmiter, R.D. (2018) 'Detecting and Avoiding Problems When Using the Cre-lox System', Trends Genet, 34(5), pp. 333-340.
Sonneveld, M.A., de Maat, M.P. and Leebeek, F.W. (2014) 'Von Willebrand factor and ADAMTS13 in arterial thrombosis: a systematic review and meta-analysis', Blood Rev, 28(4), pp. 167-78.
Soriano, P. (1999) 'Generalized lacZ expression with the ROSA26 Cre reporter strain', Nat Genet, 21(1), pp. 70-1.
Sperti, S., Montanaro, L., Mattioli, A. and Testoni, G. (1975) 'Relationship between elongation factor I-and elongation factor II-dependent guanosine triphosphatase activities of ribosomes. Inhibition of both activities by ricin', Biochemical Journal, 148(3), p. 447.
Stahl, A.L., Sartz, L. and Karpman, D. (2011) 'Complement activation on platelet-leukocyte complexes and microparticles in enterohemorrhagic Escherichia coli-induced hemolytic uremic syndrome', Blood, 117(20), pp. 5503-13.
Stevens, K.B., O'Neill, D., Jepson, R., Holm, L.P., Walker, D.J. and Cardwell, J.M. (2018) 'Signalment risk factors for cutaneous and renal glomerular vasculopathy (Alabama rot) in dogs in the UK', Veterinary Record, 183(14), pp. 448-448.
Struijk, G.H., Bouts, A.H.M., Rijkers, G.T., Kuin, E.A.C., ten Berge, I.J.M. and Bemelman, F.J. (2013) 'Meningococcal Sepsis Complicating Eculizumab Treatment Despite Prior Vaccination', American Journal of Transplantation, 13, pp. 819-820.

Takahasi, K., Yoneyama, M., Nishihori, T., Hirai, R., Kumeta, H., Narita, R., Gale, M., Jr., Inagaki, F. and Fujita, T. (2008) 'Nonself RNA-sensing mechanism of RIG-I helicase and activation of antiviral immune responses', Mol Cell, 29(4), pp. 428-40.
Tanaka, K., Adams, B., Aris, A.M., Fujita, N., Ogawa, M., Ortiz, S., Vallee, M. and Greenbaum, L.A. (2021) 'The long-acting C5 inhibitor, ravulizumab, is efficacious and safe in pediatric patients with atypical hemolytic uremic syndrome previously treated with eculizumab', Pediatr Nephrol, 36(4), pp. 889-898.
Tarr, P.I., Gordon, C.A. and Chandler, W.L. (2005) 'Shiga-toxin-producing Escherichia coli and haemolytic uraemic syndrome' Lancet, 365. [Online] Available at: http://ac.els-cdn.com/S0140673605711442/1-s2.0-S0140673605711442-main.pdf?_tid=dcce4a30-d729-11e6-89a4-00000aab0f01&acdnat=1484048728_6e066c9b2fbb05664c547960acd6590d.
Taylor, F.B., Tesh, V.L., DeBault, L., Li, A., Chang, A.C.K., Kosanke, S.D., Pysher, T.J. and Siegler, R.L. (1999) 'Characterization of the Baboon Responses to Shiga-Like Toxin: Descriptive Study of a New Primate Model of Toxic Responses to Stx-1', The American Journal of Pathology, 154(4), pp. 1285-1299.
te Loo, D.M.W.M., Monnens, L.A.H., van der Velden, T.J.A.M., Vermeer, M.A., Preyers, F., Demacker, P.N.M., van den Heuvel, L.P.W.J. and van Hinsbergh, V.W.M. (2000) 'Binding and transfer of verocytotoxin by polymorphonuclear leukocytes in hemolytic uremic syndrome', Blood, 95(11), pp. 3396-3402.
Teoh, C.W., Gorman, K.M., Lynch, B., Goodship, T.H.J., Dolan, N.M., Waldron, M., Riordan, M. and Awan, A. (2018) 'Clinical Relapses of Atypical HUS on Eculizumab: Clinical Gap for Monitoring and Individualised Therapy', Case Reports in Nephrology, 2018, p. 4.
Tesh, V.L. (2012) 'Activation of cell stress response pathways by Shiga toxins', Cell Microbiol, 14(1), pp. 1-9.
Tesh, V.L., Burris, J., Owens, J., Gordon, V., Wadolkowski, E., O'brien, A. and Samuel, J. (1993) 'Comparison of the relative toxicities of Shiga-like toxins type I and type II for mice', Infection and immunity, 61(8), pp. 3392-3402.
Thurman, J.M., Marians, R., Emlen, W., Wood, S., Smith, C., Akana, H., Holers, V.M., Lesser, M., Kline, M., Hoffman, C., Christen, E. and Trachtman, H. (2009) 'Alternative Pathway of Complement in Children with Diarrhea-Associated Hemolytic Uremic Syndrome', Clinical Journal of the American Society of Nephrology, 4(12), pp. 1920-1924.

Trachtman, H. (2003) 'Effect of an Oral Shiga Toxin–Binding Agent on Diarrhea-Associated Hemolytic Uremic Syndrome in Children<SUBTITLE>A Randomized Controlled Trial</SUBTITLE>', JAMA, 290, p. 1337.

Tschernoster, N., Erger, F., Walsh, P.R., McNicholas, B., Fistrek, M., Habbig, S., Schumacher, A.-L., Folz-Donahue, K., Kukat, C., Toliat, M.R., Becker, C., Thiele, H., Kavanagh, D., Nürnberg, P., Beck, B.B. and Altmüller, J. (2022) 'Unraveling Structural Rearrangements of the CFH Gene Cluster in Atypical Hemolytic Uremic Syndrome Patients Using Molecular Combing and Long-Fragment Targeted Sequencing', The Journal of Molecular Diagnostics, 24(6), pp. 619-631.

Ueda, Y., Miwa, T., Ito, D., Kim, H., Sato, S., Gullipalli, D., Zhou, L., Golla, M., Song, D., Dunaief, J.L., Palmer, M.B. and Song, W.C. (2019) 'Differential contribution of C5aR and C5b-9 pathways to renal thrombic microangiopathy and macrovascular thrombosis in mice carrying an atypical hemolytic syndrome-related factor H mutation', Kidney Int, 96(1), pp. 67-79.

Ueda, Y., Mohammed, I., Song, D., Gullipalli, D., Zhou, L., Sato, S., Wang, Y., Gupta, S., Cheng, Z., Wang, H., Bao, J., Mao, Y., Brass, L., Zheng, X.L., Miwa, T., Palmer, M., Dunaief, J. and Song, W.C. (2017) 'Murine systemic thrombophilia and hemolytic uremic syndrome from a factor H point mutation', Blood, 129(9), pp. 1184-1196.

UKHSA (2022) Shiga toxin-producing Escherichia coli (STEC) data: 2019 (Accessed: 21/02/23).

Ullman-Culleré, M.H. and Foltz, C.J. (1999) 'Body condition scoring: a rapid and accurate method for assessing health status in mice', Lab Anim Sci, 49(3), pp. 319-23.

Ulmke, P.A., Xie, Y., Sokpor, G., Pham, L., Shomroni, O., Berulava, T., Rosenbusch, J., Basu, U., Fischer, A., Nguyen, H.P., Staiger, J.F. and Tuoc, T. (2021) 'Post-transcriptional regulation by the exosome complex is required for cell survival and forebrain development via repression of P53 signaling', Development, 148(3).

Vaisbich, M.H., Braga, A., Gabrielle, M., Bueno, C., Piazzon, F. and Kok, F. (2017) 'Thrombotic microangiopathy caused by methionine synthase deficiency: diagnosis and treatment pitfalls', Pediatr Nephrol, 32(6), pp. 1089-1092.

Valoti, E., Alberti, M., Tortajada, A., Garcia-Fernandez, J., Gastoldi, S., Besso, L., Bresin, E., Remuzzi, G., Rodriguez de Cordoba, S. and Noris, M. (2015) 'A novel

atypical hemolytic uremic syndrome-associated hybrid CFHR1/CFH gene encoding a fusion protein that antagonizes factor H-dependent complement regulation', J Am Soc Nephrol, 26(1), pp. 209-19.
van den Hoogen, F., Khanna, D., Fransen, J., Johnson, S.R., Baron, M., Tyndall, A., Matucci-Cerinic, M., Naden, R.P., Medsger Jr, T.A., Carreira, P.E., Riemekasten, G., Clements, P.J., Denton, C.P., Distler, O., Allanore, Y., Furst, D.E., Gabrielli, A., Mayes, M.D., van Laar, J.M., Seibold, J.R., Czirjak, L., Steen, V.D., Inanc, M., Kowal-Bielecka, O., Müller-Ladner, U., Valentini, G., Veale, D.J., Vonk, M.C., Walker, U.A., Chung, L., Collier, D.H., Csuka, M.E., Fessler, B.J., Guiducci, S., Herrick, A., Hsu, V.M., Jimenez, S., Kahaleh, B., Merkel, P.A., Sierakowski, S., Silver, R.M., Simms, R.W., Varga, J. and Pope, J.E. (2013) '2013 Classification Criteria for Systemic Sclerosis: An American College of Rheumatology/European League Against Rheumatism Collaborative Initiative', Arthritis & Rheumatism, 65(11), pp. 2737-2747.
Van Quekelberghe, C., Latta, K., Kunzmann, S., Grohmann, M. and Hansen, M. (2022) 'Atypical hemolytic uremic syndrome induced by SARS-CoV2 infection in infants with EXOSC3 mutation', Pediatr Nephrol, 37(11), pp. 2781-2784.
Venables, J.P., Strain, L., Routledge, D., Bourn, D., Powell, H.M., Warwicker, P., Diaz-Torres, M.L., Sampson, A., Mead, P., Webb, M., Pirson, Y., Jackson, M.S., Hughes, A., Wood, K.M., Goodship, J.A. and Goodship, T.H.J. (2006) 'Atypical haemolytic uraemic syndrome associated with a hybrid complement gene', PLoS Medicine.
Venegas-Vargas, C., Henderson, S., Khare, A., Mosci, R.E., Lehnert, J.D., Singh, P., Ouellette, L.M., Norby, B., Funk, J.A., Rust, S., Bartlett, P.C., Grooms, D. and Manning, S.D. (2016) 'Factors Associated with Shiga Toxin-Producing Escherichia coli Shedding by Dairy and Beef Cattle', Appl Environ Microbiol, 82(16), pp. 5049-56.
Verbiest, A., Pirenne, J. and Dierickx, D. (2014) 'De novo thrombotic microangiopathy after non-renal solid organ transplantation', Blood Reviews, 28(6), pp. 269-279.
Vogt, R.L. and Dippold, L. (2005) 'Escherichia coli O157:H7 outbreak associated with consumption of ground beef, June-July 2002.', Public Health Reports, 120, pp. 174-178.

Vooijs, M., Jonkers, J. and Berns, A. (2001) 'A highly efficient ligand-regulated Cre recombinase mouse line shows that LoxP recombination is position dependent', EMBO Rep, 2(4), pp. 292-7.
Voorhees, R.M., Schmeing, T.M., Kelley, A.C. and Ramakrishnan, V. (2010) 'The Mechanism for Activation of GTP Hydrolysis on the Ribosome', Science, 330(6005), pp. 835-838.
Vu, B., Wovkulich, P., Pizzolato, G., Lovey, A., Ding, Q., Jiang, N., Liu, J.J., Zhao, C., Glenn, K., Wen, Y., Tovar, C., Packman, K., Vassilev, L. and Graves, B. (2013) 'Discovery of RG7112: A Small-Molecule MDM2 Inhibitor in Clinical Development', ACS Med Chem Lett, 4(5), pp. 466-9.
Vítor, A.C., Huertas, P., Legube, G. and de Almeida, S.F. (2020) 'Studying DNA Double-Strand Break Repair: An Ever-Growing Toolbox', Frontiers in Molecular Biosciences, 7.
Walport, M.J. (2001) 'Complement', New England Journal of Medicine, 344(14), pp. 1058-1066.
Walsh, P.R. and Johnson, S. (2018) 'Treatment and management of children with haemolytic uraemic syndrome', Archives of disease in childhood, 103(3), pp. 285-291.
Walsh, P.R., Johnson, S., Brocklebank, V., Salvatore, J., Christian, M. and Kavanagh, D. (2018) 'Glucose-6-Phosphate Dehydrogenase Deficiency Mimicking Atypical Hemolytic Uremic Syndrome', Am J Kidney Dis, 71(2), pp. 287-290.
Wan, J., Yourshaw, M., Mamsa, H., Rudnik-Schöneborn, S., Menezes, M.P., Hong, J.E., Leong, D.W., Senderek, J., Salman, M.S., Chitayat, D., Seeman, P., von Moers, A., Graul-Neumann, L., Kornberg, A.J., Castro-Gago, M., Sobrido, M.-J., Sanefuji, M., Shieh, P.B., Salamon, N., Kim, R.C., Vinters, H.V., Chen, Z., Zerres, K., Ryan, M.M., Nelson, S.F. and Jen, J.C. (2012) 'Mutations in the RNA exosome component gene EXOSC3 cause pontocerebellar hypoplasia and spinal motor neuron degeneration', Nature genetics, 44(6), pp. 704-708.
Wang, Y. and Colonna, M. (2014) 'RNA exosomes keep endogenous RNA under the radar', Nat Immunol, 15(9), pp. 830-831.
Warwicker, P., Goodship, T.H.J.J., Donne, R.L., Pirson, Y., Nicholls, A., Ward, R.M., Turnpenny, P. and Goodship, J.A. (1998) 'Genetic studies into inherited and sporadic hemolytic uremic syndrome', Kidney international, 53, pp. 836-844.

Watson, R., Lindner, S., Bordereau, P., Hunze, E.M., Tak, F., Ngo, S., Zipfel, P.F., Skerka, C., Dragon-Durey, M.A. and Marchbank, K.J. (2014) 'Standardisation of the factor H autoantibody assay', Immunobiology, 219(1), pp. 9-16.
Weick, E.-M., Puno, M.R., Januszyk, K., Zinder, J.C., DiMattia, M.A. and Lima, C.D. (2018) 'Helicase-Dependent RNA Decay Illuminated by a Cryo-EM Structure of a Human Nuclear RNA Exosome-MTR4 Complex', Cell, 173(7), pp. 1663-1677.e21.
Weisfeld-Adams, J.D., Morrissey, M.A., Kirmse, B.M., Salveson, B.R., Wasserstein, M.P., McGuire, P.J., Sunny, S., Cohen-Pfeffer, J.L., Yu, C., Caggana, M. and Diaz, G.A. (2010) 'Newborn screening and early biochemical follow-up in combined methylmalonic aciduria and homocystinuria, cblC type, and utility of methionine as a secondary screening analyte', Mol Genet Metab, 99(2), pp. 116-23.
Westra, D., Volokhina, E.B., van der Molen, R.G., van der Velden, T.J.A.M., Jeronimus-Klaasen, A., Goertz, J., Gracchi, V., Dorresteijn, E.M., Bouts, A.H.M., Keijzer-Veen, M.G., van Wijk, J.A.E., Bakker, J.A., Roos, A., van den Heuvel, L.P. and van de Kar, N.C.A.J. (2017) 'Serological and genetic complement alterations in infection-induced and complement-mediated hemolytic uremic syndrome', Pediatric Nephrology, 32(2), pp. 297-309.
Wichtowska, D., Turowski, T.W. and Boguta, M. (2013) 'An interplay between transcription, processing, and degradation determines tRNA levels in yeast', Wiley Interdiscip Rev RNA, 4(6), pp. 709-22.
Wong, C.S., Jelacic, S., Habeeb, R.L., Watkins, S.L. and Tarr, P.I. (2000) 'The risk of the hemolytic-uremic syndrome after antibiotic treatment of Escherichia coli O157:H7 infections.', The New England journal of medicine, 342, pp. 1930-1936.
Woodworth, T.G., Suliman, Y.A., Li, W., Furst, D.E. and Clements, P. (2016) 'Scleroderma renal crisis and renal involvement in systemic sclerosis', Nat Rev Nephrol, 12(11), pp. 678-691.
Xiao, T.S. and Fitzgerald, K.A. (2013) 'The cGAS-STING pathway for DNA sensing', Mol Cell, 51(2), pp. 135-9.
Yashavarddhan, M.H., Sharma, A.K., Chaudhary, P., Bajaj, S., Singh, S. and Shukla, S.K. (2021) 'Development of hematopoietic syndrome mice model for localized radiation exposure', Scientific Reports, 11(1), p. 89.
Zheng, T., Zhu, Z., Wang, Z., Homer, R.J., Ma, B., Riese, R.J., Chapman, H.A., Shapiro, S.D. and Elias, J.A. (2000) 'Inducible targeting of IL-13 to the adult lung

causes matrix metalloproteinase- and cathepsin-dependent emphysema', J Clin Invest, 106(9), pp. 1081-93.
Zhong, Z.A., Sun, W., Chen, H., Zhang, H., Lay, Y.E., Lane, N.E. and Yao, W. (2015) 'Optimizing tamoxifen-inducible Cre/loxp system to reduce tamoxifen effect on bone turnover in long bones of young mice', Bone, 81, pp. 614-619.
Zhu, J., Singh, M., Selivanova, G. and Peuget, S. (2020) 'Pifithrin-α alters p53 post-translational modifications pattern and differentially inhibits p53 target genes', Scientific Reports, 10(1), p. 1049.
Zipfel, P.F., Jokiranta, T.S., Hellwage, J., Koistinen, V. and Meri, S. (1999) 'The factor H protein family', Immunopharmacology, 42(1-3), pp. 53-60.

11.

11. Appendix

Panel	Antigen	Clone	Fluorophore	Cell expression	Vendor	Concentration
White Cell count	CD3	REA641	PerCP-Vio700	T Cells	Miltenyi	1:50
	CD19	1D3	PE	B Cells	BD Bioscience	1:200
	CD45	30-F11	PE-Cy7	Pan White cells	BD Bioscience	1:50
	Ly6G	REA526	APC	Neutrophils	Miltenyi	1:50
HSC	CD127	A7R34	BV605	Common Lymphoid progenitor	Biolegend	1:50
	CD34	HM34	Biotin (BV710 secondary)	Early HSCs	Biolegend	1:200
	CD135	A2F10	PE	Early HSCs	Biolegend	1:100
	Sca1	E13-161.7	PE-Dazzle	HSCs	Biolegend	1:160
	c-Kit	2B8	Pacific Blue	HSCs	Biolegend	1:200
	B220	RA3-6B2	APC	Lineage depletion	Biolegend	1:200
	CD3ε	17-A2	APC	Lineage depletion	Biolegend	1:200
	GR1	RB6-8C5	APC	Lineage depletion	Biolegend	1:200
	Ter119	Ter-119;	APC	Lineage depletion	Biolegend	1:200
	CD11b	M1/70;	APC	Lineage depletion	Biolegend	1:200
	Viability	N/A	Near Infrared	Viability	Biolegend	1:500
Endothelial cells	CD31	REA784	APC	Endothelial cells	Miltenyi	1:50
	CD45	30-F11	PE-Cy7	Pan White cell	BD Bioscience	1:200
	Viability	N/A	Aqua Live/Dead	Viability	Invitrogen	1:100
Platelets	CD41	MWReg30	PE	Platelets	BD	1:400
Cell Cycle Analysis	Anti-BrdU	3D4	AF700	BrdU	Biolegend	5µl
	Propidium Iodide	N/A	PI	Viability	Biolegend	10µl
Apoptosis	Annexin V	N/A	APC	Early apoptosis	Biolegend	5µl
	7-AAD	N/A	7-AAD	Viability	Biolegend	10µl

Table 11-1: Antibodies used in flow cytometry

12. Publication during this project

1. Brocklebank, V*., **Walsh, P. R*.**, Smith-Jackson, K., Hallam, T. M., Marchbank, K. J., Wilson, V., . . . Kavanagh, D. (2023). Atypical haemolytic uraemic syndrome in the era of terminal complement inhibition- An observational cohort study. *Blood*. doi:10.1182/blood.2022018833

* Contributed equally

2. Brocklebank, V., Kumar, G., Howie, A.J., Chandar, J., Milford, D.V., Craze, J., Evans, J., Finlay, E., Freundlich, M., Gale, D.P., Inward, C., Mraz, M., Jones, C., Wong, W., Marks, S.D., Connolly, J., Corner, B.M., Smith-Jackson, K., **Walsh, P.R**., Marchbank, K.J., Harris, C.L., Wilson, V., Wong, E.K.S., Malina, M., Johnson, S., Sheerin, N.S. and Kavanagh, D. (2020) 'Long-term outcomes and response to treatment in diacylglycerol kinase epsilon nephropathy', Kidney Int.
3. Elfeky, R., Lucchini, G., Lum, S.H., Ottaviano, G., Builes, N., Nademi, Z., Battersby, A., Flood, T., Owens, S., Cant, A.J., Young, H., Greener, S., **Walsh, P.,** Kavanagh, D., Annavarapu, S., Rao, K., Amrolia, P., Chiesa, R., Worth, A., Booth, C., Skinner, R., Doncheva, B., Standing, J., Gennery, A.R., Qasim, W., Slatter, M. and Veys, P. (2020) 'New insights into risk factors for transplant-associated thrombotic microangiopathy in pediatric HSCT', Blood Adv, 4(11), pp. 2418-2429
4. Glover, E.K., Smith-Jackson, K., Brocklebank, V., Wilson, V., **Walsh, P.R.**, Montgomery, E.K., Wong, E.K.S., Johnson, S., Malina, M., Kavanagh, D. and Sheerin, N.S. (2022) 'Assessing the Impact of Prophylactic Eculizumab on Renal Graft Survival in Atypical Hemolytic Uremic Syndrome', Transplantation.

5. Tschernoster, N., Erger, F., **Walsh, P.R**., McNicholas, B., Fistrek, M., Habbig, S., Schumacher, A.-L., Folz-Donahue, K., Kukat, C., Toliat, M.R., Becker, C., Thiele, H., Kavanagh, D., Nürnberg, P., Beck, B.B. and Altmüller, J. (2022) 'Unraveling Structural Rearrangements of the CFH Gene Cluster in Atypical Hemolytic Uremic Syndrome Patients Using Molecular Combing and Long-Fragment Targeted Sequencing', The Journal of Molecular Diagnostics, 24(6), pp. 619-631.
6. Wong, E.K., Hallam, T.M., Brocklebank, V., **Walsh, P.R.**, Smith-Jackson, K., Shuttleworth, V.G., Cox, T.E., Anderson, H.E., Barlow, P.N. and Marchbank, K.J. (2021) 'Functional characterization of rare genetic variants in the N-terminus of complement Factor H in aHUS, C3G, and AMD', Frontiers in immunology, 11, p. 3426.